O‘ZBEKISTON MILLIY UNIVERSITETI XABARLARI, 2024, [3/1/1]
ISSN 2181-7324

FIZIKA
http://journals.nuu.uz
Natural sciences

UDK: 530.12:531.51

Alisher ABDUVOKHIDOV,
Teacher at Andijan State University
E-mail: alisherabdulvohidovl@gmail.com
Vakhid KHAMIDOV,
Associate Professor at Tashkent University of Information Technologies, PhD
Poshshajon DAVLETOVA,
PhD student at Institute of Fundamental and Applied Research, National Research University

Ulug’bek nomidagi Astronomiya instituti, f.-m.f.d A.A.Abdujabbarov taqrizi asosida

THERMAL ANALYSIS AROUND BLACK HOLE IN $f(Q)$ GRAVITY

Annotation

This paper explores the thermodynamic properties of a newly found perturbed black hole solution in symmetric teleparallel gravity. We focus on a nonlinear model, investigating null geodesics, quasi-normal modes, thermal fluctuations, and phase transitions. Davies points are identified, and we analyze emission energy and quantum fluctuations to understand the system comprehensively.

Keywords: Black holes (BHs), Event horizon,Gravitational pull, Hawking radiation
Thermodynamics, Entropy, Holographic principle.

ТЕПЛОВОЙ АНАЛИЗ ВОКРУГ ЧЕРНОЙ ДЫРЫ В ГРАВИТАЦИИ f(Q)

Аннотация

В этой статье исследуются термодинамические свойства недавно найденного возмущенного решения черной дыры в симметричной телепараллельной гравитации. Мы фокусируемся на нелинейной модели, исследуя нулевую геодезическую, квазинормальные моды, тепловые флуктуации и фазовые переходы. Точки Дэвиса идентифицируются, и мы анализируем энергию излучения и квантовые флуктуации, чтобы всесторонне понять систему.

Ключевые слова: Черные дыры (ЧД), Горизонт событий, Гравитационное притяжение, Излучение Хокинга, Термодинамика, Энтропия, Голографический принцип.

f(Q) GRAVITATSIYADAGI QORA TUYNUK ATROFIDA TERMAL TAHLIL

Annotatsiya

Ushbu maqola simmetrik teleparallel tortishishda yaqinda topilgan bezovtalangan qora tuynuk eritmasining termodinamik xususiyatlarini o'rganadi. Biz chiziqli bo'lmagan modelga e'tibor qaratamiz, nol geodezik, kvazi-normal rejimlar, termal tebranishlar va fazali o'tishlarni o'rganamiz. Devis nuqtalari aniqlanadi va biz tizimni har tomonlama tushunish uchun radiatsiya energiyasi va kvant tebranishlarini tahlil qilamiz.

Kalit so'zlar: Qora tuynuklar (BHs), hodisalar gorizonti, tortishish kuchi, Xoking nurlanishi, Termodinamika, Entropiya, Gologrаfik printsip.

Introduction. Black holes (BHs) are crucial in understanding intense gravitational fields. Classical BHs absorb surrounding matter due to their event horizon's immense gravitational pull, while quantum mechanics predicts thermal radiation emission, known as Hawking radiation, gradually reducing BH mass and increasing its temperature [1]. Entropy, linked to BH event horizon area as S=A/4 [2], shows BHs should have maximum entropy, but this poses issues with the second law of thermodynamics. The holographic principle, relating space's degrees of freedom to its boundary, governs the area-entropy relationship [3,4]. BHs, as thermodynamic entities, establish a relationship between entropy and Hawking temperature [5–7].

Quasi-normal modes (QNMs), perturbed outcomes of BH dynamical equations, are characterized by eigenvalues indicating frequency oscillations and damping modes. These motivate exploring thermodynamic features and QNMs in symmetric teleparallel gravity, focusing on the effects of f(Q) on BH thermodynamic quantities. The paper discusses BH structure, thermodynamic quantities, thermal stability, emission energy rate, and concludes with final remarks.

Black hole in symmetric teleparallelgravity with thermodynamical implications. In this study, we consider the action for $f(Q)$ gravity [18], which is given by

$$S = \int \sqrt{-g} d^4x \left[\frac{1}{2} f(Q) + \lambda_\alpha^{\beta\mu\nu} R^\alpha_{\beta\mu\nu} + \lambda_\alpha^{\mu\nu} T^\alpha_{\mu\nu} + L_m\right], \qquad (1)$$

Where determinant of $g_{\mu\nu}$ is denoted by g, $f(Q)$ is the function of non metricity Q, $\lambda_\alpha^{\beta\mu\nu}$ are the multiplier for the Lagrangian, and L_m denotes the matter Lagrangian density. Now, we consider the solution of field equations of $f(Q)$ gravity as a 4-dimensional spherical symmetric and stationary spacetime for the ansatz $f(Q) = Q + \alpha Q^2$, where the coupling constant is denoted with α. The respective line element of BH in the modified $f(Q)$ gravity is written as [18]

$$ds^2 = g_{tt} dt^2 - g_{rr} dr^2 - r^2 d\theta^2 - r^2 \sin^2\theta \, d\phi^2, \qquad (2)$$

Here the respective metric component ($g_{tt} = 1/g_{rr}$) is defined as [18]

$$g_{tt} = -\frac{\alpha c_2 + \alpha^2 (c_3 - 16(3c_6 + c_7)m^2) + 2m}{r} - \frac{(\alpha^2 \mu) \log\left(\frac{r}{R}\right)}{r} + 1, \qquad (3)$$

with real integrating constants c_1, c_2, c_3 and c_4. Here, m represents the mass of Schwarzschild BH. Here, the coupling constant is denoted with αand its values must follow the requirement $|\alpha| < 1$for the physically acceptable configuration. In this manuscript, we also considered the values of αaccording to the required range as $|\alpha| < 1$. In order to get a dimensionless argument in the logarithm, a new scale parameter introduced as $\mu = 48m^2c_7$ and a scale R is used to shift the constant $c_6 \to c_6 - 48m^2c_7 \log(R)$ [18]. For $\alpha = 0$, it is reduced to Schwarzschild solution in GR.

The line element given in Eq.(2)with the metric function defined in Eq.(3)is not an exact solution of the theory, it is only a perturbed solution. In this regard, we rewrite the metric function as

$$\mathcal{J}(r) = g_{tt}|_{\alpha=0} + \alpha\epsilon g_{tt,\alpha} + \alpha^2\epsilon^2 g_{tt,\alpha\alpha}, \qquad (4)$$

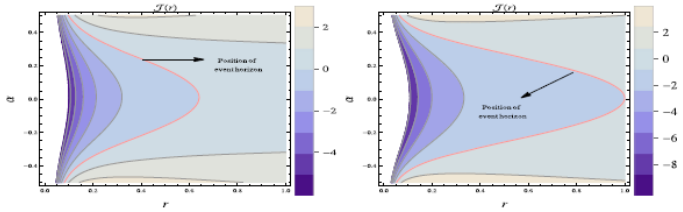

Where $\epsilon \ll 1$ is a tracking parameter. We consider the derivative of the metric function with respect to coupling constant αup to second-order terms. Hence, the corresponding metric function as a solution of considered geometry with above defined ansatze becomes

$$\mathcal{J}(r) = 1 - \frac{2m}{r} + \frac{\alpha\epsilon}{r}\left(-2\alpha(c_3 - 16(3c_6 + c_7)m^2) - c_2 - 2\alpha\mu \log\left(\frac{r}{R}\right)\right) + \frac{\alpha^2\epsilon^2}{r}\left(-2(c_3 - 16(3c_6 + c_7)m^2) - 2\mu \log\left(\frac{r}{R}\right)\right). \qquad (5)$$

Fig.1. Dependence of metric function for $m = 0.3$ (left) and $m = 0.5$ (right) on coupling constant α and radial coordinate r with $R = 0.05, \mu = -2, c_2 = 0.3, c_3 = 0.3, c_6 = 0.3, c_7 = 0.3, \epsilon = 0.3$.

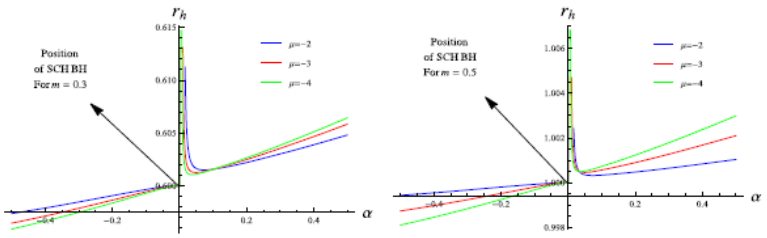

Fig.2. Plots of event horizon for $m = 0.3$ (left) and $m = 0.5$ (right) versus coupling constant α with $R = 0.05, \mu = -2, c_2 = 0.3, c_3 = 0.3, c_6 = 0.3, c_7 = 0.3, \epsilon = 0.3$.

For $\alpha = 0$, it is reduced to Schwarzschild solution in GR and the correction terms might lead to deviations from the Schwarzschild solution at large value of r. By taking $\mathcal{J}(r) = 0$, we calculate the position of event horizon in the following form

$$r_h = 2m + \alpha\epsilon\left(Re^{-\frac{c_2}{2\alpha\mu} - \frac{c_3}{\mu} + \frac{16(3c_6+c_7)m^2}{\mu}}\right) + \alpha^2\epsilon^2\left(Re^{\frac{16(3c_6+c_7)m^2}{\mu}} - \frac{c_3}{\mu}\right). \qquad (6)$$

Fig. 1 shows the graphical behavior of the metric function for different values of physical parameters. It is noted that the metric function shows symmetric behavior about positive and negative values of coupling constant α. The behavior of the metric function moves from negative to positive as r and α increase while α increases either negatively or positively. The position of event horizon is increased as the mass of BH increases. The left and right plots of Fig.2 show the graphical behavior of the position of the event horizon for different values of the mass of Schwarzschild BH. Here, it is very interesting to mention that the position of Schwarzschild event horizon ($r_h = 2m$) is recovered for $\alpha = 0$, i.e., for $m = 0.3$ and 0.5, we get $r_h = 0.6$ and $r_h = 1$, respectively. It is noted that the event horizon increases as α increases positively.

Now, we calculate the thermodynamical quantities of considered BH, i.e., Hawking temperature in terms of the mass of BH and heat capacity. These quantities are used to explore the thermodynamically stable characteristics of the BH structure.

The entropy of the system is calculated through area entropy relationship of Bekenstein [19]. It is given as

$$\mathbb{S} = \int_0^{2\pi}\int_0^{2\pi} \sqrt{g_{\theta\theta}g_{\phi\phi}}\, d\theta d\phi = \pi r_h^2 \qquad (9)$$

The corresponding expression of heat capacity $\left(\mathbb{T}\frac{\partial \mathbb{S}}{\partial \mathbb{T}}\right)$ has the following from [19]

$$\mathbb{C} = \frac{\pi r_h^2\left(\alpha\epsilon(2\alpha(\epsilon+1)(c_3 - 16(3c_6 + c_7)m^2) + c_2) + 2\left(\alpha^2\mu(-\epsilon)(\epsilon+1) + m + \alpha^2\mu\epsilon(\epsilon+1)\log\left(\frac{r_h}{R}\right)\right)\right)}{3\alpha^2\mu\epsilon(\epsilon+1) + \alpha\epsilon(-2\alpha(\epsilon+1)(c_3 - 16(3c_6 + c_7)m^2) - c_2) - 2m - 2\alpha^2\mu\epsilon(\epsilon+1)\log\left(\frac{r_h}{R}\right)}. \qquad (10)$$

The divergence point of the heat capacity is known as Davies point which plays an important role to discuss the thermodynamical stability configuration of the BH structure. It is noted that the positive region before the Devies point shows a stable region and the negative region after the Devies point represents the unstable region. These points are determined by taking the denominator of the mathematical expression of heat capacity equal to zero as

$$3\alpha^2\mu - 23\alpha^2\mu\epsilon(\epsilon+1) + \alpha\epsilon(-2\alpha(\epsilon+1)(c_3 - 16(3c_6 + c_7)m^2) - c_2) - 2m - 2\alpha - 2\alpha^2\mu\epsilon(\epsilon+1)\log\left(\frac{r_h}{R}\right) = 0$$

Hence, we get $r_{DP} = -\frac{R(-5\alpha^2\mu\epsilon(\epsilon+1)-\alpha\epsilon(-2\alpha(\epsilon+1)(c_3-16(3c_6+c_7)m^2)-c_2)+2m)}{2\alpha^2\mu\epsilon(\epsilon+1)}$,

where r_{DP} is represented the position of Davies point.

Fig.3. The position of Davies points and behavior of heat capacity for $m = 0.3$ (left) and $m = 0.5$ (right) with $R = 0.05, \mu = -2, c_2 = 0.3, c_3 = 0.3, c_6 = 0.3, c_7 = 0.3, \epsilon = 0.3$.

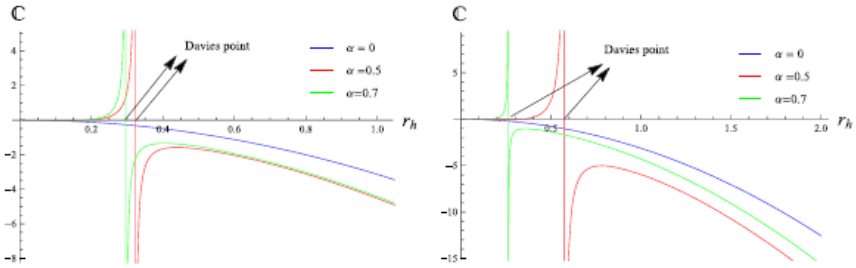

Fig.3 is used to discuss the stable and unstable configuration by using Devies points. It is interesting to mention that the thermodynamical unstable structure is observed for the choice of Schwarzschild BH ($\alpha = 0$). It is noted that presence of coupling constant enhances the stability of the Schwarzschild geometry. It shows stable behavior for smaller BHs as shown in the left plot. The stability is decreases for higher values of mass of the geometry. Hence, smaller BH represents a stable configuration while larger BH shows unstable behavior.

Emission energy. The formation and destruction of an excessive number of particles very close to the horizon is known as emission energy, and quantum fluctuations in the interior of BHs are the source of this energy. The main reason for the BH evaporation within a certain period is due to the positive-energy particles that tunnel out of the BH in the core area where Hawking radiation occurs. Here, we are interested to explore the energy emission rate associated with considered BH geometry in f(Q)gravity. At very high energy, the absorption cross-section often oscillates around a limiting constant value σ lim. The limiting value of σlimis related to the radius of the event horizon (r_h given in Eq.(6)):

$$\sigma_{lim} \approx \pi r_h^2. \qquad (11)$$

The respective expression of the rate of BH energy emission is become:

$$\frac{d^2\varepsilon}{d\omega dt} = \frac{2\pi^2\sigma_{lim}}{e^{\frac{\omega}{T}}-1}\omega^3$$

by considering the Hawking temperature T of considered BH, we get

$$\frac{d^2\varepsilon}{d\omega dt} = \frac{2\pi^3 r_h^2\omega^3}{\exp\left(\frac{4\pi r_h^2\omega}{\alpha\epsilon(2\alpha(\epsilon+1)(c_3-16(3c_6+c_7)m^2)+c_2)+2\left(\alpha^2\mu(-\epsilon)(\epsilon+)+m+\alpha^2\mu\epsilon(\epsilon+1)\,log\left(\frac{r_h}{R}\right)\right)}\right)-1} \qquad (12)$$

Fig.5 shows the behavior of the rate of emission energy along the frequency with suitable values of physical parameters. It is found that the rate of energy increases as frequency increases initially and approaches its peak value then decreases. We find the larger behavior of emission energy as μ increases negatively. The coupling constant αhas a great impact on the rate of emission energy. The right plot shows that the rate of emission energy is become smaller for higher values of α.

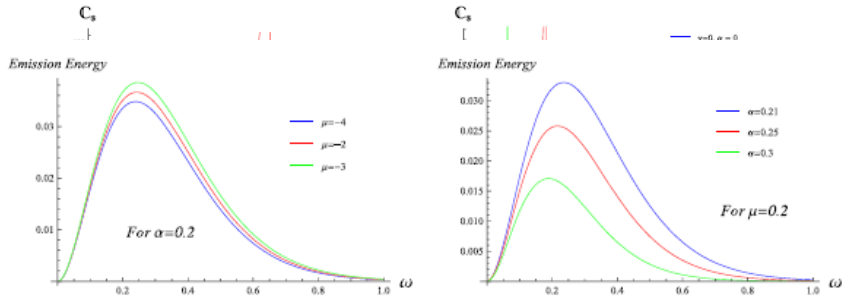

Fig.4. Stability of BH structure by using heat capacity versus r_h for $m = 0.2$ (left) and $m = 0.4$ (right) with $\mu = -2$, $c_2 = 0.3$, $c_3 = 0.5$, $c_6 = 0.5$, $c_7 = 0.03$,$\epsilon = 0.3$.

Fig.5. Graphical analysis of rate of emission energy versus frequency with different values of μ (left) and α (right) with $c_2 = 0.3, c_3 = 0.5, c_6 = 0.5, c_7 = 0.03, \epsilon = 0.3$.

Conluding remarks. We explore a novel perturbed solution for black holes within symmetric teleparallel gravity, focusing on field equations in a 4-dimensional spherically symmetric and stationary spacetime framework parameterized by α, a coupling constant. Notably, α plays a significant role, where its value influences the deviation from the Schwarzschild solution in General Relativity (GR). Teleparallel gravity, a modification of Einstein's theory, allows for black holes with similar traits as in GR but with modified equations. Our study reveals:

The lapse function's symmetric behavior with respect to α, depicted in Fig.1.

Good agreement with the Schwarzschild event horizon is observed in Fig.2.

Stability analysis, shown in Fig.3, identifies thermodynamically stable regions, with smaller black holes being stable and larger ones unstable.

Fig.5 displays the emission energy rate, indicating an initial increase with frequency before peaking and gradually decreasing.

REFERENCES

1. S.W. Hawking, Nature 248 (1974) 30; Commun. Math. Phys. 43 (1975) 199.
2. J.D. Bekenstein, Phys. Rev. D 7 (1973) 2333.
3. L. Susskind, J. Math. Phys. 36 (1995) 6377.
4. R. Bousso, Rev. Mod. Phys. 74 (2002) 825.
5. M.K. Parikh, F. Wilczek, Phys. Rev. Lett. 85 (2000) 5042.
6. R. Kerner, R.B. Mann, Class. Quantum Gravity 25 (2008) 095014.
7. A. Ejaz, et al., Phys. Lett. B 726 (2013) 827.

O‘ZBEKISTON MILLIY UNIVERSITETI XABARLARI, 2024, [3/1/1]
ISSN 2181-7324

FIZIKA
http://journals.nuu.uz
Natural sciences

UDK:2181(1296)

Nargiza ABDULXAFIZOVA,
O‘zbekiston Milliy universiteti magistranti
E-mail:abdulxafizovanargiza@gmail.com
Sherzod JUMAG‘ULOV,
O‘zbekiston Milliy universiteti tayanch doktoranti
Dilshod BOYQOBILOV,
O‘zbekiston Milliy universiteti tayanch doktoranti
Olim RO‘ZIMURADOV,
Toshkent shahridagi, Turin politexnika universiteti professori

O‘zMU professori A.Abdushukurov tahriri ostida

INVESTIGATION OF MORPHOLOGICAL CHARACTERISTICS OF TITANIUM DIOXIDE NANOTUBES

Annotation

Titanium dioxide nanotubes are important in scientific research, primarily due to their unique properties, including large surface area, chemical stability, and photocatalytic activity. This study focuses on the synthesis of TiO_2 nanotubes, highlighting the relevant factors affecting the process. The obtained results contribute to a comprehensive understanding and allow conclusions to be drawn on the different effects of different synthesis methodologies. In addition, the study investigates the underlying mechanisms of TiO_2 nanotube formation, providing valuable insights into the scientific landscape of nanomaterials.
Key words: Titanium dioxide nanotubes, anodizing, electrolyte solution.

ИЗУЧЕНИЕ МОРФОЛОГИЧЕСКИХ ХАРАКТЕРИСТИК НАНОТРУБОК ДИОКСИДА ТИТАНА

Аннотация

Нанотрубки диоксида титана играют важную роль в научных исследованиях, прежде всего, благодаря своим уникальным свойствам, включая большую площадь поверхности, химическую стабильность и фотокалитическую активность. Это исследование посвящено синтезу нанотрубок TiO_2, подчеркивая соответствующие факторы, влияющие на этот процесс. Полученные результаты способствуют всестороннему пониманию и позволяют сделать выводы о различном влиянии различных методологий синтеза. Кроме того, в данном работе исследует основные механизмы образования нанотрубок TiO_2, что дает ценную информацию о научном ландшафте наноматериалов.
Ключевые слова: Нанотрубки диоксида титана, анодирование, раствор электролита.

TITANI DIOKSID NANOTUBALARINING MORFOLOGIK XUSUSIYATLARINI O’RGANISH

Annotatsiya

Titan dioksid nanotrubkalari, birinchi navbatda, noyob xususiyatlari, jumladan, katta sirt maydoni, kimyoviy barqarorlik va fotokatalitik faolligi tufayli ilmiy tadqiqotlarda muhim ahamiyatga ega. Ushbu tadqiqot TiO_2 nanotrubkalarini sintez qilishga qaratilgan bo'lib, jarayonga ta'sir qiluvchi tegishli omillarni o’rganadi. Olingan natijalar asosida turli xil sintez metodologiyalarining turli ta'siri bo'yicha xulosalar chiqarishga imkon beradi. Bundan tashqari, tadqiqot nanomateriallarning ilmiy landshafti haqida qimmatli tushunchalar berib, TiO_2 nanotube shakllanishining asosiy mexanizmlarini o'rganadi.
Kalit so’zlar: Titan dioksid nanoporasi, anodlash, elektrolit eritmasi.

Introduction. Over the last decade, TiO_2 nanopores have garnered considerable scientific and technological attention, driven by their pivotal roles in energy conversion, environmental amelioration, potential applications as photocatalysts, and their inherent biocompatibility properties. The utilization of these nanopores spans various fields contingent upon their size, length, and wall thickness. Diverse methodologies for generating nanotubes, nanofibers, and nanopores have been explored, involving not only the deposition of metals but also semiconductors and polymer materials. Furthermore, the direct application of nanopores as filters or photonic crystals for wastewater treatment and the creation of enduring, corrosion-resistant elements has witnessed substantial advancement. The synthesis of TiO_2 nanoparticles, nanofibers, nanotubes, and nanoporous materials encompasses a spectrum of physical and chemical processes, such as electrochemical anodization, sol-gel, and chemical precipitation. Notably, the electrochemical anodization method for TiO_2 nanopore formation was selected as the focal technique in this research endeavor.

Literature review. The inaugural synthesis of titanium nanotubes through anodization was documented in 1999 by Sounart and colleagues [1], employing hydrofluoric acid as the electrolyte. Subsequently, Zwilling et al. reported the formation of a porous titanium oxide layer in a chromic acid solution with a small quantity of HF. Gong et al. [2-4] delineated the essential conditions for achieving high-quality and well-ordered (titania nanotubes)TNTs in acidic fluoride electrolytes. Pioneering advancements were made by Macak et al. [5-6] and Grimes and collaborators [7], who achieved a breakthrough in the fabrication of TiO_2 nanotubular structures. They reported the production of remarkably smooth, regular, and elongated nanotubes utilizing organic viscous electrolytes. Since then, diverse electrolytes, including HF, aqueous glycerol, carboxymethyl cellulose aqueous electrolyte, and ethylene glycol with ammonium fluoride, have proven successful in TNT fabrication. Anodizing titanium using phosphoric acid and sodium fluoride or hydrofluoric acid has also been explored [8-12]. However, titania nanotubes resulting from such processes exhibit a lack of orderliness and require extended production durations in a high-pH electrolyte [8]. Lee et

al.[9] created nanoscale biosensors by using TNTs produced through an anodization process at room temperature in an electrolyte containing ethylene glycol, NH_4F, and DI water.Macak et al. suggested that adjusting electrochemical parameters may offer potential solutions to address these challenges [10-11].

Research Methodology. SEM images of the synthesized TiO_2 nanotubes were obtained on a Focused Ion Beam Scanning Electron Microscope (FIB-SEM). Energy dispersive spectroscopy (EDS) of the samples were also investigated.

Experimental part. Main reagents: Pure titanium foil , 2% deionized water,0,5% ammonium fluoride (NH_4F) and 97,5% ethylene glycol (EG). TiO_2 nanotubes were systematically prepared through a three-step electrochemical anodization process. Initially, Ti foil was meticulously sectioned into dimensions of 2.5 x 2.5 cm and subjected to ultrasonic cleaning with acetone, distilled water, and ethanol for a duration of 10 minutes. The cleansed titanium foil underwent thorough rinsing with distilled water and was subsequently air-dried for one hour. In the second phase of anodization, the titanium foil was connected to a direct current (DC) source, sustaining a constant voltage of 60 V for a duration of 4 hours. A platinum electrode served as the counter electrode, while the electrochemical anodizing process was executed employing a copper base, Teflon cup, and GOPHERT CPS-6011 equipment. Moving on to the third step, the titanium foil underwent another round of comprehensive washing with distilled water, followed by ultrasonic treatment with acetone, deionized water, and ethanol for a period of 10 minutes. Subsequently, it was subjected to heating at 450℃ using Nabertherm heating oven for 1 hour, employing a heating rate of 20 ℃ per second.

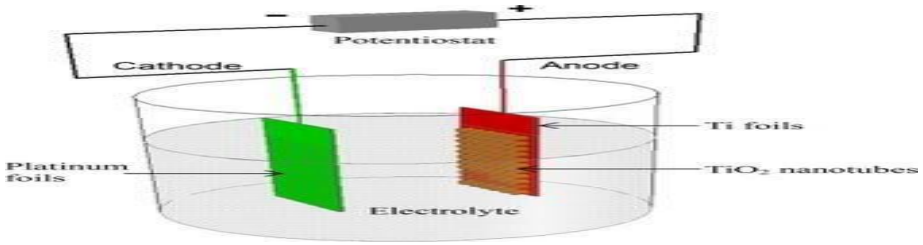

Figure 1. Illustrative diagram of anodizing cell

Results. The process is illustrated in(Fig 1), which represents the electrochemical anodization methodology. Specifically, the anodization was conducted employing titanium foil as the anode, while platinum (Pt) was employed as the counter electrode in the electrochemical cell configuration.

Post-electrochemical anodization, the surface morphology of the titanium foil was researched through SEM. The resulting micrograph (Fig 2) reveals the presence of well-organized hexagonal nanotube structures.

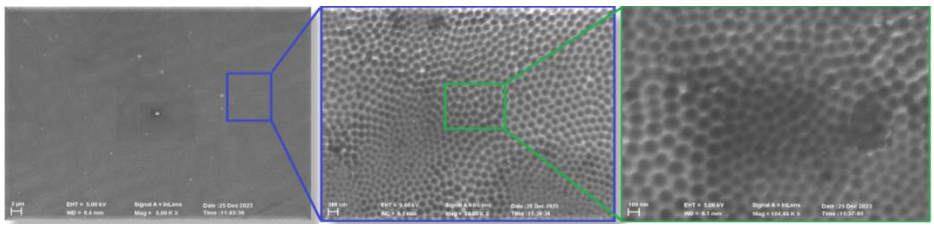

Figure 2. SEM images of as-prepared TiO_2 nanotube by anodization method at 20℃

As evidenced by the obtained results, it is imperative to underscore the pivotal role played by the dimensions of the synthesized TiO_2 nanotubes, specifically the diameter and wall thickness, as critical parameters. Consequently, an exhaustive analysis elucidating the intricate interplay between these dimensions and the applied anodizing voltage was conducted. In existing literature, this relationship can be articulated as follows: [13-15]

$$d(nm)=kV$$

$$w(nm)=hV$$

Here, k and h are the growth ratios of the nanotube wall thickness and diameter, respectively, approximately equal to 0.13 (nm V^{-1}) and 1.2 (nm V^{-1}).

In accordance with the prescribed formula, the determined dimensions of the nanotubes in our study manifest a diameter of 161.09 nm and a wall thickness of 65.43 nm.

Simultaneously, concurrent with the synthesis outcomes, electrochemical double-layer capacitance EDS analysis was performed on the nanotube surface. The analytical findings indicate the absence of additives on the foil's surface, affirming that the utilized electrolyte composition is devoid of additives (Fig 3)

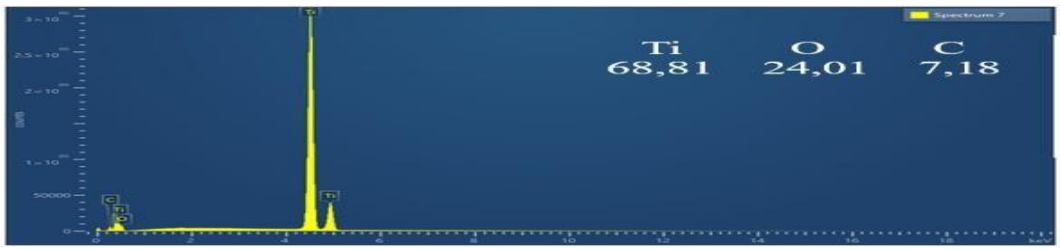

Figure 3. EDS spectrum of synthesized TiO_2

Conclusions. In summary, the investigation comprehensively examined the influencing factors on nanotube formation. Utilizing SEM and energy-dispersive EDS, detailed imaging and elemental analysis were conducted on the synthesized TiO_2 nanotubes. Additionally, an in-depth analysis of ion migration during the nanotube synthesis process was pursued. Notably,

fluorine (F) ions exhibited a migration rate two times faster than other ions, emerging as a pivotal factor in the nanotube formation mechanism.

The study contributes valuable insights into the dynamic ion migration phenomena influencing nanotube synthesis. Specifically, the accelerated migration of F^- ions plays a central role in the intricate process of nanotube formation. This newfound understanding enhances our grasp of the underlying mechanisms governing nanotube synthesis.

Moreover, it is noteworthy that the synthesis parameters, including nanotube diameter, length, and wall thickness, can be deliberately manipulated to meet specific consumer demands. This versatility underscores the adaptability and potential customization of nanotube synthesis processes to cater to diverse applications and preferences in nanomaterial engineering. Maintaining precise temperature control is crucial in the electrochemical anodization process for the creation of nanotubes. Additionally, the anodization process should be conducted within the temperature range of 20°C to 30°C, preferably at room temperature. Following anodization, the samples should be annealed at appropriate temperatures to achieve a crystalline structure. Furthermore, it is advisable to subject the titanium foil to vacuum drying following the cleaning process.

LITERATURE

1. Sounart T.L., Liu.J., Voigt J.A., JWP Hsu, ED Spoerke, Z Tian, YB Jiang. Sequential nucleation and growth of complex nanostructured films //Advanced Functional Materials. – 2006. – T. 16. – №. 3. – P. 335-344.
2. Gong, D., Grimes, C. A., Varghese, O. K., Hu, W., Singh, R. S., Chen, Z., & Dickey, E. C. (2001). Titanium oxide nanotube arrays prepared by anodic oxidation. *Journal of Materials Research*, *16*, 3331-3334.
3. Mor, G. K., Varghese, O. K., Paulose, M., Shankar, K., & Grimes, C. A. (2006). A review on highly ordered, vertically oriented TiO2 nanotube arrays: Fabrication, material properties, and solar energy applications. *Solar Energy Materials and Solar Cells*, *90*(14), 2011-2075.
4. Ding Y., Nagpal P. Titanium dioxide nanotube membranes for solar energy conversion: effect of deep and shallow dopants //Physical Chemistry Chemical Physics. – 2017. – T. 19. – №. 15. – P. 10042-10050.
5. Macak J. M., Sirotna K., Schmuki P. Self-organized porous titanium oxide prepared in Na2SO4/NaF electrolytes //Electrochimica Acta. – 2005. – T. 50. – №. 18. – C. 3679-3684.
6. Sepúlveda, M., Sopha, H., Norikawa, Y., Hromadko, L., Rodriguez-Pereira, J., Man, O., ... & Macak, J. M. (2024). Can electrodeposited Ti replace rolled Ti as substrate for the growth of anodic TiO_2 nanotube layers?. *Electrochimica Acta*, 143877.
7. Paulose, M., Prakasam, H. E., Varghese, O. K., Peng, L., Popat, K. C., Mor, G. K., ... & Grimes, C. A. (2007). TiO2 nanotube arrays of 1000 μm length by anodization of titanium foil: phenol red diffusion. *The Journal of Physical Chemistry C*, *111*(41), 14992-14997.
8. Macak, J. M., Hildebrand, H., Marten-Jahns, U., & Schmuki, P. (2008). Mechanistic aspects and growth of large diameter self-organized TiO2 nanotubes. *Journal of Electroanalytical Chemistry*, *621*(2), 254-266.
9. Lee, H. C., Zhang, L. F., Lin, J. L., Chin, Y. L., & Sun, T. P. (2013). Development of anodic titania nanotubes for application in high sensitivity amperometric glucose and uric acid biosensors. *Sensors*, *13*(10), 14161-14174.
10. Chakraborty, A. "Samriti; Ruzimuradov, O.; Gupta, RK; Cho, J.; Prakash, J. TiO_2 nanoflower photocatalysts: Synthesis, modifications and applications in wastewater treatment for removal of emerging organic pollutants." *Environ. Res* 212 (2022): 113550.
11. Lu, J., Wei, G., Yu, Y., Zhao, X., & Dai, Y. (2017). Enhanced corrosion resistance of TA2 titanium via anodic oxidation in mixed acid system. *Int. J. Electrochem. Sci*, *12*, 2763-2776
12. Hreo H.S., Holi A.M., Al-Zahrani A.A. Anodic Synthesis of Highly Ordered TiO2 Nanotube Arrays: Role of Electrolyte Composition on the Structural, Morphological, Optical, and Photoelectrochemical Properties. 2017. – T. 16. – P. 2351-2369
13. Pasikhani J.V., Gilani N., Pirbazari A.E. The effect of the anodization voltage on the geometrical characteristics and photocatalytic activity of TiO_2 nanotube arrays //Nano-Structures & Nano-Objects. – 2016. – T. 8. – P. 7-14.
14. Pang, Y. L., Lim, S., Ong, H. C., & Chong, W. T. (2014). A critical review on the recent progress of synthesizing techniques and fabrication of TiO_2-based nanotubes photocatalysts. *Applied Catalysis A: General*, *481*, 127-142.
15. Tang, D., Wang, Y., Zhao, Y., Yang, Y., Zhang, L., & Mao, X. (2014). Effect of the composition of Ti alloy on the photocatalytic activities of Ti-based oxide nanotube arrays prepared by anodic oxidation. *Applied surface science*, *319*, 181-188.

O‘ZBEKISTON MILLIY UNIVERSITETI XABARLARI, 2024, [3/1/1]
ISSN 2181-7324

FIZIKA
http://journals.nuu.uz
Natural sciences

UDK 001.38:371.80/81.811.1

Fayyozjon AZIMOV,
Shahrisabz davlat pedagogika instituti stajyor o‘qituvchisi
E-mail:fayyozjonazimov@gmail.com
Orcid: 0009-0007-6823-6916

Qarshi muhandislik-iqtisodiyot instituti “Umumtexnika fanlari” kafedrasi dotsenti I.Ismailov taqrizi asosida

ESP PROJECT FOR CIVIL ENGINEERING

Annotation

English for Specific Purposes (ESP) is an approach to language teaching and learning that meets the specific needs of learners within the particular field. The students of the ESP study the language for particular reasons (Viana, et.al, 2019). The chosen ESP context for this project is Civil Engineering. A study has been conducted according to following concepts. Firstly, needs analysis about participants has been done with the usage of quizzes and interviews. Then a task has been developed based on the needs of the learners and these tasks have been analyzed whether they work effectively or not throughout the research to develop appropriate methods and tasks for ESP students.

Key words: qualitative method, quantitative method, target situation analysis, present situation analysis, problem based learning, case study.

ПРОЕКТ ESP ДЛЯ ГРАЖДАНСКОГО ИНЖЕНЕРНОГО СТРОИТЕЛЬСТВА

Аннотация

Английский язык для специальных целей (ESP) – это подход к обучению и изучению языка, который удовлетворяет конкретные потребности учащихся в определенной области. Студенты ESP изучают язык по особым причинам (Виана и др., 2019). Выбранный контекст ESP для этого проекта - гражданское строительство. Исследование было проведено согласно следующим концепциям. Во-первых, был проведен анализ потребностей участников с использованием викторин и интервью. Затем было разработано задание на основе потребностей учащихся, и эти задания были проанализированы на предмет их эффективности в течение исследования для разработки соответствующих методов и заданий для студентов ESP.

Ключевые слова: качественный метод, количественный метод, анализ целевой ситуации, анализ текущей ситуации, обучение на основе проблем, кейс-стади.

QURILISH MUHANDISLIGI UCHUN ESP LOYIHASI

Annotatsiya

Maxsus maqsadlar uchun ingliz tili (ESP) bu til o‘rgatish va o‘rganishga bo’lgan yondashuv bo‘lib, u muayyan sohadagi o‘quvchilarning tildagi o‘z sohasiga xos ehtiyojlarini qondiradi. ESP talabalari ma'lum sabablarga ko'ra tilni o'rganishadi (Viana, va boshqalar, 2019). Ushbu loyiha uchun tanlangan ESP mavzusi - Qurilish muhandisligi. Tadqiqot quyida kelgan usullar bo'yicha o'tkazildi. Birinchidan, viktorina va intervyulardan foydalangan holda ishtirokchilarning Ingliz tiliga bo'lgan bilim ko’nikmasi tahlili o'tkazildi. O’tkazilgan ushbu tahlil asosida vazifa ishlab chiqildi. Bu vazifa orqali ESP talabalariga mos uslub va davomiy vazifalar ishlab chiqish uchun tadqiqot o’tkazildi. O’tkazilgan tadqiqot davomida yuzaga kelgan natijalar samaradorligi tahlil qilindi.

Kalit so'zlar: sifat metodi, miqdoriy usul, maqsadli vaziyat tahlili, hozirgi vaziyat tahlili, muammoli ta'lim, keys tadqiqoti.

Introduction. The growing processes of globalization in the world are having a profound impact on all aspects of the political, socio-economic and cultural life of mankind[1]. The only constant in the working life of a civil engineer is that they never have typical days. They face different challenges every day and have to solve problems to meet the specific requirements of the project they are focused on. Civil engineers may work on the same project for several years and then move on. For example, they may be working on a long-term project to plan a new housing development, and once completed, they may move on to developing a new highway system in another city or country. Many projects are very complex and require collaboration with other civil engineers and other specialties. Teamwork is a big part of this profession, as a large number of people usually have to work together to achieve large-scale actions.

At first step, an unstructured interview (qualitative method) has been taken from these learners to know background information about them to identify valid tasks and it must be known that whether they are pre-service or in service in their field (Serafini, Lake, Long, 2015). After that questionarie and structured interview have been conducted for quantitative approach. *Target situation analysis* and *present situation analysis* have been done with the help of abovementioned methods. *Target situation analysis* addresses the “needs” wheareas the *present situation analysis* includes personal information about the learners (background their names and living areas, culture and nationality, background knowledge) and teaching environment (available resources) (Flowerdew, 2013). Available resources have been taken into account for curriculum development as the target situation is essential to develop it (Chan, 2018). It is important to note that not only learner’s present situation and weaknesses were considered but also the “wants” of the learners were considered for needs analysis as it can be used as a main tool to motivate the learners towards the topic (Chan, 2018).

Participants: The learners for this study have come from different areas of Uzbekistan. Their age is between 23 and 28. Their number is 14. This group has been organized by the authority to develop civil engineering in the country. They all graduate students and work in this field. They are required to have one month course in order to develop their skills. The main reason of studying English is to get some more information and exchange program with foreign specialists on this field. They have studied English at their bachelor’s degree so they have basic information. However, they should learn more to interact with foreign experts of civil engineering.

All the learners of this group are good at working at the computer and they can work various programs to create projects. When it comes to social background, their nationality is Uzbek. Ten of them can speak Russian as a foreign language. There are only two female learners as this job is not common among women in Uzbekistan.

Literature review. Woodrow (2018) provides various examples for ESP course in his book. One of these examples named *English for cross-cultural nursing by Susan Bosher* has been chosen in order to use for this ESP project. There are number of reasons of choosing this model. First of all, it contains the aim of the course and gives information about the learners and the length of the course. Moreover, needs analysis and the results of it are clarified. According to Serafini, Lake, Long (2015), interviews, observations, questionnaires and document analysis have been used to provide the detailed information about the needs of students. When it comes to methodological approach, the strategies of reading skills, communication skills and the usage of medical terminology have been considered in this model. Course materials and extra reading materials for development are provided.

1.Approach to ESP Course Design (Method)

Problem based learning (PBL) and *Case Study approach* have been used. Wood & Head (2004, as cited in Woodrow, 2018), mentions that PBL should be in following cycle:

- Warm up activity
- PBL activity
- Reflection and evaluation activity

Warm up activity:

A picture of the construction was shown to the learners. Students discussed about this construction. The discussion part covered following questions:

- What kind of construction is this?
- What elements they can see?

PBL activity:

- Students were divided into groups and then they analyzed the problem that the shown picture had. They had to find the failure and the possible solution with discussing each other and look additional materials to provide extra information.

Reflection and evaluation activity:

- Students reflected their discussion with the help of presentation and evaluate each other’s opinion

The second approach was the **Case study,** a description of problem or situation (Woodrow, 2018).

Task:

- Selected topic: Burj Khalifa construction
- Students analyzed the project’s challenges and innovations.
- They wrote a report summarizing its technical aspects

Results. Both PBL and Case Study approaches are the same as they both focus on finding a solution to the problem. What is more, these approaches are student centered rather than teacher centered classes (Woodrow, 2018). However, Woodrow (2018), notes that PBL focus on one solution to the problem while number of solutions can be given for a case study. Looking at the PBL activities, students found a failure and gave solution for it but in the Case study task, they found various challenges and innovations. To sum up, these approaches highly increased students’ critical thinking abilities on the target field. What is more, learning centered approach was achieved with the help of choice of learning resources by students (Woodrow, 2018). This motivated students to be more active during lessons because of their interests.

Conclusion. Based on the learner’s needs and objectives abovementioned resources and methods have been used. Woodrow (2018) gave number of course designs for ESP project. All of them show us how to conduct the process of ESP and for selected ESP course examples a sample by Susan Bosher has been chosen. The main reason of choosing this material is that it focuses on specific vocabulary with nursing-related topics and the usage of following activities: Change-of-shift reports, telephone reports and documentation skills. For needs analysis, the authors Serafini, Lake, Long (2015) and Flowerdew (2013) gave brilliant information about the approaches in their articles. They helped us how to find out the needs and the wants of the learners with dividing two specific analyses (target situation analysis and present situation analysis). The job that they do is based on presenting the project so group discussions have been done throughout the lesson to exchange information. In group discussions, the usage of speaking skills about how to solve problems and how to create new projects for civil engineering have been taken into account for this project.

The selected participants, representing different regions of Uzbekistan, are well-suited for this ESP project. Their diverse backgrounds, proficiency in working with computers, and prior English language education at the bachelor's level provide a foundation for effective learning. The emphasis on group discussions and the consideration of learners' "wants" alongside their present situation and weaknesses contribute to motivation and engagement.

The project's outcomes, as highlighted in the results section, indicate the success of both PBL and Case Study approaches in fostering critical thinking and a learning-centered environment. The comparison between the two approaches demonstrates the nuanced differences in solution-focused PBL and the exploration of multiple aspects in a Case Study.

REFERENCE

1. Ergasheva Yu. A., Eralov A. J. Difficult aspects of tourism development in Uzbekistan. Spectrum Journal of Innovation, Reforms and Development. Volume 02, May, 2022. ISSN (E): 2751-1731. www.sjird.journalspark.org
2. Bocanegra-Valle, A. (2010). Evaluating and designing materials for the ESP classroom. In M. F. Ruiz-Garrido, J. C. Palmer, & I. Fortanet- Gómez (Eds.), *English for professional and academic purposes* (pp.141–165). Brill.

3. Chan, C. S. (2018). Proposing and illustrating a research-informed approach to curriculum development for specific topics in business English. *English for Specific Purposes*, 52, 27-46
4. Flowerdew, L. (2013). Needs analysis and curriculum development in ESP. In B. Paltridge & S. Starfield (Eds.), *The Handbook of English for specific purposes* (pp. 325–346). Wiley-Blackwell. https://doi.org/10.1002/9781118339855.ch17
5. O'SULLIVAN, B. (2012). Assessment issues in languages for specific purposes. *The Modern Language Journal*, 96(s1), 71-88. https://doi.org/10.1111/j.1540-4781.2012.01298.x
6. Serafini, E. J., Lake, J. B., & Long, M. H. (2015). Needs analysis for specialized learner populations: Essential methodological improvements. *English for Specific Purposes*, 40, 11-26. https://doi.org/10.1016/j.esp.2015.05.002
7. Viana, V., Bocorny, A., & Sarmentoa, S. (2019). *Teaching English for specific purposes*. TESOL Press.
8. Woodrow, L. (2018). *Introducing course design in English for specific purposes*. Routledge.

O‘ZBEKISTON MILLIY UNIVERSITETI XABARLARI, 2024, [3/1/1]
ISSN 2181-7324

FIZIKA
http://journals.nuu.uz
Natural sciences

UDK: 530.12:531.51

Husan ALIBEKOV,
Master student at National University of Uzbekistan,
E-mail :alibekov@astrin.uz
Vakhid KHAMIDOV,
Associate Professor at Tashkent University of Information Technologies, (PhD),
Maksud UMARALIYEV,
Junior researcher at Institute of Fundamental and Applied Research, National Research University TIIAME,

Ulug’bek nomidagi Astronomiya instituti, f.-m.f.d A.Abdujabbarov taqrizi asosida

PRESENTING A NOVEL APPROACH FOR COMPARING AND ANALYZING THE PHASE OF NEUTRINO OSCILLATIONS IN DIFFERENT CURVED SPACETIMES

Annotation

This paper introduces a classical approach to studying neutrino oscillations in curved spacetime, focusing on the existence of neutrino mass. It explores transition probabilities and predicts oscillations across different spacetime contexts by considering fluctuations in neutrino mass. Neutrinos are treated as classical particles following geodesic paths, particularly around massive objects like black holes and neutron stars. The investigation covers various spacetime models, including Schwarzschild, Kerr, and Kerr-like spacetimes, as well as complex non-separable domains like the γ-metric and Hartle-Thorne metric. Canonical phase formulas for neutrinos are derived, emphasizing their interaction with gravitational backgrounds. In summary, this research contributes to our understanding of curved spacetime and the cosmos by examining neutrino oscillations within this classical framework.

Keywords: Neutrino oscillation, Canonical phase, Curved spacetime

ПРЕДСТАВЛЕНИЕ НОВОГО ПОДХОДА ДЛЯ СРАВНЕНИЯ И АНАЛИЗА ФАЗЫ НЕЙТРИННЫХ КОЛЕБАНИЙ В РАЗЛИЧНЫХ ИСКРИВЕННЫХ ПРОСТРАНСТВАХ-ВРЕМЕНИ

Аннотация

В данной статье представлен классический подход к изучению нейтринных осцилляций в искривленном пространстве-времени, фокусирующийся на существовании массы нейтрино. Он исследует вероятности перехода и предсказывает колебания в различных контекстах пространства-времени, учитывая флуктуации массы нейтрино. Нейтрино рассматриваются как классические частицы, движущиеся по геодезическим путям, особенно вокруг массивных объектов, таких как черные дыры и нейтронные звезды. Исследование охватывает различные модели пространства-времени, включая пространство-время Шварцшильда, Керра и Керра, а также сложные неразделимые области, такие как γ-метрика и метрика Хартла-Торна. Выведены канонические фазовые формулы для нейтрино, подчеркивающие их взаимодействие с гравитационным фоном. Таким образом, это исследование способствует нашему пониманию искривленного пространства-времени и космоса, исследуя нейтринные колебания в рамках этой классической структуры.

Ключевые слова: осцилляции нейтрино, каноническая фаза, искривленное пространство-время.

TURLI EGRILANGAN FAZOLARDAGI NEYTRINOTLARNING TEBRANISH FAZALARINI TAQQOSLASHVA TAHLIL QILISH UCHUN YANGI USULNI TAQDIM ETISH

Annotatsiya

Ushbu maqola neytrino massasining mavjudligiga e'tibor qaratib, egri fazoda neytrino tebranishlarini o'rganishga klassik yondashuvni taqdim etadi. U o'tish ehtimolini o'rganadi va neytrino massasidagi tebranishlarni hisobga olgan holda turli fazo-vaqt kontekstlarida tebranishlarni bashorat qiladi. Neytrinolar geodezik yo'llar bo'ylab, ayniqsa qora tuynuklar va neytron yulduzlari kabi massiv ob'ektlar atrofida klassik zarralar sifatida ko'rib chiqiladi. Tekshiruv turli fazoviy vaqt modellarini, shu jumladan Shvartsshild, Kerr va Kerrga o'xshash fazo vaqtlarini, shuningdek, g-metrik va Xartl-Torn metrikasi kabi murakkab ajratilmaydigan domenlarni qamrab oladi. Neytrinolar uchun kanonik faza formulalari olingan bo'lib, ularning tortishish fonlari bilan o'zaro ta'sirini ta'kidlaydi. Xulosa qilib aytganda, ushbu tadqiqot ushbu klassik doirada neytrino tebranishlarini o'rganish orqali egri fazo va kosmosni tushunishimizga yordam beradi.

Introduction. Neutrino oscillation is a phenomenon witnessed in the field of neutrino physics, in which neutrinos transform from one flavor to another during their journey through space. This oscillation arises due to the mixing of three distinct neutrino flavors: electron neutrino (v_e), muon neutrino (v_μ), and tau neutrino (v_τ). The concept of neutrino oscillation was initially proposed by Pontecorvo (1968) [1]. It implies that neutrinos possess a mass, contrary to the previous belief that their mass was zero. The experimental confirmation of neutrino oscillation became possible through various notable endeavors such as the Super-Kamiokande experiment [2, 3], the Sudbury Neutrino Observatory (SNO) experiment [4], and the MINOS experiment [5, 6]. These experiments observed the disappearance and reappearance of different neutrino types as they traversed the Earth's atmosphere or encountered matter. The groundbreaking discovery of neutrino oscillation has been acknowledged with prestigious accolades, including the 2015 Nobel Prize in Physics, which recognized the contributions of Takaaki Kajita and Arthur B. McDonald to the Super-Kamiokande and SNO experiments, respectively.

The structure of the article is as follows: Section 2 provides a concise overview of neutrino oscillation in both flat and curved spacetimes. In Section 3, we present the calculation of the canonical phase for neutrino oscillations using separable equations within curved spacetime. Section 4 focuses on the calculation of the canonical phase for neutrino oscillations in spacetimes where non-separable equations of motion are involved. Finally, in Section 5, we provide a summary of our findings and offer comments on the results. Throughout the paper, we adopt the signature for the line element and utilize geometric units, setting $G = c = \hbar = 1$.

2. Comprehensive analysis of neutrino oscillation

Neutrinos are generated and observed in distinct flavor eigenstates, represented by $|v_\alpha\rangle$, where the flavor eigenstates are linear combinations of mass eigenstates denoted as $|v_i\rangle$. Therefore, a flavor eigenstate can be expressed in terms of mass eigenstates as follows:[6,7]

$$|v_\alpha\rangle = \sum_i \quad U_{\alpha i}|v_i\rangle$$

where, U represents the unitary matrix for neutrino flavor mixing, where α denotes the flavors (e, μ, τ), and i represents the mass eigenstates $(1,2,3)$. In the context of a curved spacetime, a neutrino wave-function can be influenced by contributions from multiple geodesics connecting the neutrino source and the detector. Consequently, when considering all possible paths, the propagation of a neutrino flavor state from the source S to the detector D, located at r_S and r_D respectively, can be expressed as follows:[5,12]

$$|v_\alpha(t_D, r_D)\rangle = \sum_i \quad e^{-i\Phi_i(r_D, r_S)} U_{\alpha i}|v_i(t_S, r_S)\rangle$$

where $\Phi_i(r_D, r_S)$ is the covariant phase of neutrino. The neutrino flavour transition probability from initial produced α flavor at the detection points is obtained as [12,15]

$$P_{\alpha\beta} = \left|\langle v_\beta | v_\alpha(t_B, x_B)\rangle\right|^2 = \sum_{i,j} \quad U_{\beta i} U_{\beta j} U_{\alpha j} U_{\alpha i} e^{-i\Delta\Phi_{ij}}$$

Moreover, in the scenario of a two-flavor system, the probability of a neutrino transitioning from the initial flavor e to the flavor μ is expressed as [13,19]

$$P_{\alpha\beta} = sin^2\, 2\Theta sin^2\left(\frac{\Delta\Phi_{ij}}{2}\right)$$

where Θ mixing angle and $\Delta\Phi_{ij} = \Phi_i - \Phi_j$ is difference of canonical phases. Finally, the generalized covariant phase is defined as [18]

$$\Phi_i = \int_{r_D}^{r_S} \quad p_\mu^{(i)} dx^\mu = -m_i \int_{r_D}^{r_S} \quad ds$$

Here, $p_\mu^{(i)}$ represents the canonical conjugate momentum to the coordinate x^μ for the i-th neutrino mass, defined as $p_\mu^{(i)} = m_i g_{\mu\nu} \dot{x}^\nu$. In this equation, $\dot{x}^\mu$ corresponds to the four-velocity of the particle, normalized as $\dot{x}_\mu \dot{x}^\mu = -1$, indicating that $p_\mu p^\mu = -m^2$. In the context of a flat spacetime, the phase can be derived as illustrated in [8]

$$\Phi_i = E_i(t_S - t_D) - p_i \cdot (x_S - x_D) \simeq (E_i - |p_i|)|x_S - x_D|,$$

In the scenario of a relativistic neutrino, under the condition $m_i \ll E_i$, the discrepancy between energy and momentum can be approximated as $E_i - |p_i| = E_i - \sqrt{E_i^2 - m_i^2} \simeq m_i^2/(2E_i)$. Consequently, the variation of the covariant phase in a flat spacetime can be expressed as

$$\Delta\Phi_{ij} = \frac{\Delta m_{ij}^2}{2E_0}|x_S - x_D|, \Delta m_{ij}^2 = m_i^2 - m_j^2$$

where, E_0 represents the mean energy of the relativistic neutrinos generated at the source.

3. Separable equation of motion

The expression of the Hamilton-Jacobi equation for a particle with mass is given by

$$g^{\alpha\beta} \frac{\partial S}{\partial x^\alpha} \frac{\partial S}{\partial x^\beta} = -m^2$$

where, m denotes the mass of the particle. By utilizing the definition of four-momentum as $p_\alpha = \partial S/\partial x^\alpha$, equation (8) can be restated as:

$$p_\alpha p^\alpha = -m^2$$

3.1. In Schwarzschild spacetime

In this section, we will explore the derivation of the canonical phase in the Schwarzschild spacetime, which represents the external solution of a black hole with mass M. The metric for this spacetime is given by $s^2 = -f(r)dt^2 + f$, where $f(r) = 1 - 2M/r$. As a result of the symmetry of the system, certain quantities, namely, energy and angular momentum, are conserved and can be denoted as $p_t = \text{const}$ and $p_\phi = \text{const}$. Ultimately, in the backdrop of the Schwarzschild spacetime, the equation of motion (9) can be separated as follows:

$$p_r = \frac{1}{f(r)}\sqrt{E^2 - f(r)\left(m^2 + \frac{K}{r^2}\right)},$$

$$p_\theta = \sqrt{K - \frac{L^2}{sin^2\,\theta}},$$

$$p_\phi = L$$

$$p_t = -E$$

In this context, E, L, and K represent the constants of motion associated with energy, angular momentum, and Carter's separation constant, respectively. By employing the definition of four-momentum as $p^{\alpha} = m\dot{x}^{\alpha}$, we can derive the following expression:

$$m\dot{r} = \sqrt{E^2 - f(r)\left(m^2 + \frac{K}{r^2}\right)},$$

$$m\dot{\theta} = \frac{1}{r^2}\sqrt{K - \frac{L^2}{sin^2\theta}},$$

$$m\dot{\phi} = \frac{L}{r^2 sin^2\theta},$$

$$m\dot{t} = \frac{E}{f(r)}.$$

In the case of radial oscillation, where $\theta = \pi/2$, the neutrino's angular momentum is zero, i.e., $K_i = L_i^2 = 0$.

In the regime of weak field approximation, the disparity in the canonical phase can be calculated as follows: as

$$\Delta\Phi_{ij} = \frac{\Delta m_{ij}^2}{E_0}(r_S - r_D)\left[1 + \frac{m_i^2 + m_j^2}{2E_0^2}\left(1 - \frac{R_s}{r_S - r_D} log\frac{r_S}{r_D}\right)\right]$$

3.2. In Kerr spacetimes

Next, we examine the canonical phase within an axially symmetric spacetime, specifically considering the Kerr spacetime described by the following line element:

$$ds^2 = \frac{-\Delta}{\Sigma}(dt - asin^2\theta d\phi)^2 + \frac{\Sigma}{\Delta}dr^2 + \Sigma d\theta^2 + \frac{sin^2\theta}{\Sigma}[(r^2 + a^2)d\phi - adt]^2,$$

Here, $\Delta = r^2 - 2Mr + a^2$ and $\Sigma = r^2 + a^2 cos^2\theta$, where M represents the mass and a denotes the spin of the black hole. In the Kerr spacetime, the equation of motion (9) in the Hamiltonian-Jacobi form is expressed as:

$$\Delta p_r^2 + p_\theta^2 - \frac{[(r^2 + a^2)E - aL]^2}{\Delta} + \left(\frac{L}{sin\,\theta} - aEsin\,\theta\right)^2 + m^2r^2 + m^2a^2cos^2\theta = 0,$$

It is worth noting that the canonical phase for a neutrino in a Kerr-like spacetime is also determined by equation (30). In the equatorial plane of the Kerr black hole, the expression can be obtained as follows:

$$\Phi_i = \int_{r_D}^{r_S} \frac{-m_i^2 dr}{\sqrt{\left[E_i - \frac{a(L_i - aE_i)}{r^2}\right]^2 - \frac{\Delta}{r^2}\left[m_i^2 + \frac{(L_i - aE_i)^2}{r^2}\right]}},$$

4. Inseparable equation of motion

The applicability of variable separation in the equation of motion is not universally valid for all spacetimes, which makes deriving the canonical phase for a neutrino in such spacetimes challenging. However, in these situations, an alternative approach can be utilized by expressing equation (5) in the following manner:

$$\Phi_i = -m_i\int_{r_D}^{r_S} ds = -m_i\int_{r_D}^{r_S} \frac{1}{\dot{r}}dr$$

This implies that it is sufficient to derive the equation for radial motion with respect to a specific angle θ_0. Our attention is directed towards certain spacetimes where variable separation is not feasible.

4.1. The γ-metric

Next, we will examine the canonical phase in the γ-metric. In Erez-Rosen coordinates, the spacetime is described by the line element:

$$ds^2 = -f^{\gamma}dt^2 + f^{\gamma^2-\gamma}g^{1-\gamma^2}\left(\frac{dr^2}{f} + r^2d\theta^2\right) + f^{1-\gamma}r^2sin^2\theta d\phi^2,$$

with

$$f = 1 - \frac{2M}{\gamma r}, g = 1 - \frac{2M}{\gamma r} + \frac{M^2sin^2\theta}{\gamma^2r^2}.$$

where, M represents the mass of the central object, and γ denotes the deformation of the spacetime. We can express the canonical phase for a neutrino as follows:

$$\Phi_i = -\int_{r_D}^{r_S} \frac{m_i^2\sqrt{-g_{tt}g_{rr}}dr}{\sqrt{g_{tt}m_i^2 + \left(E_i^2 + \frac{g_{tt}}{g_{\phi\phi}}L_i^2\right)}}.$$

In the equatorial plane ($\theta = \pi/2$)

$$\Phi_i = -\int_{r_D}^{r_S} \frac{m_i^2}{\sqrt{E_i^2 - \frac{f^{2\gamma-1}}{r^2}L_i^2 - f^{\gamma}m_i^2}}dr.$$

where $b = L_i/E_i$ is impact parameter.

The Hartle-Thorne spacetime. Let us now focus on the canonical phase for a neutrino in the Hartle-Thorne spacetime, which is described by the metric given in reference [24]. When considering the equatorial plane ($\theta = \pi/2$), the expression for the phase can be simplified as follows:

$$\Phi_i = -m_i^2 \int_{r_D}^{r_S} \frac{\sqrt{1-\frac{2M}{r}-\frac{4J^2}{r^4}}}{\sqrt{E_i^2\left(1-\frac{2M}{r}\right)^2-\left(m_i^2+\frac{rL_i^2}{4J}\right)\left[\frac{2J^2}{r^2}\left(1-\frac{2M}{r}\right)^2+\left(1-\frac{2M}{r}\right)\right]+\frac{8E_iL_iJ}{r}\left(1-\frac{2M}{r}\right)}} dr$$

Key Findings and Future Perspectives: Our study delves into the classical approach to understand vacuum neutrino oscillations in curved spacetime. We investigate transition probabilities, focusing on mass oscillations, and offer a comprehensive roadmap for predicting neutrino behavior in diverse curved spacetime scenarios.

We calculate neutrino phase transitions in various spacetimes under general relativity, including Schwarzschild and Kerr spacetimes, revealing separable equations of motion for neutrinos in both static and rotating scenarios. We also extend our analysis to the Kerr-like Johannsen metric.

In summary, our research provides valuable insights into the dynamics of neutrino oscillations in curved spacetime, offering a theoretical foundation for future studies. We anticipate that our findings will enrich our understanding of the cosmos and neutrino physics as the exploration of the universe continues.

REFERENCES

1. B. Pontecorvo, Neutrino Experiments and the Problem of Conservation of Leptonic Charge, Soviet Journal of Experimental and Theoretical Physics 26 (1968) 984.
2. Y. Fukuda, et al., Evidence for Oscillation of Atmospheric Neutrinos, Phys. Rev. Lett. 81 (1998) 1562-1567.
3. Y. Fukuda, et al., Measurement of a small atmospheric v_μ/v_e ratio, Phys. Lett. B 433 (1998) 9-18
4. Q. R. Ahmad, et al., Direct Evidence for Neutrino Flavor Transformation from Neutral-Current Interactions in the Sudbury Neutrino Observatory, Phys. Rev. Lett. 89 (2002) 011301.
5. D. G. Michael, et al., Observation of Muon Neutrino Disappearance with the MINOS Detectors in the NuMI Neutrino Beam, Phys. Rev. Lett. 97 (2006) 191801.
6. P. Adamson, et al., First observations of separated atmospheric v_μ and v_μ^-events in the MINOS detector, Phys. Rev. D 73 (2006) 072002.
7. Z. Maki, M. Nakagawa, S. Sakata, Remarks on the Unified Model of Elementary Particles, Progress of Theoretical Physics 28 (1962) 870 − 880.
8. G. Bertone, D. Hooper, J. Silk, Particle dark matter: evidence, candidates and constraints, Physics Reports 405 (2005) 279-390.
9. S. Abe, et al., Precision measurement of neutrino oscillation parameters with kamland, Phys. Rev. Lett. 100 (2008) 221803.
10. H. Swami, K. Lochan, K. M. Patel, Signature of neutrino mass hierarchy in gravitational lensing, Phys. Rev. D 102 (2020) 024043.
11. H. Duan, G. M. Fuller, Y.-Z. Qian, Collective Neutrino Oscillations, Annual Review of Nuclear and Particle Science 60 (2010) 569-594
12. C. Y. Cardall, G. M. Fuller, Neutrino oscillations in curved spacetime: A heuristic treatment, prd 55 (1997) 7960-7966.

O‘ZBEKISTON MILLIY UNIVERSITETI XABARLARI, 2024, [3/1/1]
ISSN 2181-7324

FIZIKA
http://journals.nuu.uz
Natural sciences

UDK: 530.12:531.51

Akbar DAVLATALIEV,
Master at National University of Uzbekistan,
E-mail: akbar@astrin.uz
Asalkhon ALIMOVA,
PhD student at Tashkent State Technical University,
Vakhid KHAMIDOV,
Associate Professor at Tashkent University of Information Technologies, (PhD),
E-mail:vkhamidov@tuit.uz

Ulug'bek Institute of Astronomy, PhD based on the review by A.A. Abdujabbarov

GRAVITATIONAL LENSING IN STAROBINSKY-BEL-ROBINSON GRAVITY IN NON-UNIFORM PLASMA

Annotation

This study explores optical properties of a rotating black hole in Starobinsky-Bel-Robinson (SBR) gravity, with an extra parameter β, surrounded by non-uniform plasma characterized by plasma parameter k. β significantly affects photon motion near the black hole, diminishing with distance. Photon deflection angle decreases with increasing k. β presence results in a maximum deflection angle near the black hole, diminishing as photons move away. Photon sphere radius is notably influenced by β and black hole's spin, with less dependence on plasma parameter.

Keywords: General Theory of Relativity (GR), Black holes, Shadows Gravitational waves, Quantum gravity.

ГРАВИТАЦИОННОЕ ЛИНЗИРОВАНИЕ В ГРАВИТАЦИИ СТАРОБИНСКОГО-БЕЛЯ-РОБИНСОНА В НЕОДНОРОДНОЙ ПЛАЗМЕ

Аннотация

В этом исследовании изучаются оптические свойства вращающейся черной дыры в гравитации Старобинского-Бел-Робинсона (SBR) с дополнительным параметром β, окруженной неоднородной плазмой, характеризуемой параметром плазмы k. β существенно влияет на движение фотонов вблизи черной дыры, уменьшаясь с расстоянием. Угол отклонения фотона уменьшается с увеличением k. Наличие β приводит к максимальному углу отклонения вблизи черной дыры, уменьшающемуся по мере удаления фотонов. На радиус фотонной сферы существенное влияние оказывают β и спин черной дыры, в меньшей степени зависящие от параметров плазмы.

Ключевые слова: Общая теория относительности (ОТО),Черные дыры, Тени Гравитационные волны, Квантовая гравитация, Модифицированные теории гравитации.

STAROBINSKIY-BEL-ROBINSONDAGI GRAVITASYONLI LEZONLASH NONIFORMAL PLAZMADAGI GRAVITATSIYA

Annotatsiya

Ushbu tadqiqot Starobinskiy-Bel-Robinson (SBR) tortishish kuchida, qo'shimcha b parametrga ega va plazma parametri k bilan tavsiflangan bir xil bo'lmagan plazma bilan o'ralgan aylanadigan qora tuynukning optik xususiyatlarini o'rganadi. Natijalar shuni ko'rsatadiki, b ning foton harakatiga ta'siri qora tuynuk yaqinida sezilarli, lekin masofa bilan kamayadi. Fotonlarning burilish burchagi k ortishi bilan izchil ravishda kamayadi. b ning mavjudligi qora tuynuk yaqinida maksimal burilish burchagiga olib keladi, fotonlar uzoqlashganda kamayadi. Foton sfera radiusi b va qora tuynukning spinidan sezilarli darajada ta'sirlanadi, plazma parametriga nisbatan zaifroq bog'liqlik.

Kalit so'zlar: Umumiy nisbiylik nazariyasi (UNN), Qora tuynuklar, soyalar, Gravitatsion to'lqinlar, Kvant tortishish kuchi

Introduction. Recently, Starobinsky-Bel-Robinson (SBR) gravity has emerged, augmenting the Einstein-Hilbert action with quadratic terms involving the Ricci scalar and Bel-Robinson tensor[1]. Inspired by eleven-dimensional low-energy M-theory, SBR gravity's four-dimensional formulation includes a stringy coupling parameter, β (β>0), determined through M-theory compactification. Our investigation highlights β's pronounced influence near Kerr-like black hole horizons, diminishing with distance [2]. The study on Kerr-like black holes within SBR gravity is structured as follows: Section II presents a concise overview of the spacetime metric, Section III explores photon motion and gravitational lensing phenomena, and Section IV summarizes findings and conclusions.

Kerr-type black hole in starobinsky-bel-robinson gravity. The SBR gravity action introduces two additional parameters, m and β, compared to the Hilbert action in General Relativity (GR), and has been utilized to formulate new physical models, including inflation [3]. Static Schwarzschildtype black hole solutions have been derived within SBR gravity, with the parameter m determined by solving the equation of motion [2]. It has been shown that thermodynamic quantities are modified by the stringy gravity parameter β. Consequently, the line element of this non-rotating solution is expressed as:

$$ds^2 = -f(r)dt^2 + \frac{1}{f(r)}dr^2 + r^2 d\Omega^2$$

where the metric function $f(r)$ is

$$f(r) = 1 - \frac{r_s}{r} + \beta\left(\frac{4\sqrt{2}\pi r_s}{r^3}\right)^3\left(\frac{108r - 97r_s}{5r}\right)$$

where $r_s = 2M$, with M representing the total mass parameter. Subsequently, the Newman-Janis algorithm [4, 5] can be employed for certain modified gravity models incorporating additional parameters to derive rotating black hole solutions. Specifically, in the SBR gravity, the metric line element in Boyer-Lindquist coordinates is given by:

$$ds^2 = -\left(\frac{\Delta - a^2\sin^2\theta}{\Sigma}\right)dt^2 + \frac{\Sigma}{\Delta}dr^2 + \Sigma d\theta^2$$
$$-2a\sin^2\theta\left(2 - \frac{\Delta - a^2\sin^2\theta}{\Sigma}\right)dtd\phi$$
$$+\sin^2\theta\left[\Sigma + a^2\sin^2\theta\left(2 - \frac{\Delta - a^2\sin^2\theta}{\Sigma}\right)d\phi^2,\right.$$

where new parameters

$$\Delta = a^2 + r^2\left[1 - \frac{2M}{r} + \frac{1024\pi^3\beta M^3(108r - 194M)}{5r^{10}}\right],$$

And $\Sigma = r^2 + a^2\cos^2\theta$

Two parameters, a and β, are introduced, where well-known black hole solutions are recovered: when $a = 0$, nonrotating black holes are obtained, and when $\beta = 0$, the Kerr solution is recovered with the delta function.

Photon geodesics and gravitational lensing. In this section, we explore the motion of photons and the phenomenon of gravitational lensing in the spacetime of a Kerr-type black hole within the framework of SBR gravity.

A. Photon motion. It is commonly assumed that the environment surrounding a black hole consists of a non-magnetized cold plasma. The electron plasma frequency can be expressed in terms of the electron density in the plasma, denoted as $N(x)$, as indicated in reference [6]:

$$w_p(x)^2 = \frac{4\pi e^2 N(x)}{m_e}$$

where x denotes spatial coordinates, e and m_e represent the charge and mass of the electron, respectively. In axially symmetric spacetime, it can be expressed as follows [7]:

$$w_p^2 = \frac{h(r) + g(\theta)}{\Sigma}$$

where $h(r)$ and $g(\theta)$ are the radial and angular functions, respectively. One possible choice is to set $g(\theta)$ to zero and $h(r) = k\sqrt{r}$ [7]. Given our interest in the motion of photons in the equatorial plane where $\theta = \pi/2$, the electron plasma frequency simplifies to:

$$w_p(r)^2 = \frac{k}{r^{3/2}}$$

The plasma refraction index is defined as the ratio of the plasma frequency ω_p to the photon frequency ω measured by a proper observer. It is expressed as:

$$n^2 = 1 - \frac{w_p^2}{w^2}$$

Accordingly, the trajectory of the photon is constrained to the equatorial plane. Hereafter, we adopt the convention $M = 1$ and impose the condition $\theta = \pi/2$ for the equatorial plane in our calculations.

The Hamiltonian governing the propagation of photons in curved spacetime in the presence of plasma is given by the following expression:

$$H(x^i, p_i) = \frac{1}{2}\left[g^{ik}p_i p_k + w_p^2\right] = 0$$

Using the Hamiltonian differential equations

$$\frac{dx^i}{d\tau} = \frac{\partial H}{\partial p_i},\ \frac{dp_i}{d\tau} = -\frac{\partial H}{\partial x^i}$$

additionally, two constants of motion arise from the stationarity and axial symmetry of the spacetime, which correspond to the energy and angular momentum of the particle:

$$E = -p_t = w, L = p_\phi$$

one can obtain $\dot{t}, \dot{r}, \dot{\phi}$ as

$$\frac{dt}{d\tau} = \frac{Eg_{\phi\phi} - Lg_{t\phi}}{g_{t\phi}^2 - g_{tt}g_{\phi\phi}}$$
$$\frac{d\phi}{d\tau} = -\frac{Eg_{t\phi} + Lg_{tt}}{g_{t\phi}^2 - g_{tt}g_{\phi\phi}}$$
$$V(r) = \frac{dr}{d\tau} = \sqrt{\frac{E^2 g_{\phi\phi} - \left(g_{t\phi}^2 - g_{tt}g_{\phi\phi}\right)\omega_p^2 + 2Lg_{t\phi} + L^2 g_{tt}}{g_{rr}\left(g_{t\phi}^2 - g_{tt}g_{\phi\phi}\right)}}.$$

B. Gravitational lensing. The study examines gravitational lensing by a Kerr-type black hole in SBR gravity, focusing on photon trajectories. It explores how the radius of closest approach (r_0) varies with the impact parameter (b=L/E), considering the β parameter's influence. Larger β values result in smaller b for the same r_0, especially near the black hole. Faster black hole rotation increases r_0 for photons at the same b due to stronger gravitational fields. This effect is significant for small b and decreases with increasing b. The influence of plasma, represented by the k parameter, is shown to have a nearly linear relationship with $r_0$within the chosen parameter range, where higher k values lead to higher r_0.

The relationship between the radial coordinate r and the angle ϕ can be expressed as follows:

$$\frac{d\phi}{dr} = -\sqrt{\frac{g_{rr}}{g_{t\phi}^2 - g_{tt}g_{\phi\phi}}} \frac{g_{t\phi} + bg_{tt}}{\sqrt{g_{\phi\phi} - \left(g_{t\phi}^2 - g_{tt}g_{\phi\phi}\right)\frac{k}{r^{\frac{3}{2}}} + 2bg_{t\phi} + b^2 g_{tt}}}$$

At the equatorial plane ($\theta = \pi/2$), the relationship between the radial coordinate r and the angle ϕ is derived from the second and third equations in (17).

Subsequently, the deflection angle can be expressed as:

$$\alpha = 2\int_{r_0}^{\infty} \frac{d\phi}{dr} dr - \pi$$

The integral is numerically evaluated and depicted in Figure 1. In the first plot, increasing the black hole's spin reduces the deflection angle of photons. Similar behavior is observed in the second plot, showing the dependence on the plasma parameter k. The last plot illustrates that the deflection angle's dependence on the radius of closest approach is non-monotonic, peaking near the black hole. This behavior arises from the additional term introduced in the spacetime metric involving β. Across all plots, the deflection angle decreases with an increase in the parameter β. Solutions from specific conditions reveal the dependence of the photon sphere on spacetime parameters, crucial for understanding black hole shadows in SBR gravity. Different line styles represent different plasma parameter values (k=0 solid, k=0.5 dashed, k=1 dotted). Figure 2 demonstrates that increasing β reduces the photon sphere radius, especially for lower black hole spins.

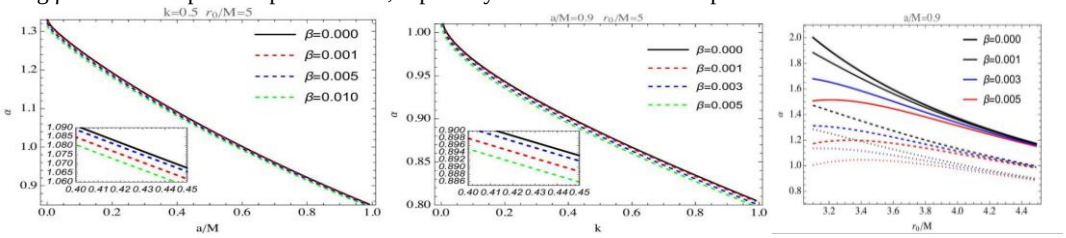

FIG. 1: Dependence of the deflection angle of photons on r_0, β, a, and k parameters.

Specifically, for a non-rotating case ($a = 0$) and in the absence of plasma around the black hole ($k = 0$), it can be observed that the radius of the photon sphere decreases sharply around $\beta \sim 0.001$, with the lines becoming smoother for higher values of the spin parameter. Moving to the second panel of Figure 2, it is evident that an increase in the plasma parameter k results in a nearly linear change in the photon sphere, while an increase in the spin of the black hole shifts the lines downwards. From the last plot, it can be observed that the rate of change of the photon sphere radius with respect to the change in the plasma parameter strongly depends on the parameter β. Specifically, larger values of β lead to smaller rates of change.

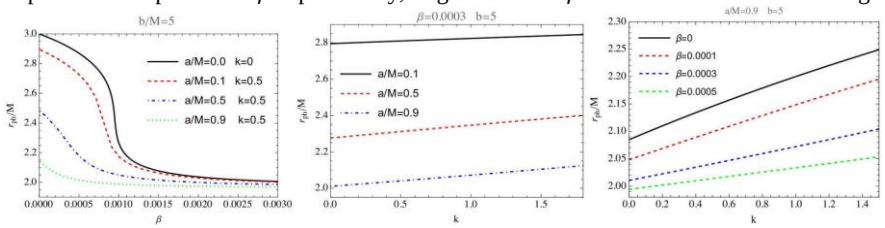

FIG. 2: The photon sphere radius is depicted as a function of spacetime and plasma parameters.

Conclusion. In our study, we explored the optical properties of a rotating black hole in SBR gravity, introducing an additional parameter β. We investigated how non-uniform plasma, quantified by parameter k, affects photon motion. Our analysis showed that β significantly impacts the radius of closest approach of photons near the black hole, but this effect diminishes with distance. Both increasing black hole spin and plasma parameter decrease the deflection angle of photons. Interestingly, the relationship between deflection angle and closest approach radius exhibits non-monotonic behavior with β, peaking before decreasing. Our findings emphasize the strong influence of β on photon behavior and spacetime in SBR gravity, revealing complex gravitational interactions. Notably, around β~0.001, there's a significant radius decrease, especially in non-rotating (a=0) and plasma-free (k=0) scenarios. We also observed a linear relationship between the photon sphere and plasma parameter k, with higher spin values causing downward shifts in the lines.

REFERENCES

1. S. V. Ketov, Universe 8 (2022), 10.3390/universe8070351.
2. R. Campos Delgado and S. V. Ketov, Phys. Lett. B 838, 137690 (2023), arXiv:2209.01574 [gr-qc] .
3. S. V. Ketov, E. O. Pozdeeva, and S. Y. Vernov, JCAP 12, 032 (2022), arXiv:2211.01546 [gr-qc] .
4. S. P. Drake and P. Szekeres, Gen. Rel. Grav. 32, 445 (2000), arXiv:gr-qc/9807001 .
5. H. Erbin, Universe 3, 19 (2017), arXiv:1701.00037 [gr-qc] .
6. G. S. Bisnovatyi-Kogan and O. Y. Tsupko, Monthly Notices of the Royal Astronomical Society 404, 1790 (2010).
7. J. Badía and E. F. Eiroa, Phys. Rev. D 104, 084055 (2021), arXiv:2106.07601 [gr-qc] .

O‘ZBEKISTON MILLIY UNIVERSITETI XABARLARI, 2024, [3/1/1]
ISSN 2181-7324

FIZIKA
http://journals.nuu.uz
Natural sciences

УДК: 512.548

Акимбек ДАВЛАТБЕКОВ,
Доцент Института предпринимательства и педагогики имени Денова, к.ф-м.н
E-mail: akimbekd@mail.ru
Mavjuda SOBIROVA,
Доцент Института предпринимательства и педагогики имени Денова, PhD
E-mail: mavjudasobirova79@gmail.com

На основе обзора профессора А.Табарова

UMUMLASHTIRILGAN CHIZIQLI KVAZIGURUHLAR VA *i*-KVAZIGURUHLAR HAQIDA

Annotatsiya

Kvaziguruhlar nazariyasining vazifalaridan biri, shuningdek, boshqa sotsiativ bo‘lmagan algebraik tizimlar nazariyasi kvaziguruhlarning morfizmlarini o‘rganish va tavsiflashdir. Gomomorfizm, endomorfizm, avtomorfizm, avtotopiya va umumlashtirilgan chiziqli kvaziguruhlarning endotopiyasi [1-3] ishlarda batafsil o‘rganilgan. Ushbu maqolada asosan umumlashtirilgan chiziqli kvaziguruhlarning gomomorfizmi va ularning parastroflari (chap kvaziguruh va ularning parastroflari, o‘ng kvaziguruh va ularning parastroflari, birinchi (ikkinchi) turdagi aralash chiziqli kvaziguruh va ularning parastroflari) o‘rganilgan. Bundan tashqari, birinchi (ikkinchi) turdagi aralash tipdagi kvaziguruhlar va ularning parastroflarining i-kvaziguruhlar bilan bog‘lanishi topilgan.

Kalit so‘zlar: o‘ngdagi chiziqli kvaziguruhlar, chapdagi chiziqli kvaziguruhlar, parastrof, endotopiya, birinchi tur aralash tipdagi kvaziguruh, ikkinchi tur aralash tipdagi kvaziguruh, avtomorfizm, antiavtomorfizm, i-kvaziguruh, endomorfizm.

ОБ ОБОБЩЕННЫХ ЛИНЕЙНЫХ КВАЗИГРУПП И *i*-КВАЗИГРУПП

Аннотация

Одной из задач теории квазигрупп, как и теория других не социативных алгебраических систем, является изучение и описание морфизмов квазигрупп. В работах [1-3] подробно изучаются гомоморфизм, эндоморфизм, автоморфизм, автотопия, эндотопия обобщенных линейных квазигрупп. В данной статье в основном изучаются гомоморфизм обобщенных линейных квазигрупп и их парастофы (линейная слева квазигруппа и их парастрофы, линейная справа квазигруппа и их парастрофы, квазигруппа смешанного типа линейности первого (второго) рода и их парастрофы). Кроме того, найдены связь квазигруппы смешанного типа линейности первого (второго) рода и их парастрофов с i-квазигруппами.

Ключевые слова: линейные справа квазигруппы, линейные слева квазигруппы, парастроф эндотопия, квазигруппа смешанного типа первого рода, квазигруппа смешанного типа второго рода, автоморфизм, антиавтоморфизм, i-квазигруппа, эндоморфизм.

ON GENERALIZED LINEAR QUASIGROUPS AND i-QUASIGROUPS

Annotation

One of the problems of the theory of quasigroups, like the theory of other algebraic systems, is the study and description of morphisms of quasigroups. In works [1-3] homomorphisms, edomorphisms, automorphisms autotopy endotopy of generalized linear quasigroups are studied in detail. This article mainly studies homomorphisms of generalized linear quasigroups and their parastrophes (left linear quasigroup and their parastrophes, right linear quasigroup and their parastrophes, quasigroups of mixed linearity type of the first (second) kind and their parastrophes). In addition, a connection was found between quasigroups of mixed type linearity of the first (second) kind and their parastrophes with i-quasigroups.

Key words: right linear quasigroups, left linear quasigroups, parastroph, endotopy, mixed quasigroup of the first kind, mixed quasigroup of the secont kind, automorvism, antiautomorphism, i-quasigroup, endomorphism.

Введение. Изучения автоморфизмов и гомоморфизмов квазигрупп была начато уже в самых первых работах по теории квазигрупп. Так, в 1944 году А.Албert [4] доказал, что группа автоморфизмов квазигруппы изоморфна подгруппе группы автоморфизмов каждой из групп: $LM, RM, M,$ то есть групп, порожденных соответственно левыми, правыми, левыми и правыми трансляциями квазигруппы. Как обычно, $L_a x = a \cdot x -$ левая, а $R_a x = x \cdot a -$ правая трансляция квазигруппы относительно элемента a.

Теория линейных квазигрупп занимает одно из центральных мест в общей теории квазигрупп. В классе квазигрупп, изотопных группам, большой интерес представляют линейные квазигруппы. Согласно В.Д. Белоусову, [5] квазигруппа $(Q,\cdot)$ называется линейной над группой $(Q,+)$, если $(Q,\cdot)$ имеет вид

$$A(x,y) = \varphi x + \psi y + c, \tag{1}$$

где $\varphi, \psi \in Aut\ (Q,+)$, $c -$ фиксированный элемент из множества Q.

Г.Б.Белявская и А.Х. Табаров в работах [6-7] ввели другие классы квазигрупп алинейные и их обобщения, а именно, алинейные слева (справа), квазигруппы смешанного типа линейности и другие. Названные эти классы такое связаны с уравновешенными и неуравновешенными тождествами.

Квазигруппа $(Q,\cdot)$ называется линейной слева (справа) над группой $(Q,+)$, если $(Q,\cdot)$ имеет вид $A(x,y)=\varphi x+\beta y+c$ $(A(x,y)=\alpha x+\psi y+c)$, где β (соответственно α) – подстановка множества Q, $\varphi\in Aut(Q,+)$ $(\psi\in Aut(Q,+))$ [8].

Квазигруппа $(Q,\cdot)$ называется квазигруппой смешнаного типа линейности I рода или II рода, если $(Q,\cdot)$ имеет вид $A(x,y)=\varphi x+\overline{\psi}\,y+c$ соответственно $A(x,y)=\overline{\varphi}\,x+\psi y+c$, где $\varphi,\psi\in Aut\,(Q,+)$, $\overline{\varphi},\overline{\psi}-$ антиавтоморфизм группы $(Q,+)$ [8].

Пусть $(Q,\cdot)-$ произвольная квазигруппа. Тройка отображений $(\alpha,\ \beta,\ \gamma)$ называется эндотопией квазигруппы $(Q,\cdot)$, если $\gamma(x\cdot y)=\alpha x\cdot\beta y.$ В случае, если $\gamma=\alpha=\beta$, то $\gamma-$ называется эндоморфизмом квазигруппы $(Q,\cdot)$.

С каждой квазигруппой $(Q,\ \cdot)$ связаны пять квазигруппы, которых называют парастрофами квазигруппы $(Q,\ \cdot)$ [9]. Поясним этот факт. Если обозначим квазигрупповую operatsiю квазигруппы $(Q,\ \cdot)$ через A, то operatsiю A можно ассоциировать следующими квазигрупповыми operatsiями:

$A(x_1,x_2)=x_3\Leftrightarrow A(12)(x_2,x_1)=x_3\Leftrightarrow A(13)(x_3,x_2)=x_1\Leftrightarrow A(23)(x_1,x_3)=x_2$

$\Leftrightarrow A(132)(x_2,x_3)=x_1\Leftrightarrow A(123)(x_3,x_1)=x_2$. Это означает, что $A_\sigma(x_{\sigma1},x_{\sigma2})=x_{\sigma3}$

$\Leftrightarrow A(x_1,x_2)=x_3$, где $\sigma\in S=\{e,\ (12),\ (13),\ (23),(123),\ (132)\}$ - группа подстановок третьего порядка. Таким образом, для квазигруппы $(Q,\ A)$ существуют следующие пять парастрофов: $(Q,\ A^{-1})$, $(Q,\ {}^{-1}A)$, $(Q,\ {}^{-1}(A^{-1}))$, $(Q,\ ({}^{-1}A)^{-1})$ и $(Q,\ A^*)$, где $A^*(x,y)=A(y,x)$.

Очевидно, что если $(Q,\ \cdot)$ квазигруппа смешанного типа первого рода $A(x,y)=\varphi x+\overline{\psi}\,y+c$, то существуют следующие пять парастрофов: $A^*(x,y)=\varphi y+\overline{\psi}\,x+c$, ${}^{-1}A(x,y)=\varphi^{-1}x+J\varphi^{-1}\overline{\psi}\,y+J\varphi^{-1}c$,

$A^{-1}(x,y)=J\overline{\psi}^{-1}\varphi x+\overline{\psi}^{-1}y+J\overline{\psi}^{-1}c$ $(({}^{-1}A)^{-1})(x,y)=\varphi^{-1}y+J\varphi^{-1}\overline{\psi}\,x+J\varphi^{-1}c$

$({}^{-1}(A^{-1}))(x,y)=J\overline{\psi}^{-1}\varphi y+\overline{\psi}^{-1}x+J\overline{\psi}^{-1}c$.

Аналогично если $(Q,\ \cdot)$ квазигруппа смешанного типа второго рода $A(x,y)=\overline{\varphi}\,x+\psi y+c$, то существуют следующие пять парастрофы: $A^*(x,y)=\overline{\varphi}\,y+\psi x+c$, ${}^{-1}A(x,y)=\overline{\varphi}^{-1}x+J\overline{\varphi}^{-1}\psi y+J\overline{\varphi}^{-1}c$,

$A^{-1}(x,y)=J\psi^{-1}\overline{\varphi}\,x+\psi^{-1}y+J\psi^{-1}c$ $(({}^{-1}A)^{-1})(x,y)=\overline{\varphi}^{-1}y+J\overline{\varphi}^{-1}\psi x+J\overline{\varphi}^{-1}c$

$({}^{-1}(A^{-1}))(x,y)=J\psi^{-1}\overline{\varphi}\,y+\psi^{-1}x+J\psi^{-1}c$.

Теорема 1. Пусть (Q,A) *линейная справа* квазигрупп вида $A(x,y)=\alpha x+\psi y+c$ и (Q,A^{-1}) $A^{-1}(x,y)=J\psi^{-1}\alpha x+\psi^{-1}y+J\psi^{-1}c$, её парастроф. Подстановка α такие что $\alpha0=0$, и $c=0$, где $0-$ нулевой элемент группы $(Q,+)$. $\gamma-$ произвольный эндоморфизм группы $(Q,+)$. Тогда γ является гомоморфизмом квазигруппы (Q,A) и (Q,A^{-1}) тогда и только тогда, когда выполняются следующие условия $\gamma\alpha=J\psi^{-1}\alpha\gamma$, $\gamma\psi=\psi^{-1}\gamma$, $c=J\psi^{-1}c$.

Доказательство. Пусть (Q,A) *линейная справа* квазигрупп вида $A(x,y)=\alpha x+\psi y+c$ и (Q,A^{-1}) $A^{-1}(x,y)=J\psi^{-1}\alpha x+\psi^{-1}y+J\psi^{-1}c$, её парастроф и $\alpha0=0$ и $c=0$. Далее γ эндоморфизм группы $(Q,+)$ и $\gamma(x\cdot y)=\gamma x\circ\gamma y.$ Тогда

$$\gamma(\alpha x+\psi y+c)=J\psi^{-1}\alpha\gamma x+\psi^{-1}\gamma y+J\psi^{-1}c,$$
$$\gamma(\gamma\alpha x+\tilde{R}_c\,\gamma\psi y)=J\psi^{-1}\alpha\gamma x+\tilde{R}_{J\psi^{-1}c}\psi^{-1}\gamma y,$$
$$\gamma\alpha x+\gamma\tilde{R}_c\psi y=J\psi^{-1}\alpha\gamma x+\tilde{R}_{J\psi^{-1}c}\psi^{-1}\gamma y,$$

Положим: $x=0,c=0.$ Тогда

$\gamma\alpha 0+\gamma\tilde{R}_0\psi y = J\psi^{-1}\alpha\gamma 0+\tilde{R}_{J\psi^{-1}0}\psi^{-1}\gamma y,$ учитывая, что $\alpha 0=0,\ \gamma 0=0,\ J\psi^{-1}0=0,$ $\tilde{R}_{J\psi^{-1}0}\Rightarrow\tilde{R}_{J0}\Rightarrow\tilde{R}_0\Rightarrow\tilde{R}_0=0$ получим: $\gamma\alpha 0+\gamma\psi y = J\psi^{-1}\alpha\gamma 0+\psi^{-1}\gamma y,$ оказано, что если квазигруппы (Q,A) и (Q,A^{-1}) изотопны $\gamma(x\circ y)=\alpha x\cdot\beta y,$ то их полугруппы эндотопий спряжены

$$\gamma\psi y=\psi^{-1}\gamma y \text{ или } \gamma\psi=\psi^{-1}\gamma.$$

Теперь, если положим $y=0,$ то $\gamma\alpha x+\gamma\psi 0=J\psi^{-1}\alpha\gamma x+\psi^{-1}\gamma 0,$

$$\gamma\alpha x=J\psi^{-1}\alpha\gamma x \text{ или } \gamma\alpha=J\psi^{-1}\alpha\gamma.$$

С другой стороны можно доказать:

$$\gamma(x\cdot y)=\gamma\left(\alpha x+\tilde{R}_c\ \psi y\right)=\gamma\alpha x+\gamma\tilde{R}_c\ \psi y=J\psi^{-1}\alpha\gamma x+\tilde{R}_{J\psi^{-1}c}\psi^{-1}\gamma y=\gamma x\circ\gamma y,$$

то есть $\gamma(x\cdot y)=\gamma x\circ\gamma y.$

Следствие 1. Пусть (Q,A) *линейные справа* квазигрупп вида $A(x,y)=\alpha x+\psi y+c$ и $(Q,{}^{-1}A)$ ${}^{-1}A(x,y)=\alpha^{-1}x+J\alpha^{-1}\psi y+J\alpha^{-1}c,$ её парастроф. Подстановка α такие что $\alpha 0=0,$ и $c=0,$ где $0-$ нулевой элемент группы $(Q,+).$ $\gamma-$ произвольный эндоморфизм группы $(Q,+).$ Тогда γ является гомоморфизмом квазигруппы (Q,A) и (Q,A^{-1}) тогда и только тогда, когда выполняются следующие условия

$$\gamma\alpha=\alpha^{-1}\gamma,\ \gamma\psi=J\alpha^{-1}\psi\gamma,\ c=J\alpha^{-1}c.$$

Следствие 2. Пусть (Q,A) линейные слева квазигрупп вида $A(x,y)=\varphi x+\beta y+c$ и $(Q,{}^{-1}A)$ ${}^{-1}A(x,y)=\varphi^{-1}x+J\varphi^{-1}\beta y+J\varphi^{-1}c,$ её парастроф. Подстановка β такие что $\beta 0=0,$ и $c=0,$ где $0-$ нулевой элемент группы $(Q,+).$ $\gamma-$ произвольный эндоморфизм группы $(Q,+).$ Тогда γ является гомоморфизмом квазигруппы (Q,A) и (Q,A^{-1}) тогда и только тогда, когда выполняются следующие условия

$$\gamma\varphi=\varphi^{-1}\gamma,\ \gamma\beta=J\varphi^{-1}\beta\gamma,\ c=J\varphi^{-1}c.$$

Следствие 3. Пусть (Q,A) линейные слева квазигрупп вида $A(x,y)=\varphi x+\beta y+c$ и (Q,A^{-1}) $A^{-1}(x,y)=J\beta^{-1}\varphi x+\beta^{-1}y+J\beta^{-1}c,$ её парастроф.

Подстановка β такие что $\beta 0=0,$ и $c=0,$ где $0-$нулевой элемент группы $(Q,+).$ $\gamma-$ произвольный эндоморфизм группы $(Q,+).$ Тогда γ является гомоморфизмом квазигруппы (Q,A) и (Q,A^{-1}) тогда и только тогда, когда выполняются следующие условия

$$\gamma\varphi=J\beta^{-1}\varphi\gamma,\ \gamma\beta=\beta^{-1}\gamma,\ c=J\beta^{-1}c.$$

Теорема 2. Пусть (Q,A) линейная слева и (Q,A^{-1}) её парастроф над группе $(Q,+)$ квазигруппа: $A(x,y)=\varphi x+\beta y+c$ и $A^{-1}(x,y)=J\beta^{-1}\varphi x+\beta^{-1}y+J\beta^{-1}c.$ То отображение $\gamma-$ гомоморфизм квазигруппы (Q,A) в $(Q,A^{-1}):\ \gamma(x\cdot y)=\gamma x\circ\gamma y.$ Тогда гомоморфизм γ можно представит в виде

$$\gamma=J\beta^{-1}\varphi\gamma\theta\varphi^{-1}=\tilde{R}_{J\beta^{-1}c}\beta^{-1}\gamma\theta\tilde{R}_c^{-1}\beta^{-1}=\tilde{L}_a\tilde{R}_b\theta.$$

Доказательство. Пусть (Q,A) и (Q,A^{-1}) гомоморфизм $\gamma(x\cdot y)=\gamma x\circ\gamma y.$

Тогда

$$\gamma(\varphi x+\beta y+c)=J\beta^{-1}\varphi x+\beta^{-1}y+J\beta^{-1}c,$$
$$\gamma(\varphi x+\tilde{R}_c\,\beta y)=J\beta^{-1}\varphi\gamma x+\tilde{R}_{J\beta^{-1}c}\beta^{-1}\gamma y,$$
$$\gamma(x+y)=J\beta^{-1}\varphi\gamma\ \varphi^{-1}x+\tilde{R}_{J\beta^{-1}c}\beta^{-1}\gamma\tilde{R}_c^{-1}\beta^{-1}y,$$

то есть, $\left(J\beta^{-1}\varphi\gamma\ \varphi^{-1},\ \tilde{R}_{J\beta^{-1}c}\beta^{-1}\gamma\tilde{R}_c^{-1}\beta,\gamma\right)$ эндотопия группы $(Q,+).$ Из [10] ясно, что, любая эндотония группы $(Q,+)$ имеет вид: $T=\left(\tilde{L}_a\theta,\tilde{R}_b\theta,\tilde{L}_a\tilde{R}_b\theta\right),$ следовательно $\tilde{L}_a\theta=J\beta^{-1}\varphi\gamma\ \varphi^{-1},$ $\tilde{R}_b\theta=\tilde{R}_{J\beta^{-1}c}\beta^{-1}\gamma\tilde{R}_c^{-1}\beta^{-1},\ \tilde{L}_a\tilde{R}_b\theta=\gamma.$ Откуда

$$\gamma = J\beta^{-1}\varphi\gamma\theta\varphi^{-1} = \tilde{R}_{J\beta^{-1}c}\beta^{-1}\gamma\theta\tilde{R}_c^{-1}\beta^{-1} = \tilde{L}_a\tilde{R}_b\theta.$$

Следствие 4. Пусть (Q,A) линейная слева и $(Q,{}^{-1}A)$ её парастроф над группой $(Q,+)$ квазигруппа: $A(x,y)=\varphi x+\beta y+c$ и ${}^{-1}A(x,y)=\varphi^{-1}x+J\varphi^{-1}\beta y+J\varphi^{-1}c$. То отображение $\gamma-$ гомоморфизм квазигруппы (Q,A) в $(Q,{}^{-1}A)$: $\gamma(x\cdot y)=\gamma x\circ\gamma y$. Тогда гомоморфизм γ можно представит в виде

$$\gamma = \varphi^{-1}\gamma\theta\varphi^{-1} = \tilde{R}_{J\varphi^{-1}c}J\varphi^{-1}\beta\gamma\theta\tilde{R}_c^{-1}\beta^{-1} = \tilde{L}_a\tilde{R}_b\theta.$$

Аналогично если можно доказать для линейной справа квазигруппой и их парастрофов и квазигруппами смешанного типа первого (второго) рода и их парастрофы.

Следствие 5. Пусть (Q,A) *линейная справа* квазигруппа вида $A(x,y)=\alpha x+\psi y+c$ и $(Q,{}^{-1}A)$: ${}^{-1}A(x,y)=\alpha^{-1}x+J\alpha^{-1}\psi y+J\alpha^{-1}c$, $\left((Q,A^{-1}):A^{-1}(x,y)=J\psi^{-1}\alpha x+\psi^{-1}y+J\psi^{-1}c\right)$ её парастрофы. То отображение $\gamma-$ гомоморфизм квазигруппы (Q,A) в $(Q,{}^{-1}A)$ и $\left((Q,A)\,в\,(Q,A^{-1})\right)$ $\gamma(x\cdot y)=\gamma x\circ\gamma y$. Тогда гомоморфизм γ можно представит в виде

$$\gamma = \alpha^{-1}\gamma\theta\alpha^{-1} = \tilde{R}_{J\alpha^{-1}c}J\alpha^{-1}\psi\gamma\theta\tilde{R}_c^{-1}\psi^{-1} = \tilde{L}_a\tilde{R}_b\theta\ ,$$

Следствие 6. Пусть (Q,A) *линейная справа* квазигрупп вида $A(x,y)=\alpha x+\psi y+c$ и $(Q,{}^{-1}A)$: ${}^{-1}A(x,y)=\alpha^{-1}x+J\alpha^{-1}\psi y+J\alpha^{-1}c$, $\left((Q,A^{-1}):A^{-1}(x,y)=J\psi^{-1}\alpha x+\psi^{-1}y+J\psi^{-1}c\right)$ её парастрофы. То отображение $\gamma-$ гомоморфизм квазигруппы (Q,A) в $(Q,{}^{-1}A)$ и $\left((Q,A)\,в\,(Q,A^{-1})\right)$ $\gamma(x\cdot y)=\gamma x\circ\gamma y$. Тогда гомоморфизм γ можно представит в виде

$$\gamma = \alpha^{-1}\gamma\theta\alpha^{-1} = \tilde{R}_{J\alpha^{-1}c}J\alpha^{-1}\psi\gamma\theta\tilde{R}_c^{-1}\psi^{-1} = \tilde{L}_a\tilde{R}_b\theta\ ,$$
$$\left(\gamma = J\psi^{-1}\alpha\gamma\theta\alpha^{-1} = \tilde{R}_{J\psi^{-1}c}\psi^{-1}\gamma\theta\tilde{R}_c^{-1}\psi^{-1} = \tilde{L}_a\tilde{R}_b\theta\right).$$

Следствие 7. Пусть (Q,A) *квазигруппа смешанного типа первого рода* $A(x,y)=\varphi x+\overline{\psi}y+c$ и $(Q,{}^{-1}A)$: ${}^{-1}A(x,y)=\varphi^{-1}x+J\varphi^{-1}\overline{\psi}y+J\varphi^{-1}c$, $\left((Q,A^{-1}):A^{-1}(x,y)=J\overline{\psi}^{-1}\varphi x+\overline{\psi}^{-1}y+J\overline{\psi}^{-1}c\right)$ её парастрофы. То отображение $\gamma-$ гомоморфизм квазигруппы (Q,A) в $(Q,{}^{-1}A)$ и $\left((Q,A)\,в\,(Q,A^{-1})\right)$ $\gamma(x\cdot y)=\gamma x\circ\gamma y$. Тогда гомоморфизм γ можно представит в виде

$$\gamma = \varphi^{-1}\gamma\theta\varphi^{-1} = \tilde{R}_{J\varphi^{-1}c}J\varphi^{-1}\overline{\psi}\gamma\theta\tilde{R}_c^{-1}\overline{\psi}^{-1} = \tilde{L}_a\tilde{R}_b\theta\ ,$$
$$\left(\gamma = J\overline{\psi}^{-1}\varphi\gamma\theta\varphi^{-1} = \tilde{R}_{J\overline{\psi}^{-1}c}\overline{\psi}^{-1}\gamma\theta\tilde{R}_c^{-1}\overline{\psi}^{-1} = \tilde{L}_a\tilde{R}_b\theta\right).$$

Следствие 8. Пусть (Q,A) *квазигруппа смешанного типа второго рода* $A(x,y)=\overline{\varphi}x+\psi y+c$ и $(Q,{}^{-1}A)$: ${}^{-1}A(x,y)=\overline{\varphi}^{-1}x+J\overline{\varphi}^{-1}\psi y+J\overline{\varphi}^{-1}c$, $\left((Q,A^{-1}):A^{-1}(x,y)=J\psi^{-1}\overline{\varphi}x+\psi^{-1}y+J\psi^{-1}c\right)$ её парастрофы. То отображение $\gamma-$ гомоморфизм квазигруппы (Q,A) в $(Q,{}^{-1}A)$ и $\left((Q,A)\,в\,(Q,A^{-1})\right)$, $\gamma(x\cdot y)=\gamma x\circ\gamma y$. Тогда гомоморфизм γ можно представит в виде

$$\gamma = \overline{\varphi}^{-1}\gamma\theta\overline{\varphi}^{-1} = \tilde{R}_{J\varphi^{-1}c}J\overline{\varphi}^{-1}\psi\gamma\theta\tilde{R}_c^{-1}\psi^{-1} = \tilde{L}_a\tilde{R}_b\theta\ ,$$
$$\left(\gamma = J\psi^{-1}\overline{\varphi}\gamma\theta\overline{\varphi}^{-1} = \tilde{R}_{J\psi^{-1}c}\psi^{-1}\gamma\theta\tilde{R}_c^{-1}\psi^{-1} = \tilde{L}_a\tilde{R}_b\theta\right).$$

Ввиду того, что доказательство следствий 1-8 почти полностью проверяют доказательство теоремы 1 и 2, поэтому считаем, что нет необходимости для доказательства следствий 1-8.

Определение 3. Квазигруппа $(Q,\cdot)$ называется i-квазигруппой если в $(Q,\cdot)$ удовлетворяет тождеству [5]

$$x\cdot\big((x\cdot y)\cdot z\big)=y\cdot\big((z\cdot x)\cdot x\big),\qquad\forall x,y,z\in Q. \tag{2}$$

Теорема 3. Пусть $(Q,\cdot)$ квазигруппа смешанного типа первого рода $A(x,y)=\varphi x+\overline{\psi}y+c$ или $x\cdot y=\varphi x+\overline{\psi}y+c$, с условием $\overline{\varphi}^{\,2}=\varepsilon$, $\overline{\psi}^{\,4}=\varepsilon$ и $\varphi x+x\in(Q,+),\forall(x)\in Q$. Тогда $(Q,\cdot)$ является i-квазигруппой, если $(Q,\cdot)$ представить в виде

$$x\cdot y=\varphi x+\overline{\psi}^{\,2}y+c, \tag{3}$$

где, $\varphi \in Aut\ (Q,+),\ \ \overline{\psi}-$ антиавтоморфизм группы $(Q,+)$.

Доказательство. Пусть $(Q,\cdot)$ квазигруппа смешанного типа первого рода $x\cdot y=\varphi x+\overline{\psi}^{2,}y+c,$ с условием $\varphi^{2,}=\varepsilon$ и $\overline{\psi}^{2}=\varepsilon$. Из равенство (2) и (3) следует, что

$$\begin{aligned} x\cdot((x\cdot y)\cdot z)&=\varphi x+\overline{\psi}^{2}\left(\varphi\left(\varphi x+\overline{\psi}^{2}y+c\right)+\overline{\psi}^{2}z+c\right)+c=\\ &=\varphi x+\overline{\psi}\,\overline{\psi}\left(\varphi^{2}x+\varphi\overline{\psi}^{2}y+\varphi c+\overline{\psi}^{2}z+c\right)+c=\\ &=\varphi x+\overline{\psi}\left(\overline{\psi}c++\overline{\psi}^{3}z+\overline{\psi}\varphi c+\overline{\psi}\varphi\overline{\psi}^{2}y+\overline{\psi}\varphi^{2}x\right)+c=\\ &=\varphi x+\overline{\psi}^{2}\varphi^{2}x+\overline{\psi}^{2}\varphi\overline{\psi}^{2}y+\overline{\psi}^{2}\varphi c+\overline{\psi}^{4}z+\overline{\psi}^{2}c+c=\\ &=\varphi x+x+\varphi y+\varphi c+z+c+c. \end{aligned} \tag{4}$$

$$\begin{aligned} y\cdot((z\cdot x)\cdot x)&=\varphi y+\overline{\psi}^{2}\left(\varphi\left(\varphi z+\overline{\psi}^{2}x+c\right)+\overline{\psi}^{2}x+c\right)+c=\\ &=\varphi y+\overline{\psi}\,\overline{\psi}\left(\varphi^{2}z+\varphi\overline{\psi}^{2}x+\varphi c+\overline{\psi}^{2}x+c\right)+c=\\ &=\varphi y+\overline{\psi}^{2}\varphi^{2}z+\overline{\psi}^{2}\varphi\overline{\psi}^{2}x+\overline{\psi}^{2}\varphi c+\overline{\psi}^{4}x+c+c=\\ &=\varphi y+z+\varphi x+\varphi c+x+c+c. \end{aligned} \tag{5}$$

Из равенство (4) и (5) следует, что

$$\begin{aligned} \varphi x+x+\varphi y+\varphi c+z+c+c&=\varphi y+z+\varphi x+\varphi c+x+c+c.\\ \varphi x+x+\varphi y+\varphi c+z&=\varphi y+z+\varphi x+\varphi c+x. \end{aligned} \tag{6}$$

Положим, в равенстве (6) $c=0,$ тогда $\varphi x+x+\varphi y+z=\varphi y+z+\varphi x+x.$

В последнем равенстве заменяя y на $\overline{\varphi}^{-1}y$ получим $\varphi x+x+y+z==y+z+\varphi x+x$, то есть в квазигруппа смешанного типа первого рода с условиям $\overline{\varphi}^{2}=\varepsilon$, $\overline{\psi}^{4}=\varepsilon$ и $\varphi x+x\in(Q,+),\forall(x)\in Q.$ выполняется тождество *i*-квазигруппа.

Следствие 9. Пусть $(Q,\cdot)$ квазигруппа смешанного типа второго рода $A(x,y)=\overline{\varphi}x+\psi y+c$ или $x\cdot y=\overline{\varphi}x+\psi y+c,$ с условиям $\overline{\varphi}^{4}=\varepsilon$, $\psi^{2}=\varepsilon$ и $\psi x+x\in(Q,+)$. Тогда $(Q,\cdot)$ является i-квазигруппой, если $(Q,\cdot)$ представить в виде

$$x\cdot y=\overline{\varphi}^{2}x+\psi y+c.$$

Следствие 10. Пусть $(Q,\cdot)$ квазигруппа смешанного типа первого рода $A(x,y)=\varphi x+\overline{\psi}\,y+c$ и $\left(Q,\ A^{-1}\right)\colon A^{-1}(x,y)=J\psi^{-1}\,\overline{\varphi}\,x+\psi^{-1}y+J\psi^{-1}c$ её парастроф. Тогда и только тогда $\left(Q,\ A^{-1}\right)$ является i-квазигруппой, если в $\left(Q,\ A^{-1}\right)$ выполняются следующие условия $\overline{\varphi}^{-2}=\varepsilon$, $\psi^{-2}=\varepsilon,\ \ x+J\,\overline{\varphi}\,x\in(Q,+),$ $\forall(x)\in Q.$

Доказательство следствие 9 и 10 аналогично как доказательство теоремы 3.

ЛИТЕРАТУРА

1. Табаров А.Х. Автотопии и антиавтотопии линейных квазигрупп /А.Х. Табаров // Доклады АН РТ, 2009, том 52, №1, С. 10-16.
2. Табаров А.Х. Гомоморфизмы и эндоморфизмы линейных и алиней-ных квазигрупп /А.Х. Табаров // Дискретная математика, РАН., 2007, том 19, вып.2, с.67-73. (Translation in Discrete Math.Appl.17 (2007), no.3, P. 253-260).
3. Давлатбеков А.А. Об автотопиях, антиавтотопиях линейных (алинейных) квазигрупп и их парастрофов. /А.А. Давлатбеков // Вестник Таджикского natsionalного университета. Серия естественных наук № 2. – с. 152 -162. Душанбе – 2022.
4. Albert A.A. Quasigroups II / A.A. Albert //Trans.Amer.Mats.Soc -1944.-Vol.54.-P.401—409.
5. Белоусов В.Д. Уравновешенные тождества в квазигруппах /В.Д.Белоусов // Мат. сборник, 1966, 70(112): 1. С. 55-97.
6. Белявская Г.Б., Табаров А.Х. Характеристика линейных и алиней-ных квазигрупп /Г.Б.Белявская., А.Х.Табаров// Дискрет-ная математика, РАН, 1992, том 4, вып.2, С. 142-147.
7. Белявская Г.Б., Табаров А.Х. Ядра и центр линейных квазигрупп /Г.Б.Белявская, А.Х. Табаров // Известия АН Республики Молдова. Математика, Кишинев, 1991, №3(6), С. 37-42.
8. Shcherbacov V. Elements of quasigroup theory and applications / V.
9. Shcherbacov RCPress, Boca Raton, 2017 - 768 C.
10. Белоусов В.Д. Основы теории квазигрупп и луп /В.Д.Белоусов-М.: Наука, 1967.- 222. С.
11. Головко И.А. Эндотопии в квазигруппах /И.А. Головко // Резюме докладов 1 Всесоюзного симпозиума по теории квазигрупп и ее приложениям. Сухуми, 1968, С. 14-15.

O‘ZBEKISTON MILLIY UNIVERSITETI XABARLARI, 2024, [3/1/1]
ISSN 2181-7324

FIZIKA
http://journals.nuu.uz
Natural sciences

UDK:535.012

Abduvakhid JUMABAEV,
DSc, professor of Samarkand State University
E-mail: jumabaev2@rambler.ru
Bekzod KHUDAYKULOV,
PhD, associate professor of Samarkand State University
Samariddin ABDUKAYUMOV,
Master student of Samarkand State University
Solihboy MAHAMMADIYEV,
Laboratory assistant of Samarkand State University
Iqboloy NORBUTAYEVA,
Student of Uzbek–Finnish Pedagogical Institute
Kamola KURBANOVA,
Master student of Samarkand State University

Based on the review by Eshonkulov G’, the Dean of the Faculty of Physics, NUUz

THE IMPORTANCE OF INTERMOLECULAR INTERACTIONS IN THE FORMATION OF TYROSINE MOLECULAR COMPLEXES

Аннотатион

The Raman spectra of neat tyrosine were investigated in this work using both experimental and quantum chemical calculations. A potential energy distribution (PED) analysis was carried out to determine the vibrational frequencies of each atom and their interactions with other atoms. Calculations were also used to investigate interaction energies, bond lengths, and vibrational frequencies. This enabled us to learn a lot about weak intermolecular interactions. C=O, N-H, and O-H vibration frequencies were also seen decreasing as the number of molecules increased.
Key words: Tyrosine, Raman, H-bonding, PED analysis.

ЗНАЧЕНИЕ МЕЖМОЛЕКУЛЯРНЫХ ВЗАИМОДЕЙСТВИЙ В ОБРАЗОВАНИИ МОЛЕКУЛЯРНЫХ КОМПЛЕКСОВ ТИРОЗИНА

Аннотация

В данной работе спектры комбинационного рассеяния чистого тирозина исследовались с использованием как экспериментальных, так и квантово-химических расчетов. Анализ распределения потенциальной энергии (PED) был проведен для определения частот колебаний каждого атома и их взаимодействия с другими атомами. Расчеты также использовались для исследования энергий взаимодействия, длин связей, частот колебаний. Это позволило нам многое узнать о слабых межмолекулярных взаимодействиях. Частоты колебаний C=O, N-H и O-H также уменьшались по мере увеличения числа молекул.
Ключевые слова: тирозин, комбинационное рассеяние света, H-связь, PED.

Annotatsiya

Ushbu ishda toza tirozining Raman spektrlari tajriba va kvantokimyoviy hisoblashlar yordamida tahlil qilindi. Har bir atomning hamda atomlarning boshqa atomlar bilan birgalikdagi tebranish chastotalarini tahlil qilish uchun potensial energiya taqsimoti (PED) analizi o‘tkazildi. Shuningdek hisoblashlar yordamida o‘zaro tasir energiyalari, bog‘ uzunliklarinng o‘zgarishi aniqlandi. Bu esa molekulalararo kuchsiz ta'sirlar haqida muhim ma'lumotlar olish imkonini berdi**.** Shuningdek molekulalar soni ortishi bilan C=O, N-H va O-H tebranish chastotalari kamayishi kuzatildi.
Kalit so‘zlar: Tirozin, Raman, H-bog‘lanish, PED analiz.

Introduction. Currently, the research of intermolecular interactions are both theoreticaly and practicaly important [1-5]. The interaction of aromatic rings is one among many noncovalent interactions mentioned in the literature. This is an interaction among strongly electronegative ring centers (π-system), which can also interact with the weakly polarized hydrogen atom in C-H. A π-system can also interact to itself by a π-π stacking interaction [6]. Such bonds also include interactions such as C-H... π, C-H-O, halogen, and other σ-holes. However, such interactions have not been thoroughly explained theoretically at this point [7]. These bonds are important in proteins and biomolecules, crystal engineering, material science, molecule self-assembly, and supramolecular structures, particularly DNA structure [8-11]. Mutual stick interaction joins adenine and temin, which are the fundamental building blocks of DNA [12]. Tyrosine is one of the chemicals participated in such bonding, and tyrosine-(4-hydroxyphenylalanine) is an essential amino acid for all living organisms. Similarly, the human body may obtain terosine, also known as L-terosine, from protein-rich diets (meat, fish, regular meals, and legumes). The substance is often used in sports nutrition because of its potential for reducing tiredness [13]. This substance, like other amino acids, contains many H-bonding sites. In the crystal phase and polar solvents, the carboxyl group (COO^-) of the tyrosine molecule functions as a proton acceptor, whereas the amino group functions as both an acceptor and a donor. Although intermolecular interactions of tyrosine are weak, they play a crucial role in protein structure.

The characteristic vibration and structure of therosin and therosinate have recently been examined using quantum mechanical approaches, specifically the DFT method [14]. Belén H. and others investigated the characteristic vibrations for different therosin and therosinate conformations using Raman spectra and calculations [15]. The optimal geometry, harmonic vibration frequency, IR intensity, and Raman activity were also investigated using the DFT/B3LYP/6-311G(d,p) method [16]. Despite the many experiments and calculations conducted by Abdelali B. and others, analyzing vibrations in the 2600-3600 cm^{-1} region remains a difficulty.

According to the review of the above literature, despite the fact that many scientific studies have been conducted to study the formation mechanisms of weak H-bonded complexes in tyrosine and their manifestations in their spectra, there are many uncertainties and contradictory opinions in the study of weak intermolecular interactions. In this work, experimental and calculated Raman spectra were analyzed. Also, with the help of quantum-chemical calculations, interaction energies, changes in bond lengths, vibration frequencies and PED were analyzed.

Experimental and Computational Details. The Raman spectra of neat tyrosine were obtained using a Renishaw Invia Raman spectrometer. As a dispersion element, this spectral instrument has a 1200 lines/mm diffraction grating. An argon laser with a wavelength of 532 nm and a power of 50 mW was utilized to generate excitation light. The scattered light was recorded using a standard Renishaw CCD camera detector. All experiments were carried out at normal atmospheric pressure and at room temperature. The exposure time is 10 seconds, and the resolution is 0.5 cm^{-1}. The Gaussian 09W program was applied for conducting calculations using the density functional theory (DFT) method [17]. DFT is used to calculate ground state optimization molecule as well as the frequency and intensity of different bands. B3LYP is a useful computational function for medium and high-order molecules. The 6-311+G (2d, p) basis set was used for finding optimal gemetry of molecular structures. The PED (potential energy distributions) analysis was carried out using the VEDA 4.0 (vibrational energy distribution analysis) tool at specific vibration frequencies.

Results and Discussion. In this work, the normal vibration frequencies of the tyrosine molecule have been calculated using methods and compared to experimental results. Tyrosine is a nonlinear molecule with 24 atoms. The formula for 3·N-6 provides 66 fundamental vibrational frequencies. 12 vibration frequencies were found through experiment. Table 1 indicates that the experimentally and theoretically obtained modes of CCN deformation and CCCC torsional vibration frequencies differ around 9%. The other frequencies are around ±5% of the experimental values.

Figure 1 also shows experimental and calculated Raman spectra. The mode formed by mixing the CCC deformation and CCCC torsional vibration frequencies at 431 cm^{-1} has been found as 429 cm^{-1} at calculation, which is precisely suitable with the observed value. The mode consisting of a combination of CC stretching and CCC deformation vibration frequencies corresponding to 630 cm^{-1} is 659 cm^{-1}, which differs from the observed result by 29 cm^{-1}. The HNH at 828 cm^{-1}, which is a combination of torsional NHCC and HCCC vibrational frequencies, is differ by 27 cm^{-1} from the determined value of 855 cm^{-1}. The mode composed of the two CC stretching, HCC and CCC deformation vibration frequencies corresponding to 1179 and 1200 is calculated to correspond to 1198 and 1224 cm^{-1}, differing from the observed value by just 2%.

Table 1. Experimental and calculated frequencies and PED analysis of tyrosine.

(*i*)	Raman	Calcul.	Exp./Calc.	PED tahlil (%)
1		30		CCCC τ (24%), CCCO τ (58%)
2		38		CCCC τ (75%), as CCCO τ (10%)
3		48		as CCN β (15%), CCCC τ (52%)
4		76		CCN β (12%), as CCCC τ (10%), CCCC τ (48%)
5	160	146	1.09	CCN β (29%), CCCC τ (27%)
6		237		CCN β (13%), as HNCC τ (11%), CCNC τ(29%)
7		245		CCN β (24%), as HNCC τ (42%)
8		282		CCN β (43%)
9		302		as CCN β (36%),CCC β (10%), as HNCC τ (34%)
10		317		as HOCC τ (95%)
11		327		CCC β (46%), as HCCC τ (12%)
12		375		CCN β (10%), CCCC τ (16%), as 17%γ (OCCC)
13		423		As CCC β (15%), HCCC τ (13%), CCCC τ (61%)
14	431	429	1.00	CCC β (64%), CCCC τ (10%)
15		469		As CC ν (12%), OCO β (13%), as CCN β (12%)
16		524		CCC β(11%), as HCCC τ(17%), as OCCC τ(17%)
17		553		as CCC β (23%), as HCCC τ (18%), OCCC τ(12%)
18		620		HOCC τ (70%)
19		638		OCO β (37%), HOCC τ (14%)
20	630	659	0.96	as CC ν (11%), as CCC β (73%)
21		726		HCCC τ(14%), as CCCC τ (45%), CCCC τ (11%)
22		767		as OCOC τ (36 %)
23		789		as CC ν (14%), CC ν (13%), as CCC β (12%)
24		798		as CC ν (14%), CCN β (14%), OCOC τ (22%)
25		817		HCCC τ (88%)
26		841		as OC ν (15%), HNCC τ (12%), HCCC τ (26%)
27	828	855	0.97	HNH β (11%), HNCC τ (38%), as HCCC τ (19%)
28		863		OC ν (51%), CCC β (14%)
29		944		HCCC τ (60%)
30		965		HCCC τ (82%), CCCC τ (12%)
31		968		HCC β (11%), HCCC τ (22%), CCNC γ (11%)
32		1024		CC ν (45 %)
33		1033	0.95	as HCC β (19%), CCC β (64%)
34		1102		NC ν (57%)
35		1123		as CC ν(21%), as HCC β (22%), HCC β (19%)
36		1148		OC ν(39%), HOC β (21%), HCN β (16%)
37		1170		as CC ν(11%), as HNC β (15%), HCC β (26%)
38		1191		HOC β (49%), HCC β (50%)
39	1179	1198	0.98	as CC ν(19%), as HCC β (66%)
40	1200	1224	0.98	as CC ν(37%), as HCC β (11%), CCC β (11%)
41		1232		HOC β (12%), HNC β (15%), HCN β (10%)
42		1279		as OC ν(65%), HCC β (13%)
43		1317		HOC β (32%), HCCO τ (12%)
44		1326		as HCCC τ (45%)
45		1348		CC ν(17%), as CC ν(17%), as HCC β (25%)
46		1363		HOC β (11%), as HCC β (28%), as HCCO τ (20%)

47	1326	1371	0.97	as HCC β (23%), HCCO τ (24%)
48		1449		as HNC β (12%), HNC β (29%)
49		1472		CC ν(20%), as HCC β (18%), HCH β (12%)
50		1485		HCH β (67%)
51		1549		CC ν(26%), HCC β (52%), CCC β (12%)
52		1630		CC ν(51%), CCC β (15%)
53		1643		HNH β(73%), HNCC τ (21%)
54		1653		as CC ν(62%), HCC β (18%)
55	1613	1801	0.90	OC ν(83%)
56		3023		CH ν(90%)
57	2931	3062	0.96	CH ν(89%)
58	2967	3081	0.96	CH ν(90%)
59		3146		as CH ν(13%), CH ν(86%)
60		3154		CH ν(94%)
61		3169		CH ν(86%), CH ν(13%)
62	3062	3189	0.96	CH ν(94%)
63		3489		NH ν(99%)
64		3571		as NH ν(99%)
65		3736		OH ν(100%)
66		3827		OH ν(100%)

Abbreviations: **ν** -stretching; **β**-deformasion; **τ**-torsion; **as**-asymmetric.

The HCC mode at 1326 cm^{-1}, formed by the combination of deformation and torsional HCCO vibrational frequencies, is calculated to be 1371 cm^{-1}, which differs by 45 cm^{-1} from the experimental result. In addition, the CO mode corresponding to 1653 cm^{-1} is calculated to be 1613 cm^{-1}, which is 10% different from the experimental measurement. The modes of the CH stretching vibration frequencies corresponding to 2931, 2967, and 3062 cm^{-1} are calculated as 3062, 3081, and 3189 cm^{-1}, respectively, with a 4% difference from the experimental values.

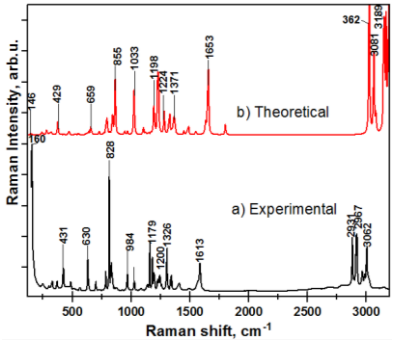

Figure 1. Raman spectra of tyrosine: a) experimental and b) theoretical

Also, calculations were performed on tyrosine molecule aggregates that ranged from monomer to trimer. Figure 2(a) depicts the tyrosine monomer, in which the carbon (C_5, C_8, C_9, and C_{11}), oxygen atoms (O_1, O_2, and O_3), and nitrogen atom (N_4) are negatively charged while the remaining atoms are positively charged. The carbon C_7 atom in the molecule has the highest positive charge (1.30), while the carbon C_5 and C_9 atoms have the most negative charges (-0.69 and -0.66). The dipole moment for tyrosine monomer is 1.47 D (Table 2-3). Figure 2(b) depicts a tyrosine dimer that is bound together by two H-bonds. The first H-bond, O-H···O, connects H_{47} and O_2 atoms and has a bond length of 1.87 Å. The second is a non-classical H-bond between H_{22} and O_{27} in the form of C-H···O with a bond length of 2.47 Å . Dimer formation energy is 0.73 kcal/mol (average H-bond 2.80 kcl/mol), and the dipole moment is 2.50 D. During dimer formation, the charge of the O_2, C_2, C_{13}, and H_{22} atoms in the H-bond changed more than the charge of the other atoms (Table 2). In addition, the bond length between C13-O12 atoms participating in H-bonding increased to most (from 1.370 Å to 1.383 Å). However, the length of the C_{12}-H_{22} bond in the second hydrogen bond has remained unchanged. This means that this bond is a non-classical H-bond that does not follow the classical H-bonding rules. Figure 2(c) depicts a tyrosine trimer that is bound together by five H-bonds.

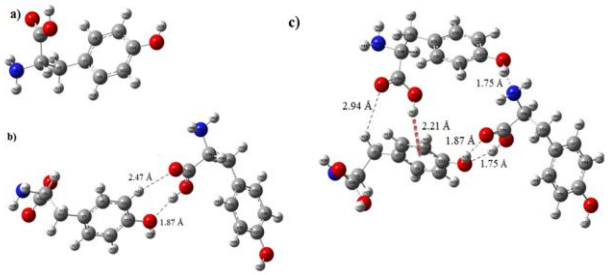

Figure 2. **Aggregations of tyrosine: a) monomer, b) dimer, c) trimer**

The first is a non-classical hydrogen bond between H_{14} and O_{27} in the form of C-H···O with a bond length of 2.94 Å. H_{48} and N_{52} form an O-H···N bond with a length of 1.75 Å. The third and fourth H-bonds are O-H···O, with bond lengths of 1.75 and 1.87 Å, respectively. These bonds are relatively strong. The fifth is a nonclassical interaction between the H^{47} atom and the adjacent to molecule's ring center in the O-H···π form, with a bond length of around 2.21Å. The trimer formation energy is 2.92 kcal/mol (average H-bonding is 10.5 kcal/mol), while the dipole moment is 4.46 D.

Table 2 depicts the frequency shifts of certain vibrational modes with high intensity in monomers, dimers, and trimers. The band corresponding to the C=O stretching vibration in the monomer was 1801 cm^{-1}. In the dimer state, there are two C=O stretching vibrational modes, which correspond to 1800 and 1777 cm^{-1} in the corresponding state, and they are displaced to a lower frequency by 1 and 24 cm^{-1}, respectively, compared to the monomer. In addition, three C=O stretching vibrational modes

(1709, 1716, and 1730 cm^{-1}) were produced in the trimer, but at a lower frequency than the monomer band. This is compatible with the notion of H-bonding, which states that the vibrational bands shift to a lower frequency.

Table 3. Parameters of tyrosine obtained in the calculation results

Structure	C=O stretching frequency, cm^{-1}	N-H symmetrical stretching frequency, cm^{-1}	N-H asymmetric stretching frequency, cm^{-1}	O-H stretching frequency, cm^{-1}	Dipole moment, D	Vibrational energy, kcal/mol	Average H-bond energy, kcal/mol
Monomer	1801	3489	3571	3736 3827	1.47		
Dimer	1777 1800	3487 3490	3569 3572	3527 3736 3824 3828	2.50	5.61	2.80
Trimer	1709 1716 1730	3476 3515 3523	3637 3645 3581	3043 3190 3420 3581 3645 3701	4.46	52.52	10.5

The N-H symmetric stretching vibration band did not change in the dimer state as it did in the monomer, indicating that the atom making this band was not involved in the formation of H-bonds. However, in the trimer state, one band shifted to a lower frequency (3489 cm^{-1} in the monomer and 3476 cm^{-1} in the trimer). Figure 2 shows that one H-bond is formed in the trimer with its help of N-H. The above considerations for symmetric stretching vibrations apply to N-H asymmetric vibrations as well. The monomer's O-H stretching vibration is represented by the frequencies 3736 and 3827 cm^{-1}. The number of these bands in dimers and trimers rose to four and six, respectively.

Conclusion. In the end, the present research investigated the Raman spectra of tyrosine using experiments and quantum chemical calculations. When the vibrational frequencies were analyzed using PED analysis, they showed a good agreement with the experimental frequencies. The atoms involved in non-classical H-bonding do not grow or change the length of bonds, but rather decrease. Non-classical hydrogen bonds are produced from the tyrosine dimer in the form of C-H·O and the trimer in the form of O–H···π. According to the calculations, the C=O, N-H, and O-H vibration bands shift to 92, 13, and 693 cm^{-1}, corresponding to low frequencies, as the number of molecules grows. As a result, the greatest shift can be found in the O-H vibration band.

REFERENCE

1. Kaplan I.G., Intermolecular Interactions: Physical Picture, Computational Methods and Model Potentials.John Wiley Sons, Ltd., 2006.
2. Khodiev, M., Holikulov, U., Jumabaev, A., ISSAOUI, N., Lvovich, L. N., Al-Dossary, O. M., Bousiakoug, L. G.. Solvent effect on the self-association of the 1, 2, 4-triazole: A DFT study. Journal of Molecular Liquids, 2023, 382, 121960.
3. Hushvaktov, H. A., Tukhvatullin, F. H., Jumabaev, A., Tashkenbaev, U. N., Absanov, A. A., Hudoyberdiev, B. G., Kuyliev, B. Raman spectra and ab initio calculation of a structure of aqueous solutions of methanol. Journal of Molecular structure, 2017. 1131, 25-29.
4. Jumabaev, A., Holikulov, U., Hushvaktov, H., Absanov, A., Bulavin, L. Interaction of valine with water molecules: Raman and DFT study. Ukr. J. Phys, 2022, 67(8), 602-610.
5. Otajonov, S., Eshchanov, B. X., Isamatov, A. S.. On possible models of thermal motion of molecules and temperature effect on relaxation of optical anisotropy in bromine benzene. Ukrainian Journal of Physics, 2011. 56(11), 1178-1178.
6. Brian J. J.T., Tiddo J.M., Intermolecular π–π Stacking Interactions Made Visible //J. Chem. Educ., 2021, 98, p.540−545.
7. Stefan G., Do Special Noncovalent π-π Stacking Interactions Really Exist?, Angew. Chem. Int. Ed., 2008, 4, p.3430–3434.
8. James T.M., John L.L., Damian L.K., Scott A.R., Probing cooperativity in C–H···N and C–H···π interactions: Dissociation energies of aniline$(CH_4)n$ (n = 1,2) van der Waals complexes from resonant ionization and velocity mapped ion imagingmeasurements //J. Chem. Phys., 2020, 153, 044303, p.153.
9. Charlotte Z., Manuel L., Martin A.S., Halogens in acetophenones direct the hydrogen bond dockingpreference of phenol via stacking interactions // Journal of Chemical Physics, 2021, Preprints (www.preprints.org), Not peer-reviewed, Posted, p.1.
10. Xiaolong L., Lorenzo S., Silvia A., Yang Z., Kevin G.L., Jens U.G., Gang F., Cristina P., Vincenzo Baron, Stacked but not Stuck: Unveiling the Role of π-π* Interactions with the Help of the Benzofuran–Formaldehyde Complex //Angew. Chem. Int. Ed., 2022, 61, p.264–270.
11. Cockroft S.L. Christopher A.H., Kevin R.L., Julie P., Christopher J.U., Electrostatic Control of Aromatic Stacking Interactions, J.Am.Chem.Soc., 2005, 127.
12. Valentino R.C., Timo T., Aaron P., Elsebeth S., Stacking Interactions and the Twist of DNA // J. Am. Chem. Soc., 2008, 130, p.1304-1308,
13. Shamoon A.S., Anoop K.P., Apoorva D., Sudha J., Neeraj M., Comparative conformational, structural and vibrational study on the molecular structure of tyrosine and L-DOPA using density functional theory //J. Chem. Pharm. Res., 2010, 2(4), pp.835-850.
14. Patricio L, Juan B, Viviana S, Carolina P, María V.C., Silvia A.B., An experimental and theoretical study of l-tryptophan in an aqueous solution, combining two-layered ONIOM and SCRF calculation // Spectrochimica Acta Part A, 2012, 88, pp.162–170,
15. Belén H., Yves M.C., Fernando P., Sergei G.K., Mahmoud G., All characteristic Raman markers of tyrosine and tyrosinate originate from phenol ring fundamental vibrations // Raman Spectrosc., 2016, 47, pp.210-220,
16. Ryouta T., Takumi N., Criteria for Determining the Hydrogen-Bond Structures of a Tyrosine Side Chain by Fourier Transform Infrared Spectroscopy: Density Functional Theory Analyses of Model Hydrogen-Bonded Complexes of *p*-Cresol // J. Phys. Chem. B, 2007, 111, p. 13833-13844,
17. Frisch, M.J., et al. Gaussian 09, Rev – D.1. Gaussian Inc, 2009.

O‘ZBEKISTON MILLIY UNIVERSITETI XABARLARI, 2024, [3/1/1]
ISSN 2181-7324

FIZIKA
http://journals.nuu.uz
Natural sciences

УДК: 524.3/4

Сардор КУТЛИМУРАТОВ,
Чирчикский государственный педагогический университет, и.о. доцент
Нилуфар ОТОЖАНОВА,
Чирчикский государственный педагогический университет, старший преподаватель
Икрам ТАДЖИБАЕВ,
Чирчикский государственный педагогический университет, доцент Национальный универестет Узбекистана

На основании рецензии Ф.Т.Шамшиевой к.ф-м.н Национальный университет Узбекистана

РАСЧЕТ ПАРАМЕТРА АНИЗОТРОПИИ ДЛЯ СКОПЛЕНИЙ ГАЛАКТИК

Аннотация

В данной работе выполнен анализ данных наблюдений по скоплениям галактик из SDSS DR8. На основе данных наблюдений распределения поверхностной плотности определены значения параметра анизотропии для 31 скопления. Предложена классификация скоплений галактик по параметрам анизотропии скоростей, согласно которой скопления разделены на три группы. Изучена зависимость между параметром анизотропии и основными физическими характеристиками скоплений галактик.

Ключевые слова: галактики, скопления галактик, поверхностная плотность, параметр анизотропии, эволюция

CALCULATION OF THE ANISOTROPY PARAMETER FOR GALAXY CLUSTERS

Annotation

This work has analyzed observational data on galaxy clusters from SDSS DR8. Based on observational data on the distribution of surface density, the values of the anisotropy parameter were determined for 31 clusters. A classification of galaxy clusters based on velocity anisotropy parameters is proposed, according to which the clusters are divided into three groups. The relationship between the anisotropy parameter and the main physical characteristics of galaxy clusters has been studied.

Key words: galaxies, galaxy clusters, surface density, anisotropy parameter, evolution

GALAKTIKA TO‘DALARI UCHUN ANIZOTROPYA PARAMETRINI HISOBLASH

Annotatsiya

Ushbu maqola SDSS DR8 bazasidan olingan kuzatuv natijalari asosida galaktika to‘dalari bo'yicha kuzatuv ma'lumotlari tahlil qilangan. Sirt zichligini taqsimoti bo'yicha kuzatuv ma'lumotlariga asoslanib, 31 ta galaktikalar to‘dasi uchun anizotropiya parametrining qiymatlari aniqlangan. Tezlik anizotropiya parametri asosida galaktika to‘dalarining sinflashtirilishi taklif qilingan, unga ko'ra to‘dalar uchta guruhga bo'lingan. Anizotropiya parametri va galaktika to‘dalarining asosiy fizik xususiyatlari o'rtasidagi bog'liqlik o'rganilgan.

Kalit so‘zlar: galaktikalar, galaktika to‘dalari, sirt zichlik, anizotropiya parametri, evolyutsiya

Введение. Скопления галактик – наиболее массивные гравитационно связанные образования во Вселенной (см., например, [1-4]). Также, в их состав входят горячий ионизованный межгалактический газ и тёмная материя. Массы скоплений галактик составляют 10^{13}–10^{15} масс Солнца, причём основная доля массы обычно приходится на тёмную материю. На втором месте по массе находится межгалактический газ, и только на третьем – сами галактики. Характерный размер массивных скоплений галактик – около 10 млн. световых лет. Скорости движения галактик внутри скопления обычно составляют 1-2 тысячи км/с. Массы скоплений галактик определяются по измерениям разброса скоростей отдельных галактик относительно среднего значения либо по температуре и распределению горячего газа, заполняющего скопление.

По скоплениям галактик опубликованы много наблюдательных работ. Здесь мы приводим основные работы. В статье [1] составлен каталог 2712 богатых скоплений галактик, обнаруженных в ходе обзора неба Паломарской обсерваторией. Из каталога выбрано 1682 скоплений, отвечающих определенным критериям для включения в однородную статистическую выборку. Авторы по исследованиям сделали следующие выводы: (1) функция распределения скоплений по богатству N(n) быстро возрастает с уменьшением n; (2) данные не позволяют сделать существенного решения о том, что пространственная плотность центров скоплений меняется с расстоянием; (3) галактическое затемнение порядка нескольких десятых звездной величины существует на высоких северных галактических широтах около 300 галактической долготы; (4) существует весьма значимое неслучайное поверхностное распределение скоплений, как когда скопления находятся на всех расстояниях и когда рассматриваются скопления на разных расстояниях.

В работе [5] выполнен спектроскопический анализ 286 богатых скоплений, ранее идентифицированных на основе наблюдений на телескопе Дюпон в обсерватории Лас-Кампанас. В работе [6] изучены радиоактивные члены скопления Эйбела и составлен каталог 150 скоплений по параметрам рентгеновского и радиодиапазона. А в работе [7] обработано изображения из проекта SDSS-III и идентифицированы 132684 скопления галактик, причем более 95 % этих скоплений имеют массы $M_{200}>10^{14}M_{\odot}$. В работе [8] исследованы динамические свойства 2092 богатых скоплений галактик на основе данных рентгеновского, оптического и радиодиапазона. В работе [9] приведены массы 1191

скоплений, и кроме того данные приведенные в работе [8] были обновлены и/или дополнены. В работе [10] даны основные физические характеристики 275 богатых скоплений, в том числе, их массы.

В космологической модели ΛCDM скопления галактик создаются возмущениями плотности на больших масштабах [11]. Также классификация этих объектов до конца еще не определена. Надо отметить, что до сих пор анализ наблюдательных данных по скоплениям галактик не выполнен и соответствующая их теория формирования не разработана. Говоря более конкретно, отметим, что отсутствуют расширенный список-каталог богатых скоплений галактик и статистический анализ всех известных скоплений галактик с целью поиска их общих физических свойств, не выполнена классификация скоплений галактик по отдельным физическим параметрам. Изучение скоплений галактик представляет большой интерес также в связи с тем, что эти объекты можно использовать в качестве индикаторов физического состояния и эволюции.

Расчет параметра анизотропии. В настоящее время, когда наблюдательная база по многим астрофизическим объектам, в том числе, по скоплениям галактик, стала достаточно богатой, имеет смысл изучение проблемы эволюции скоплений галактик. Вероятным является тот факт, что скопления на первый взгляд весьма похожи друг на друга ввиду их почти сферической формы с весьма слабой симметрией. Но физически ясно, что эти скопления должны различаться внутренней структурой, степенью распределения скоростей и т.д. Надо отметить, что теоретические аспекты происхождения и эволюции скоплений галактик требуют создания базы данных наблюдений. Поэтому мы проанализировали данные наблюдений по этим объектам и нашли значения поверхностной плотности для нескольких скоплений галактик. Для этого нами были использованы базы данных SDSS DR8.

Из результатов анализа данных наблюдений для изучения вопросов эволюции скоплений галактик нам надо найти некоторые их параметры. Одним из них, в принципе, может быть параметр анизотропии скоростей. А его разные авторы определяют по-разному: как простое отношение средних значений компонент кинетической энергии радиальных и трансверсальных движений $2<\mathrm{T_r}>/<\mathrm{T_\perp}>$, и как $1-\sigma_r^2/\sigma_t^2$, где σ_r^2 и σ_t^2 – Радиальная и трансверсальная компоненты дисперсии скоростей. В этой работе мы в качестве параметра анизотропии скоростей берем величину

$$A=\frac{(2\overline{\Pi^2}-\overline{T^2})}{\overline{\Pi^2}} \qquad (1)$$

введенную впервые в работе [12]. В (1) $\overline{\Pi^2}$ и $\overline{\mathrm{T}^2}$ – радиальная и трансверсальная дисперсии остаточных скоростей. Так же как в [12], мы полагаем его постоянным для всей системы в целом, хотя в реальности он должен зависеть от расстояния внутри скопления. Этот параметр нас интересует здесь, прежде всего, с точки зрения возможной его зависимости от других физических характеристик скоплений галактик, хотя он представляет также самостоятельной интерес. Дело в том, что параметр анизотропии удобен для анализа стадии эволюции скоплений галактик, потому что каждая стадия характеризуется определенной структурой и распределением плотности и скорости. С переходом от ранней стадии к более поздней, структура становится более сглаженной и стремится к более изотропному распределению скоростей (в отличие от радиально-вытянутого распределения на ранних стадиях). Значение параметра анизотропии скоростей A=0 соответствует сферическому распределению скоростей (поздняя стадия эволюции), A=2 соответствует радиально-вытянутому распределению (ранняя стадия эволюции системы).

Для определения параметра анизотропии скоростей в скоплениях галактик по данным наблюдений видимой поверхностной плотности мы будем рассматривать стационарную модель со сферической симметрией. Легко вывести из гидродинамического уравнения следующее

$$\frac{d}{dr}\left[\frac{r^2}{D}\frac{d}{dr}\left(\mathrm{D}\,\overline{\Pi^2}\right)+\left(2\overline{\Pi^2}-\overline{T^2}\right)r\right]=-4\pi GDr^2, \qquad (2)$$

исключая потенциал в гидродинамическом уравнении при помощи уравнения Пуассона. В (2) введена безразмерная плотность D. Если перейти к новой переменной $x=4\pi Gr/\sqrt{\overline{\Pi^2}}$ тогда уравнение (2) примет сравнительно простой вид:

$$\frac{\mathrm{d}}{\mathrm{d}x}\left(\frac{x^2}{D}\frac{\mathrm{d}D}{\mathrm{d}x}\right)=-Dx^2-A. \qquad (3)$$

Решая численно уравнение (3), получим зависимости D и $D'=\frac{dD}{dx}$ от x, причем безразмерная плотность D явно зависит от значения параметра анизотропии. Уравнение (3) мы решаем для различных значений $A\in[0;2]$. По известным значениям D и D^1 можно перейти к поверхностной плотности, т.е. к проекции пространственной плотности на картинную плоскость. Далее, вычисляем поверхностную плотность посредством выражения

$$F(r)=-A\int_{r/\alpha}^{\infty}\sqrt{x^2-(r/\alpha)^2}\,D'(x)\,dx. \qquad (4)$$

Получая для заданных значений параметра анизотропии соответствующие значения поверхностной плотности $F(r)$ и сравнивая их с наблюдаемыми поверхностными плотностями для конкретных систем, выбираем оптимальное значение A. Масштабные множители определяются путем минимизации разности наблюдаемой и теоретической плотностей. Исходя из физической природы данной задачи, удобно применение достаточно апробированного симплектического метода минимизации следующей функции

$$f = \sum_{i=1}^{N} \left[-A \int_{r_i/\alpha}^{\infty} \sqrt{x^2 - (r_i/\alpha)^2}\, D'(x)\, dx - F_0 \right]^2 \qquad (5)$$

по параметрам α, A и F_0. Здесь N - число круговых зон на фотопластинках (или изображениях), в которых подсчитывалось число звезд. Таким образом, то значение параметра анизотропии, которое дает минимум *f*, принимается как наиболее вероятное значение A.

Вышеуказанным методом нами вычислены значения параметра анизотропии A для 31 скоплений галактик, используя симплексный метод минимизации квадрата разности между теоретический и наблюдаемой функциями плотности. Результаты расчета даны ниже в таблице 1.

Таблица 1. Основные физические характеристики и значения параметра анизотропии для скоплений галактик

№	Названия скоплений галактик	rm_{mag}	R_{L^*}	z	$r_{0\ arcmin}$	A
1	J001051.4+290940	17.98	88.90	0.3320	0.1931	0.08
2	J002016.1+000446	16.73	104.60	0.2156	0.8172	0.00
3	J002712.5-193045	17.42	94.00	0.2586	0.5740	0.88
4	J002800.9+244744	18.79	73.50	0.4839	0.2310	1.50
5	J004118.5+252609	15.77	112.30	0.1675	0.2149	0.60
6	J004511.7+084111	17.28	96.06	0.3014	2.4684	0.48
7	J023127.6+065856	15.67	156.70	0.2262	0.5312	1.12
8	J023952.7-013419	17.73	144.92	0.3712	0.1613	1.44
9	J083057.3+655031	16.25	209.09	0.1853	0.4227	0.88
10	J085007.9+360414	18.33	117.09	0.3639	1.1409	0.72
11	J090912.7+105829	15.56	200.20	0.1681	0.1259	1.24
12	J091609.0-002226	18.05	125.16	0.3163	1.4599	0.56
13	J091753.4+514338	16.08	173.82	0.2161	0.1315	1.32
14	J092048.3+302818	17.04	184.93	0.2928	0.1242	0.72
15	J094951.8+170711	17.88	133.91	0.4124	0.5140	0.92
16	J100226.8+203102	18.08	141.21	0.3376	0.6505	0.76
17	J105417.5+143904	17.18	135.02	0.2956	0.2526	1.00
18	J111450.3-121351	16.10	150.92	0.1926	0.1563	1.08
19	J112358.8+212850	16.78	108.06	0.1907	0.5638	0.96
20	J131129.5-012028	15.69	168.86	0.1791	1.0006	0.84
21	J131505.2+514903	16.76	130.18	0.2838	0.5160	1.04
22	J133238.4+503336	17.33	185.14	0.2775	0.1807	1.12
23	J133520.1+410004	16.37	176.94	0.2304	0.1898	0.8.
24	J140102.1+025242	16.06	205.45	0.2615	1.1394	0.72
25	J144431.8+311336	16.65	87.06	0.2340	0.0694	1.00
26	J153940.5+342527	16.95	135.85	0.2254	0.2480	0.96
27	J155820.0+271400	14.40	157.09	0.0871	0.1008	0.20
28	J160319.0+031645	16.67	156.13	0.2383	0.5564	0.84
29	J164019.8+464242	16.55	181.34	0.2301	0.0326	1.00
30	J164325.4+132236	16.45	114.19	0.1909	0.2691	0.00
31	J212823.4+013536	17.77	144.58	0.3857	1.4662	0.80

Из таблицы 1 видно, что 5 скоплений галактик имеют значения параметра анизотропии, близкие к нулю, т.е. в около 16 % скоплений имеет место почти сферическое распределение скоростей, и они, вероятно, находятся на более поздней стадии эволюции. Заметим, что именно при найденных значениях параметра анизотропии соответствующие полученные теоретические результаты хорошо согласуются с наблюдательными функциями поверхностной плотности. Для 4 скоплений значения параметра анизотропии скоростей являются близкими к 2. Поэтому распределение скоростей в этих скоплениях соответствует радиально-вытянутому случаю, что может быть связано, вероятно, с их нестационарностью в регулярном поле. Остальные значения параметра анизотропии для скоплений галактик оказались близкими к 1.

Далее нас интересует вопрос: можно ли классифицировать скопления галактик по параметру анизотропии скоростей? С этой целью нами составлена таблица 1.

Прежде всего, сравнивая значения параметра анизотропии скоростей, замечаем, что их можно уверенно разделить на три класса:

Классы	A	Кол. скоплений
БСГ 1	0< A<0.5	5
БСГ 2	0.5< A<1	18
БСГ 3	1< A<1.5	8

Заметим, что в интервале $1.5 < A < 2$ нет ни одного скопления, а это требует поиска в будущем дополнительных данных по видимой плотности для скоплений галактик. Тем не менее, интересно сравнить средние значения основных физических параметров трех классов этих скоплений.

Таблица 2. Средние значения характеристик трех групп

Классы	<z>	$<r_m>$, [mag]	$<r_{200}>$, [Мпк]	$<R_{L^*}>$	$<r_0>$, [arcmin]
БСГ 1	0.22	16.57	1.87	112.17	0.77
БСГ 2	0.27	16.97	2.02	145.39	0.59
БСГ 3	0.25	16.46	2.10	163.13	0.26

В табл. 2. даны средние значения ряда характеристик указанных групп скоплений галактик: фотометрическое красное смещение - <z>, величина самого яркого члена в рентгеновском диапазоне - $<r_m>$, радиус, в пределах которого средняя плотность скопления в 200 раз превышает критическую плотность Вселенной - $<r_{200}>$, богатство скоплений - $<R_{L^*}>$ [7], радиус ядра скоплений - $<r_0>$.

Также отметим результаты расчетов значений коэффициента корреляции параметра анизотропии с хорошо известными данными по другим физическим характеристикам, по которым, в принципе, можно составить двумерные

или многомерные классификации. К сожалению, эти значения коэффициента очень малы и нет возможности создания таких классификаций.

Заключение. Выполнен анализ данных наблюдений по скоплениям галактик из SDSS DR8. На основе данных наблюдений вычислено количество галактик и найдены распределения поверхностной плотности в скоплениях галактик. С помощью этих данных определены значения параметра анизотропии скоростей для 31 скоплений галактик. По результатам расчета распределения скоростей, 5 скоплений галактик имеют сферическую симметрию. Также, разработана классификация скоплений галактик по параметрам анизотропии скоростей и показано, что их можно условно разделить на три группы. Изучены зависимости между параметром анизотропии и основными физическими характеристиками скоплений галактик.

ЛИТЕРАТУРА

1. Abell G.O. // Astrophys.J. Supp., Volume. 3, p.211, 1958
2. Kopylova F.G., Kopylov A.I. // Astrophys. Bull., Volume 77, Issue 4, p.347, 2022
3. Kluge M., Bender R. // Astrophys. J. Supp. Ser., Volume 267, Issue 2, id.41, 32 pp, 2023
4. Piraino-Cerda F., Jaffe Y.L., Lourenço A.C., Crossett J.P., Salinas V., Kim D., Sheen Y.K., Kelkar K., Pallero D., Bravo-Alfaro H. // MNRAS, Volume 528, Issue 1, pp.919, 2024
5. Quintana H., Ramirez A. // Astrophys. J. Suppl. Ser., Volume 96, p.343, 1995
6. Morrison G.E., Owen F.N., Ledlow M.J., Keel W.C., Hill J.M., Voges W., Herter T. // Astrophys. J. Suppl. Ser., Volume 146, p.267, 2003
7. Wen Z.L., Han J.L., Liu F.S. // Astrophys. J. Suppl. Ser., Volume 199, p.34, 2012,
8. Wen Z.L., Han J.L. // MNRAS, Volume 436, p.275, 2013
9. Wen Z.L., Han J.L. // ApJ., Volume 807, p.178, 2015
10. Andreon S. // Astron. Astrophys., Volume 587, p.158, 2016
11. Einasto J., Suhhonenko I., Hutsi G. et al. // A&A, Volume 534, p.128, 2011
12. Агекян Т.А., Петровская И.В. // Учен. записи ЛГУ, № 307, p.187, 1962

O‘ZBEKISTON MILLIY UNIVERSITETI XABARLARI, 2024, [3/1/1]
ISSN 2181-7324

FIZIKA
http://journals.nuu.uz
Natural sciences

УДК:633.511

Gulmira MO'MINOVA,
Andijon davlat tibbiyot instituti katta o‘qituvchisi,
E-mail:muminovagulmira851@gmail.com
Erkin NAIMOV,
Andijon davlat tibbiyot instituti assistenti
Xusnobod XUDAYBERDIYEVA,
Andijon davlat tibbiyot instituti katta o‘qituvchisi
Dilovar KOMILOVA,
Andijon davlat tibbiyot instituti assistenti
E’tiborxon ALIMOVA,
Andijon davlat tibbiyot instituti assistent,

Andijon davlat tibbiyot instituti professori A.Ismanova taqrizi asosida

INVESTIGATION OF ELECTROPHYSICAL PROPERTIES OF NATURAL FIBER PLANTS

Annotation

It was found that the photoconductivity spectra of different types of sorghum plant fibers added with potassium permanganate are completely different. It was found that the electrical conductivity of the fibers of the plant doped with J+KJ+C2H5OH and KMnO4 and not doped increases exponentially with the increase in temperature. Infrared quenching and long-term relaxation of the photoconductivity of sorghum plant fibers treated with potassium permanganate were found. Over time, it was found that the quality of hemp fibers improved with UV radiation at low doses and deteriorated at high doses.

Key words. latifolia plant and silk fibers, alloying, light, photoconductivity, electrical conductivity.

ИССЛЕДОВАНИЕ ЭЛЕКТРОФИЗИЧЕСКИХ СВОЙСТВ РАСТЕНИЙ НАТУРАЛЬНОГО ВОЛОКНА

Аннотация

Установлено, что спектры фотопроводимости разных видов растительных волокон сорго с добавлением перманганата калия совершенно различны. Установлено, что электропроводность волокон растения, легированных J+KJ+C2H5OH и KMnO4 и нелегированных, экспоненциально возрастает с ростом температуры. Обнаружено инфракрасное тушение и долговременная релаксация фотопроводимости волокон растений сорго, обработанных перманганатом калия. Со временем было обнаружено, что качество конопляных волокон улучшалось под действием УФ-излучения при низких дозах и ухудшалось при высоких.

Ключевые слова. рогозы и шелковые волокна, легирование, луч, фотопроводимость, электрическая проводимость.

TABIIY TOLALI O‘SIMLIKLARNING ELEKTROFIZIK XUSUSIYATLARINI TADQIQ QILISH

Annotatsiya

Kaliy permanganat bilan qo'shilgan har xil turdagi qo‘g‘a o‘simligi tolalarining fotoo'tkazuvchanlik spektrlari butunlay boshqacha ekanligi aniqlandi. J+KJ+C2H5OH va $KMnO_4$ bilan legirlangan va legirlanmagan qo‘g‘a o‘simligi tolalarining elektr o'tkazuvchanligi harorat oshishi bilan eksponensial ravishda oshishi aniqlandi. Kaliy permanganat bilan qo'shilgan qo‘g‘a o‘simligi tolalarining fotoo'tkazuvchanligining infraqizil o'chirilishi va uzoq vaqt bo'shashishi aniqlandi. Vaqt o'tishi bilan, qo‘g‘a o‘simligi tolalarini kichik dozalarda UB nurlanishi bilan qo‘g‘a o‘simligi tolalarining sifati yaxshilanishi va katta dozalarda yomonlashishi aniqlandi.

Kalit so'zlarЖ qo‘g‘a o‘simligi va ipak tolalari, legirlash, yorug‘lik, fotoo'tkazuvchanlik, elektr o'tkazuvchanligi.

Kirish. So'nggi paytlarda tabiiy tolalar fizikasi sohasida tadqiqotlar muvaffaqiyatli olib borilmoqda. Bu xususan, yarimo'tkazgich xususiyatlarining qo‘g‘a o‘simligi va ipak tolalarida aniqlanishi bilan bog'liq . Qo‘g‘a o‘simligi va ipak tolalari kabi tabiiy polimerlar ketma - ket o'zgaruvchan kristalli va amorf mintaqalarning tuzilishlariga ega. Qo‘g‘a o‘simligi va ipak tolalarining elektrofizik va optik xususiyatlari tashqi ta'sirlarga (harorat, legirlash, bir o'qli bosim, namlik, yorug'lik) juda sezgir va kerakli xususiyatlarga ega materiallarni olish uchun osongina o'zgartirilishi mumkin. Qo‘g‘a o‘simligi tolasi sirtini qayta ishlashda ma'lum bo'ldiki, xossalar asosan 10-15 mkm shartli tolali diametri 1 mm gacha qalinlikdagi qo‘g‘a o‘simligi sirt qismi bilan belgilanadi . Kaliy permanganat bilan legirlangan qo‘g‘a o‘simligi tolalarning o'ziga xos yutilish mintaqasidagi fotoluminesans va fotoo'tkazuvchanlik (FK) ham qo‘g‘a o‘simligida topilgan. Shuningdek, qo‘g‘a o‘simligi tolalariga kaliy permanganat kiritilganda hosil bo'lgan chuqur darajalarga zaryad tashuvchilarning yopishishi tufayli infraqizil so'nish va fotoo'tkazuvchanlikning uzoq vaqt bo'shashishi aniqlandi.

Bu natijalardan yuqorida aytib o'tilganidek, "Tabiiy yarimo'tkazgichlar fizikasi va yangi ilmiy natijalar fizikasi" yangi ilmiy yo'nalishi ishlab chiqilgan.

Biroq, erishilgan muvaffaqiyatlarga qaramay, hali ham ko'plab hal etilmagan muammolar mavjud, jumladan, bu hodisalarning fizikasi to'liq tushunilmagan. Binobarin, ushbu ilmiy yo‘nalishda tadqiqot sohasini kengaytirish, tabiiy polimerik nanostrukturali yarimo‘tkazgichli materiallarning elektrofizik va optik xususiyatlarini tartibga solish yo‘llarini ochib beradi va ular asosida yangi diskret yarimo‘tkazgich elementlari va elektron uskunalarni yaratish uchun keng imkoniyatlar ochadi.

Ushbu maqola qo‘g‘a o‘simligi va ipak tolalarining yangi tadqiqot natijalarini taqdim etadi.

Jumladan, bu tadqiqot namunalari quyidagi texnologiya yordamida tayyorlangan. Tadqiqot ob'ekti qo‘g‘a o‘simligi va ipak tolalari edi. Qo‘g‘a o‘simligini kaliy permanganat bilan legirlash uchun avval qo‘g‘a o‘simligi tolasi ichi nozik taroq bilan yaxshilab taraladi (pichoq davri 0,3 mm) , so'ngra qo‘g‘a o‘simligi tolasi kaliy permanganatning 2 yoki 5% li suvli eritmasiga namlangan. Keyin kaliy permanganatning tarqalishi T = 60-80^0 C da 6-8 soat davomida amalga oshirildi . Keyinchalik , ichida buyurtma ohmik kontaktlarni yaratish uchun grafit va suyuq shishaga asoslangan elektr o'tkazuvchan yopishtiruvchi ishlab chiqilgan. Ezilgan nozik taneli grafit suyuq shisha bilan qorishma holga keltirildi. Shundan so'ng, qo‘g‘a o‘simligi va ipak tolalarining so'nggi tomonlariga bunday elektr o'tkazuvchan yopishtiruvchi (R = 300 Om qalinligi 10 mm va uzunligi 1 sm) qo'llaniladi. Bu takrorlanadigan o'lchov natijalarini olish imkonini berdi. Elektr toki va kuchlanish DMM 6500 KIETHLEY millimetr yordamida o'lchandi. Tayyorlangan namunalarning to'g'ridan-to'g'ri va teskari yo'nalishdagi oqim kuchlanish xususiyatlari chiziqli. O'lchovlar shuni ko'rsatdiki, qo‘g‘a o‘simligini kaliy permanganat bilan legirlagandan so'ng, namunalar n-tipli o'tkazuvchanlikka ega bo'ldi.

J+KJ+C2H5OH yod distillangan suvda eritildi. J+KJ+C2H5OH ning 2% li spirtli eritmasi tayyorlandi. Ushbu eritma qo‘g‘a o‘simligi tolasi yuzasiga surtiladi, shundan so'ng ular xona haroratida bir kun quritiladi, so'ngra diffuziya 60-80 ^{0} C da 6-8 soat davomida amalga oshiriladi. Namunaning haroratga bog'liqligi 0-100 ^{0} S harorat oralig'ida o'lchandi. Namuna harorati kalibrlangan mis-konstantan termojufti bilan o'lchandi.

Ipak tolasining fizik xossalarini o'rganish uchun 1200 m gacha bo'linmasdan bitta bo'g'inli ipak tolasini olish imkonini beruvchi maxsus pilla yechish moslamasi yaratilgan. Yechishdan keyin choklarni distillangan suvda 75 ^{0} S haroratda 3-5 marta yuvish kerak. Qo‘g‘a o‘simligi tolasi namunalarini tayyorlashning qolgan protseduralari uchun ishlatiladigan texnologiyalardir.

Tajriba va muhokama. Tajribalardan kelib chiqadiki, bir xil boshlang'ich sharoitlarda kaliy permanganat bilan legirlangan turli xil qo‘g‘a o‘simligi tolasi markali ShK spektrlari bir-biridan farq qiladi. Buni qo‘g‘a o‘simligi tolasining yuqori qobig'i - kesikulaning shaxsiy yorug‘lik spektrlarida namoyon bo'ladigan darajasiga bog'liqligi bilan izohlash mumkin. Kaliy permanganat bilan legirlangan har xil turdagi qo‘g‘a o‘simligi tolalarning shaxsiy kompyuter spektrlari T = 300K haroratda o'lchangan holati 1- rasmda ko'rsatilgan.

Qo‘g‘a o‘simligi tolasi turli holatlarda kaliy permanganatning shaxsiy yorug‘lik spektrlarida turli xil chuqurlikdagi cho'qqilarni hosil qilishining eksperimental haqiqati qo‘g‘a o‘simligi tolasini turli legirlashlarda aniqlash uchun ishlatilishi mumkin. Tajribalar shuni ko'rsatadiki, kaliy permanganatning turli foizlardagi legirlanishi turli xil chuqurlik darajasini hosil qiladi. Qo‘g‘a o‘simligi tolalarining chuqur darajalarining ionlanish energiyalari kaliy permanganat bilan legirlanish natijasida hosil bo'lgan.

Aniqlanishicha, kaliy permanganat va J+KJ+C2H5OH bilan legirlanmagan va legirlangan qo‘g‘a o‘simligi tolasining elektr o'tkazuvchanligi harorat oshishi bilan ma'lum issiqlik ionlanish energiyasi bilan eksponensial ravishda ortadi. 1-rasmda kaliy permanganat va J+KJ+C2H5OH qo'shilgan turli xil qo‘g‘a o‘simligi tolalarning elektr o'tkazuvchanligining haroratga bog'liqligi ko'rsatilgan.

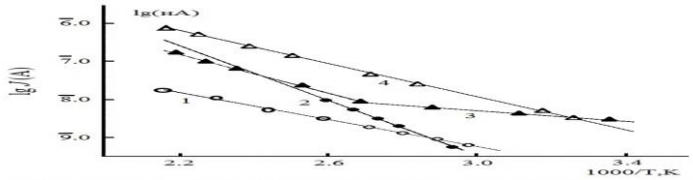

1. Qo‘g‘a o‘simligi tolasining turli legirlanishi orqali o'tadigan elektr tokining haroratga bog'liqligi. Ichi olingan va ichi olinmagan

Shuningdek, qo‘g‘a o‘simligi tolalarni legirlashdan so'ng chuqur darajadagi ionlanish energiyasi o'zgarganligi aniqlandi, bu ko'rinishidan qo‘g‘a o‘simligi tolasi tuzilmalarining kaliy permanganat bilan o'zaro ta'siri bilan bog'liq.

Kaliy permanganat bilan legirlangan har xil turdagi qo‘g‘a o‘simligi tolalarning fotoo'tkazuvchanligi (FK) o'rganildi. Aniqlanishicha, namuna yorug'lik energiyasi hν = 3,8 eV bilan yoritilsa , fototok vaqt o'tishi bilan eksponensial ravishda ortadi. Bu nisbat qorong'u oqimga fototok I_{ph} / I_d = 22-100 ga teng . Bu spektrning UB hududida ishlaydigan fotodetektorlarni yaratishga imkon beradi. Kombinatsiyalangan yoritishda qo‘g‘a o‘simligi tolasining barcha turlarida fotoo'tkazuvchanlikning IR-so’nishi kuzatildi. Qo‘g‘a o‘simligi tolasining IR-so’nishi estrodiol yorug'lik ostida chuqur darajalarni qayta zaryadlash bilan izohlanadi. Keyin yoritishning hν≥E_g yorug'likli namuna , (E_g tarmoqli bo'shlig'i), yorug'likni o'chirgandan so'ng namunaning uzoq vaqt bo'shashishi aniqlanadi. O'zining orqa yorug'ligining intensivligi oshishi bilan yutilishning ko'payishi aniqlandi. Bu qo‘g‘a o‘simligi tolasining taqiqlangan zonasida chuqur yod darajasini to'ldirish darajasining o'zgarishi bilan bog'liq.

Ko‘rinib turibdiki, nurlanishning past dozalarida kuchlanish kuchi ortib, keyin 1,6 marta kamayadi. Bu, jumladan, UB nurlarining kulrang yuzasiga ta'siri tufayli ipak qurti tırtılının o'sishi va rivojlanishi yomonlashadi. E'tibor bering, nurlanishning past dozasi (t <0,5 min.) ipak tolalari sifatini yaxshilaydi.

Xulosalar. Qo‘g‘a o‘simligi hamda ipak tolalarini kaliy permanganat va J+KJ+C2H5OH aralashmasi bilan legirlash texnologiyasi ishlab chiqilgan. Yagona tabiiy tolalarning bir o'qli mexanik kuchlanish ta'sirida yorilish vaqtini aniqlash uchun moslama yaratilgan. Aniqlanishicha, bir xil boshlang'ich sharoitlarda kaliy permanganat bilan qo'shilgan turli qo‘g‘a o‘simligi tolalarining fotoo'tkazuvchanlik spektrlari bir-biridan farq qiladi. Bu kaliy permanganatning sirt - kesikulalar bilan o'zaro ta'siri bilan bog'liq bo'lib, ular qo‘g‘a o‘simligi tolalarining turlariga qarab turli xil xususiyatlarga ega . Bu qo‘g‘a o‘simligi tolalari turlarini aniqlash uchun ishlatilishi mumkin . Har xil turdagi qo‘g‘a o‘simligi tolalarning kaliy permanganat va J+KJ+C2H5OH bilan legirlanmagan va legirlangan elektr o'tkazuvchanligi harorat oshishi bilan eksponensial ravishda oshishi aniqlangan. Aniqlanishicha, qo‘g‘a o‘simligi tolalarni legirlanganda chuqur darajadagi ionlanish energiyalari o'zgargan, bu qo‘g‘a o‘simligi tolasi strukturasining kaliy permanganat bilan o'zaro ta'siri bilan bog'liq. TF<J> ning yoritilishidan so'ng IR so‘nish va uzoq vaqt davomida yorug‘likning bo'shashishi aniqlandi. IQ o'chirish Kompyuterning ishlashi kombinatsiyalangan yorug'lik ostida chuqur darajalarni qayta zaryadlash bilan izohlanadi.

Birinchi marta qo‘g‘a o‘simligi tolasining cho’zilish kuchining UB nurlanish vaqtiga bog’liqligi o’rganildi. Aniqlanishicha, nurlanishning past dozalari qo‘g‘a o‘simligi tolalari sifatini yaxshilaydi.

ADABIYOTLAR

1. ATMamadalimov, P.K.Habibullaev, M.Shermatov, « Nekotorye muammoli modifikacii fizicheskih svojstv hlopkovyh volokon », O'zbek fizika jurnali. 1-jild, 6-son, 1999 yil, 465-479-bet.
2. AT. Mamadalimov, N.K.Hakimova, B.E.Turaev, T.A.Usmonov. The o'rganish ning paxta va ipak tolalarining yarimo'tkazgich xossalari. Yarimo'tkazgichli tuzilmalarda fotoelektrik va optik hodisalar bo'yicha xalqaro konferentsiya materiallari. 2-3 oktyabr, Farg'ona, FerPI O'zbekiston, 35-bet (2006 y.)
3. A.T.Mamadalimov, Sh.A.Gulamov, G.M.Muminova “Investigation of Me-chanical and Electrophysical Properties of Cattail Fibers”. Journal of Scientific and Engineering Research, 2018, 5(8):250-251. ISSN:2394-2630 CODEN(USA):JSERBR.
4. E.B.Rubinov, M.M.Muxamedov, L.X. Osipova, IZ Burnashev. Ipak xomashyosi va hindiston yong'og'i o'rash. Katalog. 2-nashr. " Lechprombytizdat ." - 312 b. (1986)
5. G.M.Muminova, Sh.A.Gulamov, A.T.Mamadalimov, «Izuchenie meha-nicheskih svojstv rogoza», Molodoj uchjonyj. №19(205). 2018 g. Str.144-146
6. M. Shermatov, A.T.Mamadalimov. Bir usul ning termistorni olish. Dastlabki patent № . 4946. 25.03.1996 yil. O‘zbekiston, (1996)
7. G.M.Muminova “Study of the physical properties semiconductive natural fiber plant”. Экономика и социум. №6 (109). 2023
8. Sh.A.Gulamov, G.M.Mo‘minova «Legirlangan va legirlanmagan qo‘g‘a o‘simligi tolalarini tayyorlash hamda ularning optoelektronik xossalarini tadqiq qilish usullari». Scientific Bulletin Physical and Mathematical Research, 2023, 5(1):58-63. ISSN:2181-0702
9. A.S.Zokirov, Sh.U. Yo'ldoshev, HDCho, JC Li, TW Kang va A.T.Mamadalimov. Paxta tolalari / polimer kompozitlari asosidagi organik fotodiodlar. Amaliy fizika jurnali. 110, 114522, 114522 -1-114522-6. (2011).
10. AT. Mamadalimov, B.E.To‘raev, T.T.Turg‘unov, T.A.Usmonov. Tekshiruv ning the paxta tolalariga sirt ishlov berishning ularning elektr xossalariga ta'siri . O'zbekiston Respublikasi Fanlar Akademiyasining ma'ruzalari No.3, p.48-52, (2004)
11. A.S.Zokirov, Sh.U. Yuldashev, HJ Vang, HD Cho, TW Kang, JJXamdamov, AT Mamadalimov. Sirt o'zgartirilgan va MEH-PPV bilan qoplangan paxta tolalarini fotoluminesans bilan o'rganish. Luminescence jurnali. 131 301 -305, (2011)
12. A.T.Mamadalimov, BL Oksegendler, Sh.O. Otajjnov, B.E.To'raev, TAUsmanov, N.K.Hakimova va J.A. Qodirov. Asosiy assimilyatsiya diapazonida yoritilgan yod qo'shilgan paxta tolalarining fotoo'tkazuvchanligining xususiyatlari. Texnik fizika maktublari, jild. 28, No 7, 581-583-betlar, (2002 y.)
13. DA. Mamadalimov. Yarimo'tkazgichlarda fotoelektrik hodisalar. Toshkent, NUUz, - 102 b, (2003)
14. AT. Mamadalimov, C.Sh. Rashidova, A.A.Xolmo'minov. Polimer tolar fizikasi . Toshkent. "Universitet", 124 garov. (2009)
15. A.S.Zokirov, Sh.U. Yuldashev, HJ Vang, JC Li, TW Kang, AT Mamadalimov "Yodli tsellyuloza tolalarida elektr transporti va foto o'tkazuvchanligini o'rganish." J Mater Sci, jild. 46, 896–901-betlar, (2011)
16. G.M.Mo‘minova "Exploring Methods for Assessing Electrical Conductivity in Materials and Bodies" Лучшие интеллектуальные исследования Часть-16, № 3 Март -2024. Стр.77-80.

O‘ZBEKISTON MILLIY UNIVERSITETI XABARLARI, 2024, [3/1/1]
ISSN 2181-7324

FIZIKA
http://journals.nuu.uz
Natural sciences

Shahnozahon MUMINOVA,
O‘z.RFA U.Arifov nomidagi Ion-Plazma va lazer texnologiyalari instituti tayanch doktoranti,
E-mail:shmuminova242526@gmail.com
Ishmumin YADGAROV,
O‘z.RFA U.Arifov nomidagi Ion-Plazma va lazer texnologiyalari instituti
Fizik jarayonlarni modellashtirish laboratoriyasi professori, f-m.f.d
O‘tkir O‘LJAYEV,
O‘z.RFA U.Arifov nomidagi Ion-Plazma va lazer texnologiyalari instituti
Ko‘p fazali tizimlar issiqlik fizikasi laboratoriyasi kichik ilmiy xodimi
G‘aniboy RAXMANOV,
O‘zbekiston Milliy universiteti dotsenti

O‘zMU dotsenti, PhD G’.Eshonqulov taqrizi asosida

IKKI QAVATLI UGLEROD NANONAYCHA SIRTIDA BOR ATOMLARINING ADSORBSIYA JARAYONINI MOLEKULYAR DINAMIKA USULIDA MODELLASHTIRISH

Annotatsiya

Tadqiqot ishida molekulyar dinamika usuli yordamida 300K va 900K haroratlarda ikki qavatli uglerod nanonaycha (IQUNN) sirtida bor atomlarining adsorbsiyalanish jarayoni o‘rganildi. IQUNN larning bor atomlari bilan o'zaro ta'sir jarayonlarini model hisoblashlarda ReaxFF potentsialidan foydalanilgan. IQUNN sirtida adsorbsiyalangan bor atomlari konsentratsiyasining oshishi tizimdagi qisman zaryadning o'zgarishiga olib keladi. Xususan, 300 K haroratda IQUNN larda adsorbsiyalangan bor atomlarining konsentratsiyasi 900 K dagidan yuqori, qismiy zaryad esa yuqori haroratda (900 K) pastki haroratga (300 K) qaraganda yuqori bo’lishi kuzatildi.

Kalit so‘zlar IQUNN (ikki qavatli uglerodli nanonaycha), bor atomlari, adsorbsiya, konsentratsiya, xirallik

МОДЕЛИРОВАНИЕ ПРОЦЕССА АДСОРБЦИИ АТОМОВ БОРА НА ПОВЕРХНОСТИ ДВУХСЛОЙНОЙ УГЛЕРОДНОЙ НАНОТРУБКИ МЕТОДОМ МОЛЕКУЛЯРНОЙ ДИНАМИКИ

Аннотация

В работе методом молекулярной динамики изучен процесс адсорбции атомов бора поверхностью двухслойной углеродной нанотрубки (ДСУНТ) при температурах 300К и 900К. В модельных расчетах процессов взаимодействия ДСУНТ с атомами бора был использован потенциал ReaxFF. Увеличение концентрации атомов бора, адсорбированных поверхностью ДСУНТ, приводит к изменению частичного заряда в системе. В частности, концентрация атомов бора, адсорбированных на ДСУНТ при температуре 300 К, была выше, чем при 900 К, частичный заряд был больше при верхнем значении температуры (900 К), чем при нижнем (300 К).

Ключевые слова двухслойная углеродная нанотрубка, атомы бора, адсорбция, концентрация, хиральность.

SIMULATION OF THE PROCESS OF ADSORPTION OF BORON ATOMS ON THE SURFACE OF A DOUBLE-WALLED CARBON NANOTUBE USING THE MOLECULAR DYNAMICS METHOD

Annotation

In this work, the process of adsorption of boron atoms by the surface of a double-walled carbon nanotube (DWCNT) at temperatures of 300K and 900K was studied using the molecular dynamics method. In model calculations of the processes of interaction of DWCNTs with boron atoms, the ReaxFF potential was used. An increase in the concentration of boron atoms adsorbed on the DWCNT surface leads to a change in the partial charge in the system. In particular, the concentration of boron atoms adsorbed on DWCNTs at a temperature of 300 K was higher than at 900 K, and the partial charge was higher at the upper temperature (900 K) than at the lower temperature (300 K).

Key words. double-walled carbon nanotube, boron atoms, adsorption, concentration, chirality.

Kirish. O‘zlarining noyob xususiyatlari tufayli uglerodga asoslangan nanostrukturalar bir necha o‘n yillar davomida fan va texnikaning bir qancha sohalarida eng muhum nanotexnalogiya materiallari sifatida foydalaniladi [1]. Ushbu nanostrukturalar orasida uglerodli nanonaycha (UNN) lar past og‘irligi va kimyoviy barqarorligi [2] tufayli fizika, kimyo va materialshunoslikda [1] keng qiziqish uyg‘otib, ular turli xil ilovalarda, jumladan, elektron qurilmalar [3], sensorlar, materiallarni mustahkamlash [4], adsorbentlar [5] kabi sohalarda qo‘llanilib kelinmoqda. Ular orasida ikki qavatli (devorli) uglerod nanonaychalari (IQUNN) barqarorligi va mexanik xususiyatlarining yaxshilanganligi tufayli, so‘nggi yillarda ularga katta e’tibor qaratilmoqda [6]. Bir qavatli uglerod nanonaycha (BQUNN) lar bilan solishtirganda, IQUNNlar kuchli mexanik, elektr va optik xususiyatlarga, hamda yuqori kimyoviy barqarorlikka ega [1].

IQUNN lar har bir qavati yarimo‘tkazgich (YaO‘) yoki metall (M) bo‘lishiga qarab 4 xil (YaO‘ va YaO‘; M va YaO‘; M va M hamda YaO‘ va M) konfiguratsiyada bo‘lishi mumkin [7]. Ushbu maretiallarning xususiyatlarini nazorat qilishning eng oddiy usullaridan biri IQUNN larga geteroatomlarni qo‘shish (adsorbsiya) yoki almashtirish (doping) orqali o‘zgartirishdir. Xususan, bor (B), azot (N), kalsiy (Ca), palladiy (Pd) va platina (Pt) kabi elementlarni qo‘shish orqali ularning mexanik, optik va elektron xususiyatlarini o‘zgartirish mumkin. Ushbu atomlar orasida strukturaviy tuzlishi bo‘yicha uglerod ($1s^2 2s^2 2p^2$) elementiga yaqin bo‘lgan bor ($1s^2 2s^2 2p^1$) atomining o‘zaro ta’siri yordamida IQUNN ning elektron xususiyatlari o‘zgarib ketishi

tadqiqotlarda o‘rganilgan. Bor (*B*) atomlarining IQUNN ga kiritilishi sirtning zaryadlanishini oshiradi va shuning uchun IQUNN larning adsorbsion xususiyatlarini yaxshilaydi [8]. Ushbu IQUNN larning bor atom va u asosidagi materiallar bilan o‘zaro ta’siri bo‘yicha ko‘plab nazariy (DFT), eksperimental (masalan, CVD, ALD) va modellashtirish (MD, MC) tadqiqotlari olib borilayotganiga qaramay, bor atomlarini strukturadagi miqdorini (konsentratsiyasini) boshqarish asosiy muammolardan biri bo‘lib qolmoqda.

Ushbu tadqiqotda molekulyar dinamika (MD) simulyatsiyalari yordamida turli haroratlarda IQUNN da bor atomlarining kimyosorbsiya mexanizmlarini o‘rganildi.

Hisoblash usullari. Ushbu tadqiqot ishida metal o‘tkazuvchanlikka ega bo‘lgan (5.5) va (10.10) xirallikdagi IQUNN va bor atomlarining o‘zaro ta’siri MD usulidan foydalanib LAMMPS dasturiy paketi [9] yordamida kompyuterda modellashtirilib o‘rganildi. (5.5) va (10.10) xirallikdagi IQUNN ning ichki va tashqi diametrlari mos ravishda 0.678 va 1.357 nm ga teng bo‘lib, eksperimentlarda olingan IQUNN lardagi qiymatlari mos keladi. [10]. IQUNN va bor atomlari orasidagi o‘zaro bog‘lar hosil bo‘lishi va uzilish jarayonlarini hisoblashda ReaxFF ta’sir potensialidan foydalanildi [11].

Dastlab, barcha model tizimlarining energiyasi konfiguratsiyalangan gradiyent usuli bilan minimallashtirildi. Tizimlarning harorati va bosimi NpT ansamblida Berendsen termostati va barostat [12] yordamida kerakli qiymatga (300 K) tenglashtiriladi. Tanlangan isitish tezligi (ya'ni, 1 K/ps) ilgari xabar qilingan qiymatlar diapazoniga (0,1-10,0 K/ps) mos keladi va harorat oshishi vaqtida model tizimlarining termodinamik muvozanatidagi og‘ishlar ahamiyatsiz ekanligini ko‘rsatadi. IQUNN da bor atomlarining kimyosorbsiyasi holatida tizimning harorati kanonik NVT ansamblida Bussi termostati [13] yordamida 100 ps uchun 300 K da ushlab turildi.

Modellashtirishlarda tizimdagi bor atomlarning bosimi 1,94 MPa ga teng. Bor atomlari NVT ansamblida 10 ps oralig‘i bilan nanonaycha yuzasini o‘rab turgan muhitga tasodifiy ravishda adsorbsiyalangan va atomlar orasidagi minimal masofa 1nm qilib tanlangan.

Harorat (300 K) ta’sirida IQUNN yuzasida qolgan bor atomlarining konsentratsiyasi quyidagicha hisoblangan:

$$\rho\ (\%) = N_B/N_C * 100\%) \qquad (1)$$

bu yerda N_C va N_B – IQUNN dagi uglerod atomlari va unga adsorbsiya bo‘lgan bor atomlari soni.

Simulyatsiyalar har bir holat uchun bir necha marta takrorlangan va yakuniy natijalar individual qiymatlarni o‘rtachalash yo‘li bilan olingan.

Hisoblash natijalari. 300 K va 900 K tizimlar uchun (5,5) va (10,10) xirallikdagi IQUNN yuzasida adsorbsiyalangan bor atomlar konsentratsiyasi (ρ (%)) harakat tezligi (kinetik energiya, E_k) ga qarab o‘zgarib borgan. E_k ning ortishi bilan (ya’ni, 1 eV dan 32 eV gacha) adsorbsiyalangan bor atomlarining ρ (%) qiymati 300 K va 900 K ga mos ravishda 2.2 %-16.1 % va 1.2 %-15.7 % oralig’ida o’zgargan (1-rasm). Borning past konsentratsiyasi (masalan, <0,5 %) UNN larning mexanik xususiyatlarni o‘zgartirmaydi, biroq ularning elektron o‘tkazuvchanligini sezilarli darajada yaxshilanishiga olib kelishi mumkin [14].

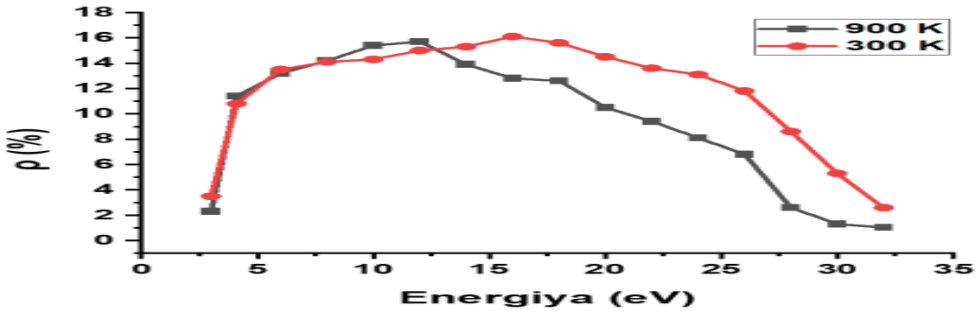

1-rasm. IQUNN sirtida bor atomlarining adsorbsiya ko‘rsatgichining uning kinetik energiyasiga bog‘liqligi

2a-rasmda sistemadagi (ya’ni, IQUNN) atomlar qismiy zaryadining o‘zgarishi tasvirlangan bo‘lib, qizil rangdan ko‘k rangga o‘tish holati qismiy zaryadlarning ortishini (ya’ni, -16*e* va 16*e*) ifodalaydi. 2b-rasmda adsorbsiya energiyasining bor atomlari qismiy zaryadlarining o‘zgarishiga bog’liqligi keltirilgan. Rasmdan ko‘rinadiki, 300 K va 900 K haroratlarda uglerod (*C*) va bor (*B*) atomlarining maksimal qismiy zaryadlari yig‘indisi, mos ravishda 16*e* va -16*e* (18 eV) hamda 20.61*e* va 20.61*e* (32 eV) qiymatlariga to‘g‘ri keladi. Bu shuni ko‘rsatadiki, bor kontsentratsiyasining ortishi IQUNN ning musbat (p-tip) qismiy zaryadlarining oshishiga olib keladi. (5,5) va (10,10) xirallikka ega IQUNN dagi bor va uglerod *(B-C)* orasidagi bog‘lanish uzunligi 1.4-1.8 Å oralig‘ida bo‘lib, bu boshqa tadqiqot natijalariga yaqin [15].

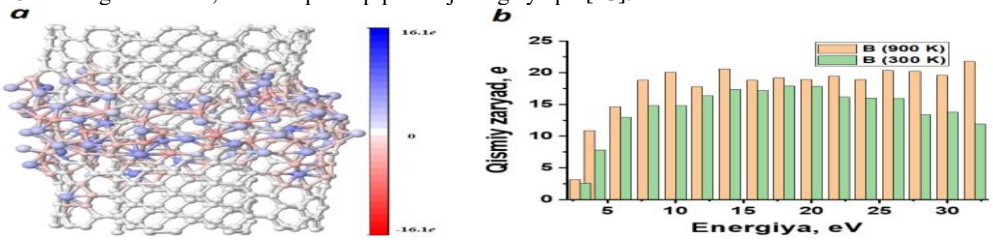

2-rasmda *a*) IQUNN sirtiga bor atomlarining adsorbsiyasi keltirilgan, tizimdagi atomlar musbat zaryadli ko‘k va manfiy zaryadli qizil rangda, zaryadsiz (0) atomlar esa oq rangda tasvirlangan. Rasmdagi holat 300 K uchun. *b*) Adsorbsiyalangan bor atomlarining qismiy zaryadlarining o‘zgarishiga bog’liqligi.

IQUNN da bor atomlarining kimyosorbsiyasi ko‘plab omillarga, jumladan, nanonaycha yuzasining egriligi, olti a’zoli uglerod halqalarining joylashishi bog‘liq [16]. Bor atomlari UNN ning olti burchakli (geksoganal) tuzilishi ichidagi joylashuviga (para, orto, meta) qarab, UNN yuzasidan harorat ta’sirida sirtdan chiqib ketishi mumkin [17]. IQUNN yuzasida adsorbsiyalangan bor atomlarga boshqa bor atomlarining sirtga kelishi ta'sir qiladi, bu esa Lengmyur-Hinshelvud rekombinatsiya mexanizmi orqali molekulalarning hosil bo‘lishiga olib keladi (bu yerda sirtdagi ikki bor atom kovalent bog‘lanib, bor molekulasini hosil qiladi)

yoki kiruvchi bor atomlarning adsorbsiyalangan bor atomiga ta’siri tufayli yuzada Eley-Rideal mexanizmi orqali desorbsiyalanadi [18].

Xulosa. Nanonaychalarda bor atomlarining mavjudligi geterostrukturada zaryadning qayta taqsimlanishi hisobiga ularning reaksiya imkoniyatlarini yaxshilaydi. Bor atomlarining kiritilishi bir qator muhim kimyoviy birikmalarni aniqlash va nanonaychalardagi turli xil konsentratsiyalarni boshqarish nanosensorlarning sezgirligini nazorat qilish imkonini beradi. Ushbu ishda 300 K va 900 K haroratlarda uglerod (*C*) va bor (*B*) atomlarining maksimal qismiy zaryadlari yig‘indisi, mos ravishda 16*e* va -16*e* (18 eV) hamda 20.61*e* va 20.61*e* (32 eV) qiymatlariga to‘g‘ri keldi. Xulosa qilib aytish mumkinki, bor UNN dagi o‘rnini bosuvchi reaktsiyalar uchun eng istiqbolli materiallardan biridir.

ADABIYOTLAR

1. G. Speranza, "Carbon Nanomaterials: Synthesis, Functionalization and Sensing Applications", *Nanomaterials*, vol. 11, no. 4, (2021), p. 967.
2. H. Lee, Y.-S. Kang, S.-H. Kim, and J.-Y. Lee, ‘Hydrogen desorption properties of multiwall carbon nanotubes with closed and open structures’, *Applied Physics Letters*, vol. 80, no. 4, (2002), pp. 577–579.
3. M. Soto *et al.*, ‘Effect of interwall interaction on the electronic structure of double-walled carbon nanotubes’, *Nanotechnology*, vol. 26, no. 16, (2015), p. 165201.
4. R. Qin, A. Zhou, Z. Yu, Q. Wang, and D. Lau, ‘Role of carbon nanotube in reinforcing cementitious materials: An experimental and coarse-grained molecular dynamics study’, *Cement and Concrete Research*, vol. 147, (2021), p. 106517.
5. M. Inagaki, M. Toyoda, Y. Soneda, and T. Morishita, ‘Nitrogen-doped carbon materials’, *Carbon*, vol. 132, (2018) pp. 104–140.
6. V. Zólyomi *et al.*, ‘Intershell interaction in double walled carbon nanotubes: Charge transfer and orbital mixing’, *Phys. Rev. B*, vol. 77, no. 24, (2008) p. 245403.
7. M. Damnjanović, I. Milošević, T. Vuković, and R. Sredanović, ‘Full symmetry, optical activity, and potentials of single-wall and multiwall nanotubes’, *Phys. Rev. B*, vol. 60, no. 4, (1999) pp. 2728–2739.
8. M. Endo *et al.*, ‘Atomic Nanotube Welders: Boron Interstitials Triggering Connections in Double-Walled Carbon Nanotubes’, *Nano Lett.*, vol. 5, no. 6, (2005) pp. 1099–1105.
9. Q. Mao, M. Feng, X. Z. Jiang, Y. Ren, K. H. Luo, and A. C. T. van Duin, ‘Classical and reactive molecular dynamics: Principles and applications in combustion and energy systems’, *Progress in Energy and Combustion Science*, vol. 97, (2023) p. 101084.
10. G. Chen *et al.*, ‘Chemically Doped Double-Walled Carbon Nanotubes: Cylindrical Molecular Capacitors’, *Phys. Rev. Lett.*, vol. 90, no. 25, (2003), p. 257403.
11. K. Chenoweth, A. C. T. Van Duin, and W. A. Goddard, ‘ReaxFF Reactive Force Field for Molecular Dynamics Simulations of Hydrocarbon Oxidation’, *J. Phys. Chem. A*, vol. 112, no. 5, (2008), pp. 1040–1053.
12. H. J. C. Berendsen, J. P. M. Postma, W. F. Van Gunsteren, A. DiNola, and J. R. Haak, ‘Molecular dynamics with coupling to an external bath’, *The Journal of Chemical Physics*, vol. 81, no. 8, (1984), pp. 3684–3690.
13. G. Bussi, D. Donadio, and M. Parrinello, ‘Canonical sampling through velocity rescaling’, *The Journal of Chemical Physics*, vol. 126, no. 1, (2007), p. 014101.
14. M. Terrones a, A. Jorio b, M. Endo c, A.M. Rao d, Y.A. Kim c, T. Hayashi c, H. Terrones a, J.-C. Charlier e, G. Dresselhaus f, M.S. Dresselhaus, "New direction in nanotube science" Volume 7, Issue 10, (2004), pp. 30-45
15. M. Endo, T. Hayashi, S.-H. Hong, T. Enoki, and M. S. Dresselhaus, ‘Scanning tunneling microscope study of boron-doped highly oriented pyrolytic graphite’, *Journal of Applied Physics*, vol. 90, no. 11, (2001), pp. 5670–5674.
16. W. Su *et al.*, ‘Chirality-dependent electrical transport properties of carbon nanotubes obtained by experimental measurement’, *Nat Commun*, vol. 14, no. 1, (2023), p. 1672.
17. U. Khalilov, A. Bogaerts, B. Xu, T. Kato, T. Kaneko, and E. C. Neyts, ‘How the alignment of adsorbed ortho H pairs determines the onset of selective carbon nanotube etching’, *Nanoscale*, vol. 9, no. 4, (2017), pp. 1653–1661.
18. X. Sha, B. Jackson, and D. Lemoine, ‘Quantum studies of Eley–Rideal reactions between H atoms on a graphite surface’, *The Journal of Chemical Physics*, vol. 116, no. 16, (2002), pp. 7158–7169.

O‘ZBEKISTON MILLIY UNIVERSITETI XABARLARI, 2024, [3/1/1]
ISSN 2181-7324

FIZIKA
http://journals.nuu.uz
Natural sciences

UDK: 546.26.043:535

Qayum MUSURMONOV,
Ion plazma va lazer texnologiyalari instituti kichik ilmiy xodimi
Email: abduqayummusulmonov@gmail.com
Urol MAXMANOV,
Ion plazma va lazer texnologiyalari instituti, “Optika va spektroskopiya” laboratoriyasi mudiri, f.-m.f.d
Shohboz ESANOV,
Ion plazma va lazer texnologiyalari instituti tayanch doktoranti
Bobir ASLONOV,
Ion plazma va lazer texnologiyalari instituti tayanch doktoranti
Tohirjon CHO‘LIYEV,
Guliston davlat universiteti tayanch doktoranti
Akbar SHUKUROV,
Ion plazma va lazer texnologiyalari instituti katta ilmiy xodimi

O‘zbekiston Milliy universiteti professori, f.-m.f.d. Sh.Otajonov taqrizi asosida

C_{60} FULLEREN GEKSAN-TOLUOL ERITUVCHILAR SISTEMASIDA: KOMPONENTLAR KONSENTRATSIYASINING TA’SIRI

Annotatsiya

Ushbu tadqiqot ishida C_{60} fullerenning “geksan+toluol” erituvchilarning binar aralashmalaridagi eritmalarning fizikaviy xususiyatlarini optik yutilish spektroskopiyasi, refraktometriya va yorug’likning dinamik sochilishi metodlarida tadqiq qilindi. Eritmalarning optik va morfologik xossalari komponentlarning konsentratsiyalariga bog’liq ravishda o’zgarish natijalari bayon etilgan. Olingan natijalar o’lchamli va fizik xususiyatlarini oldindan boshqariladigan fulleren tarkibli funktsional nanomateriallar yaratish mumkinligini ko’rsatadi.

Kalit so‘zlar: C_{60} fulleren, o‘z-o‘zidan tashkillanish, sindirish ko‘rsatkichi, optik zichlik, yorug‘likning dinamik sochilishi, gidrodinamik diametr.

ФУЛЛЕРЕН C_{60} В СИСТЕМЕ РАСТВОРИТЕЛЕЙ ГЕКСАН-ТОЛУОЛ: ВЛИЯНИЕ КОНЦЕНТРАЦИИ КОМПОНЕНТОВ

Аннотация

В данной работе методами спектроскопия оптической поглощения, рефрактометрии и динамического рассеяния света исследованы физические свойства растворов фуллерена C_{60} в бинарных смесях растворителей «гексан+толуол». Описаны результаты изменения оптических и морфологических свойств растворов в зависимости от концентрации компонентов. Полученные результаты показывают возможность создания фуллеренсодержащих функциональных наноматериалов с заранее контролируемыми размером и физическими свойствами.

Ключевые слова: Фуллерен C_{60}, самосборка, показатель преломления, оптическая плотность, динамическое рассеяние света, гидродинамический диаметр.

FULLERENE C_{60} IN A HEXANE-TOLUENE SOLVENT SYSTEM: INFLUENCE OF COMPONENT CONCENTRATIONS

Annotation

In this work, the physical properties of solutions of C_{60} fullerene in binary mixtures of hexane+toluene solvents were studied using optical absorption spectroscopy, refractometry and dynamic light scattering. The results of changes in the optical and morphological properties of solutions depending on the concentration of components are described. The results obtained show the possibility of creating fullerene-containing functional nanomaterials with pre-controlled size and physical properties.

Key words: C_{60} fullerene, self-assembly, refractive index, optical density, dynamic light scattering, hydrodynamic diameter.

Kirish. Turli nanoo‘lchamli materiallar orasida uglerod nanomateriallari noyob optik, elektr, issiqlik va mexanik xususiyatlarga egaligi bilan ajralib turadi [1-2]. Hozirgi vaqtda uglerod nanozarrachalarining, xususan, C_n (n = 60, 70, …) fullerenlar eritmalarini o‘z-o‘zini tashkil etuvchi tizimlarning tabiiy modellari sifatida qaralishi fiziklar va kimyogarlarning e’tiborini tobora ko‘proq jalb qilmoqda [3-4]. Bir qator eksperimental ishlarda [5-10] eritma tayyorlashda ishlatiladigan erituvchilarning turi va miqdorini, erigan moddaning konsentratsiyasini va tashqi sharoitlarni (atrof-muhit harorati, eritma tayyorlash usuli va boshqalar) nazorat qilish orqali o‘z-o‘zini tashkil etuvchi tizimlarni boshqarish imkoniyati bor ekanligini ko‘rsatildi. Eritmalarda sintezlangan uglerod tarkibli nanoklasterlarning fizikaviy xususiyatlari ularning yakuniy geometrik o‘lchamlariga bog‘liq bo‘ladi va ularni tashkil etuvchi diametri ~0,7 nm bo‘lgan fulleren molekulalari xususiyatlaridan sezilarli darajada farq qiladi [11-12]. Fullerenlar molekulasi va erituvchilar o‘rtasida sodir bo‘ladigan o‘zaro ta’sir va agregatsiya jarayonlarini yaxshiroq tushunish fullerenlar asosida yangi nanomateriallarni yaratish uchun muhimdir. Hozirgi vaqtda fulleren nanomateriallari diodlar, tranzistorlar, quyosh fotoelementlari tayyorlashda [13-15], tibbiyot sohasida antioksidantlar sifatida [16-17], tribologiyada [18], yangi molekulyar tarmoqlarni yaratishda [19], shuningdek sensor texnologiyalarida [20] samarali foydalanilishi bilan ajralib turadi. Shu bilan birga, hozirgi vaqtda binar eritmalarda fulleren molekulalarining o‘z-o‘zini tashkil

qilishiga olib keladigan eritma ichidagi va tashqarisidagi molekulalararo (zarralararo) o‘zaro ta’sirlar haqidagi ko‘plab muhim savollar munozarali bo‘lib qolmoqda.

Ushbu ishning maqsadi fulleren C_{60} eritmalarining optik yutilish spektrlarini va sindirish ko‘rsatkichlarini eksperimental ravishda “geksan+toluol” erituvchilarning binar aralashmalarida turli konsentratsiyalarda o‘rganish, undan tashqari, yorug‘likning dinamik sochilishi (YDS) metodlari bilan C_{60} fulleren nanostrukturalarining o‘lchamlari va morfologik xususiyatlarini aniqlashdan iborat.

Tadqiqot metodi va reagentlar. Belgilangan konsentratsiyadagi C_{60} eritmalarini tayyorlash uchun oldindan aniq o‘lchangan C_{60} fulleren kukuni (tozaligi >99,8%, Sigma Aldrich, AQSH), geksan, toluol yoki geksan/toluol aralashmalari bo‘lgan shisha kolbaga qo‘shiladi. Olingan aralashma germetik yopilgan shisha kolbada xona haroratida 4 soatgacha vaqt davomida 2,2 Hz chastotada laboratoriya magnit aralashtirgichi “MS-11 H” (WIGO, Polsha) yordamida mexanik aralashtirish bilan eritildi.

Turli konsentratsiyali C_{60}/geksan va C_{60}/toluol/geksan tizimining nur sindirish ko‘rsatgichi yuqori aniqlikka ega (<0,0001) raqamli refraktometr PAL BX/RI (ATAGO, Yaponiya) yordamida o‘lchandi.

Tajribalarda C_{60} eritmalarining optik yutilish spektrlari o‘lchovlari spektral aniqligi ~0,1 nm bo‘lgan UV-2700 spektrofotometrida (Shimadzu, Yaponiya) olib borildi. C_{60}/geksan va C_{60}/toluol/geksan optik yutilish spektrlari ular tayyorlangandan so‘ng darhol olingan.

NanoSight LM10 (Malvern Instruments Ltd.) qurilmasida YDS usulidan foydalangan holda, C_{60} fulleren dispers fazasining eritmalardagi o‘rtacha gidrodinamik diametri (D_h) bo‘yicha taqsimlanish xarakteri o‘rganildi.

Natijalar va ularning muhokamasi. Komponentlar konsentratsiyasining o‘zgarishi bilan fulleren eritmalarining nur sindirish ko‘rsatgichining o‘zgarishi turli o‘lchamdagi klasterlarning yorug‘likka sezgirligi haqida tasavvur beradi, bu esa ma’lum bir sensorlar uchun nano o‘lchamdagi fulleren klasterlarini tanlashga yordam beradi. C_{60} fullerenning ikkita konsentratsiyasida (~10 va ~14 mg/dm^3) C_{60}/toluol/geksan eritmalarining nur sindirish ko‘rsatkichlarining (n) o‘lchangan eksperimental qiymatlari shuni ko‘rsatadiki, C_{60}/geksan/toluol eritmasida fulleren C_{60} kontsentratsiyasi ortishi bilan n ning qiymati oshib boradi. C_{60} konsentratsiyasi ~10 va ~14 mg/dm^3 bo‘lgan C_{60}/toluol eritmasida n ning qiymatlari mos ravishda 1,4907 va 1,4912 ni tashkil qiladi. Shu bilan birga, C_{60}/geksan eritmasida n ning qiymatlari C_{60} konsentratsiyasi ~10 mg/dm^3 dan ~14 mg/dm^3 gacha ortishi bilan 1,3671 dan 1,3682 gacha ortib borishi kuzatildi. Bunday o‘zgarishlar o‘rganilayotgan eritmalarda C_{60} kontsentratsiyasining oshishi bilan individual C_{60}–C_{60} molekulalarining o‘z-o‘zidan tashkillanish jarayonlari kuchayishi bilan bog‘liq. Bu esa yorug‘lik fotonlari bilan ko‘proq o‘zaro ta’sirga olib keladi, natijada eritmalarning nur sindirish ko‘rsatgichlari qiymatlari oshishiga sabab bo‘ladi.

1-rasmda C_{60}/geksan (nuqta-nuqta chiziq) va C_{60}/geksan/toluol (uzuq-uzuq chiziq va tutash chiziq) yangi tayyorlangan past konsentratsiyali eritmalarining ko‘zga ko‘rinadigan sohadagi optik yutilish spektrlari keltirilgan bo‘lib, bu eritmalarda C_{60} fullerenning konsentratsiyasi ~14 mg/dm^3. C_{60}/geksan eritmasida C_{60} ning quyidagi xarakterli yutilish sohalari yaqqol va zaif maksimumlar sifatida kuzatildi: ~404,35 nm, ~406,7 nm, ~535 nm, ~568 nm, ~590 nm, ~598 nm va ~620 nm (1-rasm, nuqta-nuqta chiziq). C_{60}/geksan/toluol eritmada toluolning mol ulushi oshishi bilan spektrning qisqa va uzun to‘lqinli qismlarida optik yutilish maksimumlarining amplitudalari ortishi, ~404,35 nm va ~406,7 nm ga mos keluvchi yutilish maksimumlari o‘zaro qo‘shilib ketishi, ~620 nm ga mos keluvchi yutilish maksimumining batoxromik siljishi (~3.2 nm ga) kuzatildi (1-rasm, uzuq-uzuq chiziq va tutash chiziq). Bu o‘zgarishlar bu jarayonda eritmada zaryad almashishi hisobiga C_{60}-C_{60} va C_{60}-erituvchi molekulalari o‘rtasida molekulalararo o‘zaro ta’sirlar qayta taqsimlanishini ko‘rsatadi.

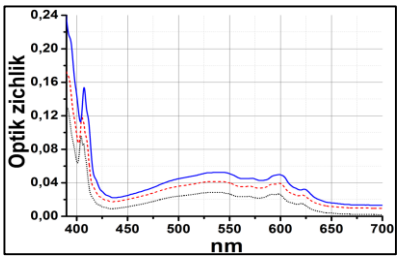

1-rasm. C_{60} fullerenning geksan/toluol aralashmalaridagi eritmalarida toluolning mol fraksiyalari (M) funksiyasi sifatida ko‘zga ko‘rinadigan sohadagi optik yutilish spektrlari: 0,00 (nuqta-nuqta chiziq), ~0,32 (uzuq-uzuq chiziq) va ~0,6 (tutash chiziq). C_{60} fullerenning konsentratsiyasi ~14 mg/dm^3.

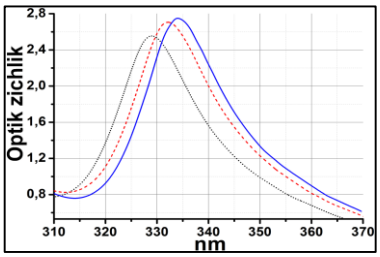

2-rasm. C_{60} fullerenning geksan/toluol aralashmalaridagi eritmalarida toluolning mol fraksiyalari (M) funksiyasi sifatida ~328,8 nm yutilish maksimumi o‘zgarishi: 0,00 (nuqta-nuqta chiziq), ~0,32 (uzuq-uzuq chiziq) va ~0,6 (tutash chiziq).

2-rasmda C_{60}/geksan (nuqta-nuqta chiziq) va C_{60}/geksan/toluol (uzuq-uzuq chiziq va tutash chiziq) eritmalarining ultrabinafsha sohadagi optik yutilish spektrlari keltirilgan bo‘lib, bu eritmalarda C_{60} fullerenning konsentratsiyasi ~14 mg/dm^3. Bu sohada C_{60}/geksan eritmasida fullerenning ~328,7 nm xarakterli yutilish maksimumi mavjud (2-rasm, nuqta-nuqta chiziq). Bu holda aralashmada toluolning molyar ulushi ortishi bilan geksandagi C_{60} spektriga nisbatan optik spektrlarida sezilarli o‘zgarishlar (solvatoxrom effekti) kuzatiladi. Xususan, eritmadagi toluolning ~0,6 M molyar ulushida ~328,7 nm xarakterli yutilish maksimumi intensivligi ortishi va uning ~4,8 nm ga batoxromik siljishi bir paytda kuzatildi (2-rasmga qarang). Bu o‘zgarishlar erituvchi almashtirilgandan so‘ng C_{60} molekulalarning asosiy holatiga nisbatan uyg‘otilgan elektron holatda π-elektronlarining zaryad taqsimotining sezilarli darajada farqlanishini ko‘rsatadi.

YDS metodi bo‘yicha tajriba o‘lchovlari C_{60}/geksan/toluol eritmasidagi molekulalarning o‘z-o‘zidan tashkillanishi natijasida sintez qilingan C_{60} nanoklasterlarining geometrik o‘lchamlari haqida qo‘shimcha ma’lumot beradi. 3-rasmda C_{60}/geksan/toluol eritmalarida C_{60} klasterlari o‘lchamlarining hajm bo‘yicha taqsimoti toluolning ~0,6 (*1*) va ~0,32 (*2*) mol fraktsiyalariga bog‘liq o‘zgarishlari keltirilgan. Ushbu eritmalarda C_{60} fullerenning konsentratsiyasi bir xil va u ~14 mg/dm^3 ga teng. Past konsentratsiyali C_{60} eritmasida C_{60} nanoklasterlarining gidrodinamik o‘lchamlari taqsimoti butun o‘lcham oralig‘ida monomodal cho‘qqi ekanligi ko‘rinib turibdi. C_{60}/geksan/toluol eritmalarida sintez qilingan C_{60} nanoklasterlari gidrodinamik

diametri eritmadagi toluol miqdori ortishi bilan kamayadi. C_{60}/geksan/toluol eritmasida toluol ulushi ~0,6 M bo‘lganda, eritmada sintezlangan nanoklasterlarning maksimal diametri ~8,23 nm ga teng bo‘lsa, toluol ulushi ~0,32 M bo‘lganda maksimal diametr ~10,36 nm ga tengligi ko‘rinib turibdi (3-rasm). Toluol mol fraksiyasi ~0,6 M bo‘lgan C_{60}/geksan/toluol eritmasida fulleren nanoklasterlari gidrodinamik diametrlari taqsimlanishi ~3,35÷13,92 nm o‘lcham oralig‘ida, ~0,32 M molyar fraktsiyasida nanoklasterlar gidrodinamik diametrlari ~5,1 nm dan ~18,8 nm gacha kengroq taqsimlanadi. C_{60}/geksan/toluol muhitida sintezlangan C_{60} klasterlarining o‘lcham xususiyatlaridagi bunday keskin farqlar C_{60} molekulalarining o‘z-o‘zidan tashkillanish xarakterini aniqlashda ishlatiladigan erituvchi rolini ko‘rsatadi. Bu holda taxmin qilish mumkinki, tizimdagi toluol miqdori ortishi bilan C_{60} fulleren molekulalari eritmada yaxshi eruvchanlikka moyil bo‘ladi va nanoklasterlar o‘lchami kamayadi.

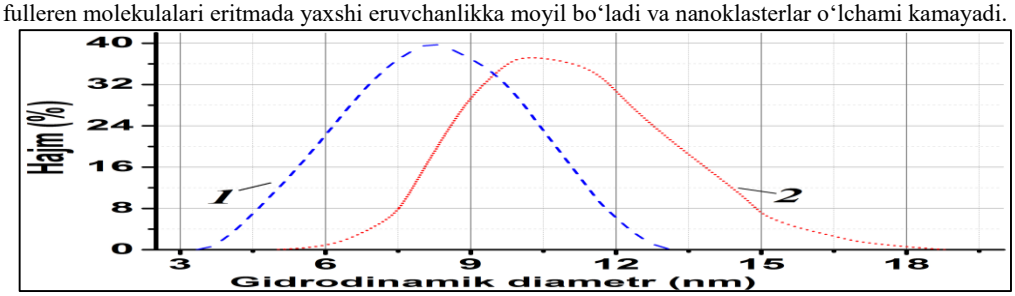

3-rasm. C_{60}/geksan/toluol eritmasida sintez qilingan C_{60} nanoklasterlarining o‘lchamlari taqsimoti toluolning turli mol fraksiyalarida (M): ~0,6 (*1*) va ~0,32 (*2*). Eritmalarda C_{60} fullerenning konsentratsiyasi ~14 mg/dm^3.

Xulosa. C_{60} fullerenning “geksan+toluol” binar aralashmasidagi yangi tayyorlangan eritmalarining sindirish ko‘rsatkichi qiymatlari o‘zgarishlarining “C_{60}-C_{60}” va “C_{60}-erituvchi” molekulalararo o‘zaro ta’sir darajalariga bog‘liqligi refraktometriya metodida tadqiq qilindi. Eritmalarda toluolning ulushi kamayishi va C_{60} konsentratsiyasining oshishi “C_{60}-C_{60}” molekulalararo o‘zaro ta’sirlar “C_{60}-erituvchi” o‘zaro ta’sirlardan kuchli bo’lishiga olib kelishi va eritma nur sindirish ko‘rsatkich qiymatlarining oshishiga sabab bo’lishi aniqlandi.

Tajribalarda C_{60} eritmalarining optik yutilish spektral o‘lchovlari aralashmada toluolning molyar ulushi ortishi bilan geksandagi C_{60} spektriga nisbatan optik spektrlarida sezilarli o‘zgarishlar (solvatoxrom effekti) kuzatiladi. Bu o‘zgarishlar erituvchi almashtirilgandan so‘ng C_{60} molekulalarning asosiy holatiga nisbatan uyg‘otilgan elektron holatda π-elektronlarining zaryad taqsimotining sezilarli darajada farqlanishini ko‘rsatadi.

YDS metodi yordamida C_{60}/geksan/toluol eritmasida toluol ulushining oshishi erigan modda va erituvchi o‘rtasidagi ta’sirga sezilarli o‘zgarishlarga olib kelishi, eritmada sintezlangan fulleren zarralari qayta tashkillanishi hisobiga nanoagregatlarining maksimal geometrik o‘lchami kamayishi o’rnatidi.

Ushbu ish O‘zbekiston Respublikasi Fanlar akademiyasining fundamental tadqiqotlar jamg‘armasi moliyaviy ko‘magida amalga oshirildi: “Suyuq sistemalarda organik nanoo'lchamli materiallarning o'z-o'zidan tashkillanish yarayonlarining fizik qonuniyatlarini tadqiq etish”.

ADABIYOTLAR

1. D. Jariwala, V.K. Sangwan, L.J. Lauhon, T.J. Marks, M.C. Hersam, Chemical Society Reviews, 42 (№7), 2824-2860 (2013).
2. Z. Li, L. Dev, Y. Li, Y. Feng, Chinese Journal of Aeronautics, 179, 1215–1221 (2019).
3. U.K. Makhmanov, S.A. Esanov, D.T. Sidigaliyev, K.N. Musurmonov, B.A. Aslonov, T.A. Chuliev, Liquids, 3, 385-392 (2023).
4. O.A. Kyzyma, Ukr. J. Phys., 65, 761–767 (2020).
5. U.K. Makhmanov, S.A. Esanov, B. Aslonov, Z. Bekmurodov, K. Musurmonov, D. Sidigaliyev, A. Shukurov, Узбекский физический журнал, 25 (№2), 30-34 (2023).
6. P.V. Lebedev-Stepanov, R.M. Kadushnikov, S.P. Molchanov, A.A. Ivanov, V.P. Mitrokhin, K.O. Vlasov, M. Alfimov, Nanotechnologies in Russia, 8, 137-162 (2013).
A. Kumar, A. Srivastava, I.Y. Galaev, B. Mattiasson, Progress in polymer science, 32 (№10), 1205-1237 (2007).
7. U.K. Makhmanov, A.M. Kokhkharov, S.A. Bakhramov, S.A. Esanov, D. Erts, Fullerenes, Nanotubes and Carbon Nanostructures, 30, (№ 1), 80-84 (2022).
8. T. Guo, P. Nikolaev, A.G. Rinzler, D. Tomanek, D.T. Colbert, R.E. Smalley, The Journal of Physical Chemistry, 99 (№27), 10694-10697 (1995).
9. L. Jinrui, C. Mengjun, Z. Shengju, L. Hongguang, H. Jingcheng, Chemical Society Reviews, 51 (№8) 3226-3242 (2022).
10. Y. Zhuo, D. Zhong, H. Miaoa, X. Yang, RSC Advances, 5 (№.41), 32669-32674 (2015).
11. C.L.Cheung, A. Kurtz, H. Park, C.M. Lieber, The Journal of Physical Chemistry, 106 (№10), 2429-2433 (2002).
12. D. Mi, Journal of nanoscience and nanotechnology, 14 (№2), 1064-1084 (2014).
13. J. Liu, L. Qiu, S. Shao, Journal of Materials Chemistry, 9 (№45), 16143-16163 (2021).
14. J.R. Pinzon, A. Villalta-Cerdas, L. Echegoyen, Curr Chem, 127–174 (2012).
15. H. Kazemzoda, M. Mozafari, Drug Discovery Today, 24 (№3), 898-905 (2019).
16. M.J. Axtar, M. Ahamed, H.A. Alhadlaq, A. Alshamsan, Biochimica et Biophysica Acta (BBA)-General Subjects, 1861 (№4), 802-813 (2017).
17. W. Zhai, N. Srikanth, L.B. Kong, K. Zhou, Carbon, 119, 150-171 (2017).
18. S.G. Radhakrishnan, D.M. Guldi, E.M. Perez, I. Perez, M. Bietti, N. Martin, Advanced Materials, 22 (№38) 4220-4248 (2010).
19. N.P. Shetti, A. Mishra, S. Basu, T.M. Aminabxavi, Materials Today Chemistry, 20, 100454 (2021).

O‘ZBEKISTON MILLIY UNIVERSITETI XABARLARI, 2024, [3/1/1]
ISSN 2181-7324

FIZIKA
http://journals.nuu.uz
Natural sciences

UDK: 530.12:531.51

Dilmurod ORTIQBOYEV,
Teacher at Presidential school in Gulistan,
E-mail: artdima93@gmail.com
Pahlavon YOVQOCHEV,
Master student at National University of Uzbekistan
Tolibjon IBROKHIMOV,
Master student at National University of Uzbekistan
Vakhid KHAMIDOV,
Associate Professor at Tashkent University of Information Technologies, PhD

Ulug'bek Institute of Astronomy, PhD based on the review by A.A. Abdujabbarov

GRAVITATIONAL LENSING IN JANIS-NEWMAN-WINICOUR SPACETIME IN PLASMA

Annotation

The Janis-Newman-Winicour (JNW) metric represents a comprehensive static spherically symmetric solution to the Einstein massless scalar equations, introducing an additional parameter ν. This metric encompasses the Schwarzschild metric as a special case. Notably, it features a globally naked strong curvature singularity. We investigate the weak-field lensing effects caused by JNW spacetime naked singularities surrounded by plasma, considering three distribution scenarios: uniform, singular isothermal spheres.

Key words: Gravitational lensing (GL), General relativity,Event Horizon Telescope Collaboration, Supermassive black hole, Kerr metric, Naked singularity, Janis-Newman-Winicour (JNW) spacetime, Reissner-Nordström naked singularity, Light propagation,Weak lensing.

ГРАВИТАЦИОННОЕ ЛИНЗИРОВАНИЕ В ПЛАЗМЕ В ПРОСТРАНСТВЕ-ВРЕМЕНИ ДЖЕНИСА-НЬЮМЕНА-ВИНИКУРА

Аннотация

Метрика Яниса-Ньюмана-Виникура (JNW) представляет собой комплексное статическое сферически симметричное решение безмассовых скалярных уравнений Эйнштейна, вводя дополнительный параметр n. Эта метрика включает в себя метрику Шварцшильда как особый случай. Примечательно, что он имеет глобально обнаженную сингулярность сильной кривизны. Мы исследуем эффекты линзирования слабого поля, вызванные голыми сингулярностями пространства-времени JNW, окруженными плазмой, рассматривая три сценария распределения: однородные, сингулярные изотермические сферы.

Ключевые слова: гравитационное линзирование (ГЛ), общая теория относительности, сотрудничество с телескопами горизонта событий, сверхмассивная черная дыра, метрика керра, голая сингулярность, пространство-время дженисаньюмана-виникура (JNW), обнаженная сингулярность рейсснера-нордстрема, свет. распространение, слабое линзирование.

PLAZMADAGI JANIS-NYYMEN-VINİKUR KOMOV VAQTIDA GRAVITASYONLI LEZONLASH

Annotation

Janis-Nyuman-Vinikur (JNW) metrikasi Eynshteynning massasiz skalyar tenglamalarining keng qamrovli statik sferik simmetrik yechimini ifodalaydi va qo'shimcha n parametrini kiritadi. Ushbu ko'rsatkich Shvartsshild ko'rsatkichini alohida holat sifatida o'z ichiga oladi. Shunisi e'tiborga loyiqki, u global yalang'och kuchli egrilik o'ziga xosligi bilan ajralib turadi. Plazma bilan o'ralgan JNW fazoviy vaqtning o'ziga xosligi tufayli yuzaga keladigan zaif maydonli linzalash effektlarini uchta taqsimlash stsenariysini ko'rib chiqamiz: bir xil, yagona izotermik.

Kalit so‘zlar: Gravitatsion linzalash (GL), Umumiy nisbiylik, Voqea gorizonti teleskopi bilan hamkorlik, Supermassiv qora tuynuk, Kerr metrikasi, Yalang‘och singularlik, Janis-Nyuman-Vinikur (JNW) fazoviy vaqt, Reissner-Nordströmsikulyarlik, yalang‘ochlik tarqalish, zaif linzalash.

Introduction. Gravitational lensing (GL) is a phenomenon predicted by general relativity, where light bends in a gravitational field, producing multiple images of a single source. GL offers valuable insights into astrophysical phenomena and the Universe's geometry, serving as a tool to study gravity's strong-field aspects and detect exotic objects[1–4]. Recent observations of the shadow image of the supermassive black hole M87* have highlighted GL's significance[5–7]. Early work by Synge initiated investigations into GL and plasma effects[8], further advanced by Perlick and Bisnovatyi-Kogan & Tsupko, which expanded to include rotational aspects and shadows of black holes[11–17]. Studies have also analyzed plasma's influence on photon trajectories around compact gravitating objects[17].

Weak-field lensing in the presence of plasma. We are intrigued by a solution to the Einstein equations that satisfies the criteria of being static, spherically symmetric, and asymptotically flat, while incorporating a massless scalar field as the energy-momentum source, as proposed by JNW. This solution, known as the JNW solution, depicts a spherically symmetric gravitational field that seamlessly transitions into the exterior Schwarzschild spacetime. The JNW metric arises as a solution to the Einstein-massless scalar field equations.

$$\mathcal{R}_{\mu\nu} = 2\nabla_\mu\phi\nabla_\nu\phi, \quad \nabla_\mu\nabla^\mu\phi = 0 \qquad (1)$$

It is described by the metric

$$ds^2 = -F^\nu dt^2 + F^{-\nu}dr^2 + r^2F^{1-\nu}(d\theta^2 + \sin^2\theta\, d\phi^2). \quad (2)$$

where the lapse function F and the scalar field Φ, respectively read

$$F = \left(1 - \frac{r_g}{r}\right) \text{ and } \Phi = \left(\frac{1-\nu^2}{2}\right)\ln F \qquad (3)$$

The JNW solution is governed by two parameters ν and r_g are, respectively, given by

$$\nu = \frac{2M}{r_g} \text{ and } r_g = 2\sqrt{M^2 + q^2} \qquad (4)$$

Here, M and q are, respectively, the ADM mass and scalar charge of the compact object. The parameter lies in the range $0 \le \nu \le 1$. The range of the radial coordinate is given by $r_g < r < \infty$.

When the scalar field is zero $q = 0$, the solution should reduce to the Schwarzschild solution, which happens when $\nu = 1$ or the JNW solution differs from the Schwarzschild solution for $q \neq 0$. The JNWsolution, for non-trivial scalar fields, does not possess an event horizon and describes a naked curvature singularity located at radial distance at $r = r_g$ when $\nu < 1$ which could be globally naked as it can be visible to distant observers not being covered by a horizon. Thus, an introduction of the static scalar field in the Schwarzschild black hole becaomes a JNW spacetime containing a naked singularity, and the event horizon or coordinate singularity at $r = r_g$ is then deformed into a naked singularity. The Stress-tensor for the JNW metric is

$$T_{\nu\mu} = diag[-\rho, P_1, P_2, P_3]. \qquad (5)$$

where [3]

$$\rho = -P_1 = P_2 = P_3 = \frac{r_q^2(1-\nu^2)\left(1-\frac{r_g}{r}\right)^\nu}{r^2\left(r-r_g\right)^2} \qquad (6)$$

The JNW spacetime satisfies the weak energy condition and it has a globally naked strong curvature singularity $r = r_g$ for $q \neq 0$. Next, we use a more general approach and derive the deflection angle for the photon moving in a weak gravitational field, in the JNW metric (2), in the arbitrary inhomogeneous plasma [13,14]. In the JNW spacetime (2), the metric tensor $g_{\alpha\beta}$ is independent of the time. We assume that the gravitational field is weak, hence we have

$$g_{\alpha\beta} = \eta_{\alpha\beta} + h_{\alpha\beta}$$

where $\eta_{\alpha\beta}$ and $h_{\alpha\beta}$, respectively, refer to the Minkowski metric and a perturbation metric.

$$\eta_{\alpha\beta} = diag(-1,1,1,1),$$

$h_{\alpha\beta} \ll 1$, $h_{\alpha\beta} \to 0$ under $x^\alpha \to \infty$.

$$g^{\alpha\beta} = \eta^{\alpha\beta} - h^{\alpha\beta}, \quad h^{\alpha\beta} = h_{\alpha\beta}. \qquad (8)$$

Now, we consider the distribution of plasma surrounds the mass M, located at the origin and that the spacetime is filled with a static inhomogeneous plasma whose electron plasma frequency ω_e is a function of the radius coordinate only

$$\omega_e = \frac{4\pi e^2}{m_e}N_p \qquad (9)$$

in terms of the electric charge e and the number density N_p. m is the electron mass. The refraction index n of this plasma is

$$n^2 = 1 - \frac{\omega_e^2}{\omega^2} \qquad (10)$$

We describe photon paths through the plasma in the JNW spacetime by the Hamiltonian in the geometric optics limit described by

$$H(x^\alpha, \boldsymbol{p}_\alpha) = \frac{1}{2}\left[g^{\alpha\beta}\boldsymbol{p}_\alpha\boldsymbol{p}_\beta - (n^2-1)\left(\boldsymbol{p}^0\sqrt{-g_{00}}\right)^2\right]. \qquad (11)$$

The paths of light rays are then described

$$\frac{dx^\alpha}{d\lambda} = \frac{\partial H}{\partial \boldsymbol{p}_\alpha},$$
$$\frac{d\boldsymbol{p}_\alpha}{d\lambda} = \frac{\partial H}{\partial x^\alpha},$$

where λ is the affine parameter. The plasma has an index of refraction $n = n(x^\alpha, \omega)$, where the photon frequency is ω, and p_α the linear momentum of the photon. Let us assume that ω_e be the plasma frequency in terms of the electron charge e and number density N_p, it depends on the spatial coordinates x^μ because of the gravitational field. In order to proceed further we assume refractive index is of the form [8,13]

$$n^2 = 1 - \frac{\omega_e^2}{[\omega(x^i)]^2}, \quad \omega_e^2 = \frac{4\pi e^2 N(x^i)}{m} = K_e N(x^i). \qquad (12)$$

The validity of the inequality, $\omega^2 > \omega_e^2$ is important for the propagation of light through the plasma medium. We can assume photon moving along the z-axis and take in the null approximations [13] a in curved spacetime in an inhomogeneous plasma. The photon will move along the curved trajectory because of the curved spacetime metric and plasma inhomogeneity. We use the approximation in which deviations of the photon trajectory from the straight line are small [8] and hence

$$\boldsymbol{p}^0 = \left(\frac{\hbar\omega}{c}, 0, 0, \frac{n\hbar\omega}{c}\right), \qquad \boldsymbol{p}_\alpha = \left(-\frac{\hbar\omega}{c}, 0, 0, \frac{n\hbar\omega}{c}\right) \qquad (14)$$

Henceforth, for definitences we utilize the following notations

$$\omega(\infty) = \omega, \qquad \omega_e(\infty) = \omega_0, \qquad n(\infty) = \sqrt{1 - \frac{\omega_0^2}{\omega^2}} = n.$$

Since we are considering a diagonal metric therefore the components of the metric tensor $g_{\alpha\beta}$ dissolves for all $\alpha \neq \beta$. On using Eqs.(11) and (12), yields the following equations of motion

$$\frac{dx^i}{d\lambda} = g^{ij}\boldsymbol{p}_j. \quad (15)$$

$$\frac{d\boldsymbol{p}_i}{d\lambda} = -\frac{1}{2}g_{,i}^{lm}\boldsymbol{p}_l\boldsymbol{p}_m - \frac{1}{2}g_{,i}^{00}\boldsymbol{p}_0^2 - \frac{1}{2}\frac{\hbar^2}{c^2}K_eN,i\,. \quad i = 1,2. \qquad (19)$$

We consider only those components of the unit vector perpendicular to the initial direction of propagation [13] since the motion takes place only along the z-axis. The deflection angle, in a weak gravitational field (18), appears as $\hat{a} = \boldsymbol{u}_{+\infty} - \boldsymbol{u}_{-\infty}$. Hence, The deflection angle of the photon moving from infinity to the central object and then to infinity reads

$$\hat{a} = \frac{1}{2}\int_{-\infty}^{+\infty}\left(h_{33,i} + \frac{\omega^2}{\omega^2-\omega_e^2}h_{00,i} - \frac{K_e}{\omega^2-\omega_e^2}N,i\right)dz \qquad (20)$$

Thus, the deflection angle α_i could be $-ve$ or $+ve$, respectively, according to the deflection of light towards or away w.r.t. spacetime.

Gravitational lensing in JNW metric. Next, we analyse the deflection angle for a photon moving in the plasmamedium for the JNWmetric (2)We take the series expansion of f up to $O(r_g^2)$ for the weak field regime and we use $\frac{r_g}{r} >> \left(\frac{r_g}{r}\right)^2$, in additional, the JNW metric (2) takes the form

$$ds^2 = ds_0^2 + \frac{\nu r_g}{r}(dt^2 + dr^2) + (\nu-1)r_g r(d\theta^2 + \sin^2\theta\, d\phi^2) \qquad (21)$$

with $ds_0^2 = -dt^2 + dr^2 + r^2(d\theta^2 + \sin^2\theta\, d\phi^2)$. The components $h_{\alpha\beta}$ in Cartesian coordinates, reads

$$h_{00} = \frac{\nu r_g}{r},$$

$$h_{11} = \frac{(4\nu - 3 - \cos 2\theta + \cos 2\phi \sin^2\theta)r_g}{4r},$$

$$h_{22} = \frac{(4\nu - 3 - \cos 2\theta + \cos 2\phi \sin^2\theta)r_g}{4r},$$

$$h_{33} = \frac{(2\nu - 1 + \cos 2\theta)r_g}{2r},$$

$$h_{12} = \frac{\sin^2\theta \sin 2\phi\, r_g}{2r},$$

$$h_{13} = \frac{\cos\phi \sin 2\phi\, r_g}{r},$$

$$h_{23} = \frac{\sin 2\theta \sin\phi\, r_g}{r}.$$

where $r = \sqrt{b^2 + z^2}$ and $cos\,\theta = z/r$ are introduced in [13], and b is the impact parameter of photon’s orbit. From the general equation (20) of the deflection angle, we can determine the deflection angle of light relative to the impact parameter b for a black hole in the presence of a plasma medium

$$\hat{a}_b = \int_{-\infty}^{+\infty}\frac{b}{2r}\left[\partial_r\left(\frac{(2\nu - 1 + \cos 2\theta)r_g}{2r}\right) + \partial_r\left(\frac{\nu r_g}{r}\right)\frac{\omega^2}{\omega^2-\omega_e^2}\partial_r N\right]dz\,. \qquad (22)$$

The formula (22) allows us to calculate the deflection angle of the photonmoving in the JNWspacetime in the presence of a spherically symmetric distribution of plasma for both inhomogeneous and homogeneous plasma and depends on the photon frequency.

a. *Uniform plasma* In a homogeneous plasma with $\omega_e^2 = const$, the refractive index does not explicitly depend on the space coordinates, so refractive action is absent, i.e., $\partial_r N$ vanish for a homogeneous plasma, and from the equation (22), one can compute the deflection angle of light in a uniform plasma as

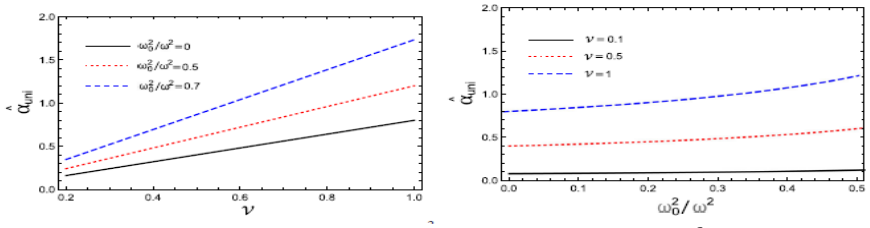

Fig. 1 The dependence of the parameter ν and surrounding plasma parameter $\frac{\omega_0^2}{\omega^2}$on the deflection angle with a fixed impact parameter $b = 5$

$$\hat{a}_{uni} = \frac{\nu r_g}{b}\left[1 + \frac{1}{1 - \frac{\omega_0^2}{\omega^2}}\right]. \qquad (23)$$

The most exciting result following our calculation is that even in a homogeneous or uniform plasma, the photon deflection angle differs from the vacuum case and depends on the plasma and photon frequency. The formula (23) holds when $\omega > \omega_0$ as the waves with $\omega < \omega_0$ do not propagate in the plasma. In the limit $\omega \to \omega_0$, the gravitational deflection in plasma can be much larger than in the vacuum We have shown the influence of the plasma parameter and the JNV ν parameter on the

angle of light deflection around the central object in the Fig. 1. It is clear that as the parameter ν decreases, the deflection angle also increases.

b. *Singular Isothermal sphere* Here,we consider situations of lensing with a non uniform plasma distribution. Indeed, we consider a model non-uniform plasma medium of a singular isothermal sphere (SIS) which is frequently used in the lens modelling of galaxies and clusters of galaxies. The SIS density distribution can be written as

$$\rho(r) = \frac{\sigma_v^2}{2\pi r^2}, \qquad (25)$$

where σ_v^2 corresponds to a 1-dimensional velocity dipersion which can be for stars in galaxies. The concentration of plasma medium reads

$$N(r) = \frac{\rho(r)}{\kappa m_p}, \qquad (26)$$

where κ is a dimensionless constant coefficient may correspond to the dark matter contribution to the Universe and *mp* is the proton mass [13]. On using Eqs.(12),(25) and (26), the plasma frequency takes the form

$$\hat{a}_{SIS} = \frac{2\nu r_g}{b} + \frac{r^2\omega_c^2}{b^2\omega^2}\left(\frac{1}{2} - \frac{2\nu r_g}{3\pi b}\right). \qquad (28)$$

Thus, we have obtained correction to the gravitational deflection due to the plasma. Here, we introduced a new plasma frequency ω_c^2 for SIS to simplify below

Fig. 2 The dependence of the parameter ν and surrounding plasma parameter $\frac{\omega_c^2}{\omega^2}$on the deflection angle with a fixed

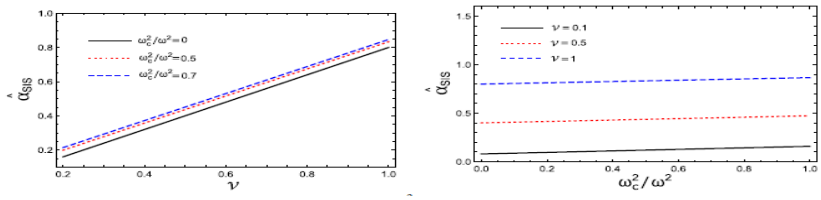

impact parameter $b = 5$

$$\omega_c^2 = \frac{\sigma_v^2 K_e}{2\kappa m_p R_s^2}. \qquad (29)$$

Conlusions. We examined light propagation around JNW naked singularities and its interaction with plasma. Three scenarios, including uniform plasma and singular isothermal sphere (SIS), were explored to estimate light deflection angles under weak conditions. Key findings include:

Exact expressions for deflection angles in weak gravitational lensing around JNW naked singularities with plasma were derived.

The influence of plasma on deflection angles in JNW spacetime was analyzed for various ν values, showing a decrease with decreasing JNW parameter and an increase with plasma presence.

Calculations included models with non-uniform plasma distributions, like SIS within JNW naked singularities' backdrop.

REFERENCES

1. K.S. Virbhadra, Phys. Rev. D **79**, 083004 (2009). http://arxiv.org/abs/0810.2109 [gr-qc]
2. K.S. Virbhadra, C.R. Keeton, Phys. Rev. D **77**, 124014 (2008). http://arxiv.org/abs/0710.2333 [gr-qc]
3. K.S. Virbhadra, G.F. Ellis, Phys. Rev. D **65**, 103004 (2002)
4. K.S. Virbhadra, D. Narasimha, S.M. Chitre, Astron. Astrophys. **337**, 1 (1998). http://arxiv.org/abs/astro-ph/9801174 [astro-ph]
5. K. Akiyama, et al. (Event horizon telescope collaboration), Astrophys. J. **875**, L1 (2019a), http://arxiv.org/abs/1906.11238 [astro-ph.GA]
6. K. Akiyama, et al. (Event horizon telescope collaboration), Astrophys. J. **875**, L5 (2019b), http://arxiv.org/abs/1906.11242 [astro-ph.GA]
7. K. Akiyama and et al. (Event horizon telescope collaboration), Astrophys. J. **875**, L6 (2019c), http://arxiv.org/abs/1906.11243 [astro-ph.GA]
8. J.L. Synge, *Relativity: the general theory* (North-Holland, Amsterdam, 1960)
9. D.O. Muhleman, I.D. Johnston, Phys. Rev. Lett. **17**, 455 (1966)
10. D.O. Muhleman, R.D. Ekers, E.B. Fomalont, Phys. Rev. Lett. **24**, 1377 (1970)
11. V. Perlick, *Ray optics, fermat's principle, and applications to general relativity*, Vol. 61 (2000)
12. B.-K.G.S. Tsupko, O. Yu, Gravit. Cosmol. **184**, 15 (2009)
13. G.S. Bisnovatyi-Kogan, O.Y. Tsupko, Mon. Not. R. Astron. Soc. **404**, 1790 (2010)
14. V. Morozova, B. Ahmedov, A. Tursunov, Astrophys. Space. Sci. **346**, 513 (2013)
15. G.Z. Babar, A.Z. Babar, F. Atamurotov, Eur. Phys. J. C. **80**, 761 (2020)
16. V. Perlick, O.Y. Tsupko, G.S. Bisnovatyi-Kogan, Phys. Rev. D. **92**, 104031 (2015). http://arxiv.org/abs/1507.04217 [gr-qc]
17. V. Perlick, O.Y. Tsupko, Phys. Rev. D. **95**, 104003 (2017). http://arxiv.org/abs/1702.08768 [gr-qc]

O‘ZBEKISTON MILLIY UNIVERSITETI XABARLARI, 2024, [3/1/1]
ISSN 2181-7324

FIZIKA
http://journals.nuu.uz
Natural sciences

UDK: 520.16

Dilshod RAUPOV,
O`zR FA Astronomiya instituti katta ilmiy xodimi
E-mail:dilshod@astrin.uz
Sabit ILYASOV,
O`zR FA Astronomiya instituti laboratoriya mudiri, f.m-f.d
E-mail:ilyasov@astrin.uz

“TIQXMMI” qoshidagi FATI bosh ilmiy hodimi, f.m-f.d A.A.Abdujabbarov taqrizi asosida

RESULTS OF THE MONITORING OF THE AMOUNT OF PRECIPITATED WATER IN THE ATMOSPHERE OF THE SUFFA PLATEAU

Annotation

The results of measurements of the amount of precipitated water at the RT-70 Radio Astronomy Observatory on the Suffa Plateau (Uzbekistan, λ=65°26, ϕ=39°37, h=2500 m) are presented. Observations were carried out automatically every 11 minutes throughout the year, starting from January 2015 to November 2020 using the MIAP-2 measuring complex. Seasonal changes of the amount of precipitated water in the atmosphere are considered and statistical diagrams are constructed. The main result of the work is statistical data characterizing the astroclimate, allowing one to predict the possibility of radio astronomical observations in the transparency windows of the wavelength range.

Key words: interstellar atoms and molecules, ground-space communication, sounding, precipitated water.

SUFFA YASSITOG’I ATVOSFERASIDAGI CHO’KMA SUV MIQDORINING MONITORINGI NATIJALARI

Annotatsiya

Maqolada Suffa yassitog’da joylashgan RT-70 radioastronomiya observatoriyasida (O‘zbekiston, λ=65°26, ϕ=39°37, h=2500 m) cho‘kma suv miqdorini o‘lchash natijalari keltirilgan. Kuzatishlar 2015-yil yanvaridan 2020-yil noyabrigacha MIAP-2 o‘lchash majmuasi yordamida yil davomida har 11 daqiqada avtomatik ravishda amalga oshirildi. Atmosferadagi cho’kma suv miqdorining mavsumiy o'zgarishlari hisobga olindi va statistik diagrammalar tuzildi. Ishning asosiy natijasi astroiqlimni tavsiflovchi statistik ma'lumotlar bo'lib, to'lqin uzunligi diapazonining shaffof oynalarida radioastronomik kuzatishlarni prognoz qilish imkonini beradi.

Kalit so'zlar: yulduzlararo atomlar va molekulalar, yer-kosmos aloqasi, masofadan zondlash.

РЕЗУЛЬТАТЫ МОНИТОРИНГА КОЛИЧЕСТВА ОСАЖДЁННОЙ ВОДЫ НА ПЛАТО СУФФА

Аннотация

Представлены результаты измерений количества осаждённой воды в Радиоастрономической обсерватории РТ-70 на плато Суффа (Узбекистан, λ=65°26, ϕ=39°37, h=2500 м). Наблюдения проводились в автоматическом режиме в каждые 11 минут в течение года, начиная с января 2015 г. по ноябрь 2020 г., с помощью измерительного комплекса МИАП-2. Рассмотрены сезонные изменения количества осаждаемой воды в атмосфере и построены статистические диаграммы. Основным результатом работы являются статистические данные, характеризующие астроклимата, позволяющие прогнозировать возможность радиоастрономических наблюдений в окнах прозрачности диапазона длин волн.

Ключевые слова: межзвездные атомы и молекулы, наземно-космическая связь, дистанционное зондирование.

Введение. Известно, что наиболее перспективной областью спектра электромагнитных колебаний в решении фундаментальных проблем космологии, поиска и исследования органических молекул космического происхождения и других фундаментальных проблем астрофизики, а также решении прикладных задач, имеющих народно-хозяйственное значение, таких как наземно-космическая связь, дистанционное зондирование Земли, создание глобальной навигационной системы и многих других, является миллиметровый диапазон длин волн [1].

Преимущества миллиметрового диапазона в радиоастрономии помимо того, что доминирующим в этом диапазоне является реликтовое космологическое излучение, слабое рассеяние и поглощение радиоволн в космической плазме, богатый спектр вращательно-колебательных линий большинства межзвездных атомов и молекул, является возможность реализовать самое высокое угловое разрешение [2].

В последнее десятилетие, благодаря стремительному развитию техники сверхвысоких частот, созданию адаптивных радиотелескопов большой апертуры и возможности объединения их в систему наземных и наземно-космических интерферометров со сверхдлинными базами, появилась реальная возможность в полной мере реализовать преимущество миллиметрового диапазона в решении фундаментальных проблем космологии, а также в решении ряда прикладных задач на совершенно новом уровне [3].

Однако нестабильность многих параметров атмосферы Земли, благодаря как глобальная циркуляция, так и перемешивание атмосферных слоев и локальной турбулентности вызывают неоднородности земной поверхности и их влияние на прохождение электромагнитных волн микроволнового диапазона, исключают возможность построение универсальной радио модели атмосферы, необходимость постоянного наблюдения за состоянием атмосферы, в дополнение к использованию наблюдаемых параметров для решения фундаментальных проблем физики атмосферы и

продиктованы по экономической целесообразности, с точки зрения более эффективного использования больших (дорогих) радиотелескопов в реализации исследовательских программ [4].

Поэтому в настоящее время во всех крупных радио обсерваториях мира (в местах установки радиотелескопов) проводятся систематические наблюдения параметров атмосферы с использованием современных измерительных систем для накопления статистического материала для прогнозирования условии прохождения микроволнового излучения от космических объектов [5-9].

В данной работе мы представляем результаты мониторинга осаждаемой воды в атмосфере, проводимого на Плато Суффа, в период с января 2015 года по ноябрь 2020 г. с использованием измерительного комплекса МИАП-2.

Измерительная аппаратура. Измерительный комплекс состоит из двух независимых канала регистрации атмосферного поглощения в так называемых окнах прозрачности атмосферы Земли – 84-99 ГГц ($\lambda_{ср}$ = 3 мм) и 132-148 ГГц ($\lambda_{ср}$ = 2 мм), расположенных в общем корпусе с амплитудно-цифровым преобразователем (АЦП), устройства для сканирования зенитных углов от 0° (зенит) до 90° (горизонт) и рупорных антенн. Все радиометрическое оборудование установлено на единой платформе, с герметичный жесткий корпус из нержавеющей стали, обеспечивающий надежную защита от неблагоприятных погодных условий и имеет радиопрозрачное фторопластовое окно. Ширина луча рупорные антенны радиометра на половинном уровне мощности в оба диапазона составляют 2,5°. Строение и принцип работы комплекса МИАП-2 подробно описаны в [10,11]. Измерение полного вертикального поглощения радиоволн на указанных частотах осуществляется метод вертикальных сечений, основанный на измерении собственного теплового излучения атмосферы при различных углы над горизонтом (60,5°, 76,3°, 81,4°, 84,2°, 88,6°).

Последний угол находится как можно ближе к горизонту. метод реализуется путем сравнения приращений яркостные температуры двух участков атмосферы под разными зенитными углами с температурой рефренный регион. Эта область обычно используется как атмосферная излучения в направлении горизонта, если предположить, что яркостная температура атмосферы в направлении антенны близка к термодинамической температуре

приземный слой воздуха, а сама атмосфера изотермическая в горизонтальных координатах.

Расчетное значение атмосферного поглощения в зените, выражается в Неперах (1 Неп = 8,686 дБ), т. е. так называемая оптическая толщина атмосферы отображается на графике. Цикл регистрации длится около минуты. Возможность обеспечивается непрерывный контроль радио прозрачности. Как отмечалось выше, измерения параметров атмосферы на плато Суффа проводятся с января 2015 по ноябрь 2020 г. За этот период нами были получены более 250 000 значений параметров атмосферы. Результаты мониторинга параметров атмосферы представлены в [12].

Количество осаждённой воды. Основная проблема наблюдений на вышеуказанных радиодиапазонах для целей радиоастрономии и телекоммуникаций является значительное поглощение излучения атмосферными газами и, прежде всего, водяным паром [13]. Он подвержен значительным сезонными и суточными колебаниями, существенно зависящих от климата, рельефа и высотой над уровнем моря.

Наблюдения в двух окнах атмосферного поглощения позволяют рассчитать количество осаждённой воды по методу, представленному в работе [14], используя методы расчета удельного коэффициенты поглощения для данного радиометра, приведенные в работе [15]. Результаты расчетов количества осаждённой воды находятся отдельно для каждого канала, но в чистом времени они совпадают с точностью до погрешности измерения. Результат - среднее арифметическое между значениями для двух каналов в каждой точке время.

В качестве примера на рис. 1 показан временной ряд количества осаждённой воды, полученной на плато Суффа за 2015, 2017 и 2020 гг. Как видно из рисунка, среднее значение количества осаждённой воды остается стабильным.

Для визуального представления статистики атмосферных поглощения и тенденции его изменения, были выбраны времена года по принципу погодных условий: ноябрь, декабрь, январь и февраль относятся к зимнему сезону; переходный сезон включает март, апрель, сентябрь и октябрь, летний сезон - май, июнь, июль и август. В зимний сезон, среднее значение осажденной воды для диапазона 2 мм - 5,04 мм, а для диапазона 3 мм – 9,90 мм. В переходный сезон количество выпадающих осадков вода для диапазона 2 мм составляет 7,71 мм, а для диапазона 3 мм это 13,17 мм. В летний сезон – 7,29 мм на 2 мм диапазона, а для диапазона 3 мм – 13,17.

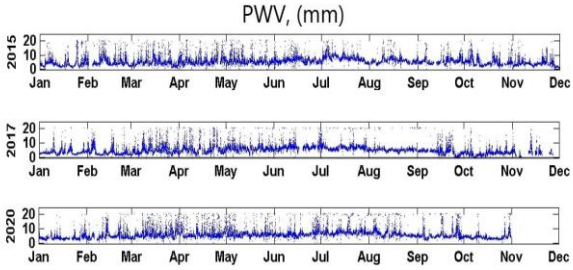

Рис. **1.** Временной ряд количества осаждённой воды, полученный на плато Суффа.

Известно, что облака не влияют на работу радиотелескоп кроме крайних сантиметров и миллиметровые диапазоны. Поскольку в данная работа посвящена измерениям в миллиметровом диапазоне нами были проанализированы данные радиоизмерений, полученных на абсолютно ясных и пасмурных дней. Зимой в ясные дни величина осаждённой воды всегда ниже на 30%, чем в пасмурные дни в 3 мм диапазоне, а 2 мм диапазоне – 35%.

Количество осаждённой воды при переходном периоде в пасмурные дни на 60% выше, чем в ясные дни для диапазона 2 мм, а для 3 мм диапазона – 57%. Летом в пасмурные дни значение осаждаемой воды всегда на 31% выше, чем в ясные дни в 2 мм диапазоне и 46% в 3 мм диапазоне.

Суточный ход осаждаемой воды в летний период более значителен, чем зимний. На некоторых ночи в декабре и январе количество осаждаемой воды опускается до минимума примерно на 2 мм, летом поднимается до 15 мм.

Заключение. На основе проведенных исследований можно сделать вывод, что за шестилетний период параметры атмосферы на плато Суффа остаются довольно стабильными. Значения, представленные здесь осаждаемой

воды соответствуют значениям всей толщи атмосферы в зените. Он может сводиться к значениям любого угла, а также экстраполироваться на любую высоту с учетом стандартной модели атмосферы.

ЛИТЕРАТУРА

1. Калмыков Ю.П., Титов С.В. Применение метода функций памяти для расчета вращательного спектра поглощения паров воды. Радиотехника и электроника, 1989, Т.33, №1. С.13-20
2. Артеменко Ю.Н., Бубнов Г.Н., Большаков О.С.Вдовин В.Ф., Данилевский Д.Б., Зинченко И.И., Никифоров П.Л., Носов В.И., Федосеев Л.И.,Шевцов А.А., Шанин Г.И., Узбекский физический журнал, 2014. №6, 421
3. Д.Б. Данилевский, А.И. Железнякова, Д.А. Раупов, Г.И. Шанин, Узбекский физический журнал, Т.18, № 1, 206-213 (2016).
4. Bubnov G.M., Artemenko Yu.N., Vdovin V.F., Danilevsky D.B., Zinchenko I.I., Nosov V.I., Nikiforov P.L., Shanin G.I., Raupov D.A. The Results of Astroclimate Observations in the Short-Wave Length Interval of the Millimeter-Wave Range on the Suffa Plateau // Radio physics and Quantum Electronics, 2017. V.59, Issue: 8-9, P. 763-771. DOI: 10.1007/s11141-017-9745-7
5. Radford, S. J. E., The Atacama Large Millimeter Array: Observing the Distant Universe, in Observing Dark Energy // ASP Conf. Ser. 339, eds. Wolff, S. C., & Lauer, T. R., (San Francisco: ASP, 2005, ISBN: 1-58381-206-7) P.177. Bibcode: 2005ASPC. 339.77R.
6. Radford, S. J. E. ALMA Site and Configurations // National Radio Science Meeting (Washington, D. C.: National Academy of Sciences), 2002, P. 364.
7. Calisse, P. G., Ashley, M. C. B., Burton, M. G., Phillips, M. A., Storey, J. W. V., Radford, S. J. E., & Peterson, J. B. Submillimeter site testing at Dome C // Antarctica in Third International Workshop on Astrophysics at Dome C, PASA , 2004, 21(3), P. 256 – 263. DOI: 10.1071/AS03018
8. Calisse, P. G., Ashley, M. C. B., Burton, M. G., Lawrence, J. S., Travouillon, T., Peterson, J. B. Phillips, M. A., Radford, S. J. E., & Storey, J. W. V., Dome C, Antarctica: The Best Accessible Sub-millimeter Site on the Planet? // The Dense Interstellar Medium in Galaxies, Springer Proceedings in Physics 91, ed. Pfalzner, S., Kramer, C., Staubmeier, C., & Heithausen, A., (Berlin: Springer, ISBN: 3-540-21254-X), 2004, P. 353. DOI: 10.1007/978-3-642-18902-9_64
9. Calisse, P. G., Ashley, M. C. B., Burton, M. G., Lawrence, J. R., Phillips, M. A., Storey, J. W. V., Peterson, J. B., & Radford, S. J. E. New Submillimeter Site Testing Results from Dome C, Antarctica // Astronomy in Antarctica, ed. Burton, M., Highlights of Astronomy, 13 = Astronomy in Antarctica, 25th GA of the IAU, SS 2, 18 July, 2003 in Sydney, Australia, meeting abstract, P.33.
10. Peterson, J. B., Radford, S. J. E., Ade, P. A. R., Chamberlin, R. A., O'Kelly, M. J., Peterson, K. M., & Schartman, E. Stability of the Submillimeter Brightness of the Atmosphere Above Mauna Kea, Chajnantor and the South Pole // PASP, 2003, V. 115, P. 383-388. DOI: 10.1086/368101
11. Артеменко Ю.Н., Бубнов Г.Н., Большаков О.С.Вдовин В.Ф., Данилевский Д.Б., Зинченко И.И., Никифоров П.Л., Носов В.И., Федосеев Л.И.,Шевцов А.А., Шанин Г.И., Узбекский физический журнал, 2014. №6, 421-423.
12. Raupov D, Ilyasov S, Shanin G //The results of atmospheric parameters measurements in the millimeter wavelength range on the radio astronomy observatory “Suffa Plateau” // Acto IMEKO, T.12, №2, P.1-5. DOI:10.21014/actaimeko.v12i2.1430
13. Zuev VE, Makushkin YS, Ponomarev YN (1987) Modern Problems of Atmospheric Optics. Atmospheric Spectroscopy Leningrad.
14. Liebe HJ, Rosenkranz PW, Hufford GA (1992) J Quant Spectrosc Radiat Transfer 48(5/6): 629.
15. Ulich BL (1980) Improved correction for millimeterwavelength atmospheric attenuation Astroph. Lett 21: 21.

O‘ZBEKISTON MILLIY UNIVERSITETI XABARLARI, 2024, [3/1/1]
ISSN 2181-7324

FIZIKA
http://journals.nuu.uz
Natural sciences

UDK: 530.12:531.51

Gulzoda RAKHIMOVA,
PhD Student at Tashkent State Technical University
E-mail: phisic_96@mail.ru
Alisher ABDUVOKHIDOV,
Teacher at Andijan State University
Vakhid KHAMIDOV,
Associate Professor at Tashkent University of Information Technologies, PhD

Ulug'bek Institute of Astronomy, based on the review by A. A. Abdujabbarov, PhD

PARTICLE DYNAMICS AROUND CHARGED ROTATING BLACK HOLE IN PERFECT FLUID DARK MATTER

Annotation

This paper is devoted to studying particle acceleration around charged rotating black holes surrounded by perfect fluid dark matter(PFDM) as medium. In the beginning, we discuss black hole(BH) horizons, ergosphere and inner stable circular orbits in the framework of PFDM. Next, we investigate the collision of particles in the vicinity of extremal and non-extremal BHs. It is found that in the non-extremal case E_{cm} energy can be finite for some values of charge Q in the presence of PFDM.
Key words: Horizons; Ergosphere; Particle acceleration.

ДИНАМИКА ЧАСТИЦ ВОКРУГ ЗАРЯЖЕННОЙ ВРАЩАЮЩЕЙСЯ ЧЕРНОЙ ДЫРЫ В ИДЕАЛЬНОЙ ЖИДКОЙ ТЕМНОЙ МАТЕРИИ

Аннотация

Данная статья посвящена исследованию ускорения частиц вокруг заряженных вращающихся черных дыр, окруженных идеальной жидкой темной материей (PFDM) в качестве среды. Вначале мы обсуждаем горизонты черных дыр (ЧД), эргосферу и внутренние стабильные круговые орбиты в рамках PFDM. Далее мы исследуем столкновение частиц вблизи экстремальных и неэкстремальных ЧД. Установлено, что в неэкстремальном случае энергия E_cm может быть конечной для некоторых значений заряда Q при наличии PFDM.
Ключевые слова: Горизонты; Эргосфера; Ускорение частиц.

MUKAMMAL SUYUQ QORA MATERIYADA ZARYADLI AYLANADIGAN QORA TUYNUK ATROFIDAGI ZARRACHALAR DINAMIKASI

Annotatsiya

Ushbu maqola vosita sifatida mukammal suyuqlik qora materiya (PFDM) bilan o'ralgan zaryadlangan aylanadigan qora tuynuklar atrofida zarrachalar tezlashishini o'rganishga bag'ishlangan. Boshida biz PFDM doirasida qora tuynuk (BH) gorizontlari, ergosfera va ichki barqaror dumaloq orbitalarni muhokama qilamiz. Keyinchalik, ekstremal va ekstremal bo'lmagan BHlar yaqinida zarrachalarning to'qnashuvini tekshiramiz. Aniqlanishicha, ekstremal bo'lmagan holatda E_cm energiya PFDM ishtirokida Q zaryadining ba'zi qiymatlari uchun chekli bo'lishi mumkin.
Kalit so'zlar: Ufqlar; Ergosfera; Zarrachalarning tezlashishi.

Introduction. Several experiments and observations reveal that normal matter constitutes only a small fraction (4%) of the Universe, with dark matter (~21%) and dark energy (~75%) comprising the majority[1][2]. While these new forms of matter are not directly observed, their presence is inferred through gravitational interactions. In the context of astrophysical processes around compact objects, the impact of dark energy is typically negligible, yet strong evidence supports the existence of dark matter around giant galaxies[3].

Understanding the effect of dark matter on various astrophysical processes around compact gravitating objects is a key challenge in modern relativistic astrophysics. Modifications to standard theory are often tested through experiments and observations, particularly by studying the dynamics of test particles around black hole (BH) horizons. Analyzing particle dynamics, including orbits, oscillations, and acceleration, provides valuable insights into gravity theories and their modifications[4-6].

Previous studies have investigated particle dynamics around compact objects with nonvanishing electric charge and/or magnetic dipole momentum in the presence of electromagnetic fields, offering insights into important physical processes[7-10]. Additionally, the Kerr BH exhibits intriguing features, such as its role in particle acceleration and the divergence of the center of mass energy of colliding particles at the event horizon of extreme rotating Kerr BH[11]. Studies exploring particle acceleration mechanisms and energetic processes around rotating BHs in modified or alternative theories of gravity contribute to our understanding of these phenomena[12-13].

The paper is organized as follows: In Sect. II we review the spacetime around rotating BH with electric charge and in the presence of perfect fluid dark matter. We consider the particle acceleration mechanism and explored the center of mass energy of colliding article around rotating charged BH surrounded by PFDM in Sect. III. We have concluded our results in Sect. IV. Throughout the work, we have used units that fix the speed of light and the gravitational constant via $8\pi G = c^4 = 1$.

Charged BH in perfect fluid dark matter. The action for the gravity theory minimally coupled with gauge field in PFDM reads as [14]

$$\mathcal{I} = \int dx^4\sqrt{-g}\left(\frac{1}{16\pi G}R + \frac{1}{4}F^{\mu\nu}F_{\mu\nu} + \mathcal{L}_{DM}\right)$$

Here, $g = \det(g_{ab})$ is the determinant of the metric tensor, R is the Ricci scalar, G is Newton's gravitational constant, $F_{\mu\nu} = \partial_\mu A_\nu - \partial_\nu A_\mu$($A_\mu$ is the gauge potential) is the Maxwell field strength and $\mathcal{L}_{DM}$ is the Lagrangian density for PFDM. Charged rotating BH in PFDM is [14]:

$$ds^2 = -\frac{1}{\rho^2}(\Delta - a^2\sin^2\theta)dt^2 + \frac{\rho^2}{\Delta}dr^2 + \rho^2 d\theta^2$$
$$-\frac{2a\sin^2\theta}{\rho^2}\left[2Mr - Q^2 - \gamma r\ln\left(\frac{r}{\gamma}\right)\right]dtd\phi$$
$$+\sin^2\theta\left[r^2 + a^2 + \frac{a^2\sin^2\theta}{\rho^2}(2Mr - Q^2\right.$$
$$\left.-\gamma r\ln\left(\frac{r}{\gamma}\right)\right)\Bigg]d\phi^2,$$

here Δ and ρ defined as

$$\Delta = r^2 + a^2 - 2Mr + Q^2 + \gamma r\ln\left(\frac{r}{\gamma}\right)$$
$$\rho^2 = r^2 + a^2\cos^2\theta$$

where M, a, Q and γ are the mass, rotational parameter, charge and PFDM parameter of the black hole, respectively.

On the other hand, the condition $g_{tt} = 0$ gives us two static limit surfaces: $r_{sls}^-$and r_{sls}^+. The region between r_{sls}^+ and r_h^+corresponds to the ergosphere region. With the help of numerical computation of $\Delta = 0$ and $g_{tt} = 0$ we can easily evaluate the horizon and static limit surfaces of the charged rotating BH in PFDM. The Fig. 1) shows the behavior of the regions of the horizon and ergosphere of the charged rotating BH in PFDM for non-extremal BH for different values of charge Q and spin parameter a at fixed PFDM parameter $\gamma = 0.1$. One can see from the plot that by increasing the charge Q gradually the regions of the ergosphere and horizon are converging and merging into one region, taking an almost spherical shape.

Particle acceleration near charged rotating BH in PFDM. This section is devoted to study the collision of two particles around charged rotating black hole in PFDM and energy extraction produced by the collision. We assume that the collision of particles occurs near the horizon of the charged rotating black hole. Furthermore, as the metric (2) is rotating black hole we consider two cases to evaluate the center-of mass energy E_{cm} produced by the collision: an extremal and non-extremal BHs.

A. Equation of motion and effective potential. Now our goal is to find the equation of motion and effective potential for a time-like particle around charged rotating black hole in PFDM. To achieve this, the simplest way is to use the constants of motions, such as P_t and P_ϕ :

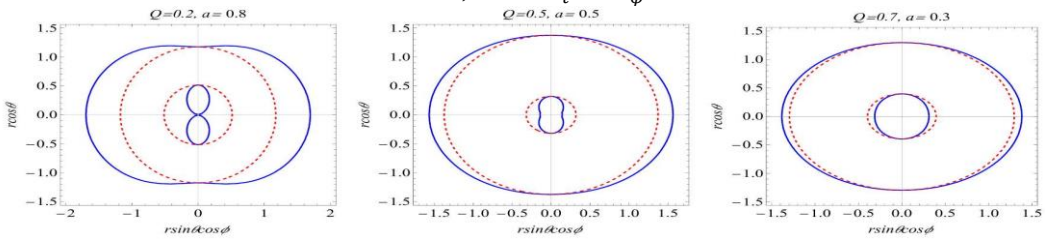

FIG. 1: The variation of the shape of ergosphere of the rotating charged non-extremal BH in PFDM for the fixed PFDM parameter $\gamma = 0.1$

$$P_t = g_{tt}\dot{t} + g_{t\phi}\dot{\phi} = -E$$
$$P_\phi = g_{\phi\phi}\dot{\phi} + g_{t\phi}\dot{t} = L$$

Here, E and L are the energy and the angular momentum of the particle, respectively. Let's consider the motion at $\theta = \pi/2$, which means that $\dot{\theta} = 0$. By utilizing the expressions for the generalized momenta of the particle (4) and the normalization condition $u_\mu u^\mu = -m^2$ we get the following equation of motion:

$$\dot{t} = \frac{1}{r^2}\left[\frac{(a^2 + r^2)}{\Delta}(E(a^2 + r^2) - aL) + a(L - aE)\right],$$
$$\dot{\phi} = \frac{1}{r^2}\left[\frac{a^2}{\Delta}(E(a^2 + r^2) - aL) + (L - aE)\right]$$
$$\dot{r} = \pm\frac{\sqrt{(aL - (a^2 + r^2)E)^2 - \Delta(m^2r^2 + (L - aE)^2)}}{r^2}$$

The + and - signs in the radial velocity $\dot{r}$ indicate the outgoing and incoming geodesics, respectively. It is useful to derive the expression for the effective potential in order to acquire more information about the character of the motion of the particle. With the help of (7) and the following expression:

$$\frac{1}{2}r^2 + V_{eff} = 0$$

it is not difficult to find the effective potential in the form:

$$V_{eff} = -\frac{(aL - (a^2 + r^2)E)^2 - \Delta(m_0^2r^2 + (L - aE)^2)}{2r^4}$$

By utilizing the expression for the effective potential V_{eff} we can easily determine the innermost stable circular orbit of the particle. The following conditions must be satisfied to evaluate the ISCO:

1.$V'_{eff}(r) = 0$
2.$V''_{eff}(r) = 0$

The dependence of the innermost stable circular orbits (ISCO) on parameters γ, and a at fixed value of charge $Q = 0.5$ is presented in the Fig. (2). The graph on the left hand-side illustrates the ISCO radius versus γ parameter for different values of the spin parameter a. It can be noticed that increase in the rotational parameter a leads to the decrease of the radius of ISCO when the charge Q and parameter γ are fixed. In addition, there is a gradual drop in the radius of ISCO with the grow of the γ. Meanwhile the second graph on the right hand-side illustrates the variation of ISCO with respect to a at fixed $Q = 0.5$ for various values of the parameter γ.

FIG. 2: The variation of the innermost stable circular orbits for PFDM parameter γ and rotating parameter a at fixed charge $Q = 0.5$

B. Collision of Particles Near Horizon. In this section we are aimed to determine the center-of-mass (CM) energy E_{cm} produced by the collision of two timelike particles around charged rotating black hole in PFDM. In our case, particles have the

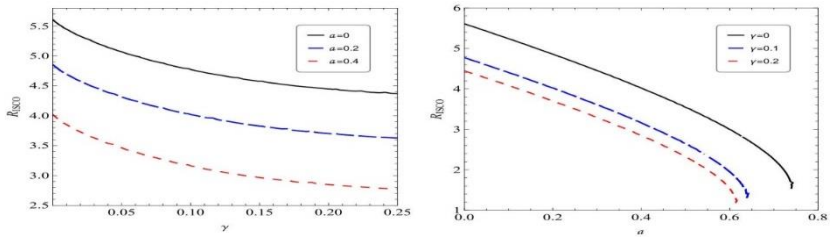

same mass $m_1 = m_2 = m_0$ but different four-velocities u_1 and u_2, respectively. The CM energy E_{cm} of collision between two particles at the radial coordinate r is given by the following expression: $E_{cm} = m_0\sqrt{2}\sqrt{1 - g_{\mu\nu}u_1^{\mu}u_2^{\nu}}$

By substituting (5-7) into the equation (10) we get the following expression:

$$\frac{\mathcal{E}_{cm}^2}{2} = -\frac{K}{r^2\Delta}$$

where $\mathcal{E}_{cm} = E_{cm}/m_0$ and K has the form:

$$K = (r^2 + a^2 - aL_1)(r^2 + a^2 - aL_2) + (r^2 - (a - L_1)(a - L_2)\Delta) - \sqrt{(r^2 + a^2 - aL_1)^2 - (m^2r^2 - (a - L_1)^2)\Delta}\sqrt{(r^2 + a^2 - aL_2)^2 - (m^2r^2 - (a - L_2)^2)\Delta}$$

In order to get the ultrahigh-energy we need the particle to approach the BH with the critical angular momentum L_{cr}. We can get the critical value of the angular momentum L_{cr} from the condition $\dot{t} \geq 0$ (see 5), when $r \longrightarrow r_h^E$. So, the expression for the critical angular momentum L_{cr} is:

$$L_{cr} = \frac{\left(a^2 + \left(r_h^E\right)^2\right)E}{a}$$

The limiting values of the angular momentum along with the corresponding spin parameters and the horizons for the extremal and nonextremal charged rotating BH in PFDM are presented in the Tab. (I) and Tab. (II), respectively. Fig. (3) illustrates the collision energy for an extremal BH at fixed PFDM parameter $\gamma = 0.2$ for different values of charge Q. In this case, the CM energy diverges sharply close to the region of the horizon. On the other hand, in Fig. (4) the collision energy diverges beyond the radius of the event horizon and maybe even finite at some values for Q.

TABLE I: Limiting cases for angular momentum for an extremal BH

Q	a_E	L_1	L_2
0.2	0.836371	-3.40392	1.53746
0.3	0.805926	-3.36789	1.53350
0.4	0.761261	-3.31489	1.53152
0.5	0.699655	-3.24148	1.53774
0.6	0.61605	-3.14123	1.56787
0.7	0.499517	-3.00021	1.67339
0.8	0.315463	-2.77392	1.94426

TABLE II: Limiting cases for angular momentum for a non-extremal BH

Q	a	r_-	r_+	L_1	L_2
0.2	0.8	0.537845	0.996355	-3.38472	1.82852
0.3	0.7	0.39476	1.14429	-3.31002	2.02628
0.4	0.6	0.331881	1.21029	-3.22286	2.13517
0.5	0.5	0.313006	1.23025	-3.12092	2.20061
0.6	0.4	0.331881	1.21029	-3.00059	2.23378
0.7	0.3	0.39476	1.14429	-2.85571	2.23662

0.8	0.2	0.537845	0.996355	-2.67415	2.20285

Conclusion. In this paper we have studied the particle acceleration around charged rotating black hole in PFDM.

We have investigated the horizons and ergosphere of the metric (2) and considered the effects of the PFDM parameter γ on the shapes of the horizon and ergosphere regions. As is shown, the γ parameter decreases both regions considerably.

We have also derived the equations of motion for the time-like particle and found the expression for the effective potential V_{eff} of the particle. Moreover, the effect of the γ parameter along with the spin parameter a and the charge Q of the black hole on the innermost stable circular orbits has been analysed and is shown in Fig. (1). It has been found that the ISCO radius is decreasing within the scope of all parameters (γ, Q, a).

We have also studied the collision of two particles with the same mass m near the horizon of the charged rotating BH in PFDM. For this, we have analysed two cases of the black hole: extremal and non-extremal. We have evaluated the

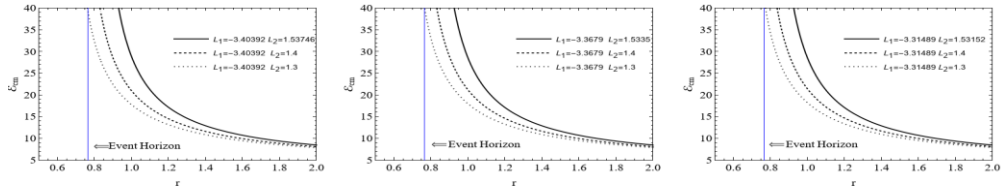

(a) $Q = 0.2$ (b) $Q = 0.3$ (c) $Q = 0.4$

FIG. 3: The center-of-mass energy $\mathcal{E}_{cm}$ dependence of the radial coordinate r for an extremal BH for $\gamma = 0.2$ and various Q values with $r_h^E = 0.765747$ critical values of the spin parameter a_E for different values of the charge Q where the black hole becomes extremal. The limiting cases for the charge Q, rotational parameter a and angular momentum L for the extremal and non-extremal black hole are presented in the Tabs. (I) and (II), respectively.

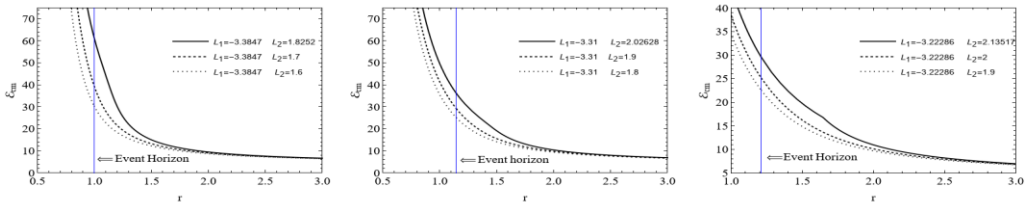

(a) $Q = 0.2$ (b) $Q = 0.3$ (c) $Q = 0.4$

FIG. 4: The center-of-mass energy $\mathcal{E}_{cm}$ dependence of the radial coordinate r for a non-extremal BH for $\gamma = 0.2$ and various Q values.

Finally, we have derived the expression for the CM energy E_{cm} of colliding particles near the horizon of the BH in PFDM and got its radial dependence for extremal and non-extremal black hole at fixed $\gamma = 0.2$ for different values of charge Q (Fig. (3) and Fig. (4), in turn). It is found that the colliding energy diverges near the horizon of the black hole sharply for the extremal case, while in the non-extremal case it diverges beyond the radius of the horizon and even can be finite when the charge of the black hole increases.

REFERENCES

1. G. Bertone and D. Hooper, Reviews of Modern Physics 90, 045002 (2018), arXiv:1605.04909 [astro-ph.CO] .
2. D. Huterer and D. L. Shafer, Reports on Progress in Physics 81, 016901 (2018), arXiv:1709.01091 [astro-ph.CO].
3. V. C. Rubin, J. Ford, W. K., and N. Thonnard, Astrophys. J. 238, 471 (1980).
4. M. Bañados, J. Silk, and S. M. West, Physical Review Letters 103, 111102 (2009).
5. A. Jawad, F. Ali, M. Jamil, and U. Debnath, Communications in Theoretical Physics 66, 509 (2016), arXiv:1610.07411 [gr-qc] .
6. S. Hussain and M. Jamil, Phys. Rev. D 92, 043008 (2015), arXiv:1508.02123 [gr-qc] .
7. R. M. Wald, Phys. Rev. D. 10, 1680 (1974).
8. V. P. Frolov, Phys. Rev. D. 85, 024020 (2012), arXiv:1110.6274 [gr-qc] .
9. A. Abdujabbarov, B. Ahmedov, and A. Hakimov, Phys.Rev. D 83, 044053 (2011), arXiv:1101.4741 [gr-qc] .
10. J. Rayimbaev, A. Abdujabbarov, M. Jamil, and W.-B. Han, Nuclear Physics B 966, 115364 (2021), arXiv:2009.04898 [gr-qc].
11. M. Bañados, J. Silk, and S. M. West, Phys. Rev. Lett 103, 111102 (2009), arXiv:0909.0169 [hep-ph] .
12. O. B. Zaslavskii, Phys. Rev. D 82, 083004 (2010), arXiv:1007.3678 [gr-qc] .
13. O. B. Zaslavskii, Phys. Rev. D 86, 084030 (2012), arXiv:1205.4410 [gr-qc] .
14. F. Atamurotov, U. Papnoi, and K. Jusufi, Classical and Quantum Gravity 39, 025014 (2022), arXiv:2104.14898 [gr-qc] .

O‘ZBEKISTON MILLIY UNIVERSITETI XABARLARI, 2024, [3/1/1]
ISSN 2181-7324

FIZIKA
http://journals.nuu.uz
Natural sciences

UDK: 004.896:621.311

Muzaffar SOBIROV,
Renessans ta’lim universiteti v.b dotsenti
E-mail:muzaffarsobirov538@gamail.com

TATU professori, t.f.d D.Muhammadiyeva taqrizi asosida

ANALYSIS OF AUTOMATION OF THE MONITORING SYSTEM IN INTELLECTUAL HYBRID ENERGY SYSTEMS

Annotation

This article presents an approach to solve the problem of forecasting electric loads of the electric network based on intelligent systems monitoring of hybrid intelligent energy systems. Such systems include both expert systems and artificial neural networks. The main directions of application of the neural network methodology in the field of energy are considered. A functional and infological model of a power system design automation system based on poorly formalized processes such as functional and parametric synthesis has been developed.

Key words: hybrid, artificial neural networks, structural, parametric, synthesis methods, model, hybrid expert systems, technology, functional, infological model as well as parametric synthesis.

АНАЛИЗ АВТОМАТИЗАЦИИ СИСТЕМЫ МОНИТОРИНГА В ИНТЕЛЛЕКТУАЛЬНЫХ ГИБРИДНЫХ ЭНЕРГЕТИЧЕСКИХ СИСТЕМАХ

Аннотация

В данной статье представлен подход к решению задачи прогнозирования электрических нагрузок электрической сети на основе интеллектуальных систем мониторинга гибридных интеллектуальных энергетических систем. К таким системам относятся как экспертные системы, так и искусственные нейронные сети. Рассмотрены основные направления применения нейросетевой методологии в сфере энергетики. Разработана функционально-инфологическая модель системы автоматизации проектирования энергосистемы, основанная на плохо формализованных процессах типа функционального и параметрического синтеза.

Ключевые слова: гибридные, искусственные нейронные сети, структурные, параметрические, методы синтеза, модель, гибридные экспертные системы, технология, функциональная, инфологическая модель и параметрический синтез.

INTELLEKTUAL GIBRID ENERGIYA TIZIMLARIDA MONITORING TIZIMINI AVTOMATLASHTIRISHNI TAHLILI QILISH

Annotatsiya

Ushbu maqolada gibrid intellektual energiya tizimlari monitoringini aqlli tizimlar asosida elektr tarmog‘ining elektr yuklarini bashorat qilish muammosini hal qilish yondashuvi keltirilgan. Bunday tizimlarga ham ekspert tizimlari, ham Sun’iy neyron tarmoqlar kiradi. Energetika sohasida neyron tarmoq metodologiyasini qo‘llashning asosiy yo‘nalishlari ko‘rib chiqilgan. Bunda muhandislik bilimlari bankini o‘z ichiga olgan va funktsional va parametrik sintez kabi noto‘g‘ri rasmiylashtirilgan jarayonlarga asoslangan energiya tizimini loyihalashni avtomatlashtirish tizimining funktsional va infologik modeli ishlab chiqilgan.

Kalit so‘zlar: gibrid, sun’iy neyron tarmoqlari, strukturaviy, parametrik, sintez qilish usullari, model, gibrid ekspert tizimlari, texnologiya, funktsional, infologik modeli hamda parametrik sintez.

Kirish. Hozirgi vaqtda ilg‘or texnologiyalar va raqamli innovatsiyalarni joriy etish bilan bog‘liq ishlab chiqarish sanoati rivojlanishining yangi bosqichlaridan hisoblanadi. Birinchi marta Sanoat 4.0 atamasi Germaniyada paydo bo‘lgan va ishlab chiqarishni yanada samaraliroq qilishga qaratilgan to‘rtinchi sanoat inqilobini aks ettiradi. Sanoat 4.0 bir nechta asosiy texnologiyalar, jumladan:

buyumlar internet - (inglizcha: internet of things, IoT) – bu bir-biri bilan yoki tashqi muhit bilan o‘zaro ta’sir qilish uchun o‘rnatilgan vositalar va texnologiyalar bilan jihozlangan jismoniy obyektlar (“narsalar”) o‘rtasida ma’lumotlarni uzatish tarmog‘i tushunchasi; - *Sun’iy intellekt* - (SI; inglizcha: artificial intelligence, AI) – inson intellektiga taqlid qilishga qodir bo‘lgan mashinalar yaratishga qaratilgan fan va texnologiya sohasi. - *bulutli hisoblash* - bulutli hisoblash xizmati asosan 3 xil modelga ko‘rsatiladi:

infrastruktura xizmati (iglizcha Infrastructure as a Service); platforma xizmati (iglizcha Platform as a Service); dasturiy vosita xizmati (iglizcha Software as a Service).

Bunda infrastruktura xizmati eng quyi xizmat turi bo‘lib, qolgan yuqori xizmat turlari pastkilarining detallarini yanada abstraktlash asosida quriladi.

avtomatlashtirish – bu fan va texnologiya sohasida, insonning bevosita ishtirokisiz texnologik jarayonlarni amalga oshirishning texnik vositalari va usullarini ishlab chiqadi.

Hozirgi vaqtda ekspert tizimlarining sinflaridan biri gibrid ekspert tizimlari bo‘lib, ular nafaqat bilimlar bazalarida bilimlarni taqdim etishning turli modellarini birlashtirishga, balki ularni qayta ishlash uchun bir nechta texnologiyalardan foydalanishga imkon beradi [1].

Mavzuga oid adabiyotlar tahlili. 1940-va 1950-yillar oralig‘ida matematik Alan Tyuring “Fikrlash mashinasi” konsepsiyasini taqdim etish orqali sun’iy intellektning rivojlanish tarixiga o‘z hissasini qo‘shdi. Uning asosiy g‘oyasi mashinalar,

xuddi odam kabi, mavjud ma’lumotlarni qayta ishlashi va ular asosida qaror qabul qilishi mumkinligini ta’kidlash edi. Amerikalik ilm-fan tadqiqotchisi Jorj Jonson sun’iy intellekt sohasining o‘ziga xos xususiyatlarini quyidagicha tavsiflaydi: “sof va amaliy bo‘lmagan o‘rtasidagi bo‘linish qutblanish kabi bo‘linish emas – maydonni harakatga keltiradigan kuchlanishdir” degan fikrlarni bildirishgan.

Tadqiqot metodologiyasi. Bugungi kunda sun’iy intellektning asosiy jihatlari quyidagilarni o‘z ichiga oladi:

Mashinani o‘rganish. Bu kompyuter tizimlari tajriba va ma’lumotlar asosida avtomatik ravishda o‘rganishi va ish faoliyatini yaxshilashi mumkin bo‘lgan metodologiyadir. Mashinani o‘rganish Sun’iy intellektni rivojlantirishda muhim rol o‘ynaydi, bu tizimlarga ma’lumotlarni tahlil qilish va natijalarni bashorat qilish imkonini beradi. - *Chuqur o‘rganish.* Bu ma’lumotlarni qayta ishlash va tahlil qilish uchun ko‘p qatlamli neyron tarmoqlardan foydalanadigan mashinani o‘rganishning kichik bo‘limi bo‘lib chuqur o‘rganish tizimlarga naqshlarni tan olish, tabiiy tilni tushunish, murakkab ma’lumotlarga asoslangan qarorlar qabul qilish va boshqa murakkab vazifalarni bajarish imkonini beradi. - *Neyron tarmoqlar.* Bu inson miyasining ishlashiga taqlid qiluvchi kompyuter modellari hisoblanadi. Neyron tarmoqlar axborotni uzatuvchi va qayta ishlovchi ulangan neyronlardan tashkil topgan bo‘lib, ular naqshni aniqlash, ma’lumotlarni tasniflash, prognozlash va katta hajmdagi ma’lumotlarni qayta ishlashni talab qiladigan vazifalar uchun ishlatiladi. - *Tabiiy tilni qayta ishlash.* Bu Sun’iy intellektning bo‘limi bo‘lib, u odamlar tomonidan ishlatiladigan tabiiy tilni qayta ishlash, tahlil qilish va tushunish bilan shug‘ullanadi. Bu kompyuterlarga tabiiy tilda odamlar bilan muloqot qilish, nutqni tan olish, matnni tahlil qilish va tilni qayta ishlash vazifalarini bajarish imkonini beradi. - *Jarayonlarni avtomatlashtirish va optimallashtirish.* Sun’iy intellekt yordamida faoliyatning turli sohalarida turli jarayonlarni avtomatlashtirish va optimallashtirish mumkin. Masalan, ishlab chiqarish sohasida Sun’iy intellekt uskunalar va ishlab chiqarish jarayonlarining ishlashini nazorat qilishi va optimallashtirishi mumkin. Logistika sohasida esa transport yo‘nalishlari tovarlarni etkazib berishni va boshqarishni optimallashtirishi mumkin.

1-rasm. Sanoat 4.0 asoslangan texnologiyalar ro‘yxati keltirilgan.

Industry 4.0 texnologiyasida ishlab chiqarishning asosiy xususiyati uning modulliligidir. Unda barcha aloqalar simsizdir. Smart komponentlar quyidagi xususiyatlarga iborat:

– ma’lumotlar almashinuvi uchun standart interfeys va yagona manzilga ega bo‘lish; - ularning holati va joylashuvi haqidagi ma’lumotlarni uzatishi va saqlashi mumkin; - matematik modellar bilan tavsiflanadi.

Energetika tizimida sun’iy intellekt tizimlarini qo‘llash sohalari.

Quyida hal qilish zamonaviy energiya tizimlarida Sun’iy intellekt tizimlaridan foydalanish bilan bog‘liq bo‘lgan asosiy vazifalar ro‘yxati keltirilgan:

– yukni bashorat qilish uchun yukni bashorat qilish va atrof-muhit haroratini bashorat qilish; - tarmoqlarda elektr energiyasi oqimlarini boshqarish va maksimal quvvatni ta’minlash; - kuchlanishni tartibga solish; - nosozliklarni aniqlash maqsadida energiya tizimlarining diagnostikasi tuzish; - energiya tizimlarining xavfsizligini nazorat qilish uchun sensorni joylashtirishni optimallashtirish; - energiya tizimlarining xavfsizligini nazorat qilish; - transformatorlarni himoya qilishni ta’minlash; - barqarorlikni ta’minlash, dinamik holatni baholash va generatorlarni diagnostika qilish; - turbogeneratorlarni boshqarish; - generator tarmog‘ini boshqarish; - kuchli kommutatsiya tizimlarini boshqarish.

Energiya tizimlarini boshqarishni avtomatlashtirishda Sun’iy intellekt tizimlaridan foydalanish bo‘yicha vazifalar ro‘yxati doimiy ravishda o‘sib bormoqda. Ilgari ushbu muammolarning ba’zilari statistik va raqamli usullar bilan hal qilingan. Elektr energiya tizimlarining ish rejimlarini modellashtirish va operativ boshqarish usullaridan foydalanilgan. Ammo ekspert tizim texnologiyalari va neyron tarmoqlarining rivojlanishi energiya tizimining holatini baholashda hal qilinishi kerak bo‘lgan vazifalar doirasini kengaytirish imkonini berdi.

Gibrid aqlli tizim (*Hybrid intelligent system*-HIS) bu odatda muammoni hal qilish uchun insonning intellektual faoliyatini taqlid qilishning bir nechta usullari qo‘llaniladigan tizim sifatida tushuniladi.

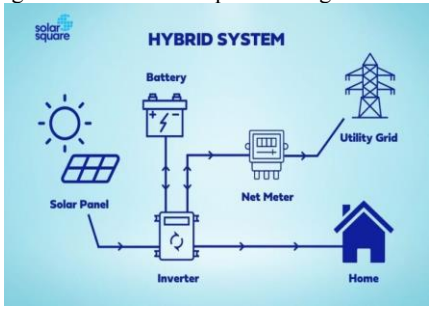

2-rasm. Gibrid aqlli tizimi.

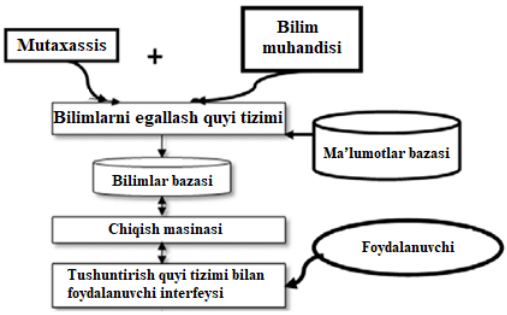

3-rasm. Espert tizimining tuzilishi.

Gibrid aqlli tizim parallel ravishda Sun’iy intellektning pastki maydonlaridan quyidagi usullar va metodlarni qo‘llaydigan dasturiy ta’minot tizimini bildiradi:

– Neyro-loyqa tizimlar; - Gibrid konnektistik-ramziy modellar; - Asabiy-simvolik hisoblash; - Xira ekspert tizimlari; - Connectionist ekspert tizimlari; - Evolyutsion asab tarmoqlari; - Genetik loyqa tizimlar; - Qattiq loyqalashtirish;

Ushbu tizimning asosiy komponentlari ekspert tizimlari va Sun’iy neyron tarmoqlaridir. **Ekspert tizimlari** - bu ma’lum bir mavzu bo‘yicha mutaxassislarning qarorlariga o‘xshash qarorlar qabul qila oladigan kompyuter tizimlarini yaratish uchun Sun’iy intellekt sohasidagi tadqiqot yo‘nalishidir. Ekspert tizimlarining boshqa Sun’iy intellekt tizimlaridan farqi bor: ular neyron tarmoqlar yoki genetik algoritmlar kabi universal muammolarni hal qilish uchun mo‘ljallanmagan. Ekspert tizimlari ishlab chiquvchilar tomonidan belgilangan sohada, kamdan-kam hollarda, sohalarda muammolarni yuqori sifatli hal qilish uchun mo‘ljallangan. Ekspert tizimi ma’lum bir fan sohasidagi mutaxassislar, bilim muhandislari va dasturchilarning birgalikdagi faoliyati natijasidir (2-rasm). **Neyron** - bu kirish signallari yig‘indisidan chiqish signalini (ma’lum qoidaga muvofiq) hisoblaydigan o‘z elementi [2]. **Sun’iy neyron tarmoq (SNT)** - bu og‘irlik koeffitsientlari bilan belgilangan ulanishlar yordamida bir-biriga va tashqi muhitga ma’lum bir tarzda bog‘langan Sun’iy neyronlarning tuzilgan to‘plami [3,4,…6]. Sun’iy neyron tarmoq quyidagi xususiyatlaridan iborat: - pretsedentlar (misollar) asosida o‘qitish; - oldingi tajribani umumlashtirish; - ortiqcha va shovqinli ma’lumotlardan mazmunli ma’lumotlar va naqshlarni olish; - o‘zgaruvchan ish sharoitlariga moslashish. Sun’iy neyron tarmoqdan foydalanish tavsiya etiladi, agar: - masalani yechish algoritmi yo‘q yoki uni yechish printsipi noma’lum, lekin uni hal qilish bo‘yicha eksperimental ma’lumotlar mavjud; - vazifa katta hajmdagi ma’lumotlar bilan tavsiflanadi; - ma’lumotlar to‘liq emas, shovqinli, ortiqcha yoki nomuvofiq. Sun’iy neyron tarmoqlar uchun muammoning bayoni: Bunday xaritalashni qurish kerak X→Y, shuning uchun har bir kirish signali X uchun to‘g‘ri chiqish signali Y hosil bo‘ladi.

Sun’iy neyron tarmoqni qo‘llash sohalari:

- tasniflash va naqshni aniqlash (X – kirish tasviri; Y – kirish tasviri tegishli sinf raqami); - klasterlash/kategorizatsiya (X – kirish vektori; Y – kirish vektori tegishli bo‘lgan klaster); - funksiyaning yaqinlashuvi (X – kirish o‘zgaruvchilari vektori; Y – taxminiy chiqish o‘zgaruvchisi); - bashorat/prognoz (X - ma’lum vaqt oralig‘idagi vaqt seriyasi; Y - kirish signali o‘zgaruvchilari to‘plami); - identifikatsiya (X va Y tizimning kirish va chiqish signallarini ifodalaydi, jarayon aniqlanadi); - optimallashtirish; - assotsiativ xotira; - boshqaruv.

Sun’iy neyron. 2-rasmda Sun’iy neyronning tipik tuzilishi ko‘rsatilgan.

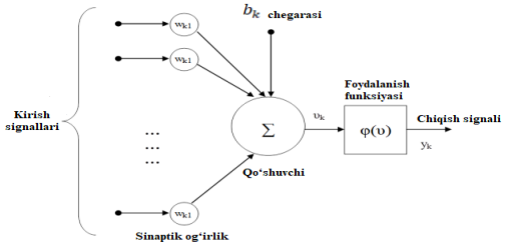

2-rasm. Sun’iy neyron diagrammasi.

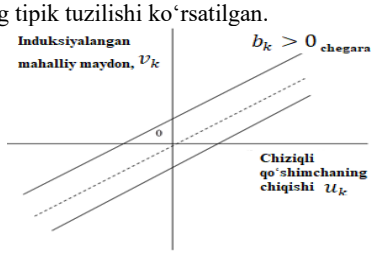

3-rasm. Neyron chiqishiga chegaraning ta’siri

$$b_k > 0$$

Neyronning asosiy elementlari: - har biri xarakterli bo‘lgan sinapslar / ulanishlar to‘plami; - k neyron bilan bog‘langan j sinapsining kirishidagi x_j signali w_{kj} og‘irligiga ko‘paytiriladi (birinchi indeks ko‘rib chiqilayotgan neyronga, ikkinchisi esa bu og‘irlik bog‘langan sinapsning kirish uchiga ishora qiladi); - sinaptik og‘irlik ijobiy yoki salbiy bo‘lishi mumkin; - adder neyronning mos keladigan sinapslariga nisbatan og‘irlikdagi kirish signallarini qo‘shadi; - faollashtirish funktsiyasi neyronning chiqish signalining amplitudasini cheklaydi; neyron chiqish amplitudalarining normallashtirilgan diapazoni [0, 1] yoki [-1, 1] oralig‘idagi diapazonda ko‘rsatilgan. Neyron k ning ishlashi quyidagi iboralar bilan tavsiflanadi:

$$u_k = \sum_{j=1}^{m} w_{kj}\, x_j, \qquad y_k = \varphi(u_k + b_k)$$

bu yerda $x_1, x_2, \dots x_m$ – kirish signallari; - $w_1, w_2, \dots w_{km}$ – k ning sinaptik og‘irliklari neyron; - u_k – kirish ta’sirlarining chiziqli birikmasi; - b_k – chegara siljishi (qo‘shiluvchi chiqishining affin o‘zgarishi effektini ta’minlaydi); - φ - faollashtirish funktsiyasi; y_k- neyronning chiqish signali. b_k chegarasidan foydalanish. Neyronda postsinaptik potentsial quyidagicha hisoblanadi:, $v_k = u_k + b_k$. Xususan, b_k chegarasi qanday qiymat olishiga qarab, musbat yoki manfiy bo‘lsa, k-neyronning induktsiyalangan mahalliy maydoni yoki faollashuv potentsiali u_k 3-rasmda ko‘rsatilganidek o‘zgaradi.

– **Tahlil va natijalar.** Sun’iy neyronning faollashuv funksiyalari 4-rasmda misollari asosida ko‘rsatilgan: a) bitta sakrash funktsiyasi: $f(s) = \begin{cases} 0, s < \Theta, \\ 1, s \geq \Theta; \end{cases}$, b) qismli chiziqli funksiya: $f(s) = \begin{cases} 0, s < -a, \\ \frac{1}{2a}(s + a), -a < s < a, \\ 1, s > a; \end{cases}$, c) logistika (sigmasimon): $f(s) = \frac{1}{1+e^{-as}}$; , d) giperbolik tangent (sigmoid): $f(s) = \frac{e^{as} - e^{-as}}{e^{as} + e^{-as}}$.

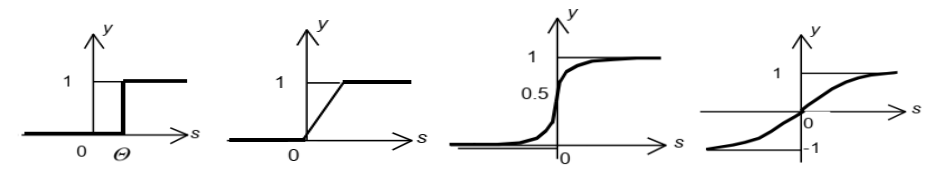

a) b) c) d)

4-rasm. Neyronni faollashtirish funktsiyalariga misollar.

Sun’iy neyron tarmoq neyronlarining turlari:

- kirish neyronlari kirish ta’sirini kodlaydi va neyron tarmog‘ining oraliq neyronlariga “vaznli” ma’lumotlarni uzatadi; - oraliq neyronlar neyron tarmog‘ida asosiy ma’lumotlarni o‘zgartirishni amalga oshiradi; - chiqish neyronlari hosil bo‘lgan transformatsiyalarni amalga oshiradi; ularning chiqish qiymatlari neyron tarmoqning chiqishlaridir. Gibrid ekspert tizimlarida qo‘llaniladigan usullar va algoritmlar odatda mantiqiy va evristik turlarga bo‘linadi. Ular elektr tarmoqlarini loyihalashni avtomatlashtirish uchun mos keladi [6]. Olingan natijalardan kelib chiqib, GESlarni rivojlantirishga yondashuv taklif etilmoqda, u quyidagilardan iborat GES tarkibiga Sun’iy neyron tarmoqlari (SNT) apparatlarini joriy etish orqali gidroelektrostantsiya kengaymoqda. SNTning shubhasiz afzalliklari quyidagilardan iborat: - tuzilishning moslashuvchanligi; - tezkor o‘rganish algoritmlarini qo‘llash; - ko‘p miqdordagi shovqin mavjud bo‘lganda ishlash qobiliyatidagi, - signallar; - har xil turdagi axborotlar bilan ishlash qobiliyati; - o‘qitilgan SNT o‘zining alohida elementlarining ishdan chiqishiga chidamli bo‘ladi.

Gibrid ekspert neyron tizimining blok diagrammasi 5-rasmda ko‘rsatilgan. Gibrid ekspert neyron tizimi quyidagi komponentlarni o‘z ichiga oladi:

– o‘qitilgan neyron tarmoq; - ekspert tizim; - qaror qabul qilish va tushuntirish moduli; - neyron tarmoq va ekspert tizimidan ma’lumotlarni o‘zaro o‘zgartirish imkonini beruvchi interfeys moduli.

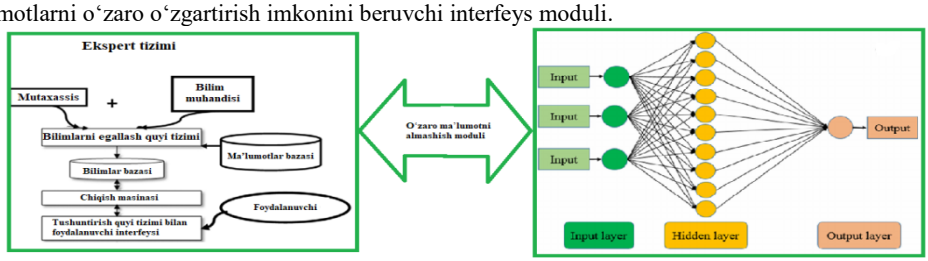

5-rasm. Gibrid ekspert neyron tizimining tuzilishi.

Mualliflar neyron tarmoqlardan foydalangan holda modellashtirish usullaridan foydalanish imkoniyatini ko‘rsatdilar. tarmoq ob’ektlari yukini bashorat qilishda SNTga asoslangan kompyuter prognozlash modeli ko‘rib chiqiladi [7].

Xulosa va takliflar. Ushbu maqolada elektr tarmoqlarini loyihalash va monitoring qilish muammolarini hal qilishda gibrid intellektual tizimlardan foydalanish imkoniyatlari ko‘rsatilgan. Gibrid ekspert tizimlari va Sun’iy neyron tarmoqlari strukturasi tahlili qilingan. Gibrid aqlli tizim parallel ravishda sun’iy intellekt bilan metodlarni qo‘llaydigan dasturiy ta’minot tizimining ishlash prinspri tahlil qilindi hamda gibrid aqlli neyron tizimlardan foydalanishga asoslangan energiya muammolarini hal qilishga yondashuv taklif etildi. Sun’iy neyronning faollashuv funksiyalari misollar bilan ko‘rsatildi hamda neyron diagrammasi yoritib berildi. Gibrid ekspert neyron tizimining blok diagrammasida neyron tarmoqlardan foydalangan holda modellashtirish usullaridan foydalanish imkoniyatini ko‘rsatib o‘tilgan.

ADABIYOTLAR

1. Ковалев, К. В. Искусственный интеллект в промышленности. Перспективы / К. В. Ковалев // 69-я научно-техническая конференция учащихся, студентов и магистрантов, 2-13 апреля 2018 г., Минск : сборник научных работ : в 4 ч. Ч. 4 / Белорусский государственный технологический университет. - Минск : БГТУ, 2018. – С. 471-474.
2. Борисов В.В., Бобряков А.В., Мисник А.Е. Экспертные системы. Учебное пособие
3. по направлению «Информатика и вычислительная техника» [Текст]: учебное пособие. – Смоленск: Универсум, 2021. – 110 с
4. Сухоцкий, А. Б. Нетрадиционные и возобновляемые источники энергии : курс лекций для студентов специальности 1-43 01 06 "Энергоэффективные технологии и энергетический менеджмент" / А. Б. Сухоцкий, В. Н. Фарафонтов ; БГТУ. - Минск : БГТУ, 2009. - 244 с.
5. Башева М. А. "Индустрия 4.0" в России: на пороге промышленного переворота // Молодой ученый. - 2019. - №13. - С. 100-102. – URL https://moluch.ru/archive/251/57602/ (дата обращения: 11.12.2019).
6. Колесников, А.В. Методология и технология решения сложных задач методами функциональных гибридных интеллектуальных систем. / Колесников, А.В., Кириков И.А. - М.: ИПИ РАН, 2007.
7. Алдошина, А. Н. Экспертная система на основе нейросетевых технологий для мониторинга и диагностики корпоративной локальной сети // Молодой ученый. - 2016. - №18. - С. 35-38. - URL https://moluch.ru/archive/122/33814/ (дата обращения: 07.12.2019).
8. Борисов В.В., Круглов В.В., Федулов А.С. Нечеткие модели и сети. 2-е изд. стереотип. – М.: Горячая линия – Телеком, 2018. – 284 с.

O‘ZBEKISTON MILLIY UNIVERSITETI XABARLARI, 2024, [3/1/1]
ISSN 2181-7324

FIZIKA
http://journals.nuu.uz
Natural sciences

UDK: 524

Sobir TURAEV,
PhD student of National university of Uzbekistan
E-mail: sobr8488@mail.ru

Based on the review of professor K.Mirtadjiyeva

PROBLEMS OF DETERMINING THE AGES OF GLOBULAR CLUSTERS

Annotation

In this work, the literature on the ages of Globular Clusters (GCs) is analyzed. The problems of determining the age of the clusters are thoroughly reviewed. Also, the relationship between the concentration parameter and the age of GCs found based on the observations of the HST and Gaia DR2 space telescopes has been studied. Connections based on the found concentration parameter and the absolute magnitude and mass of GCs are presented.

Key words: age estimation, concentration parameter, globular clusters, modeling, xi-square method, space observations.

ПРОБЛЕМЫ ОПРЕДЕЛЕНИЯ ВОЗРАСТА ШАРОВЫХ СКОПЛЕНИЙ

Аннотация

В данной работе анализируется литература о возрасте шаровых скоплений (ШС). Подробно рассмотрены проблемы определения возраста скоплений. Также изучена связь параметра концентрации с возрастом ШС, найденных по наблюдениям космических телескопов HST и Gaia DR2. Представлены связи на основе найденного параметра концентрации, а также абсолютной величины и массы ШС.

Ключевые слова: оценка возраста, параметр концентрации, шаровые скопления, моделирование, метод хи-квадратов, космические наблюдения.

SHARSIMON TO’DALARNING YOSHLARINI ANIQLASH MUAMMOLARI

Annotatsiya

Bu ishda Globular klasterlar (GK) yoshiga oid adabiyotlar tahlil qilingan. Klasterlarning yoshini aniqlash muammolari har tomonlama ko'rib chiqiladi. Shuningdek, HST va Gaia DR2 kosmik teleskoplari kuzatuvlari asosida aniqlangan kontsentratsiya parametri va GK yoshi o'rtasidagi bog'liqlik o'rganildi. Topilgan konsentratsiya parametri va GK larning mutlaq kattaligi va massasiga asoslangan ulanishlar keltirilgan.

Kalit so'zlar: yoshni baholash, konsentratsiya parametri, sharsimon to’dalar, modellashtirish, xi-kvadrat usuli, kosmik kuzatuvlar.

Introduction. Globular clusters, ancient enclaves of stars, hold the keys to unraveling the cosmic timeline. Their ages provide crucial constraints on the age of the Universe itself. However, determining these ages is no straightforward task. A key distinguishing feature of globular clusters in the Galaxy is their uniformly old age. Globular clusters are composed of Population II objects (old stars). Determined by comparing the stellar population of globular clusters with stellar evolutionary models, the ages of all those so far measured range from 11 billion to 13 billion years. They are the oldest objects in the Galaxy and so must have been among the first formed. Composed of stars belonging to the extreme Population II, as well as the high-latitude halo stars, these nearly spherical assemblages apparently formed before the material of the Galaxy flattened into the present thin disk. The present interstellar gas in the solar neighborhood contains elements heavier than helium, which are called metals by astronomers, at a level of about 2 percent by mass, while the globular clusters contain as little as 0.02 percent of the same elements. The color magnitude diagram of co-eval stellar populations in the Milky Way can be used to infer the age of its oldest stars. The age can also be estimated for individual stars if their metallicity and the distance to them are known. For resolved stellar populations, however, an independent measurement of the distance is not strictly necessary as the full morphology of the color-magnitude diagram can, in principle, provide a determination of the absolute age [1–3]. It has long been recognized that they are among the most metal poor (∼ 1% of the solar metallicity) stellar systems in the Milky Way, and exhibit color-magnitude diagrams characteristic of old (> 10 Gyr) stellar populations [1, 3, 4]. As argued in Ref. [5], it is possible to estimate the probability distribution of Δt by considering that the first galaxies are found at $z \sim 11$ and a significant number of galaxies are found at $z > 8$. Many of these galaxies contain stellar populations that indicate that star formation started at $z \sim 15 - 40$ [6-8]. Since the mid 90’s, estimates of the ages of GCs have been in the range 12−14 Gyr consistently [9]. According to the result of D. Valcin et al. (2020) the average age of the oldest (and most metal poor) GCs is $t_{GC} = 13.32 \pm 0.1$ Gyr. [10]. As first pointed out in Refs. [11, 12], the full color-magnitude diagram has features that allow for a joint fit of the distance scale and the age (see Appendix A for a visual rendering of this). On the one hand, in Ref. [13] shows how the different portions of the color-magnitude diagram constrain the corresponding physical quantities. On the other, in Ref. [12] show how the luminosity function is not a pure power law but has features that contain information about the different physical parameters of the GC. This technique enabled the estimation of the ages of the GCs M68 [11], M5 and M55 [13]. Moreover, in principle, exploiting the morphology of the horizontal branch makes it possible to determine the ages of GCs independently of the distance [9].

About age estimation for some Globular Clusters. We delve into the challenges and methods associated with estimating the ages of GCs, shedding light on the discrepancies and uncertainties that persist. GCs are celestial time capsules, preserving the earliest stellar generations. Their stars, densely packed and gravitationally bound, offer unique insights into the

universe’s past. Yet, pinpointing their ages remains a puzzle. We explore the complexities involved in this endeavor. But there are enough problems with determining the age of GCs. There are two conflicting accounts of the age of Globular Clusters. The first suggests a relatively young age of the universe of less than 14 billion years due to cosmological expansion and the Hubble constant. Second, ancient celestial objects: globular clusters, with their metal-poor stars, consistently give ages over 14 billion years. Some even go as close as 18 billion years [14].

The primary tool for age determination is the main sequence turnoff (TO) [15]. Hertzsprung-Russell Diagram (H-R Diagram): By plotting a star’s temperature (color) against its intrinsic brightness (luminosity), we trace its evolutionary path. Massive, blue stars exhaust their hydrogen fuel first and evolve off the main sequence. Their transition to red giants shifts their position on the H-R diagram. In addition, the horizontal line of red giants marks their post-main-sequence phase. Challenges and Solutions:

Stars within a cluster have varying masses and mass influences their lifetimes. It is used the TO region, where stars burn hydrogen, to estimate the cluster age. O-type stars live about a million years, G-type stars (like our Sun) survive around 8 billion years and red M-type stars can endure 56 billion years. Globular clusters harbor stars formed at different times. Some clusters exhibit multiple episodes of star formation. Untangling this complexity is essential. Recent statistical methods aim to combine various age indicators including Global Fitting: Simultaneously fitting multiple properties of the cluster CMD (color-magnitude diagram) using isochrones and comparing synthetic CMDs to observed data statistically. Applying these techniques to clusters like NGC 6397, M92, and M3, are found [16]:

- NGC 6397: Estimated age of 14.0 Gyrs (range: 13.8–14.4 Gyrs).
- M92: Age around 14.75 Gyrs (range: 14.50–15.40 Gyrs).
- M3: Approximately 16.0 Gyrs (range: 15.9–16.3 Gyrs).

The search is on to determine the age of the GC. As we improve our methods and encounter inconsistencies, finding the exact age of these ancient witnesses will increase the accuracy of our calculations and lead to a deeper understanding of cosmic history.

Results. From the surface density observation data of 26 GCs obtained by HST [17], we calculated the concentration parametric (γ), which represents the concentration of stars towards the center, using the model (1) based on the King model, using the chi-square method and, we examine the relationship between this parameter and the age of GCs.

$$\sigma(r, \gamma, r_0, \sigma_0) = \sigma_0(1+(r/r_0)^2)^{-\gamma} \quad (1)$$

Here γ, r_0 and σ_0 are free parameters, γ is the degree of concentration of stars towards the center of the cluster, is the radius of the cluster core, σ_0 is the surface density of the core.

We examined relatively observational data published by Dotter et al. (2010) [18]. Using the data, we found that the correlation is −0.57. For the last case, for the sake of interest, we decided to find corresponding empirical dependence. So it is obtained that

$$\gamma = (4.36 \pm 1.15) - (0.26 \pm 0.09)\tau. \quad (2)$$

From here it can be seen that the cluster becomes denser if the age grows.

We calculated concentration parameters based on surface density observations of 81 GCs obtained by Gaia DR2 [19]. Unfortunately, no correlation was found between this parameter and the Age of GCs. This is because the quality of the Gaia DR2 observation data is lower than that of the HST observations [20]. Furthermore, in literature several researches have been done estimation ages of GCs using different methods. But the results of these researches differ from each other’s. For example, In [21], GCs range in age from ~[8–13.75] Gyr, in [10] in the range ~[8–15] Gyr, in [22] in the range ~[10–13] Gyr, In [23] it varies between ~[9–13] Gyr, and in [24] between ~[7–14] Gyr. But we found correlations between concentration parameter and absolute magnitude (M_V) and GCs mass (M_{GC}) values. Below we show empirical formulas of these relationships.

a). Relationship between γ and the absolute value of MV. The correlation coefficient between these values is 0.63. The corresponding empirical formula has the form

$$\gamma = 0.24(\pm0,05)M_V + 3,01(\pm0,39), \quad (3)$$

or vice versa

$$M_V = 1,64(\pm0,33)\gamma - 9,91(\pm0,37). \quad (4)$$

b). Dependence between γ and GC mass. The correlation coefficient is - 0.62. Empirical formula:

$$\gamma = - 0,58(\pm0,12)\lg M/M_\odot + 4,22(\pm0,65), \quad (5)$$

or vice versa

$$\lg M/M_\odot = - 0.67(\pm0,14)\gamma + 6,18(\pm0,15). \quad (6)$$

Conclusion. We have discussed in detail that there are serious problems in determining the age of GCs. These issues have a material impact on our results. In addition, errors and inaccuracies in the observations of GCs have a negative impact on the results. Nevertheless, we tried to find a connection between the concentration parameter we calculated and the age of GCs. We also found connections between this parameter and cluster mass and absolute magnitude. In the future, the increase in the accuracy of finding the age of GCs, the improvement of the quality of observations will help us to make more accurate conclusions based on our results.

REFERENCES

1. M. Catelann et al., *The ages of (the oldest) stars, in Rediscovering Our Galaxy*, vol. 334 of IAU Symposium, pp. 11–20, Aug., 2018, DOI [1709.08656].
2. D. R. Soderblom, *The Ages of Stars*, ARAA 48 (2010) 581 [1003.6074].
3. D. A. Vandenberg et al., *The Age of the Galactic Globular Cluster System*, ARAA 34 (1996) 461.
4. E. M. O’Malley et al., *Absolute Ages and Distances of 22 GCs Using Monte Carlo Main-sequence Fitting*, ApJ 838 (2017) 162 [1703.01915].
5. R. Jimenez, A. Cimatti et al., *The local and distant Universe: stellar ages and H_0*, JCAP 2019 (2019) 043 [1902.07081].
6. T. Hashimoto et al., *The onset of star formation 250 million years after the Big Bang*, Nature 557 (2018) 392 [1805.05966].
7. V. Strait et al., *Stellar Properties of z > 8 Galaxies in the Reionization Lensing Cluster Survey*, ApJ 888 (2020) 124 [1905.09295].

8. C. Binggeli et al., *Balmer breaks in simulated galaxies at z > 6*, MNRAS 489 (2019) 3827 [1908.11393].
9. R. Jimenez et al., *Ages of globular clusters: a new approach*, MNRAS 282 (1996) 926 [astro-ph/9602132].
10. David Valcin et al., *Inferring the Age of the Universe with Globular Clusters*, arXiv:2007.06594v2 [astro-ph.CO] 17 Oct 2020.
11. R. Jimenez and P. Padoan, *A New Self-consistency Check on the Ages of Globular Clusters*, ApJL 463 (1996) L17.
12. P. Padoan and R. Jimenez, *Ages of Globular Clusters: Breaking the Age-Distance Degeneracy with the Luminosity Function*, ApJ 475 (1997) 580 [astro-ph/9603060].
13. R. Jimenez and P. Padoan, *The Ages and Distances of Globular Clusters with the Luminosity Function Method: The Case of M5 and M55*, ApJ 498 (1998) 704 [astro-ph/9701141].
14. A. Dotter, *MESA Isochrones and Stellar Tracks (MIST) 0: Methods for the Construction of Stellar Isochrones*, ApJS 222 (2016) 8 [1601.05144].
15. V. Strait et al., *Stellar Properties of z & 8 Galaxies in the Reionization Lensing Cluster Survey*, ApJ 888 (2020) 124 [1905.09295].
16. L. Knox, N. Christensen and C. Skordis, *The Age of the Universe and the Cosmological Constant Determined from Cosmic Microwave Background Anisotropy Measurements*, ApJL 563 (2001) L95 [astro-ph/0109232].
17. P. Miocchi, et al., *Star count density profiles and structural parameters of 26 galactic globular clusters*, The Astrophysical Journal, 774:151 (16pp), 2013.
18. Dotter A et al., *The ACS Survey of galactic globular clusters. IX. Horizontal branch morphology and the second parameter phenomenon*, 2010. ApJ. 708:698-716.
19. T.J.L. de Boer et al., Globular cluster number density profiles using Gaia DR2, arXiv:1901.08072v2 [astro-ph.GA] 5 Mar 2019.
20. S.J.Turaev et al., *Problems of determining the degree of concentration of stars towards the center of globular clusters*. Astrophysical Bulletin, 2024, volume 79, no. 1, p. 89–95.
21. M. Koleva et al., *Spectroscopic ages and metallicities of stellar populations:validation of full spectrum fitting*, Mon. Not. R. Astron. Soc. 000, 1–14 (2008).
22. A. T. Baldwin et al.,*Hubble space telescope proper motion (hstpromo) catalogs of galactic globular clusters. IV. kinematic profiles and average masses of blue straggler stars*, The Astrophysical Journal, 827:12 (12pp), 2016 August 10.
23. Don A. VandenBerg et al., *The ages of 55 globular clusters as determined using an improved* ΔV_{HB} *to method along with color-magnitude diagram constraints, and their implications for broader issues*, arXiv:1308.2257v1 [astro-ph.GA] 9 Aug 2013.
24. F. Meissner and A. Weiss, *Global fitting of globular cluster age indicators*, A&A 456, 1085–1096 (2006).

O‘ZBEKISTON MILLIY UNIVERSITETI XABARLARI, 2024, [3/1/1]
ISSN 2181-7324

FIZIKA
http://journals.nuu.uz
Natural sciences

UDK: 577.95.541

Gulbakhor URMANOVA,
Associate Professor of Tashkent Pediatric Medical Institute
E-mail:g.urunbayevna@gmail.com

According to reviews of M.I. Asrorov, professor at the Institute of Biophysics and Biochemistry, Doctor of Biological Sciences.

INFLUENCE OF DISSYMPATIZATION ON ENTEROCYTES

Annotation

This study highlights the influence of physicochemical desympatization on the functional state of enterocytes*(enterocytes (lat. enterocytes) is the general name for a number of intestinal epithelial cells)* and some morphometric indicators of the small intestine.

The experiments were carried out during the transition to feeding of newborn rats, during the formation of skeletal muscle tone and thermoregulation mechanisms**.** Experiments confirm that disruption of sympathetic innervation negatively affects the function of a number of parameters of the small intestine, as well as functional states associated with enterocyte adhesion.

Key words: function, diameter, system, cell, segment, rat, enterocyte, intestine, section, guanethidine, mechanism.

ВЛИЯНИЕ ДИССИМПАТИЗАЦИИ НА ЭНТЕРОЦИТЫ

Аннотация

В данном исследовании выделено влияние физико-химической десимпатизации на функциональное состояние энтероцитов *(энтероциты (лат. enterocytus)* - общее название ряда клеток эпителия кишечника*)* и некоторые морфометрические показатели тонкой кишки.

Эксперименты проводились в период перехода к питанию новорожденных крысят, в период формирования тонуса скелетных мышц и механизмов терморегуляции.

Эксперименты подтверждают, что нарушение симпатической иннервации отрицательно влияет на функцию ряда параметров тонкой кишки, а также на функциональные состояния, связанные с адгезией энтероцитов.

Ключевые слова: функция, диаметр, система, клетка, сегмент, крыса, энтероцит, кишечник, раздел, гуанетидин, механизм.

DISSIMPATIYANING ENTEROTSITLARGA TA’SIRI

Annotatsiya

Mazkur tadqiqot ishida fiz-kimyoviy desimpatizatsiya, enterotsitlar *(enterotsitlar (lot. enterocytus)* - bir qator ichak epiteliy hujayralarining umumiy nomi) ning funksional xolatiga va ingichka ichakning ayrim morfometrik ko‘rsatkichlariga ta’siri yoritildi.

Eksperimentlar yangi tug‘ilgan kalamushlarning oziqlanishga o‘tish davrida, skelet mushaklari tonusi va termoregulyatsiya mexanizmlarining shakllanishi davrlarida olib borildi.

Tajribalar, simpatik innervatsiyaning buzilishi ingichka ichakning bir qator ko‘rsatkichlarining funksiyasini izdan chiqishiga, hamda enterotsitlar adgeziyasiga bog‘liq funksional holatlarga salbiy ta’sir etishini asoslaydi.

Kalit so‘zlari: funksiya, diametr, tizim, hujayra, segment, kalamush, enterotsit, ichak, bo‘lim, guanetidin, mexanizm.

Introduction. Transport, barrier, rheological properties and the mechanism of action of the mucous membrane of the stomach, thin and thick men, and many of them are determined by adhesion between enterocytes. [1,3]. The activity of the membrane-attachment complexes of the basal part of the cell is due to its close connection with the desmosomes of the apical part of the cell [3,4,7]. Adhesion of epithelial cells, including enterocytes, reflects individual patterns of development. This describes the current functional state of the body, which depends on the influence of external environmental factors.

For example, adhesion of different species depends on their emotional and behavioral reactions. Therefore, its function changes under stress and under the influence of a number of pharmacological drugs [4,5].

Izucheno vliyanie physiko-khimicheskoy desimpatizatsii na adgezivnye svoystva enterotsitov i nekotorye morphometricheskie pokaseteli tonkoy kishki.

Literature review. Intramural ganglia and neurocytes of the small intestine of white laboratory rats have different morphometric characteristics. Under the influence of gunetidine, changes in the age-related dynamics of cholinesterase and monoamine oxidase activity are observed

Chemical desympatization under ultrasound control is a minimally invasive, pathogenetically based intervention in patients with open trophic ulcers of venous etiology. The method is economically feasible and can be used both in inpatient and outpatient settings [4,5,6].

When de-empathized with guanethidine (60-70 mg/kg per day, from the second to the fortieth day of life), the age-related dynamics of the studied indicators is disrupted. changes in the stomach are significantly higher than in the duodenum. As a result, the parameters of gastric neurocytes are restored more slowly. It is known from the literature that there are different degrees of influence of the sympathetic and parasympathetic parts of the nervous system on the intramural ganglia.

After chemical desympatization, the functional state of metasympathetic neurocytes in the intestinal ganglia of white rats is disrupted. As a result, which leads to more pronounced changes in the gastric ganglia. There are relatively few functional disorders in the duodenum.

Chemical desymptization partially affects the neuronal apparatus of the ganglia. This shows the extreme resistance of the nervous system to extreme chemicals such as guanethidine.

We can say that the reason for this may be the nature of the origin of the metasympathetic innervation of the internal organs, their inherent flexibility and resistance to chemical influences [2,7,9].

Research Methodology. White laboratory rats of different ages were used in research experiments. For this purpose, animals of different sexes weighing 140-180 g were selected. Pregnant female rats were kept in individual cages.

Newborn rats were allocated five per lactating rat. The experiments were carried out during a critical period of growth and development of rats [2,3,8].

In this case: 12-14th day is the period of opening the eyes of rats; 21-22 days of transition to full nutrition; Day 30 – period of liberation from the mother (emancipation); 55-60 days – the period of formation of skeletal muscle tone and thermoregulation mechanisms; 85-90 days is the period of puberty of animals.

Six rats were used for each experiment. Enterocyte adhesion and morphometric parameters were studied in various sections of the small intestine and sections below the duodenum.

In the first part of the experiments (control group), the mechanism specific to the adhesive properties of various physical parameters of the small intestine was studied;

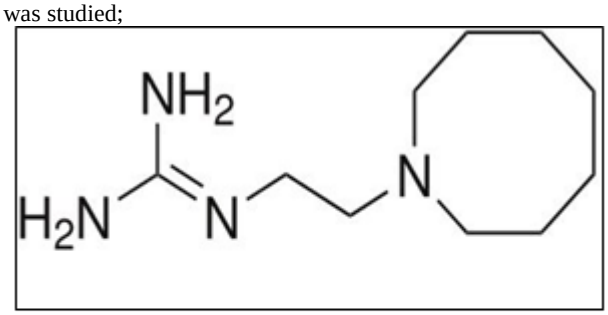

Fig. 1. Chemical formula of the studied guanethidine

In the second series of experiments, the state of these indicators was determined after physical-chemical desympathization. In these experiments, physicochemical desympathization was performed using guanethidine sulfate. The chemical formula of the studied guanethidine is presented in Fig. 1. Guanethidine is a white crystalline powder with a bitter taste. Slightly soluble in water [6,9].

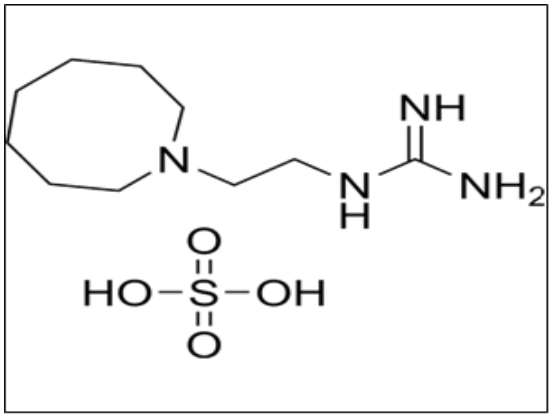

Fig. 1. Chemical formula of the studied guanethidine sulfate

Guanethidine sulfate (Guanethidine monosulfate) ia an antihypertensive agents. Guanethidine is also an adrenergic neurone blocking agent, enters noradrenergic nerve terminals by the neuronal amine carrier. The chemical formula of the studied guanethidine sulfate is shown in Fig.2 [6,8].

Newborn rat pups were administered guanethidine sulfate at a dose of 20 mg/kg daily intraperitoneally from the 1st to the 14th day of life. As a result of these experiments, the number of nerve cells in the sympathetic ganglia decreased to approximately 75-85-90 percent.

To determine enterocyte adhesion in subsequent experiments, rats were decapitated. The abdominal cavity was opened and the small intestine isolated.

Appropriate 2 cm pieces of small intestine were inverted and thoroughly washed with chilled Hanks' solution. The pH value is 7.4.

Then they placed it in a special glass and poured in 5 ml of Hanks' solution. The test tubes prepared in this way are placed in a shaker and strainer for 1 to 5 minutes. For easy counting of the number of enterocytes, the time was determined according to the release of enterocytes into the surrounding solution.

A drop of the solution was introduced into Goryaev's chamber. The collected enterocytes were counted using a special microscope. It has been established that the more enterocytes are exfoliated from the small intestinal mucosa during the determination process, the weaker the adhesion of enterocytes.

The results obtained were statistically processed using the Student and Fisher method.

Analysis and results. The results of the study showed that the weight of the mucous membrane of intact rats increased rapidly from the 2nd to the 7th day of life of rats in all parts of the small intestine. Then, by day 85-90, the growth rate slowed down. When comparing the processes of growth of the mass of the mucous membrane in each of the four sections of the intestine, it was found that the mass of the mucous membrane increased everywhere in the same proportion.

In 2-day-old rats, the intestinal diameter was very small and was the same in all four intestinal segments. By days 6 and 14, the intestinal diameter increased, but remained the same in all segments. By the 22nd day, the intestinal diameter increased, especially in the duodenum. An increase in diameter was also observed on the 55-60th day of life of rats, after which the diameter of the duodenum became wider than other sections.

Enterocyte adhesion increased from the 2nd to the 28-30th day of life in rats and stabilized by the 85-90th day. In each age group, enterocyte adhesion was approximately the same in different parts of the small intestine.

After physico-chemical desensitization, the development of the small intestine is disrupted. While the length and diameter of the small intestine increased at a normal rate, mucosal mass increased slowly in the duodenum and proximal portion and gradually increased in the medial and distal portions until days 21-22.

The adhesion of enterocytes decreased maximally in the duodenum and paroxysmal region according to the number of heared enterocytes on days 21-22 and 30 after the disruption of sympathetic innervation, was less observed in the medial section and did not differ from the control group in the distal section

It is a growing rat, it is an adult, it plays a vital role in the regulation of the functions of the thin intestine, and it plays the role of zaputyvaniya mejmyshechnyh and mucous nerves, as well as humoral factors. Sympathetic and parasympathetic nerves play a secondary role [5,9]. However, the results showed that the disturbance of sympathetic innervation negatively affects the development of parameters in men, for example, adhesion of enterocytes.

Guanetidin has a sympatholytic effect, and adrenergic neuron transmitter. Izbirateln nakaplivaetsya v granulax sympathicheskix postganglionarnyx nervnyx okonchaniy i vydavlivaet iz nix noradrenaline. Chast vydelivshegosya noradrenaline dostigaet postsynapticheskikh a-adrenoretseptorov i okazyvaet kraktovremennoe pressornoe deystvie. No, it is often inactivated. As a result, the function of the adrenergic junction is disturbed.

Guanethidine has a blocking ability and affects β2-adrenergic receptors. But it has almost no effect on the mechanism of the nervous system and adrenal glands.

The effect of guanethidine develops in two stages: tachycardia - a transient reaction occurs in the heart, followed by a gradual decrease in systolic and diastolic blood pressure, a decrease in heart rate and cardiac output. This process is associated with a violation of vascular resistance [5,8,9].

Conclusion. After chemical desensitization, i.e., administration of guanethidine to rats from the 1st to the 14th day of life, enterocyte adhesion decreased maximally in the duodenum and proximal section, less in the medial section and less than control in the distal section. matter. Studies on rats of different ages showed that on days 20 and 30, enterocyte adhesion increased in all parts of the small intestine. By the end of the experiment, this increase stabilized. It can be said that sympathetic innervation is important for restoring the adhesive properties of enterocytes compared to the initial parts of the intestine.

The results are statistically significantly different from the results of the control group. During the postnatal ontogenesis of rats, the adhesion of enterocytes in various parts of the small intestine decreases depending on the number of exfoliated enterocytes.

Based on the results of the experiments and instead of a conclusion, we can say that disruption of sympathetic innervation after desympatization causes functional changes in a number of indicators of the small intestine. As a result, there is a negative impact on the functional states associated with the adhesion of enterocytes.

Most disturbances occur in the oral portions of the small intestine, but may be related to the presence of oral-caudal gradients of control mechanisms. The neural mechanisms of this condition are clearly expressed in the upper gastrointestinal tract. In the caudal direction, the process of dominance of humoral mechanisms gradually decreases.

LITERATURE

1. Воробьева О.Б. Возрастные преобразования сократительной активности двенадцатиперстной кишки белой крысы в норме и при химической денервации. https://www.dissercat.com/content/vozrastnye-preobrazovaniya-sokratitelnoi-aktivnosti-dvenadtsatiperstnoi-kishki-beloi-krys.2005.
2. Воробьева О. Б. и др. Энзимохимическая характеристика метасимпатических нейроцитов желудка и двенадцатиперстной кишки у десимпатизированной белой крысы. // Вестник СПбГУ. Сер. 3, 2003, вып. 3 (№ 19).
3. Нигматулина Р.Р. и др. Фармакологическая десимпатизация изменяет реакцию инотропной функции сердца на серотонин в постнатально. //Росс.физиол.журн. 2017. №10.С.1132-1142.
4. Johnson E. M. et al. The effects of drug which destroy the sympathetic nervous system on the retrograde transport of nerve growth factor. 1999.
5. https://allmed.pro/drugs/oktadin/2020.
6. https://ru.wikipedia.org/wiki/2023.
7. https://studfile.net/preview//Механизм антигипертензивного действия гуанетидина. 2023.
8. https://www.medchemexpress.com/Guanethidine-sulfate.2022.
9. https://www.vidal.ru/drugs/molecule/Гуанетидин (Guanethidine).2020.

O‘ZBEKISTON MILLIY UNIVERSITETI XABARLARI, 2024, [3/1/1]
ISSN 2181-7324

FIZIKA
http://journals.nuu.uz
Natural sciences

UDK: 530.12:531.51

Husanboy HOSHIMOV,
Teacher at Fergana State University, Murabbiylar St 19,
E-mail:hoshimovhusanboy25@gmail.com
Vakhid KHAMIDOV,
Associate Professor at Tashkent University of Information Technologies, (PhD),
E-mail:vkhamidov@tuit.uz
Maksud *UMARALIYEV,*
Junior researcher at Institute of Fundamental and Applied Research,
National Research University TIIAME, Kori Niyoziy 39,
E-mail: umaraliyevmaksud@mail.com

Ulug'bek nomidagi Astronomiya instituti, f.-m.f.d A.A.Abdujabbarov taqrizi asosida

WEAK GRAVITATIONAL LENSING OF A GUP-MODIFIED SCHWARZSCHILD BLACK HOLE IN THE PRESENCE OF PLASMA

Annotation

In this work, we have studied weak gravitational lensing effect around black hole. We started with orbits of photons around black hole in S-GUP. In addition, we have studied gravitational weak lensing around such black hole in plasma medium.

Keywords: Generalized Uncertainty Principle (GUP), General relativity (GR), Schwarzschild black hole, Accretion disk, Kerr black hole.

СЛАБОЕ ГРАВИТАЦИОННОЕ ЛИНЗИРОВАНИЕ GUP-МОДИФИЦИРОВАННОЙ ЧЕРНОЙ ДЫРЫ ШВАРЦШИЛЬДА В ПРИСУТСТВИИ ПЛАЗМЫ

Аннотация

В этой работе мы изучили эффект слабого гравитационного линзирования вокруг черной дыры. Мы начали с орбит фотонов вокруг черной дыры в S-GUP. Кроме того, мы исследовали слабое гравитационное линзирование вокруг такой черной дыры в плазменной среде.

Ключевые слова: Обобщенный принцип неопределенности (ОПН), Общая теория относительности (ОТО), черная дыра Шварцшильда, Аккреционный диск, Черная дыра Керра.

WEAK GRAVITATIONAL LENSING OF A GUP-MODIFIED SCHWARZSCHILD BLACK HOLE IN THE PRESENCE OF PLASMA

Annotatsiya

Ushbu ishda biz qora tuynuk atrofida zaif tortishish linzalash effektini o'rgandik. Biz S-GUPdagi qora tuynuk atrofidagi fotonlarning orbitalaridan boshladik. Bundan tashqari, biz plazma muhitida bunday qora tuynuk atrofida tortishish kuchsiz linzalarini o'rgandik.

Kalit so'zlar: Umumlashtirilgan noaniqlik printsipi (UNP), Umumiy nisbiylik (UN), Shvartsshild qora tuynugi, Akkretsiya diski, Kerr qora tuynuk.

Introduction. The generalized uncertainty principle (GUP) offers insights into the limitations of general relativity (GR) by incorporating nonlinear terms in the uncertainty relationship between position and momentum operators[1]. These terms, motivated by string theory and loop quantum gravity, have been studied extensively, including their effects on the accretion disk onto Schwarzschild black holes[2][3]. Estimates of the GUP parameters have been derived from various physical phenomena, such as gravitational wave events, perihelion precession, and weak lensing, providing constraints on modified gravity models[4-10]. Recent observations, including gravitational waves and images of supermassive black holes by the LIGO-Virgo and Event Horizon Telescope collaborations, respectively, offer new avenues for testing alternative gravity theories[11-13]. The presence of magnetized plasma near supermassive black holes, as observed by the Event Horizon Telescope, highlights the need for better theoretical models to understand such environments[19]. In this context, we focus on studying non-magnetized plasma near black holes, considering its effects on the deflection of light and weak gravitational lensing[20]. Understanding photon motion and weak lensing around black holes provides fundamental insights into gravity's behavior and can reveal deviations from established theories[21-22]. By integrating these tests, we aim to refine our understanding of gravity and its role in the universe's evolution. In this paper, we calculate the deflection angle in the weak field limit (Sect. II) and summarize our results (Sect. III).

Gravitational weak lensing in presence of the plasma medium. In this section, our main objective is to investigate the effects of gravitational lensing in the Schwarzschild black hole with corrections from the Generalized Uncertainty Principle (GUP), while considering the presence of surrounding plasma. We undertake this analysis using a weak-field approximation, as defined by [23]. In Boyer-Lindquist coordinates, S-GUP metric is given by [5]

$$ds^2 = -f(r)dt^2 + f(r)^{-1}dr^2 + r^2(d\theta^2 + \sin^2\theta d\phi^2),$$

with

$$f(r) = 1 - \frac{2M}{r} + \epsilon\frac{M^2}{r^2}$$

Here, ϵ serves as a dimensionless parameter representing the GUP correction [5], which has been bounded within the range $-44.9 < \epsilon \leq 1$ [7]. Additionally, it's important to note that this metric simplifies to the Schwarzschild metric as ϵ approaches 0 .

$$g_{\alpha\beta} = \eta_{\alpha\beta} + h_{\alpha\beta},$$

Here, $\eta_{\alpha\beta}$ and $h_{\alpha\beta}$ denote the Minkowski metric and perturbation metric, respectively, with their properties outlined in [23].

$$\eta_{\alpha\beta} = \text{diag}(-1,1,1,1),$$
$$h_{\alpha\beta} << 1,\ h_{\alpha\beta} \to 0 \text{ under } x^{\alpha} \to \infty$$
$$g^{\alpha\beta} = \eta^{\alpha\beta} - h^{\alpha\beta},\ h^{\alpha\beta} = h_{\alpha\beta}.$$

We are interested in examining the effects of plasma on the deflection angle of light rays. In the presence of a plasma medium, the deflection angle can be expressed as described in [23].

$$\hat{\alpha}_i = \pm\frac{1}{2}\int_{-\infty}^{\infty}\left[\frac{1}{2}\left(h_{33,i} + \frac{\omega^2}{\omega^2-\omega_e^2}h_{00,i} - \frac{K_e}{\omega^2-\omega_e^2}\omega^2 N_{,i}\right)\right]dz$$

$N(x^i)$ represents the number density of particles in the plasma surrounding the black hole, and $K_e = 4\pi e^2/m_e$ is a constant. The $\pm$ signs of $\hat{\alpha}_\iota$ determine the deflection towards or away from the central object, respectively. For large distances, we can approximate the black hole metric as follows:

$$ds^2 = ds_0^2 + \left(\frac{R_s}{r} - \epsilon\frac{R_s^2}{4r^2}\right)dt^2 + \left(\frac{R_s}{r} - \epsilon\frac{R_s^2}{4r^2}\right)dr^2,$$

Here, $ds^2 = -dt^2 + dr^2 + r^2(d\theta^2 + \sin^2\theta d\phi^2)$, and for further calculations, we utilize $R_s = 2M$ as the Schwarzschild radius. In Cartesian coordinates, the components $h_{\alpha\beta}$ can be expressed as:

$$h_{00} = \left(\frac{R_s}{r} - \epsilon\frac{R_s^2}{4r^2}\right),$$
$$h_{jk} = \left(\frac{R_s}{r} - \epsilon\frac{R_s^2}{4r^2}\right)n_j n_k,$$
$$h_{33} = \left(\frac{R_s}{r} - \epsilon\frac{R_s^2}{4r^2}\right)\cos^2 x,$$

Here, $\cos x = \frac{z}{\sqrt{b^2+z^2}}$ and $r = \sqrt{b^2+z^2}$, where b represents the impact parameter, indicating the closest approach of the photons to the black hole. By employing the aforementioned expressions in the formula, one can calculate the light deflection angle with respect to b for a black hole surrounded by plasma.

$$\hat{\alpha}_b = \int_{-\infty}^{\infty}\frac{b}{2r}\left[\partial_r\left(\left(\frac{R_s}{r} - \epsilon\frac{R_s^2}{4r^2}\right)\cos^2 x\right) + \partial_r\left(\frac{R_s}{r} - \epsilon\frac{R_s^2}{4r^2}\right)\frac{\omega^2}{\omega^2-\omega_e^2} - \frac{K_e}{\omega^2-\omega_e^2}\partial_r N\right]dz$$

In light of the preceding discussion, we can readily examine the impact of different plasma mediums on the photon deflection angle, as depicted in Figure.1.

Uniform plasma. In the first case, we consider homogeneous plasma with $\omega_0^2 = \text{const}$. In this plasma state, the refractive index does not explicitly depend on spatial coordinates, so we can disregard the refractive action. In other words, we do not consider the last term of Eq. (13). By integrating Eq. (13), we obtain the following result for the deflection angle.

$$\hat{\alpha}_{uni} = \left(\frac{R_s}{b} - \epsilon\frac{\pi R_s^2}{16b^2}\right) + \left(\frac{R_s}{b} - \epsilon\frac{\pi R_s^2}{8b^2}\right)\frac{1}{1-\frac{\omega_0^2}{\omega^2}}$$

Graphs illustrating the impact parameter b for different GUP parameter ϵ (left) and plasma parameters $\frac{\omega_0^2}{\omega^2}$ (right) are depicted in Fig.1. The deflection angle increases with decreasing impact parameter b, indicating that a massless particle approaching the vicinity of a black hole experiences

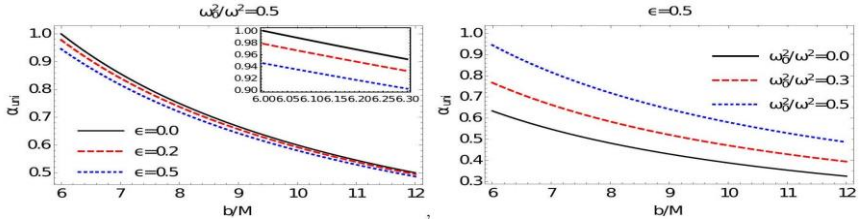

FIG. 1:The plot illustrates how the deflection angle $\hat{\alpha}_{uni}$ varies with the impact parameter b.

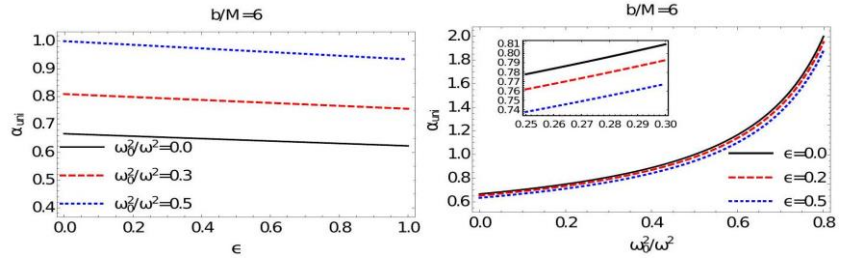

FIG. 2: The graph displays the deflection angle $\hat{\alpha}_{\text{uni}}$ plotted against the parameters $\frac{\omega_0^2}{\omega^2}$ and ϵ, with a fixed impact parameter $b/M = 6$.

a greater deviation. Fig. 2 visually illustrates the variation of the deflection angle concerning $\frac{\omega_0^2}{\omega^2}$ and ϵ. Specifically, the deflection angle is maximized with higher plasma distribution (right panel) and is observed to decrease significantly with increasing GUP parameter ϵ (right panel).

B. Singular isothermal sphere. The Singular Isothermal Sphere (SIS) serves as a highly suitable model for comprehending the characteristics of photons undergoing gravitational lensing. Initially introduced to investigate lens properties and clusters, the SIS represents a spherical distribution of matter with a density feature

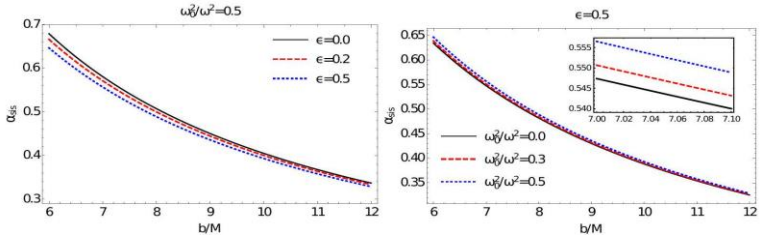

FIG. 3: The figure illustrates the change in $\hat{\alpha}_{sis}$ concerning b under different ϵ values (left panel) and $\frac{\omega_0^2}{\omega^2}$ (right panel).

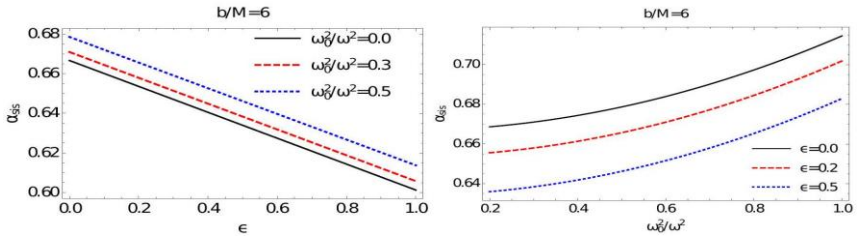

FIG. 4: Plot of the deflection angle $\hat{\alpha}_{sis}$ as a function of ϵ (left panel) and $\frac{\omega_0^2}{\omega^2}$ (right panel) for a fixed impact parameter $b/M = 6$.

that extends to infinity at its center. The density distribution of a SIS is given by [20]

$$\rho(r) = \frac{\sigma_v^2}{2\pi r^2}$$

where σ_v^2 refers to a one-dimensional velocity. The plasma concentration follows the given analytical dispersion and admits the following analytic expression [23, 24].

$$N(r) = \frac{\rho(r)}{\kappa m_p}$$

here m_p is the proton mass and k is a dimensionless constant coefficient generally associated with the dark matter universe. Utilizing the plasma frequency takes the form

$$\omega_e^2 = K_e N(r) = \frac{K_e \sigma_v^2}{2\pi\kappa m_p r^2}$$

We consider the aforementioned properties of the SIS and compute the angle of deflection $\hat{\alpha}_{SIS}$ as follows:

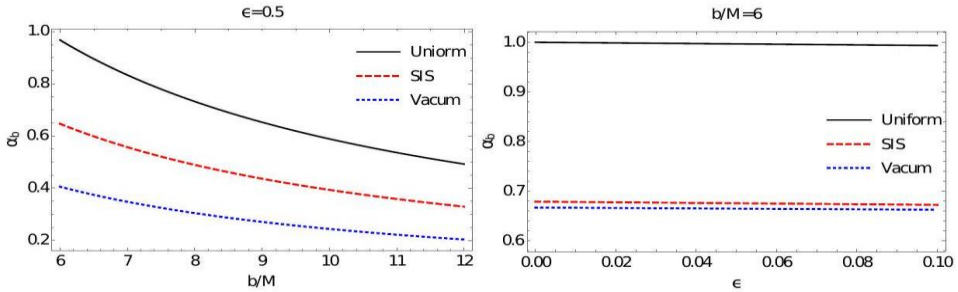

FIG. 5: Plot of the deflection angle $\hat{\alpha}_b$ as function of the impact parameter b and ϵ. The correspoding fixed parameters used are $\frac{\omega_0^2}{\omega^2} = 0.5, \frac{\omega_c^2}{\omega^2} = 0.5, b/M = 6, r_c = 3$

$$\hat{\alpha}_{SIS} = \left(\frac{2R_s}{b} - \epsilon\frac{3\pi R_s^2}{16b^2}\right) + \frac{R_s^2\omega_c^2}{b^2\omega^2}\left(\frac{1}{2} - \frac{2R_s}{3\pi b} + \epsilon\frac{3\pi R_s^2}{16b^2}\right)$$

These calculations result in an additional plasma constant ω_c^2, which can be expressed analytically as follows [24]:

$$\omega_c^2 = \frac{K_e\sigma_v^2}{2\pi\kappa m_p R_s^2}$$

In order to understand the impact of the Singular Isothermal Sphere (SIS) on the trajectory of photons, we have plotted the deflection angle $\hat{\alpha}_{SIS}$ as a function of the impact parameter b, as shown in Fig. 3. Interestingly, we observe common characteristics in the behavior of b for both the uniform plasma and SIS medium. Additionally, the quantity $\frac{\omega_c^2}{\omega^2}$ represents the distribution of the SIS in the vicinity of the black hole, allowing us to analyze the sensitivity of photons to this specific parameter along with the coupling constant parameter ϵ. This analysis is depicted graphically in Fig. 4. We observe that $\hat{\alpha}_{SIS}$ decreases with

increasing ϵ (left panel), while it increases with increasing $\frac{\omega_c^2}{\omega^2}$ (right panel). Thus, the presence of the SIS in the vicinity of the black hole has a noticeable effect on the trajectory of massless particles. Fig. 5 is a visual juxtaposition of the $\hat{\alpha}_{uni}, \hat{\alpha}_{SIS}$ as a function of the impact parameter and the parameter ϵ. It is quite obvious that the deflection is maximum when the black hole is surrounded by a uniform plasma medium. The final result can therefore be encapsulated in a mathematical expression as, $\hat{\alpha}_{uni} > \hat{\alpha}_{SIS}$

Conclusion. In this paper, we have investigated gravitational weak lensing in Schwarzschild spacetime with a modified GUP parameter. When studying weak gravitational lensing, it is observed that the presence of the GUP modification parameter ϵ leads to a decrease in the deviation angle. As the impact parameter b decreases, an increase in the deflection angle is observed, indicating that a massless particle moving closer to the black hole's surroundings experiences a higher degree of deviation. The deflection angle is maximized in the presence of high plasma distribution and is observed to decrease steadily with increasing GUP parameter ϵ. For instance, when $\epsilon = 0$, Schwarzschild gravity ensures the highest degree of deviation $\hat{\alpha}_{uni}$. We conclude that, as expected, the presence of plasma in the vicinity of the black hole, contrary to the vacuum case $\frac{\omega_0^2}{\omega^2} = 0$, contributes to the motion of photons.

REFERENCES

1. A. F. Ali, S. Das, and E. C. Vagenas, Phys. Lett. B 678, 497 (2009), arXiv:0906.5396 [hep-th] .
2. M. Moussa, Annals Phys. 453, 169305 (2023).
3. D. B. Lenat, Artif. Intell. 21, 61 (1983).
4. Z.-W. Feng, S.-Z. Yang, H.-L. Li, and X.-T. Zu, Phys. Lett. B 768, 81 (2017), arXiv:1610.08549 [hep-ph] .
5. F. Scardigli and R. Casadio, Eur. Phys. J. C 75, 425 (2015), arXiv:1407.0113 [hep-th] .
6. J. C. S. Neves, Eur. Phys. J C 80, 343 (2020), arXiv:1906.11735 [gr-qc] .
7. O. Ökcü and E. Aydiner, Nucl. Phys. B 964, 115324 (2021), arXiv:2101.09524 [gr-qc] .
8. K. Jusufi, M. Azreg-Aïnou, M. Jamil, and T. Zhu, Int. J. Geom. Meth. Mod. Phys. 19, 2250068 (2022), arXiv:2008.09115 [gr-qc] .
9. J. L. Synge, Relativity: The General Theory (New York,: Interscience Publishers, 1960).
10. M. Azreg-Aïnou, Z. Chen, B. Deng, M. Jamil, T. Zhu, Q. Wu, and Y.-K. Lim, Phys. Rev. D 102, 044028 (2020), arXiv:2004.02602 [gr-qc] .
11. B. P. Abbott and et al., Phys. Rev. Lett 116, 061102 (2016), arXiv:1602.03837 [gr-qc] .
12. K. Akiyama and et al., ApJ. 875, L1 (2019), arXiv:1906.11238 [astro-ph.GA] .
13. K. Akiyama and et al., Astrophys. J. Lett 930, L12 (2022).
14. S. Vagnozzi and et al., Classical and Quantum Gravity 40, 165007 (2023), arXiv:2205.07787 [gr-qc] .
15. R. C. Pantig and A. Övgün, Annals of Physics 448, 169197 (2023), arXiv:2206.02161 [gr-qc] .
16. R. K. Walia, S. G. Ghosh, and S. D. Maharaj, Astrophys. J. 939, 77 (2022), arXiv:2207.00078 [gr-qc]
17. F. Atamurotov, I. Hussain, G. Mustafa, and A. Övgün, Chinese Physics C 47, 025102 (2023).
18. F. Atamurotov, I. Hussain, G. Mustafa, and K. Jusufi, Eur. Phys. J. C 82, 831 (2022), arXiv:2209.01652 [gr-qc] .
19. K. Akiyama et al. (Event Horizon Telescope), Astrophys. J. Lett. 910, L13 (2021), arXiv:2105.01173 [astro-ph.HE] .
20. Q. Li, Y. Zhu, and T. Wang, Eur. Phys. J. C 82, 2 (2022), arXiv:2102.00957 [gr-qc]
21. W. Chou and T. Tajima, Astrophys. J. 513, 401 (1999).
22. A. E. Broderick et al., Astrophys. J. 935, 61 (2022), arXiv:2208.09004 [astro-ph.HE] .
23. G. S. Bisnovatyi-Kogan and O. Y. Tsupko, Mon. Not. R. Astron. Soc 404, 1790 (2010), arXiv:1006.2321 [astro-ph.CO] .
24. G. Z. Babar, F. Atamurotov, and A. Z. Babar, Physics of the Dark Universe 32, 100798 (2021).

O‘ZBEKISTON MILLIY UNIVERSITETI XABARLARI, 2024, [3/1/1]
ISSN 2181-7324

FIZIKA
http://journals.nuu.uz
Natural sciences

UO‘K: 524.4

Fazliddin SHAMSHIYEV,
Ozbekiston Milliy unversiteti, f.-m.f.n
E-mail: shamshiyev_f@nuu.uz

Chirchiq davlat pedagogika universiteti, f.-m.f.dok., dotsent I.U.Tadjibaev taqrizi asosida

YULDUZLAR DINAMIKASIDA UCHINCHI VA LOKAL INTEGRALARNING MUAMMOLARI HAQIDA

Annotatsiya

Ushbu maqolada harakat tenglamalarining uchinchi integrali va ikkinchi invarianti – lokal integralining yulduzlar dinamkasida qo‘lanilishi haqida gisqacha gap boradi. Statsionar gravitatsion maydon uchun lokal integralining ma’nosi va ularining mavjud bo‘lgan ba‘zi holarini keltiramiz.

Kalit so‘zlar: yulduzlar dinamikasi, gravitasion potensial, harakat integrallari.

ON THE PROBLEMS OF THE THIRD AND LOCAL INTEGRALS IN STELLAR DYNAMICS

Annotation

This article briefly discusses the application of the third integral and the second invariant - the local integral of the equations of motion in stellar dynamics. We present the value of the local integral and some cases of their existence.

Key words: stellar dynamics, gravitational potential, integrals of motion.

О ПРОБЛЕМАХ ТРЕТЬЕГО И ЛОКАЛЬНОГО ИНТЕГРАЛОВ В ЗВЕЗДНОЙ ДИНАМИКЕ

Аннотация

В этой статье кратко рассматривается применение третьего интеграла и второго инварианта -локального интеграла уравнений движения в звездной динамике. Приведем значение локального интеграла и некоторые случаи их существования.

Ключевые слова: звездная динамика, гравитационный потенциал, интегралы движения.

Введение. Проблема существования дополнительного интеграла движения, в регулярном стационарном гравитационном поле, независимого от интегралов энергии и площадей, обсуждалась во многих работах [2-32] и [60-80].

В течение долгого времени предполагалось, что третий интеграл движения отдельной звезды в регулярном стационарном гравитационном поле Галактики, с помощью которого определяется возможные виды выражения фазовой плотности в звездных системах, не является однозначным [33-38], на том основании, что, несмотря на многочисленные усилия, не было обнаружено явный вид третьего интеграла, выражаемого в аналитической форме, подобной как интегралов энергии и площадей. Но это предположение, как часто отмечалось, вступает в противоречие с наблюдаемым распределением скоростей звезд вблизи Солнца, поскольку из него следует, что разброс скоростей должен быть одинаковыми в направлении центра Галактики R и в направлении перпендикулярный к плоскости галактики z, тогда как наблюдаемые дисперсии скоростей по этим координатам, соответственно, имеют соотношение приблизительно 2:1, т.е., для всех подсистем Галактики дисперсия вертикального компонента скорости меньше, чем радиального почти в два раза [39, 40]. А также, численно вычисленные орбиты звезд оказались такими, как если бы у них было не два, а три однозначных интеграла движения [41-44].

В работах [45-46, 49] были предприняты попытки теоретически доказать существование третьего интеграла, но каждый дополнительный интеграл может быть однозначным или многозначным. Действительно, аргументами фазовой плотности должны быть именно однозначные интегралы (они иногда называются также «*изолирующими*»), иначе сама фазовая плотность также получится многозначной, что лишено физического смысла. Однако, Г.М.Идлис рассматривает случаи, когда интеграл, вообще многозначный, но для определенных форм потенциала $U(x,y,z)$ вырождается в однозначную функцию [4-7].

В работе [5] Г.Г.Кузмин подробно описывает применимость *квадратичного интеграла движения* для моделирования стационарной Галактики, допускающее трехосное распределение скоростей, а также в статьях [8, 49] много раз обсуждались свойства этого интеграла. Были также попытки определения и других форм третьего интеграла, например, Г.М.Идлис в работе [11] ищет интеграл движения, представляющий собой сумму членов нулевого, второго и четвертого порядков относительно компонентов скорости.

D. Lynden-Bellom исследовано, что каждый из известных до сих пор интегралов движения для стационарных систем сохраняет силу для целого класса таких систем. При этом весь класс или его часть можно получить, варьируя некоторую функцию одной переменной. Сама эта функция входит как в потенциал, так и в интеграл движения локальным образом, т.е. без помощи действий дифференцирования и интегрирования [46].

Третий интеграл G. Contopoulos представляет собой разложение в ряд по степеням отклонений в фазовом пространстве от какой-либо фиксированной круговой орбиты или, что обычно эквивалентно первому определению, ряд по степеням малого параметра, характеризующего отклонение гравитационного потенциала от квадратичной формы [61-65].

Таким образом, понятно, что если рассматриваемый потенциал не имеет осевой или ротационной симметрии, то интеграла площадей не существует и третий интеграл как правило, является многозначным, [46, 48, 62, 72], и тогда проблемой становится уже второй интеграл после интеграла энергии.

В работе [1] В.А. Антоновым было введено понятие локального интеграла, отличного от интеграла Линден-Белла [46, 48]. Фундаментальная работа В.А.Антонова, положила начало поискам второго инварианта в виде одной изолированной гиперповерхности, существование которой дает некоторую ориентировку в свойствах множества возможных траекторий, поскольку локальный интеграл играет в фазовом пространстве роль барьера, через которой изображающая точка не может никогда перейти [1, 51, 52, 54-56].

Локальный интеграл Антонова, построенный в аналитическом виде, в отличие от настоящего интеграла, вообще говоря, не позволяет найти сами траектории, а только инвариантные множества в фазовом пространстве. Однако, возможны случаи полного нахождения области движения или траектории и с локальным интегралом [53, 56].

Известные случаи интегрируемости уравнения движения.

Отыскание точных траекторий движения пробной частицы в произвольном потенциальном поле, стационарном лишь во вращающейся системе координат, представляет, вообще говоря большие трудности, чем для неподвижной системы. Для такой системы как известно существует только интеграл Якоби [2]. Так, например, для системы с ненулевым вращением не удаётся разделить переменные при потенциале и представить его в виде

$$U = U_1(x) + U_2(y), \tag{1}$$

кроме некоторых довольно простых случаев. К числу этих простых случаев относятся следующие:

а) Ротационно-симметричный потенциал.

$$U = U(\rho, z), \ (\rho = \sqrt{x^2 + y^2}); \tag{2}$$

(вращение по существу не играет никакой роли).

в) Уравновешенность по одной из координат,

$$U = -\frac{\Omega^2 x^2}{2} + U_0(y); \tag{3}$$

с) Квадратичный потенциал,

$$U = \frac{Ax^2}{2} + \frac{By^2}{2}, \tag{4}$$

соответственно с линейными уравнениями движения.

Известно, что во всех этих случаях можно найти дополнительный интеграл движения, не зависящий от интеграла энергии [53].

Случаи существования локального интеграла.

Само понятие локального интеграла в используемом здесь смысле первые было в введено в звездную динамику В.А. Антоновым [1], хотя по существу такое же понятие использовалось ранее в теории волчка [81]. То есть речь идет об отдельной инвариантной поверхности в фазовом пространстве. В работе [1] выражение такого локального интеграла давалось формулой

$$A(x,y)u^2 + 2B(x,y)uv + C(x,y)v^2 = 1, \tag{5}$$

где $x, y -$ декартовы координаты; $u, v -$компоненты скорости; $A(x,y), B(x,y)$ и $C(x,y) -$ некоторые неизвестные функции, подлежащие определению. Ясно, что такое описание топологических свойств траекторий звезды возможно только при наличии интеграла энергии

$$\frac{u^2+v^2}{2} - U(x,y) = h, \tag{6}$$

для любого значения $h -$постоянной интеграла энергии.

В [1] В.А. Антоновым определен класс потенциалов, для которых инвариантность (5) существует. Поверхность, задаваемой формулой (5), играет роль барьера, через которой посторонняя изображающая точка не может перейти. Движение же, удовлетворяющее (5), происходит на плоскости (x, y) в некотором ящике. Форма самой траектории, в отличие от случая существования настоящего интеграла, не определяется в квадратурах, но порядок системы дифференциальных уравнений движения локальный интеграл позволяет понизить.

В работе [52] дано обобщение локального интеграла на случай вращения координатной системы, с постоянной угловой скоростью Ω, но только для формы первого порядка относительно компонентов скорости

$$a(x,y)u + b(x,y)v = \varphi(x,y,u,v). \tag{7}$$

где $a(x,y), b(x,y)$- некоторые неизвестные функции, подлежащие определению, $\varphi(x,y,u,v)$ – сам локальный интеграл. Тогда, искомый общий потенциал имеет форму,

$$U = \frac{1}{2}[S(\psi) + \varphi^2 - \Omega^2(x^2 + y^2)]. \tag{8}$$

Областью движения в типичных случаях является некоторое кольцо, сама же траектория оказывается принадлежащей к категории условно-периодических и часто показывает либо локальные «завитки», либо «волны» вблизи внутренней границы, что похоже на результаты численного интегрирования в более реалистических потенциалах. Доказано также существования периодического решения с отношением частот 1:3.

В [51] дано трехмерно обобщение, причем поле скоростей заранее ищется в виде

$$\left.\begin{aligned} u &= u_0(x,y,z) \pm \alpha(x,y,z)\sqrt{S(x,y,z)+2h} \\ v &= v_0(x,y,z) \pm \beta(x,y,z)\sqrt{S(x,y,z)+2h} \\ w &= w_0(x,y,z) \pm \gamma(x,y,z)\sqrt{S(x,y,z)+2h} \end{aligned}\right\} \quad (9)$$

где h −постоянная энергии.

$$U(x,y,z) = \frac{1}{2}\left[U_0(L) + \frac{H}{r^2}\right] \quad (10)$$

где функция H зависит только от угловых координат, а не от r.

В [54, 55] мы рассмотрим случаи когда система вращается с постоянной угловой скорости Ω. Предполагаем, что поле скоростей представляется в виде

$$\left.\begin{aligned} u &= u_0 \pm \alpha\sqrt{S+2h} + \Omega y \\ v &= v_0 \pm \beta\sqrt{S+2h} - \Omega x \\ w &= w_0 \pm \gamma\sqrt{S+2h} \end{aligned}\right\} \quad (11)$$

где $S, u_0, v_0, w_0,\ \alpha, \beta, \gamma$ −функции координат, h −произвольная постоянная энергии.

Известен для таких систем интеграл Якоби

$$\frac{u^2+v^2+w^2}{2} - \frac{\Omega^2(x^2+y^2)}{2} - U(x,y,z) = h. \quad (12)$$

Также найден общий вид допустимых потенциалов

$$U(x,y,z) = \frac{1}{2}\left[(grad\Phi)^2 + U_0(L) + \Omega\left(y\frac{\partial\Phi}{\partial x} - x\frac{\partial\Phi}{\partial y}\right)\right]. \quad (13)$$

Построен нетривиальный пример потенциала анализом топологии поверхностей уровня $U(x,y,z)$.

Результаты исследования могут быть применены для изучения движения звезд в системах, близких к сферической симметрии.

4. **Заключение.** Подчеркнем, что проблема регулярности движений актуальна не только в звездной динамике, но и вообще в различных областях механики и физики, причем встречающиеся при этом силы не обязательно имеют потенциал. Среди наиболее известных примеров можно указать движение заряженной частицы в магнитном поле [35,36], вращение твердого тела вокруг неподвижной точки [81] и проблему движения катящегося шара в бильярде (или, что математически то же самое, фотона в области с зеркальной границей) [25]. Последняя проблема интересна тем, что представляет собой предельный случай движения частицы в потенциальном поле: вместо непрерывно меняющегося потенциала здесь имеем «яму» с резкими высокими стенками. В частности, вырождение потенциала модели Г.Г. Кузьмина [8-15] дает эллиптический бильярд. В исследовании локального интеграла этот предельный случай «фотона» нередко играет важную подсобную роль.

Следует отметит, что существование локального интеграла с точки зрения удержания частиц в магнитных ловушках, часто решает практическую задачу пространственного ограничения области движения частицы, хотя бы настоящий интеграл при этом не существовал. Также и в теории бильярда известны примеры, когда движение частицы не распространяется на всю область, допустимую внешне по условиям задачи, хотя настоящий интегрируемости в этих примерах нет.

Благодарность. Работа выполнена в рамках гранта FZ-20200929344 Министерства образования, науки и инновации Республики Узбекистан.

ЛИТЕРАТУРА

1. Антонов В.А., Вестник Ленинград. гос. универ. 19, 97 (1981).
2. Jacobi's, Lectures on Dynamics, Second Revised Edition, Hindustan Book Agency (India), 2009
3. Whittaker, E. T., & Watson, G. N. 1902, A course of Modern Analysis (Cambridge University Press) Fifth edition 2021
4. Идлис Г.М., Астрон. журнал, 1959, 36, N 1, 85-88
5. Идлис Г. М., Труды Астрофиз. ин-та АН КазССР. Том. 1, 1961, 1963, 6.51.330 К
6. Идлис Г.М., Известия Астрон. ин-та АН КазССР, 1962, 13, 3-15
7. Идлис Г.М., Известия Астрон. ин-та АН КазССР, 1959, 8, 24-52.
8. Кузмин Г. Г. Астрон. журнал, 1956, 33, № 1, 27-45, 1957, № 3, 2042
9. Кузмин Г.Г., Бюллетень Абаст. обсерв., 1962, N 27, 89-92
10. Кузмин Г.Г., Публ. Тартус. астрон. обсерв., 1963, 34. N 1. 9-37
11. Кузмин Г.Г., Публ. Тартус. астрон. обсерв., 1963. 34. N 1. 457-484
12. Кузмин Г.Г., Маласидзе Г.А., Публ. Тартус. астр. обсерв., 1969. 38. 181-250
13. Кузьмин Г.Г., Динамика галактик и звездных скоплений. Алма-Ата, с. 71. (1973)
14. Кузьмин Г.Г., Дин. галактик и звездных скоплений. Алма-Ата. 1973. 71-75
15. Кузмин Г.Г., Публ. Тартус. астрофиз. обсерв., 1973. 40, 3-10
16. Огородников К.Ф., Динамика звездных систем, М. Физматгиз., с.636, 1958.
17. Агекян Т.А., Астрономический журнал, т. 49, с. 371 (1972)
18. Агекян Т. А., Астрон. журнал, 1972, 49, N 2, с. 371.
19. Агекян Т. А., Астрон. журнал, 1994, 71, N 2. (принята к печати).
20. Агекян Т.А., Вьюга А.А., Вестник Ленинград. ун-та. 1973, N 7. с. 128.
21. Агекян Т. А., Орлов В.В. Письма в Астрон. журнал, 1989, т. 15, с. 771.
22. Агекян Т. А., Питьев Н. П. Астрон. журнал, 1977, 54, N 5.
23. Агекян Т.А., Якимов С. П. Вестник Ленинград. ун-та, 1975. N 1. с. 185.
24. Агекян Т.А., Якимов С. П. Вестник Ленинград. ун-та, 1976, N 13. с. 177.

25. Антонов В. А., Итоги науки и техники. Сер. астрон., 1968, т. 4.
26. Антонов В. А., Итоги науки и техники. Сер. астрон. 1985, т. 26.
27. Антонов В.А., Вестник Ленинград. ун-та, 1981, N 19, с. 97.
28. Осипков Л.П., АЦ. 1971, N 623, 1-2
29. Осипков Л.П., Астрофизика, 1972, N 1, 139-147
30. Осипков Л.П., Тр. АО ЛГУ, 1972, 29
31. Осипков Л.П., Астрофизика, 1972, 8, N 2, 295-304
32. Орлов В.В., Вестник Ленинград. ун-та. 1988. N 1. 4
33. Jeans, J. H., Monthly Notices Roy, Astron. Soc. 76, 81, 1915
34. Jeans, J. H., Problems of Cosmogony and Stellar Dynamics (Cambridge University Press, New York), p. 233, 1919
35. Lindblad, B. Handbuch der Astrophysik (Springer-Verlag, Berlin), Vol. V/2, p. 1038, 1933
36. Lindblad, B. Handbuch der Astrophysik (Springer-Verlag, Berlin), Vol. 53, p. 28, 1959
37. Smart, W. M., Stellar Dynamics (Cambridge University Press, New York), p. 338, 1938
38. van der Pahlen, E., Einfükrung in die Dynamik von Stern-systemen (Verlag Birkhäuser, Basel), p. 61, 1947
39. Локтин А.В., Марсаков В.А., Лекции по звёздной астрономии, Типография ЮФУ, 282 с. (2009)
40. Binney J., Tremaine S., Galactic Dynamics: Second Edition, Series: Princeton Series in Astrophysics, Edition: REV-Revised, 2, Published by: Princeton University Press, DOI.org/10.2307/j.ctvc778ff, (2008)
41. Contopoulos G., Stockholms Obs. Ann. 19, No. 10. ibid. 20, No. 5. 1958,
42. Contopoulos G., Astron., Journal, 68,273, 1963
43. Ollongren A., Bull. Astron. Inst. Neth., 16, 241, 1962
44. Hénon M., & Heiles C., The Astronomical Journal v. 69, Num. 1, (1964)
45. Wintner A., The Analytical Foundalions of Celestial Mechanics (Princeton University Press, Princeton, New Jersey), p. 96, 1947
46. Lynden-Bell D., Monthly Notices Royal Astron. Soc. 124, 95 DOI:10.1093/mnras/ 124.2.95, (1962)
47. de Zeeuw, Lynden-Bell D., Monthly Notices Royal Astron. Soc. (1985)
48. Lynden-Bell D., Monthly Notices Royal Astron. Soc. 458 (1), 726 (2016). DOI:10.1093/mnras/stw229
49. Ollongren A. Three-dimensional galactic stellar orbits. Bull. Astron. Inst. Netherl.», 1962, 16. № 521, 211-295. 1963, 5.51.365 55.
50. Bienaymé O., “Integrals of motion for non-axisymmetric potentials”, A&A, vol.627 (2019)
51. Антонов В.А., Шамшиев Ф. Т., Астрономический журнал. 69 (5), 971 (1992)
52. Antonov V.A. and Shamshiev F.T., Celestial Mechanics and Dynamical Astronomy 56 (3), 451 (1993). DOI:10.1007/BF00691813
53. Antonov V.A. and Shamshiev F.T., Celestial Mechanics and Dynamical Astronomy 59 (3), 209 (1994). DOI:10.1007/BF00692872
54. Shamshiev F.T., Astronomical and Astrophysical Transactions 7 (4), 269 (1995). DOI:10.1080/10556799508203273
55. Shamshiev F.T., in Proc. All-Russian Conf. on Astronomy at the Epoch of Multimessenger Studies, Moscow, Russia, 2021, Ed. by A. M. Cherepashchuk (Janus-K, Moscow, 2022), pp. 468–470. DOI:10.51194/VAK2021.2022. 1.1.195
56. Шамшиев Ф.Т., Астрофизический бюллетень, том 79, №1, с. 153–161 (2024)
57. Власов А.К., Курс высшей математики. Том I. Аналитическая геометрия. Дифференциальное и интегральное исчисления (часть первая), URSS, 480 с. ISBN 978-5-9710-8821-9, (2021)
58. Сокольников И.С., Тензорный анализ (с приложениями к геометрии и механике сплошных сред), М.: Наука, с. 376, (1971)
59. Мозер Ю., КАМ-теория и проблемы устойчивости, перевод под. ред. Трещёва, Ижевск: НИЦ «Регулярная и хаотическая динамика», 448 с. (2001)
60. de Zeeuw P.T., Lynden-Bell D., “Best approximate quadratic integrals in stellar dynamics”, Monthly Notices Royal Astron. Soc., Vol. 215. P. 713-730 (1985)
61. Contopoulos G., Astron. J. 1971, 76, N 2, 147-156
62. Contopoulos G., Astron. and Astrophys., 1978, 64, N 3, 323-332
63. Contopoulos G., Astron. and Astrophys., 1980, N 1-2, 198-209
64. Contopoulos G., Celeste. Mech., 1981, 24, N 4, 355-366
65. Contopoulos G., Celeste. Mech., 1983, 21, N 2, 193-211
66. Contopoulos G., P.O. Vandervoort, The Astrophys. J., 1992, 389, 118-128
67. de Zeeuw P.T., MNRAS, 1985, 216, 273
68. de Zeeuw P.T., C. Hunter, Astrophys. J., 1990, 356, 365
69. de Zeeuw P.T., D. Lynden-Bell, MN RAS, 1985, 215, 713
70. de Zeeuw P.T., C. Hunter, M. Schwarschild, Astrophys. J., 1987, 317,607
71. Stodolkiewicz J.S., Acta Astronomica, 1972, N 4, 22, 375-386
72. Stodolkiewicz J.S., Acta Astronomica, 1974, N 2, 24, 153-164
73. Stodolkiewicz J.S., Acta Astronomica, 1974, N 3, 24, 265-274
74. Stodolkiewicz J.S., Acta Astronomica, 1974, N 4, 24, 321-326
75. Vandervoort P.O., The Astrophys. J., 1970, 161, 67
76. Vandervoort P.O., The Astrophys. J., 1973, 180, 739
77. Vandervoort P.O., The Astrophys. J., 1975, 201, 50
78. Vandervoort P.O., The Astrophys. J., 1978, 221, 539
79. Vandervoort P.O., The Astrophys. J., 1979, 232, 91-105
80. Vandervoort P.O., Monet D.G., The Astrophys. J., 1975, 232, 91-105
81. Голубев В.В., Лекции по интегрированию уравнения движения тяжелого твердого тела около неподвижной точки. М.: Гос.изд.тех.теор.л-ры, 288 с., 1953

O‘ZBEKISTON MILLIY UNIVERSITETI XABARLARI, 2024, [3/1/1]
ISSN 2181-7324

FIZIKA
http://journals.nuu.uz
Natural sciences

UDK:621.315.592.9

Latofat SHUHRATOVA,
O‘z.R.FA Fizika texnika instituti tayanch doktoranti
Rustam KABULOV *Rashidovich*
O‘z.R.FA Fizika texnika instituti f.-m.f.n., katta ilmiy xodimi
E-mail:shuhratovalatofat2@gmail.com

TDTU dotsenti, t.f.n M.Tulyagov taqrizi asosida

GUIDELINES FOR USING THERMAL VACUUM EVAPORATION METHOD FOR PRODUCING THIN FILMS OF PEROVSKITE

Annotation

This article provides an overview of thermal vacuum sputtering for producing high-quality perovskite thin films, essential for optoelectronic applications. It covers substrate preparation, deposition process of perovskite materials, controlled parameters, monitoring techniques, post-deposition treatments, and device integration. Highlighting its versatility, the article serves as a roadmap for researchers and practitioners in advancing perovskite-based optoelectronics.

Key words: thermal vacuum evaporation, perovskite thin films, deposition techniques, optoelectronic applications, film morphology.

РУКОВОДСТВО ПО ИСПОЛЬЗОВАНИЮ МЕТОДА ТЕРМОВАКУУМНОГО ИСПАРЕНИЯ ДЛЯ ПОЛУЧЕНИЯ ТОНКИХ ПЛЕНОК ПЕРОВСКИТА

Аннотация

В данной статье представлен обзор материала для получения коммерческих высококачественных тонких пленок перовскита методом термического вакуумного испарения для оптоэлектронных приложений. Он охватывает подготовку подложки, процесс осаждения перовскитного материала, контроль параметров, методы мониторинга, обработку после осаждения и изготовление устройств. Подчеркивая его универсальность, статья служит дорожной картой для исследователей и практиков в развитии оптоэлектроники на основе перовскита.

Ключевые слова: термическое вакуумное испарение, тонкие пленки перовскита, методы осаждения, оптоэлектронные приложения, морфология пленок.

PEROVSKIT YUPQA QATLAMLARNI TAYYORLASHDA TERMIK VAKUUM PURKASH USULINI QO‘LLASH BO‘YICHA QO‘LLANMA

Annotatsiya

Ushbu maqola optoelektronik qurilmalar uchun zarur bo‘lgan yuqori sifatli perovskit yupqa qatlamlarni termik vakuumli uchirish usuli yordamida tayyorlash bo‘yicha umumiy ma’lumot beradi. Ushbu maqola taglik tayyorlash, perovskit materiali, purkash jarayoni, parametrlarni boshqarish usullari, purkashdan keyingi ishlov berish va qurilmada qatlamni integratsiyalasni o‘z ichiga oladi. Maqola tadqiqotchilar va amaliyotchilar uchun perovskit asosidagi optoelektronikani rivojlantirishda yo‘l xaritasi bo‘lib xizmat qiladi.

Kalit so’zlar: termik vakuumli purkash, perovskit yupqa qatlamlar, purkash texnikasi, optoelektronik qurilmalar, qatlam morfologiyasi.

Introduction. In contemporary materials science and engineering, the pursuit of advanced materials with tailored properties has led to significant interest in perovskite materials [1]. These materials, with their versatile crystal structures and remarkable optoelectronic properties, hold immense promise for various applications ranging from solar cells to light-emitting diodes (LEDs) and beyond. Among the plethora of methods available for thin film fabrication, thermal vacuum evaporation has emerged as a versatile and efficient technique. Thermal vacuum evaporation stands out as a versatile and efficient technique for thin film fabrication due to its material compatibility, precise control over film properties, high deposition rates, vacuum environment advantages, compatibility with complex structures, and scalability for industrial production, distinguishing it from other methods available in the field [2]. This article aims to provide a detailed exploration of the process of using thermal vacuum evaporation to create perovskite thin films, offering insights into its advantages, challenges, and potential applications.

Thermal Vacuum Evaporation Method: An Overview

Research from leading research centers in 10 countries, coordinated by the National Renewable Energy Laboratory in the United States (NREL) and the Karlsruhe Institute of Technology (KIT) in Germany, has determined that the use of vapor deposition processes for perovskite layers holds promise for accelerating the commercialization of photosensitive structures based on perovskites [3]. Thermal vacuum evaporation stands as a prominent and extensively utilized technique within thin film fabrication processes due to its efficacy and versatility [4]. The methodology of thermal vacuum evaporation hinges upon the principle of sublimating a solid source material, often in the form of pellets or powder, followed by the subsequent condensation of the evaporated material onto a substrate surface, ultimately yielding a thin film product. This entire process unfolds within a vacuum environment, meticulously crafted to prevent the intrusion of contaminants and to optimize the quality of the resulting film. Let's understand the intricacies of the process; a thermal vacuum evaporation system consists of several essential components, each of which plays a vital role in ensuring the efficiency and accuracy of the deposition process. Firstly, the

vacuum chamber serves as the main protective vessel in which the entire process of creating a perovskite layer is carried out and the necessary conditions of vacuum purity are maintained. Within this chamber, a crucible or boat accommodates the solid source material intended for sublimation. This chamber is created in such a way as to provide controlled heating of the starting material, thereby initiating its transition to the gaseous phase. Central to the process is the heating element, designed to provide the necessary thermal energy to induce sublimation of the source material. This component ensures that the temperature within the crucible or boat reaches the threshold required for the material to undergo the phase transition from solid to vapor. Through meticulous temperature control, the heating element regulates the rate of sublimation, thereby exerting influence over crucial aspects such as deposition rate and film thickness. Finally, a substrate holder is incorporated into the system to support and secure the substrate upon which the thin film is to be deposited. This holder plays a pivotal role in positioning the substrate within the vacuum chamber, ensuring optimal exposure to the vaporized source material for uniform film formation. Moreover, the substrate holder may incorporate mechanisms for precise manipulation, enabling controlled movement or rotation to further enhance film uniformity and consistency across the substrate surface. Figure 1 shows a schematic diagram of a thermal evaporation system.

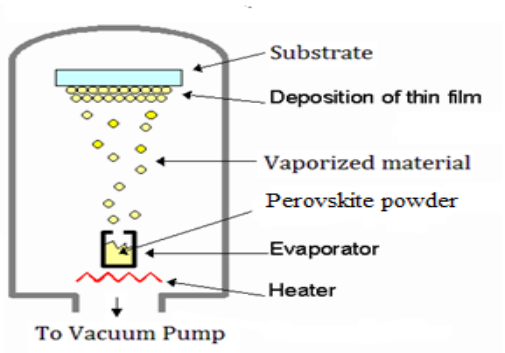

Figure 1. Schematic diagram of the thermal evaporation system [5]

Methodology of deposition. Thermal vacuum sputtering is a method used to deposit thin layers of materials onto substrates under controlled conditions of vacuum and temperature. In the context of the formation of thin layers of perovskite, the process must begin with the preparation of substrates on which thin layers of perovskite will be deposited. Substrates are typically made of materials like glass, silicon, or flexible polymers, depending on the application requirements. Substrates undergo thorough cleaning to eliminate contaminants such as dust, oils, and residues. Methods include ultrasonic cleaning, solvent rinsing, and plasma treatment. Ultrasonic cleaning employs high-frequency sound waves in a solvent-filled bath, while solvent rinsing uses organic solvents like acetone or ethanol. Plasma treatment exposes substrates to low-pressure plasma, removing organic contaminants and activating surfaces. Surface treatments, like deposition of functional layers or chemical modifications, enhance adhesion and promote uniform perovskite thin film growth. Techniques such as UV-ozone treatment or oxygen plasma treatment modify surface chemistry, facilitating uniform deposition. The next step is to prepare a source of high purity perovskite material. This target is typically made of the specific elements or compounds required to form the desired perovskite structure. For instance, for a lead halide perovskite, the target might contain lead, iodine, and other appropriate elements. The cleaned substrate is loaded into the vacuum deposition chamber, along with the perovskite target material. The chamber is then evacuated to create a vacuum environment, typically reaching pressures in the range of 10^{-6} to 10^{-7} torr (1torr=133,322 Pa). The sputtering process begins by bombarding the perovskite sources with high-energy ions. These ions dislodge adsorbed foreign atoms or molecules from the perovskite sources.

The perovskite film deposition process begins with a gradual increase in the heater temperature until sublimation begins. The sublimated atoms or molecules from the perovskite sources then condense on the surface of the substrate, forming a thin film. Various parameters are carefully controlled during the deposition process to achieve the desired thin film characteristics, such as thickness, composition, and crystal structure. These parameters include the evaporator temperature of the perovskite source, the substrate temperature, the deposition rate, and the pressure inside the chamber. Throughout the deposition process, the thickness and quality of the growing perovskite thin film are monitored using techniques such as in-situ spectroscopy, ellipsometry, or quartz crystal microbalance. After deposition, the thin film may undergo further characterization using techniques like X-ray diffraction (XRD), scanning electron microscopy (SEM), and atomic force microscopy (AFM) to assess its structural and morphological properties. Depending on the specific application requirements, post-deposition treatments such as annealing or surface passivation may be performed to improve the performance and stability of the perovskite thin film. Finally, the perovskite thin film may be integrated into devices such as solar cells, light-emitting diodes (LEDs), or photodetectors, depending on the intended application.

Analysis and result. Advantages of Thermal Vacuum Evaporation for Perovskite Thin Film Deposition: The vacuum environment minimizes impurities and contaminants, resulting in high-purity thin films with enhanced properties. By adjusting deposition parameters such as deposition rate and substrate temperature, precise control over the thickness of the perovskite thin film can be achieved [6]. Thermal evaporation ensures uniform coverage of the substrate surface, leading to consistent film quality and performance [7]. Thermal vacuum evaporation is compatible with a wide range of substrates, including glass, silicon, and flexible substrates, offering versatility in device fabrication [8].

Challenges and Considerations: Perovskite materials are sensitive to temperature variations, and excessive heating during evaporation can lead to degradation or phase transitions. Careful control of substrate temperature is essential to maintain the desired crystal structure and properties [9]. Achieving the desired stoichiometry in perovskite thin films is crucial for optimal

device performance. Controlling the deposition rate and the ratio of precursor materials is necessary to ensure proper composition [10]. The morphology of perovskite thin films significantly influences their optoelectronic properties. Optimization of deposition parameters is required to minimize defects such as pinholes, grain boundaries, and non-uniformity [11]. Perovskite materials are susceptible to environmental factors such as moisture and oxygen, which can degrade film quality and stability. Deposition under controlled vacuum conditions is essential to mitigate these effects [12].

Conclusion. In summary, thermal vacuum evaporation offers a versatile method for fabricating high-quality perovskite thin films with tailored properties for optoelectronic applications. While it provides advantages such as high-purity deposition, precise control over film thickness, and compatibility with various substrates, challenges like temperature sensitivity and stoichiometry control must be addressed. Nonetheless, with careful optimization and post-deposition treatments, thermal vacuum evaporation holds promise for advancing perovskite-based devices such as solar cells, LEDs, and photodetectors. Further research is essential to unlock its full potential in next-generation optoelectronics.

REFERENCES

1. Stranks, S. D., & Snaith, H. J. (2015). Metal-halide perovskites for photovoltaic and light-emitting devices. Nature Nanotechnology, 10(5), 391–402.
2. Liu, M., & Johnston, M. B. (2018). A Review of the Fabrication of Perovskite Solar Cells: Inorganic-Organic Hybrid Lead Halide Perovskite Active Layers. Solar RRL, 2(4), 1700186.
3. Tobias Abzieher, et.all. Vapor phase deposition of perovskite photovoltaics: short track to commercialization. Energy & Environmental Science. Volume 17 Number 5 7 March 2024 Pages 1627–2070. DOI: 10.1039/d3ee03273f
4. Park, N. G. (2015). Perovskite Solar Cells: An Emerging Photovoltaic Technology. Materials Today, 18(2), 65–72.
5. https://www.youtube.com/watchv=f7UxBawRPj4
6. Yang, W. S., Noh, J. H., Jeon, N. J., Kim, Y. C., Ryu, S., Seo, J., & Seok, S. I. (2015). High-performance photovoltaic perovskite layers fabricated through intramolecular exchange. Science, 348(6240), 1234–1237.
7. Green, M. A., & Ho-Baillie, A. (2017). Perovskite Solar Cells: The Birth of a New Era in Photovoltaics. ACS Energy Letters, 2(4), 822–830.
8. Saliba, M., Correa-Baena, J. P., Grätzel, M., Hagfeldt, A., & Abate, A. (2017). Perovskite Solar Cells: From the Atomic Level to Film Quality and Device Performance. Angewandte Chemie International Edition, 56(27), 7180–7194.
9. Jiang, Q., Zhang, L., Wang, H., Yang, X., Meng, J., Liu, H., Yin, Z., Wu, J., Zhang, X., You, J., & Li, Y. (2017). Enhanced electron extraction using SnO2 for high-efficiency planar-structure HC(NH2)2PbI3-based perovskite solar cells. Nature Energy, 2(1), 16177.
10. Yang, W. S., Park, B. W., Jung, E. H., Jeon, N. J., Kim, Y. C., Lee, D. U., Shin, S. S., Seo, J., Kim, E. K., Noh, J. H., & Seok, S. I. (2017). Iodide management in formamidinium-lead-halide–based perovskite layers for efficient solar cells. Science, 356(6345), 1376–1379.
11. Zhang, T., Yang, M., & Benson, J. C. (2018). Effects of Precursor Stoichiometry on the Morphology and Photovoltaic Performance of Perovskite Solar Cells. ACS Applied Energy Materials, 1(9), 4606–4614.
12. Zhao, J., Deng, Y., Wei, H., Zheng, X., Yu, X., Shao, Y., & Huang, J. (2017). Efficient two-dimensional Ruddlesden–Popper perovskite solar cells with enhanced moisture stability. Nature Communications, 8(1), 16045.

O‘ZBEKISTON MILLIY UNIVERSITETI XABARLARI, 2024, [3/1/1]
ISSN 2181-7324

FIZIKA
http://journals.nuu.uz
Natural sciences

UDK: 530.12:531.51

Odil YUNUSOV,
Master student at National University of Uzbekistan
E-mail: odilbekhamroev@gmail.com
Vakhid KHAMIDOV,
Associate Professor at Tashkent University of Information Technologies, PhD
E-mail:vkhamidov@tuit.uz
Inomjon IBRAGIMOV,
Junior Researcher at Institute of Fundamental and Applied Research, National Research University
E-mail: i.ibragimov@mail.ytit.uz

Ulug’bek nomidagi Astronomiya instituti, f.-m.f.d A.A.Abdujabbarov taqrizi asosida

SHADOW OF A GUP-MODIFIED SCHWARZSCHILD BLACK HOLE IN THE PRESENCE OF PLASMA

Annotation

In this research, we examined the shadow radius within the context of the Schwarzschild spacetime modified by Generalized Uncertainty Principle (GUP), denoted as S-GUP, in the presence of a plasma environment. Our investigation began by analyzing the photon orbits around a black hole in the S-GUP framework. Furthermore, we explored the characteristics of the shadow cast by such a black hole. Utilizing observational data from the Event Horizon Telescope (EHT) project related to M87* and Sgr A*, we derived constraints on the parameter ϵ within the gravitational framework of S-GUP.

Key words: black holes, generalized uncertainty principle (gup), string theory, loop quantum gravity,planck scale, plasma effects, photon motion, weak gravitational lensing.

ТЕНЬ GUP-МОДИФИЦИРОВАННОЙ ЧЕРНОЙ ДЫРЫ ШВАРЦШИЛЬДА В ПРИСУТСТВИИ ПЛАЗМЫ

Аннотация

В этом исследовании мы исследовали радиус тени в контексте пространства-времени Шварцшильда, модифицированного обобщенным принципом неопределенности (GUP), обозначенного как S-GUP, при наличии плазменной среды. Наше исследование началось с анализа орбит фотонов вокруг черной дыры в рамках S-GUP. Кроме того, мы исследовали характеристики тени, отбрасываемой такой черной дырой. Используя данные наблюдений проекта Event Horizon Telescope (EHT), связанные с M87* и Sgr A*, мы получили ограничения на параметр ϵ в рамках гравитационной структуры S-GUP.

Ключевые слова: черные дыры, обобщенный принцип неопределенности (ОПН), теория струн, петлевая квантовая гравитация, масштаб Планка, плазменные эффекты, движение фотонов, слабое гравитационное линзирование.

PLAZMA BO'LGAN SHVARJSCHILD QORA TUYNIGINING SOYASI

Annotatsiya

Ushbu tadqiqotda biz plazma muhiti mavjudligida S-GUP deb ataladigan Umumiy noaniqlik printsipi (GUP) tomonidan o'zgartirilgan Shvartsshild fazo vaqti kontekstida soya radiusini ko'rib chiqdik. Bizning tadqiqotimiz S-GUP tizimidagi qora tuynuk atrofidagi foton orbitalarini tahlil qilishdan boshlandi. Bundan tashqari, biz bunday qora tuynuk soyasining xususiyatlarini o'rganib chiqdik. M87* va Sgr A* bilan bog‘liq Event Horizon Telescope (EHT) loyihasidan olingan kuzatuv ma’lumotlaridan foydalanib, biz S-GUP gravitatsion doirasidagi ϵ parametriga cheklovlarni oldik.

Kalit so'zlar: kvant tortishish, umumiy nisbiylik, qora tuynuklar, umumlashtirilgan noaniqlik printsipi (UNP), iplar nazariyasi, halqa kvant tortishish, plank shkalasi, plazma effektlari, foton harakati, zaif tortishish linzalari.

Introduction. The challenge of unifying quantum theory and gravity stands out as one of the most captivating and formidable issues in contemporary physics. At the core of this endeavor is the effort to harmonize two highly successful yet inherently different theories: quantum mechanics, governing particle behavior at the subatomic level, and general relativity, describing spacetime curvature in response to mass and energy.

While quantum mechanics adeptly explains phenomena at atomic and subatomic scales, general relativity offers an elegant framework for comprehending the gravitational effects across solar to cosmic scales. Various attempts to merge these theories, such as string theory, loop quantum gravity, and others, have shed light on the intricate nature of this task. Fortunately, black holes, being both gravitational and quantum mechanical entities, serve as a unique laboratory to test predictions of quantum gravity. They also provide a theoretical foundation for advancing towards the overarching goal of formulating a theory of quantum gravity [1].

The Generalized Uncertainty Principle (GUP) is utilized as a valuable tool to address the limitations of general relativity (GR). The uncertainty relationship between position and momentum operators, introduced by GUP, incorporates nonlinear terms arising from uncertainties in momentum, expressed as $[\hat{x},\hat{p}] = \imath\hbar(1+\beta\hat{p}^2)$. This formulation is motivated by insights from both string theory and loop quantum gravity, as highlighted in [2]. GUP implies a minimal length at the Planck scale, mitigating the singularity predicted by standard GR. Since its introduction, physicists have extensively and profoundly explored GUP [3].

Numerous tests of GUP-corrected black holes have been considered in the literature [4-9]. The influence of GUP on the accretion disk around a Schwarzschild black hole is discussed in Ref. [10], where the quantum corrections to the Schwarzschild black hole

metric based on GUP are derived [11]. GUP parameter estimates have been applied to various physical effects, including constraints from gravitational wave events [12], perihelion precession for planets and binary pulsars [13], shadow phenomena [14], Shapiro time delay, gravitational redshift, and geodetic precession for the GUP-modified Schwarzschild metric [15].

In the study of GUP-modified Schwarzschild black holes, plasma effects play a crucial role, influencing shadow features. The presence of plasma introduces modifications to spacetime geometry, impacting the trajectory of light rays and observable characteristics. Understanding these effects is essential for accurate interpretations of astrophysical observations, shedding light on the intricate interplay between quantum gravity corrections and the surrounding plasma environment [5-18]. It is crucial to rigorously test gravity models using various observational techniques particle motion, to obtain meaningful constraints on these models [18]. The test particle and photon motion, serves as a fundamental probe of gravity's behavior under different conditions.

The integration of above mentioned tests contributes to refining our understanding of gravity's intricacies and its role in the universe's evolution. Ultimately, these observations play an indispensable role in constraining and validating gravity models, steering us toward a more comprehensive and accurate portrayal of the fundamental forces that shape our cosmos. With this aim, here we plan to study the photon motion and effect of weak gravitational lensing around black hole within GUP modified gravity model. The paper is organized as follows. In Sect. II, we provide null geodesic in presence of plasma. In Sect. III. Finally, in Sect. IV, we summarize obtained results.

Null geodesic in GUP-modified schwarzschild spacetime. In Boyer-Lindquist coordinates, S-GUP metric is given by [13]

$$ds^2 = -f(r)dt^2 + f(r)^{-1}dr^2 + r^2(d\theta^2 + \sin^2\theta d\phi^2) \quad (1)$$

with

$$f(r) = 1 - \frac{2M}{r} + \epsilon\frac{M^2}{r^2} \quad (2)$$

where ϵ is a dimensionless parameter representing the GUP correction [13]. In addition, this metric reduces to the Schwarzschild metric when $\epsilon \to 0$.

For a photon moving in a plasma, the Hamiltonian is written as

$$H(x^\alpha, p_\alpha) = \frac{1}{2}(g^{\alpha\beta} + \left(\frac{\omega_p(r)^2}{\omega(r)^2}\right)u^\alpha u^\beta)p_\alpha p_\beta, \quad (3)$$

here x^α describe the spacetime coordinates and $\omega_p^2(r) = 4\pi e^2 N(r)/m_e$ and $\omega(r) = \frac{\omega_0}{\sqrt{f(r)}}$, here $\omega_0 = \text{const}$.

Using the constraint $H = 0$ for the photon motion, we can rewrite the above equation as

$$\frac{dr}{d\phi} = \pm r\sqrt{f(r)}\sqrt{h^2(r)\frac{\omega_0^2}{p_\phi^2} - 1} \quad (4)$$

where we define [22]

$$h^2(r) \equiv r^2\left[\frac{1}{f(r)} - \frac{\omega_p^2(r)}{\omega_0^2}\right] \quad (5)$$

The radius of a circular orbit of light around black hole, particularly the one that forms a photon sphere of radius r_p, is determined by solving the following equation as

$$\frac{d(h^2(r))}{dr}\Big|_{r=r_p} = 0. \quad (6)$$

we will consider a few simplifed cases below.

A. Homegeneous plasma with $\omega_p^2(r) = $ const. First of all, in the case of homogeneous plasma medium with a constant plasma frequency throughout the medium From Fig.(1) one can easily see that the photon's radius around black hole decreases with increasing GUP parameters ϵ. As well as, the plasma medium increases radius of the photon sphere.

B. Inhomogeneous plasma with $\omega_p^2(r) = z_0/r^q$. In this subsection we probe photon spheres in the presence of an non-uniform plasma, where the plasma frequency must satisfy a simple power-law of the from [19, 22],

$$\omega_p^2(r) = \frac{z_0}{r^q} \quad (7)$$

where z_0 and $q > 0$ are free parameters. To analyze the primary features of the power-law model, we restrict ourselves to the following cases: $q = 1$ and $q = 3$ based on Goldreich-Julian(GJ) density.

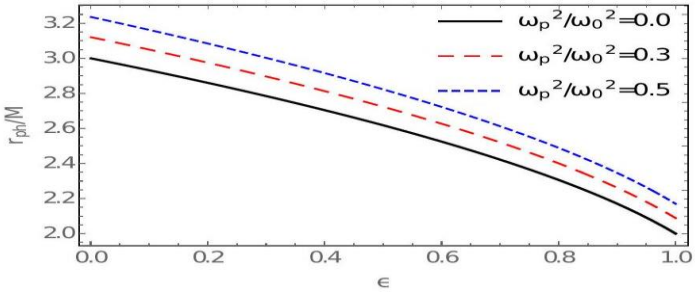

FIG. 1. This graph describes radius of the photon sphere in a homogeneous plasma medium with constant frequency $\omega_p = \text{const}$.

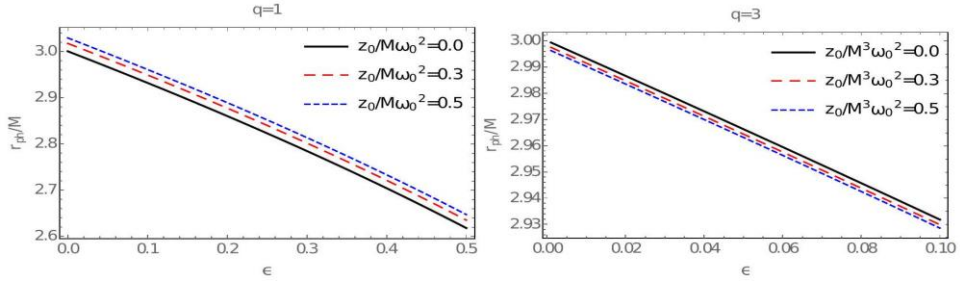

FIG. 2. This graph shows a variation of r_{ph}/M with respect to ϵ for the case $q = 1$ (left panel) and $q = 3$ (right panel).

Using Eqs (6, 7) we obtain the radius of the photon sphere based on numerical scheme for the inhomegeneous plasma medium, as illustrated in Fig.(2). This profile shows that the radius of photon sphere decreases when ϵ parameter increases. On the other hand, plasma medium leads to the widening of the photon sphere radius if its distribution obeys $\omega_p^2(r) = z_0/r$ law (shown in left panel), contrarily, in the case of $q = 3$, the effect of plasma is negative i.e. the presence of plasma around black hole slightly shrinks the photon radius (shown in right panel). Furthermore, difference of the photon radius in the case of without and with plasma is enough small. This suggests that testing and distinguishing the homogeneous plasma from inhomogeneous plasma around BHs based on their shadows may be quite challenging.

Shadow of a bh surrounded by plasma medium. We investigate the radius of the shadow of S-GUP spacetime metric in a plasma medium.

Notably, if the observer is located at a sufficiently large distance from the BH, one can approximate the radius of the BH shadow as follows

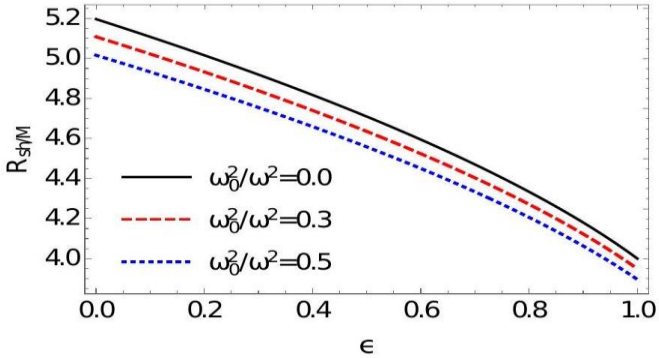

FIG. 3. This graph describes a variation of R_{sh}/M with respect to ϵ in uniform plasma

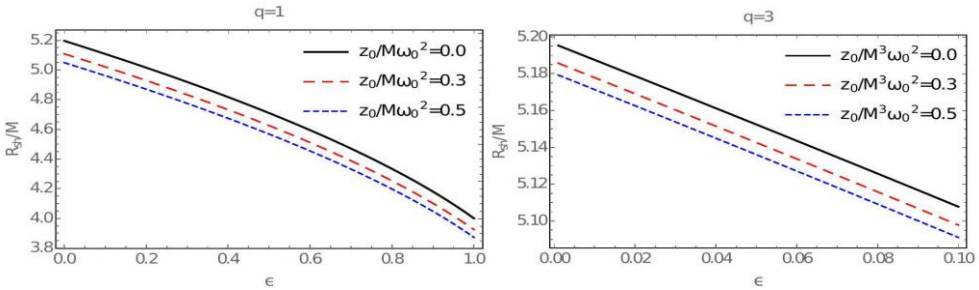

FIG. 4. Variation of R_{sh}/M with respect to ϵ for $q = 1$ (left panel) and $q = 3$ (right panel).

[22]

$$R_{sh} \approx r_0 \sin \alpha_{sh} = \sqrt{r_p^2 \left[\frac{1}{f(r_p)} - \frac{\omega_p^2(r_p)}{\omega_0^2}\right]} \qquad (8)$$

The radius of the BH shadow is depicted for different parameter ϵ in Fig (3) for a homogeneous plasma frequency. This figure illustrates that the shadow radius decreases much more steeply with ϵ as well as plasma frequency. Furtermore, we have investigated inhomogeneous plasma with $q = 1$ and $q = 3$ in Eq.(8). One can see that due to the presence of plasma radius of the BH's shadow is decreasing.

Now we assume that the supermassive BHs M87* and Sgr A* are spherically symmetric static. Although the observation got by the EHT collaboration does not support the assumption taken here. However, here we explore theoretically the constrain on the parameter ϵ, from the data provided by the EHT project. To constrain this parameter ϵ we use the observational data released by the EHT project for the BH shadows of the supermassive BHs M87* and Sgr A*. The angular diameter of the shadow, the distance from sun system and the mass of the BH at the centre of the galaxy M87, are $\Omega_{\mathrm{M87^*}} = 42 \pm 3\mu\mathrm{as}, D = 16.8 \pm 0.8\mathrm{Mpc}$ and $M_{\mathrm{M87^*}} = (6.5 \pm 0.7) \times 10^9 M_\odot$, respectively [24]. For the Sgr A* the data recently obtained by the EHT project is $\Omega_{\mathrm{SgrA^*}} = 48.7 \pm 7\mu$ as, $D = 8277 \pm 9 \pm 33\mathrm{pc}$ and $M_{\mathrm{Sgr\,A}} = 4.297 \pm 0.013 \times 10^6 M_\odot$ (VLTI) [18].

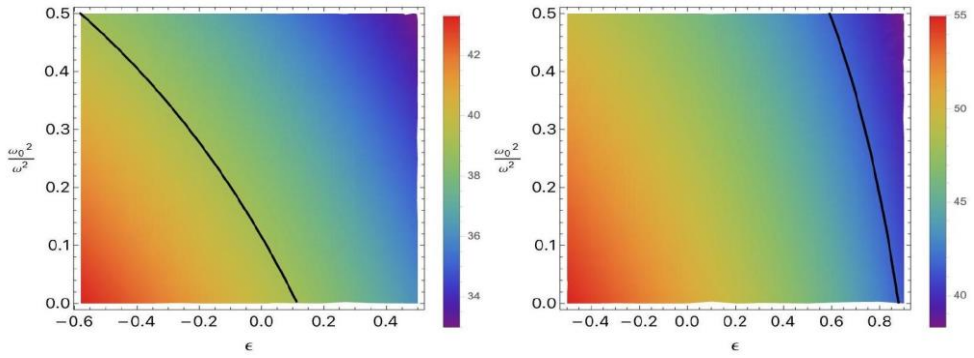

FIG. 5. Relationship between ϵ and plasma parameter via observational shadow angular diameter of M87* (left panel) and Sgr A* (right panel) black holes. Black lines correspond to black hole shadow angular diameter $\theta_{sh} = 39\mu as$ for M87* (left panel)

and $\theta_{sh} = 41.7\mu as$ for Sgr A* (right panel), respectively. Regions contained within it satisfy M87*(left panel) and Sgr A^* (right panel) black holes shadow $1-\sigma$ bound.

Now we can obtain the diameter of the shadow from the expression $d_{\rm sh}^{\rm theo} = 2R_{\rm sh}$. Thus, the diameter of the BH shadow image is $d_{\rm sh}^{\rm M87^*} = (11 \pm 1.5)M$ and $d_{\rm sh}^{\rm SgrA^*} = (9.5 \pm cc - by)M$. From the data by the EHT collaboration, we obtain the constrain on the parameter ϵ for the supermassive BHs at the centre of the galaxy M87 and the Sgr A. We present our results obtained here in the Fig. 5. In this figure, it is observed that the angular diameter of BH shadow decreases with the increasing value of parameter ϵ. It is also observed that the angular diameter of shadow for M87* and Sgr A* BH in the context of the S-GUP black hole is smaller than the other ordinary astrophysical BH such as Schwarzschild BH. In addition, by using observational data of EHT project, we can get constrains parameter ϵ. Fig.(5) shows that the region that is coincided observation. As a result, we can get upper bound of parameter ϵ of GUP-modified Schwarzschild black hole. This value is $\epsilon_{\rm upper} = 0.2$ in the case of M87*, while it can be $\epsilon_{\rm upper} = 0.9$ in the case of SgrA*.

Conclusion. In this paper, we have tested Schwarzschild spacetime with modified GUP parameter through studying null geodesic and shadow. From above investigating, we can summarize as follows:

- Studying of the null geodesic we can observe that photon orbits decrease due to presence of the parameter ϵ. As well as Radius of the BHs shadow decrease with increasing of the parameter ϵ.
- Also, we have obtained influence of plasma in photon radius and shadow. From Figs.(1) and (2), photon and shadow radius decreasing with increasing plasma parameter in the case $q = 1$ and for the case $q = 3$ photon radius falls when plasma parameter growth.

REFERENCES

1. L. Susskind and J. Uglum, Nucl. Phys. B Proc. Suppl. 45BC, 115 (1996), arXiv:hep-th/9511227.
2. A. F. Ali, S. Das, and E. C. Vagenas, Phys. Lett. B 678, 497 (2009), arXiv:0906.5396 [hep-th].
3. A. Nasser Tawfik and A. Magied Diab, Rep. Prog. Phys. 78, 126001 (2015), arXiv:1509.02436 [physics.gen-ph].
4. R. J. Adler, P. Chen, and D. I. Santiago, Gen. Rel. Grav. 33, 2101 (2001), arXiv:gr-qc/0106080 [gr-qc].
5. Ö. Ökcü, C. Corda, and E. Aydiner, EPL (Europhysics Letters) 129, 50002 (2020), arXiv:2003.11369 [gr-qc].
6. R. Karmakar, D. J. Gogoi, and U. D. Goswami, Int. J. Mod. Phys. A 37, 2250180-2409 (2022), arXiv:2206.09081 [gr-qc].
7. Z.-Y. Fu and H.-L. Li, Nucl. Phys. B 969, 115475 (2021).
8. H.-L. Li and S.-R. Chen, Gen. Rel. Grav. 49, 128 (2017), arXiv:1705.00297 [gr-qc].
9. M. Rizwan and K. Saifullah, Int. J. Mod. Phys. D 26, 1741018 (2017).
10. M. Moussa, Annals Phys. 453, 169305 (2023).
11. D. B. Lenat, Artif. Intell. 21, 61 (1983).
12. Z.-W. Feng, S.-Z. Yang, H.-L. Li, and X.-T. Zu, Phys. Lett. B 768, 81 (2017), arXiv:1610.08549 [hep-ph].
13.] F. Scardigli and R. Casadio, Eur. Phys. J. C 75, 425 (2015), arXiv:1407.0113 [hep-th].
14. J. C. S. Neves, Eur. Phys. J C 80, 343 (2020), arXiv:1906.11735 [gr-qc].
15. O. Ökcü and E. Aydiner, Nucl. Phys. B 964, 115324 (2021), arXiv:2101.09524 [gr-qc].
16. K. Jusufi, M. Azreg-Aïnou, M. Jamil, and T. Zhu, Int. J. Geom. Meth. Mod. Phys. 19, 2250068 (2022), arXiv:2008.09115 [gr-qc].
17. K. Jusufi, P. Channuie, and M. Jamil, Eur. Phys. J. C 80, 127 (2020), arXiv:2002.01341 [gr-qc].
18. G. S. Bisnovatyi-Kogan and O. Y. Tsupko, Mon. Not. R. Astron. Soc 404, 1790 (2010), arXiv:1006.2321 [astro-ph.CO].

O‘ZBEKISTON MILLIY UNIVERSITETI XABARLARI, 2024, [3/1/1]
ISSN 2181-7324

FIZIKA
http://journals.nuu.uz
Natural sciences

UDK: 528.4

Otabek YUSUPJONOV,
O‘zbekiston Milliy universiteti tayanch doktoranti
E-mail: yusupjonov_otabek@mail.ru
Maxsud ABDUKARIMOV,
O‘zbekiston Milliy universiteti o‘qituvchisi
Jahongir IBRAGIMOV,
O‘zbekiston Milliy universiteti o‘qituvchisi

TAQI, Geomatika muhandisligi kafedrasi dotsenti D.Tog‘ayeva taqrizi asosida

IN THE ESTABLISHMENT OF STATE BASE NETWORKS THEORETICAL ISSUES OF APPLICATION OF SATELLITE GNSS OBSERVATIONS

Annotation

The article provides information about navigational system GPS and GLONASS applicable when making the state geodetic supporting network. The Requirements to receiver companion (satellite) for performing on making the state geodetic supporting network.

Keywords: reference system, GPS, ГЛОНАСС, СК-42, RTK method, WGS-84 coordinate system.

ПОСТРОЕНИИ ГОСУДАРСТВЕННЫХ БАЗОВЫХ СЕТЕЙ ТЕОРЕТИЧЕСКИЕ ВОПРОСЫ ПРИМЕНЕНИЯ СПУТНИКОВЫХ НАБЛЮДЕНИЙ GNSS

Аннотация

В статье представлена информация о системах спутниковой навигации GPS и ГЛОНАСС, применяемых при возведении государственных геодезических базовых сетей. Рассмотрены требования к спутниковым приемопередающим устройствам для проведения работ по сооружению государственных геодезических опорных сетей.

Ключевые слова: система отсчета, GPS, ГЛОНАСС, СК-42, метод RTK, система координат WGS-84.

DAVLAT TAYANCH TARMOQLARINI BARPO QILISHDA YO‘LDOSHLI GNSS KUZATISHLARNI QO‘LLASHNI NAZARIY MASALALARI

Annotatsiya

Maqolada davlat geodezik tayanch to‘rlarini barpo etish bo‘yicha qo‘llaniladigan GPS va GLONASS sun’iy yo‘ldoshli navigatsiya tizimlari haqida ma’lumotlar berilgan. Davlat geodezik tayanch to‘rlarini barpo etish bo‘yicha ishlarni amalga oshirish uchun sun’iy yo‘ldosh qabul qiluvchi qurilmalariga bo‘lgan talablar ko‘rib chiqilgan.

Kalit so‘zlar. referens sistema, GPS, GLONASS, CK-42, RTK usuli, WGS–84 koordinatalar sistemasi.

Kirish. Ma’lumki mamlakatimizda geografik koordinatalar sistemasidan foydalanishda asosiy tayanch bo‘lib geodezik ishlar xizmat qiladi. Hozirgi kunga kelib, butun dunyo bo‘ylab koordinata sistemasining turlicha ko‘rinishlari mavjud. O‘zbekistonda barcha geodezik, topografik tashkilotlar 1942 yilda joriy etilgan CK-42 (Krasovskiy) koordinata sistemasi qo‘llanilib kelmoqda.

Yuqoridagilarni xisobga olib, davlat geodezik tarmoqlari qayta qurish va ularni rivojlantirish shuningdek respublikamiz hududi uchun WGS-84 umumyer koordinatalar sistemasini joriy qilish maqsadida so‘nggi yillarda sun’iy yo‘ldosh navigatsion tizimlariga asoslangan davlat geodezik tarmoqlarini qurish va rivojlantirish borasida respublikamizda loyihalar ishlab chiqildi va amaliyotga tadbiq etilmoqda.

Mavzuga oid adabiyotlar tahlili. Ushbu masalani hozirgi kunga kelib malakali ilmiy tadqiqotchi olimlar tomonidan o'rganilib kelinmoqda. Xususan, davlat tayanch geodezik tarmoqlarini barpo qilishda yo‘ldoshli GNSS kuzatishlarni qo'llashga bag'ishlangan tadqiqotlar bo'yicha soha olimlaridan J.A.Yunes, T.Sh.Chan, V.N.Balandin, I.V.Men’shikov, YU.G.Firsov, X.A.Mohamed, M.G.Godjamanov, A.V.Gordeev, A.V.Maslov, YU.K.Neumivakin, M.Y.Brin, T.M.Pimshina, A.V.Voytenko, M.A.Monaxova, K.M.Antonovich, F.Molodensky, F.Xelmert, A.P.Gerasimov, A.A.Genike, G.G.Pobedinskiy, K.F.Afonin, V.N.Xarisov, A.I.Perov, V.A.Boldin, B.B.Serapinas, V.F.Xabarov, A.V.Yuskevich va boshqa bir qator olimlarning ilmiy ishlarida o‘z ifodasini topgan. O‘zbekistonda ham yo‘ldoshli GNSS kuzatishlari bo‘yicha amaliy, nazariy va metodologik masalalari E.R.Mirmaxmudov, X.Muborakov, A.Ro‘ziyevlar va bir qator olimlarning ilmiy ishlarida o'z aksini topgan.

Tadqiqot metodologiyasi. O‘zbekiston Respublikasi hududida hozirgi kunga kelib jami 14145 ta davlat geodezik tayanch punktlari mavjud bo‘lib, ular astronomo-geodeziya, triangulyatsiya, poligonometriya punktlari va nivelir reperlaridan tashkil topgan.

Mavjud geodezik tayanch tarmoqlarini qurish ishlari 1939-yildan boshlangan. Barcha geodezik punktlar Gauss-Kryugerning 1942 yilda qabul qilingan davlat koordinatalar sistemasi va boltiq balandliklar tizimiga ega (1 va 2 sinf astronomo-geodeziya tarmog‘i – AGT punktlari shuningdek, CK-95 koordinatalar sistemasiga ega, biroq ushbu koordinatalar sistemasi O‘zbekiston Respublikasida davlat koordinatalar sistemasi xisoblanmaydi va faqatgina maxsus ishlarni bajarishda foydalaniladi). Barcha punktlarning koordinatalari va balandliklari to‘g‘risidagi ma’lumotlar xozirgi kunda tizimlashtirilgan kataloglar ko‘rinishida xamda elektron kompyuter bazasi tizimida shakllantirilgan.

Bundan tashqari Respublikamizning shaxarlari va tuman markazlarida poligonometriya punktlari yaratilgan bo‘lib, ular davlat va maxalliy koordinatalar tizimiga ega.

Butun dunyo bo‘yicha olib borilayotgan kosmik tadqiqotlar natijasida geodeziya, kartografiya, yer tuzish va davlat kadastri sohalariga kosmik uskunalar va yangi o‘lchash usullarining kirib kelishi xamda o‘lchashlar aniqlik darajasining oshganligi tufayli mavjud davlat geodezik tarmog‘idagi kamchiliklar yuzaga chiqdi. Bir tomondan, Davlat geodezik tarmog‘i punktlarining juda ko‘p qismi yo‘qotilgan bo‘lsa, boshqa tomondan an’anaviy yer usti geodezik o‘lchash usullari asosida yaratilgan davlat koordinatalar sistemasi CK-42 foydalanuvchilar talabini to‘la qanoatlantirmay qo‘ydi. Ushbu kamchiliklar global navigatsion sun’iy yo‘ldosh tizimlariga (GNSYT) asoslangan geodezik texnologiyalar yordamida zamonaviy davlat geodezik tarmoqlarini qurish orqali bartaraf etilishi mumkin.

Sun’iy yo‘ldosh geoedezik balandlik tarmoqlari triangulyatsiya va poligonometriya kabi an’anaviy usullarda qurilgan geodezik tarmoqlarga nisbatan o‘zining yuqori darajadagi aniqligi va samaradorligi bilan ajralib turadi. Ushbu texnologiyalarda balandliklarni topish o‘rta kvadratik xatosi 2 sm va undan xam kam ko‘rsatkichni tashkil etadi.

Hozirgi vaqtda geodezik o‘lchashlarni bajarishda asosan ikkita sun’iy yo‘ldosh navigatsion tizimlari qo‘llaniladi – AQSh ga tegishli GPS (boshqa nomi NAVSTAR - Navigation Satellite Timing And Ranging) va Rossiyada ishlab chiqarilgan GLONASS (Globalnaya Navigatsionnaya Sputnikovaya Sistema). Ushbu ikkita tizimdan tashqari Yevropa kosmik agentligiga tegishli Galileo navigatsion tizimi xam mavjud.

GPS va GLONASS tizimlari turli umumyer geotsentrik koordinatalar sistemasida ishlaydi. GPS tizimida nuqtalar o‘rni WGS-84 (World Geodetic System, 1984) koordinatalar sistemasida topilsa, PZ-90 (Parametri Zemli, 1990) koordinatalar sistemasida ishlaydi [1].

O‘zbekiston Respublikasi xududi bo‘yicha yer resurslaridan samarali foydalanish, yer fondini bir tizimga solib boshqarish, ya’ni davlat kadastrlari yagona tizimini (DKYaT) yuritish kabi qator masalalarni yechish maqsadida Respublikamiz xududida sun’iy yo‘ldosh texnologiyalariga asoslangan davlat geodezik tarmoqlarini barpo etish borasida ishlar olib borilmoqda.

Tahlil va natijalar. O‘zbekiston Respublikasining sun’iy yo‘ldosh navigatsion tizimlariga asoslangan Davlat geodezik tarmoqlari (Davlat Sun’iy Yo‘ldosh Geodezik Tarmoqlari - DSYGT) GPS va GLONASS tizimlaridan, shuningdek kosmik geodeziyaning boshqa usullaridan foydalanib umumiydan xususiyga o‘tish tarzida quriladi va quyidagilarni o‘z ichiga oladi: referens geodezik punktlar tarmog‘i (RGP); 0-sinf sun’iy yo‘ldosh geodezik tarmog‘i (SYGT-0); 1-sinf sun’iy yo‘ldosh geodezik tarmog‘i (SYGT-1).

RGP tizimi umumyer fazoviy koordinatalar sistemasini (WGS-84) bevosita O‘zbekiston Respublikasi xududiga o‘rnatish uchun mo‘ljallangan. Hozirgi kunda Respublikamiz xududida bunday referens geodezik punktlarining beshtasi mavjud bo‘lib ular Farg‘ona, Toshkent, Urganch, Termiz va Kitob shaxarlarida joylashgan. Ushbu RGP larning barchasida o‘lchash ishlari yakuniga yetkazilgan. RGP uchun boshlang‘ich punktlar sifatida geodinamika uchun Xalqaro GPS-xizmatining (International GPS-Service for Geodinamics – IGS) muntazam ishlab turuvchi punktlari xizmat qiladi. Bunday punktlar, shu jumladan O‘zbekiston Respublikasi xududida xam joylashgan (Kitob sh.).

RGP tizimi orqali umumyer fazoviy koordinatalar sistemasi quyi sinf sun’iy yo‘ldosh tarmog‘i punktlariga uzatiladi. Ishlash rejimlariga qarab RGP muntazam ishlab turuvchi (aktiv) va davriy (passiv) larga bo‘linadi. Barcha referens geodezik punktlar uchta IGS punktlari bilan va qolgan qo‘shni RGP lar o‘lchashlari bilan bog‘langan bo‘lishi kerak. Referens geodezik punktalri orasidagi masofa o‘rtacha 500-800 km ni tashkil qilishi kerak.

RGP ni yaqin IGS punktiga nisbatan o‘rnini topishning o‘rta kvadratik xatosi plandagi koordinatalar bo‘yicha 2 sm dan va geodezik balandlik bo‘yicha 3 sm dan oshmasligi kerak.

RGP punktlarning o‘zaro o‘rnini topishning o‘rta kvadratik xatosi plandagi koordinatalar bo‘yicha **3 mm + 5×10^{-8} D mm** (D – RGP punktlari orasidagi masofa, mm) dan va geodezik balandlik bo‘yicha **5 mm + 7×10^{-8} D** dan oshmasligi kerak [3].

0-sinf sun’iy yo‘ldosh geodezik tarmog‘i (SYGT-0) umumyer fazoviy koordinatalar sistemasini (WGS-84) respublikaning butun xududiga uzatish uchun shuningdek, umumyer va referens koordinatalar sistemalari aro o‘tish parametrlarini aniqlash uchun mo‘ljallangan. SGS-0 punktlari, RGP bilan bir qatorda quyi sinf geodezik tarmoqlarini rivojlantirish uchun boshlang‘ich asos xisoblanadi. Barcha SYGT-0 punktlari kamida 2 ta RGP va barcha qo‘shni SYGT-0 punktlari o‘lchashlari bilan bog‘langan bo‘lishi kerak [5, 6].

Hozirgi kunda Respublikamiz xududida bunday punktlarning 15 tasi mavjud. Ular orasidagi o‘rtacha masofa 100-300 km ni tashkil etadi. RGP tarmog‘ining va SYGT-0 ning Respublikamiz xududi bo‘yicha joylashuvi quyidagi shaklda keltirilgan (1-rasm).

I-sinf sun’iy yo‘ldosh geodezik tarmog‘i (SYGT-1) turli maqsadlar uchun foydalanish qulay bo‘lgan geodezik punktalar tizimi bo‘lib, sun’iy yo‘ldosh o‘lchash vositalarini qo‘llash uchun optimal sharoitlarni ta’minlash va ular imkoniyatidan maksimal tarzda foydalanish uchun mo‘ljallangan.

SYGT-1 punktlari o‘zaro RGP tizimi orqali bog‘lanuvchi aloxida fragmentlar ko‘rinishida quriladi.

SYGT-1 yaratilayotgan fragmenti bitta boshlang‘ich punktga ega mustaqil tarmoq xisoblanadi. SYGT-1 fragmenti uchun boshlang‘ich punktlar bo‘lib RGP va SYGT-0 xizmat qiladi.

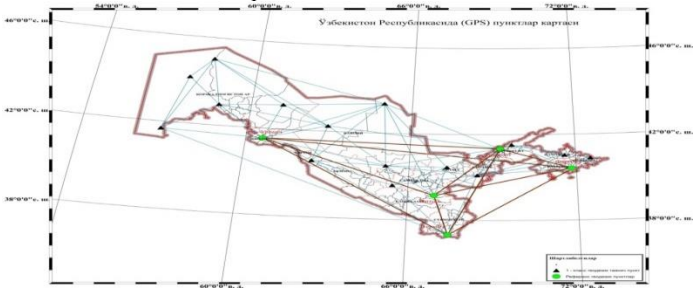

1-rasm. RGP, SYGT-0 va DSYGTning joylashuv sxemasi

SYGT-1 punktlari orasidagi o‘rtacha masofa quyidagilarga teng bo‘lishi kerak: 5-10 km – axolisi 300 ming kishidan ortiq bo‘lgan shaxarlar xududida (zichligi – 20-80 km^2 ga 1 punkt); 10-20 km – intensif xo‘jalik faoliyatidagi shuningdek, seysmik

aktivligi 6 va undan yuqori ballga ega bo‘lgan xududlarda (zichligi – 80-350 km^2 ga 1 punkt); 20-30 km – sanoat majmualari bilan band bo‘lgan xududlarda (zichligi 350-800 km^2 ga 1 punkt) [1, 3].

Yuqoridagilardan istisno tariqasida aloxida xududlarda SYGT-1 punktlari zichligi oshirilishi yoki kamaytirilishi mumkin.

SYGT-1 qo‘shni punktlari o‘rnini topishning o‘rtacha kvadratik xatosi plandagi koordinatalar bo‘yicha 3 mm + 1×10^{-7} D mm dan geodezik balandlik bo‘yicha 5 mm + 2×10^{-7} D mm dan oshmasligi kerak.

SYGT-1 ni yaqin SYGT-0 va RGP ga nisbatan o‘rnini topishning o‘rta kvadratik xatosi 2 sm dan oshmasligi kerak.

1-jadval

RGP da va SYGT-1 punktlarida sun’iy yo‘ldosh o‘lchashlarini bajarishga qo‘yiladigan talablar

RGP	SYGT-1
-o‘lchash davomiyligi – 3 sutkadan kam bo‘lmasligi kerak; -o‘lchash intervali – 30 sek.; -sun’iy yo‘ldosh minimal ko‘tarilish burchagi - 15°; -o‘lchashlar bajariladigan su’iy yo‘ldoshlar soni – 6 tadan kam emas (uzoq vaqt davomiyligi uchun); -DOP ko‘rsatkichi – 4 tadan kam emas (uzoq vaqt davomiyligi uchun).	-o‘lchash davomiyligi – ikki (yoki undan ko‘p) seansdan, xar bir seansda 4 soatdan; -o‘lchashlar bajariladigan sun’iy yo‘ldoshlar soni – 5 tadan kam emas; -yozish intervali – 20 sek; -sun’iy yo‘ldosh minimal ko‘tarilish burchagi - 15°; -DOP ko‘rsatkichi – 4 tadan kam.

Sun’iy yo‘ldosh geodezik tarmoqlarida sun’iy yo‘ldosh o‘lchashlari bitta seansda iloji boricha ko‘p miqdordagi priyomniklarni qo‘llab bajarilishi kerak. Bunda qo‘llaniladigan priyomniklar mumkin qadar bir xil tipda bo‘lmog‘i lozim.

SYGT-0 va SYGT-1 larni qurishda Leica firmasining ikki chastotali Leica Viva GS16, Leica GS 16, LeicaGS08plus, Sino GNSS T300 PLUS GNSS kabi sun’iy yo‘ldosh priyomniklari keng qo‘llanilmoqda.

Sun’iy yo‘ldosh orqali o‘lchashlarni bajarish uchun quyidagi usullardan foydalaniladi: statik (Static); tezstatik (Fast Static, Rapid Static); RTK usuli (soxtastatik, reokkupatsiya); kinematik.

Respublikamiz shahar hududlarida mavjud geodezik tarmoqlar zamonaviy talablarini qanoatlantira olmaydi. Shuning uchun xam keyingi yillarda GPS-texnologiyalari asosida geodezik tarmoqlarni qurishga qaratilgan ishlar olib borilmoqda. Respublikamizda xozirgi kunda RGP, SYGT-0 va SYGT-1 kabi sun’iy yo‘ldosh geodezik tarmoqlarini qurish borasida loyixalar ishlab chiqilgan va ba’zi o‘lchashlar olib borilgan. Shulardan, SYGT-1 ni qurish loyixasi bo‘yicha “Respublika aerogeodeziya markazi” xodimlari tomonidan ilmiy va amaliy izlanishlar olib borildi va Namangan viloyatida barpo etildi. Keyinchalik ushbu tarmoqlarni quyi sinf tarmoqlari bilan zichlashtirish, xamda shaharlar hududlarida sun’iy yo‘ldosh texnologiyalariga asoslangan geodezik tarmoqlarni qurish rejalari xam mavjud. Biroq, ba’zi sabablarga ko‘ra xozirda ishlar to‘xtab turibdi.

Shuning uchun xam respublikamiz shaharlarida s’yomkalari uchun aniqlik va sifat jixatlari bilan tavsiflanuvchi geodezik tarmoqlarini qurish masalasi xozirgi kunda dolzarb masalalardan biri bo‘lib turibdi. Bunda sun’iy yo‘ldosh va yer usti texnologiyalarni birga qo‘llash masalasi katta axamiyat kasb etadi.

Shularni xisobga olib shahar hududlarida s’yomkalarni bajarish uchun geodezik tarmoqlarni sun’iy yo‘ldosh texnologiyalari va yer usti o‘lchashlariga asoslangan usullar yordamida rivojlantirishni quyidagi 2-sxema (variant) asosida ko‘rib chiqaldi.

SYGT-1 ning har bir punkti uchun alohida ikkita sessiyadagi qo‘shma o‘lchashlarga dastlabki ishlov berish va ularni tenglash Trimble Business Center dasturining 5.52 versiyasi bo‘yicha WGS-84 tizimida keyinchalik ularni 1942 yilgi koordinatalar tizimiga transformatsiyalagan holda bajarildi [9].

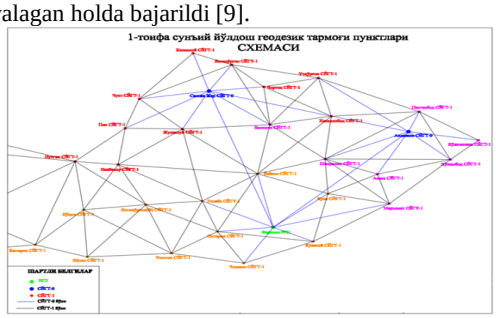

2-rasm. Farg‘ona vodiysi 1-sinf sun’iy yo‘ldosh geodezik tarmog‘i (SYGT-1) punktlari

2-jadvalda **Farg‘ona vodiysi** hududida o‘rnatilgan SYGT-1 punktlarida olib borilgan o‘lchash natijalari keltirilgan.

2-jadval

**Punktlar koordinatalari (WGS84) **

Nuqta	Kenglik	σ, mm	Uzoqlik	σ, mm	Balandlik, m	σ, mm
Andi	40° 46' 35.16069"	0.9	72° 20' 41.08785"	0.7	450.1002	2.5
Asak	40° 39' 01.64864"	0.9	72° 14' 06.82586"	0.7	461.8710	2.5
Balik	40° 54' 04.83701"	0.8	71° 48' 57.36675"	0.7	438.8937	2.6
Besh	40° 25' 01.46833"	0.7	70° 36' 02.04850"	0.6	489.6569	1.8
Chim	40° 11' 58.47634"	1.1	71° 42' 41.73164"	0.9	636.3988	1.1
...						

Xulosa va takliflar. O‘zbekistonda xozirgi kunga kelib xam 1942-yilda qabul qilingan SK-42 koordinat tizimi qullanilib kelmoqda. Barcha topogeodezik ishlar shu tizimga asoslangan. Lekin xozirgi zamonaviy asboblar va GAT Umumyer koordinata tizimi WGS84 koordinata tizimiga asoslangan. O‘zbekiston Respublikasida qurilayotgan suniy yuldosh geodezik punktlari (SYuGP) RGP (Referens Geodezik Punkt) va bazi SYGT 1 tarmoqlari GPS va DORIS punktlariga bog‘langan. Bu punktlar yuqori aniqlikka yega bo‘lgan fundametal punkt xisoblanadi ushbu punktlardan mamlakatimizda boshlang‘ich geodezik asosni yaratish masalalarni xal qilishda foydalanish lozim.

ADABIYOTLAR

1. Антонович К.М. Исползование спутниковых радионавигационных систем в геодезии. М.: Картгеоцентр, 2006, Том.2.

2. Базлов Ю.А., Герасимов А.П., Ефимов Г.Н., Насретдинов К.К. Параметры связи систем координат. Геодезия и картография. 1996. № 8.
3. ГКИНП (ОНТА)-02-262-02. Инструкция по развитию съёмочного обоснования и съёмке ситуации и рельефа с применением глобальных навигационных спутниковых систем ГЛОНАСС И ГПС. 2002.
4. Клюшин Е.П., Куприянов А.О., Шлапак В.В. Спутниковые методы измерений в геодезии. М.,2006. Ч.1. стр. 5-6.
5. Мубораков Х., Юсупжонов О.Ғ., Рўзиев А.С., Мирмахмудов Э.Р. Некоторые требования к созданию национальной референцной системы координат узбекистана. Ўзбекистон География жамияти ахбороти. 58-жилд. Т.2020. Б. 316-322.
6. Мирмахмудов Э.Р. Предварителный анализ точности координат уровенных постов Узбекистана Научный журнал. Наука, техника и образование. Москва, 2020. №4(68). С.114-118.
7. Инструкция о построении государственной геодезической сети СССР. М., Недра,1966.
8. Постановление Кабинета министров Республики Узбекистана от 26 декабря 2017 г. № 1022 «О применении и открытом использовании на территории Республики Узбекистан международных геодезических систем координат».
9. ҳттпс://гэоспатиал.тримблэ.ком/эн/продустс/софтwарэ/тримблэ-бусинэсс-сэнтэр